

University of Southampton

**Effects of Lipids on the Structure of the Mechanosensitive
Channel MscL**

By Joanne Carney

**School of Biological Sciences
University of Southampton
UK**

February 2007

University of Southampton

Abstract

FACULTY OF MEDICINE, HEALTH AND LIFE SCIENCES

SCHOOL OF BIOLOGICAL SCIENCES

Doctor of Philosophy

Effects of Lipids on the Structure of the Mechanosensitive Channel MscL

By Joanne Carney

Tryptophan (Trp) fluorescence spectroscopy has been used to characterise interactions between the mechanosensitive channel of large conductance (MscL) of *Mycobacterium tuberculosis* (*Tb*) and its surrounding lipid bilayer. MscL is a homopentamer, each monomer containing two transmembrane α -helices, one lipid-exposed (TM2) and one lining the pore (TM1). Native MscL contains no Trp residues. Trp residues were incorporated into TbMscL at lipid-facing and pore-facing sites. Results from Trp-mutants of pore-lining residues suggest that water is able to penetrate into the channel pore, in the closed channel, upto the pore constriction formed by Thr-25. Trp residues located below Thr-25 and incorporated at helix-helix contact positions resulted in gain-of-function (GOF) mutants causing the channel to adopt an open conformation at zero tension. Reconstitution of Trp mutants of TbMscL into lipids of different chain lengths and different head group structures resulted in no significant change in fluorescence emission maxima, suggesting that any changes in structure are small or result in no change in polarity for the Trp residue. Lipid-facing residues at the N-terminal end of TM1 are buried below the transmembrane surface of the protein. Fluorescence emission maxima for lipid-facing Trp residues in TM1 vary with position in the bilayer comparably to those for Trp residues in TM2, despite the fact that residues in TM2 are on the surface of the protein. Fluorescence emission spectra for most Trp residues on the periplasmic sides of TM1 and TM2 fit well to a model proposing a trough-like variation of dielectric constant across the membrane but the relationship between location and fluorescence emission maximum on the cytoplasmic side of the membrane is more complex. The fluorescence of Trp residues in TM1 is quenched efficiently by phospholipids with bromine-containing fatty acyl chains, showing that the lipid chains must be able to enter the Trp-containing cavities on the surface of MscL, resulting in efficient solvation of the surface.

Contents

	Page
Chapter One - Introduction	1
1.1 Biological Membranes	1
1.2 Lipids	2
1.2.1 Phospholipids	3
1.2.2 Glycolipids	3
1.2.3 Sterols	4
1.2.4 Prokaryotic Lipids	4
1.3 Lipid Phase	7
1.4 Phase transition of the lipid bilayer	10
1.5 Lipid composition	11
1.6 Lateral Pressure Profile	11
1.7 Membrane Proteins	11
1.8 Membrane Protein Topology	12
1.9 Protein Lipid Interactions	13
1.10 Ion Channels	17
1.11 Prokaryotic Osmoregulation	17
1.12 TbMscL Structure	20
1.13 Gating Mechanism of TbMscL	26
Chapter Two – General Methods and Materials	31
2.1 Materials	31
2.2 General Methods	33
2.2.1 Sterilisation	33
2.2.2 Antibiotic Stocks	33
2.2.3 Luria Broth	33
2.2.4 LB Agar	33
2.2.5 SOB Medium	34
2.2.6 SOC Medium	34

2.2.7	Transformation Buffer	34
2.2.8	Escherichia coli strains	35
2.2.9	Glycerol Stocks	35
2.2.10	Purification of Plasmid DNA	36
2.2.11	Restriction Digests	37
2.2.12	Agarose Gel Electrophoresis	38
2.2.13	Quik-change [®] site-directed mutagenesis	39
2.2.14	Ethanol Precipitation of DNA	39
2.2.15	DNA Sequencing	40
2.2.16	Sequence Analysis	40
2.2.17	Preparation of ultra-competent cells	40
2.2.18	Transformation of DNA into ultra-competent cells	41
2.2.19	Expression of TbMscL	41
2.2.20	Purification of TbMscL	41
2.2.21	SDS-PAGE	43
2.2.22	Determination of protein concentration	45
Chapter Three – Mutagenesis of TbMscL		46
3.1	Introduction	46
3.2	Methods	49
3.2.1	Cloning of TbMscL	49
3.2.2	Generation of Trp mutants of TbMscL	50
3.2.3	Quik-change [®] site-directed Mutagenesis	51
3.2.4	Expression and purification of TbMscL	54
3.3	Results	55
3.3.1	Restriction Digests of TbMscL	55
3.3.2	Quik-change [®] site-directed Mutagenesis	56
3.3.3	Sequencing of TbMscL Trp constructs	57
3.3.4	Expression and purification of TbMscL	60
3.4	Discussion	62

Chapter Four - Fluorescence Properties of Lipid Exposed mutants on TM1	63
4.1 Introduction	63
4.2 Fluorescence	65
4.2.1 Tryptophan Fluorescence	67
4.2.2 Quenching of Tryptophan Fluorescence	68
4.3 Methods and Materials	70
4.3.1 Materials	70
4.3.2 Methods	71
4.3.2.1 In vivo cell viability assay for GOF mutants	71
4.3.2.2 Preparation of Lipid Stocks	71
4.3.2.3 Preparation of brominated Lipid Stocks	71
4.3.2.4 Hepes Buffer	71
4.3.2.5 Preparation of Potassium Cholate	71
4.3.2.6 Reconstitution of TbMscL into lipid bilayers by dilution	72
4.3.2.7 Fluorescence Quenching of TbMscL by Acrylamide	72
4.3.2.8 Fluorescence Quenching of TbMscL by Iodide	72
4.3.2.9 Fluorescence Measurements	73
4.3.2.10 Statistical Analysis	73
4.4 Results	74
4.4.1 Functional Analysis of Trp-mutants of TbMscL	75
4.4.2 Fluorescence Emission Spectra for Trp Mutants of TbMscL	77
4.4.3 Polarity Profile of lipid-exposed residues in TbMscL	79
4.4.4 Fluorescence Quenching of TbMscL by brominated Phospholipids	82
4.4.5 Fluorescence Quenching of TbMscL by Acrylamide	84

4.4.6	Fluorescence Quenching of TbMscL by Iodide	86
4.5	Discussion	87
4.5.1	Effects of Trp mutants of TbMscL on channel function	87
4.5.2	Accessibility of Trp residues to acrylamide and iodide	95
4.5.3	Penetration of lipid chains into the surface of TbMscL	96
4.5.4	Conclusions	105
 Chapter Five - Fluorescence Properties of pore exposed residues on TM1		106
5.1	Introduction	106
5.2	Methods and Materials	108
5.2.1	Materials	108
5.2.2	Methods	108
5.3	Results	109
5.3.1	Functional Analysis of Trp-mutated TbMscL	109
5.3.2	Fluorescence Emission Spectra of Trp-mutated TbMscL	110
5.3.3	Fluorescence quenching of TbMscL by brominated phospholipids	113
5.3.4	Fluorescence quenching of TbMscL by acrylamide	114
5.3.5	Fluorescence quenching of TbMscL by Iodide	115
5.4	Discussion	116
5.4.1	Properties of pore lining Trp mutants of TbMscL	116
5.4.2	Accessibility of Trp residues from the lipid and aqueous phases.	118
5.4.3	Conclusions	119
 Chapter Six – Gain-of-function Mutants		120
6.1	Introduction	120
6.2	Methods and Materials	122
6.2.1	Materials	122
6.2.2	Methods	122

6.2.2.1	Small scale expression of TbMscL	122
6.2.2.2	Expression of TbMscL GOF mutants	123
6.2.2.3	Production of charge mutants of TbMscL	123
6.3	Results	124
6.3.1	Functional Analysis of Trp-mutated TbMscL	124
6.3.2	Fluorescence emission spectra of Trp-mutated TbMscL	126
6.3.3	Fluorescence quenching of TbMscL by brominated phospholipids	128
6.3.4	Fluorescence quenching of TbMscL by Acrylamide and Iodide	129
6.3.5	V21K mutants of TbMscL	130
6.4	Discussion	134

Chapter Seven - Effects of lipid headgroup and chain length on TbMscL

		140
7.1	Introduction	141
7.2	Methods and Materials	143
7.2.1	Materials	143
7.2.2	Methods	143
	7.2.2.1 Reconstitution into mixed lipid bilayers	144
	7.2.2.2 Reconstitution of Trp analogue into mixed bilayers	144
	7.2.2.3 Analysis of Fluorescence Measurements	144
7.3	Results	147
7.3.1	Effects of lipid chain length on emission maxima	147
7.3.2	Fluorescence Quenching of TbMscL by brominated phospholipids	149
7.3.3	Effects of lipid chain length on fluorescence quenching of TbMscL by acrylamide	151
7.3.4	Effects of lipid chain length on fluorescence quenching of TbMscL by Iodide	153
7.3.5	Fluorescence quenching of TbMscL as a function of	

lipid headgroup	155
7.3.6 Fluorescence quenching for Trp residues on the periplasmic side of TbMscL	169
7.3.7 Effects of lipid headgroup on fluorescence emission Maxima	176
7.4 Discussion	181
7.4.1 Effects of fatty acyl chain length	181
7.4.2 Effects of lipid headgroup	183
Chapter Eight – General Discussion	186
References	191

List of Figures

Chapter One-Introduction

1.1	Structure of Phospholipid Bilayer.	2
1.2	Classification of Membrane lipids	5
1.3	Lipid Headgroup Structures	6
1.4	Geometric Shapes of Lipids	8
1.5	Hexagonal Phase Lipids	9
1.6	Phase Transitions of Lipid Bilayers	10
1.7	Structure of a Bilayer	15
1.8	Structures of KscA and Rhodopsin	16
1.9	Structure of TbMscL	22
1.10	Representation of TbMscL Transmembrane Helices	23
1.11	Sequence Alignments of MscL Homologues	24
1.12	Helix-Helix Interactions between TM1 and Tm2 of TbMscL	25
1.13	Conformational Structures of TbMscL during Channel Gating	30

Chapter Three-Mutagenesis of TbMscL

3.1.1	Wild Type amino acid sequence of TbMscL	46
3.1.2	Nucleotide Sequence of TbMscL	47
3.1.3	TbMscL monomer showing α -carbons of residues mutated to Trp.	48
3.2.1	pET-19b vector map	49
3.2.2	Quik-change® site-directed Mutagenesis overview	53
3.3.1	Agarose gel of TbMscL Digests	55
3.3.2	Agarose gel of PCR products	56
3.3.3	Electroferragraph of V22W TbMscL	58
3.3.4	Electroferragraphs of TbMscL mutants	59
3.3.5	SDS-PAGE gel of F27W and V22W TbMscL	61

Chapter Four- Fluorescence Properties of Lipid Exposed mutants on TM1

4.1.1	Surface representation of TbMscL showing lipid facing residues	64
4.2.1	Structures of aromatic amino acids	65
4.2.2	Jablonski Diagram	66
4.2.3	Fluorescence emission spectra of Tryptophan	67
4.4.	Lipid-exposed surface of TbMscL	74
4.4.1	<i>In vivo</i> assay for gain-of-function mutants	76
4.4.2	Fluorescence emission spectra of lipid exposed Trp-mutants	78
4.4.3	TbMscL monomer showing α -carbons of lipid facing residues on TM1	80
4.4.4	Polarity profile of lipid facing residues on TM1 and TM2 of TbMscL	81
4.4.5	Fluorescence quenching of lipid facing residues on TM1 by brominated phospholipids	83
4.4.6	Stern-Volmer plots for quenching of the Trp fluorescence of TbMscL by acrylamide	84
4.4.7	Fluorescence quenching of lipid facing residues on TM1 by iodide	86
4.5.1	Surface representation of TbMscL	88
4.5.2	Dielectric profile of a bilayer	90
4.5.3	Dependence of fluorescence emission maxima on position within a bilayer.	93
4.5.4	Fits of fluorescence emission maxima for Trp residues in TM1 and TM2 of TbMscL	94
4.5.5	Fluorescence quenching of TbMscL by iodide	96
4.5.6	Quenching of Trp fluorescence in TbMscL by di(Br ₂ C18:0)PC	98
4.5.7	Molecular modeling of PE onto surface of TbMscL at A20W	100
4.5.8	Diagram of the location of TbMscL in a bilayer of di(C18:1)PC	101
4.5.9	Parameters required to calculate expected efficiencies of quenching	102
4.5.10	Minimum Trp to Br distance	103
4.5.11	van der Waals contact of hexane and PE with I23W and F34W	104

Chapter Five- Fluorescence Properties of pore exposed residues on TM1

5.1	View of TbMscL showing pore lining residues chosen for Trp substitution in TM1 in CPK format	107
5.3.1	<i>In Vivo</i> assay for Gain of Function mutants	110
5.3.2	Fluorescence emission spectra of pore exposed Trp-mutants of MscL	112
5.3.3	Fluorescence quenching of pore lining residues on TM1 by KI	115
5.4.1	The inside surface of the MscL pentamer	117

Chapter Six- Gain-of-function mutants

6.3.1	<i>In Vivo</i> assay for Gain of Function mutants	125
6.3.2	Fluorescence emission spectra of pore exposed GOF Trp-mutants of TbMscL	127
6.3.3	<i>In Vivo</i> assay for V21K Gain of Function mutants	132
6.3.4	Effects of gadolinium on expression of TbMscL	133
6.4.1	representation of TbMscL showing contacts between Gly-24 and Val-22 on neighbouring TM1 helices	138

Chapter Seven- Effects of lipid headgroup and chain length on TbMscL

7.1.1	Ribbon diagram of EcoMscL showing predicted positions of TM1 helices in the closed-intermediate state and the open state.	142
7.2.1	showing lipid binding sites on the transmembrane surface of a membrane protein	146
7.3.1	Quenching of Trp fluorescence by brominated phospholipids	150
7.3.2	Quenching of Trp fluorescence by acrylamide	152
7.3.3	Quenching of Trp fluorescence by iodide	154
7.3.4	The structure of TbMscL	156
7.3.5	Effect of n , the number of lipid binding sites on a protein from which a bound BrPC molecule can quench the fluorescence of a given Trp residue in a protein.	157
7.3.6	Effect of K on the level of fluorescence quenching of a Trp residue	158

7.3.7	Quenching of Trp fluorescence of I23W and F27W by brominated phospholipids	160
7.3.8	Fluorescence quenching of I23W and F27W in mixtures of zwitterionic phospholipids	164
7.3.9	Fluorescence quenching of I23W and F27W in mixtures of anionic phospholipids PC and PA	165
7.3.10	Fluorescence quenching of I23W and F27W in mixtures of anionic phospholipids PC and PS	166
7.3.11	Fluorescence quenching of I23W and F27W in mixtures of anionic phospholipids PC and PG	167
7.3.12	Fluorescence quenching of I23W and F27W in mixtures of anionic phospholipids. PC and PG	168
7.3.13	The structure of TbMscL	170
7.3.14	Quenching of Trp fluorescence of L30W and F34W by brominated phospholipids	171
7.3.15	Fluorescence quenching of L30W and F34W in mixtures of phosphatidic acid and and phosphatidylcholine	175
7.3.16	Relative fluorescence intensity for Trp mutants of TbMscL as a function of phospholipid headgroup	178
7.3.17	Effect of PA on fluorescence intensity of the Trp analogue NPTH (N-palmitoyl-Trp-hexyl)	179
7.3.18	Effect of PS on fluorescence intensity of the Trp analogue NPTH (N-palmitoyl-Trp-hexyl).	180

List of Tables

3.2.1	Oligonucleotides designed to generate lipid exposed tryptophan mutants of TbMscL.	50
3.2.2	Oligonucleotides designed to generate pore lining tryptophans mutants of TbMscL.	51
3.2.3	Oligonucleotides designed to generate open channel tryptophans mutants of TbMscL	51
4.4.1	Fluorescence properties of lipid-exposed Trp-mutants of TbMscL	78
4.4.2	Positions of lipid facing residues on TM1 and TM2 of TbMscL	81
4.4.3	Quenching of Trp fluorescence by brominated phospholipids	82
4.4.4	Quenching of Trp fluorescence by brominated acrylamide	85
4.5.1	Calculated parameters obtained by fitting values of wavelengths for maximum fluorescence for lipid-exposed residues on the periplasmic and cytoplasmic sides of TbMscL	92
4.5.2	Quenching data for Trp mutants in TM2	102
4.5.3	Distances of Trp residues from a lipid molecule docked onto the surface of TbMscL	104
5.3.1	Fluorescence emission maxima for pore-exposed Trp-mutants of TbMscL	112
5.3.2	Quenching of Trp fluorescence by brominated phospholipids	113
5.3.3	Fluorescence quenching of pore facing residues on TM1 by Acrylamide	114
6.3.1	Fluorescence emission maxima for pore-exposed GOF Trp-mutants of TbMscL	127
6.3.2	Quenching of Trp fluorescence by brominated phospholipids	128
6.3.3	Fluorescence quenching of pore facing GOF mutants on TM1 by the aqueous quenchers acrylamide and iodide	129
6.4.1	Fluorescence quenching by brominated phospholipids for lipid-exposed residues and GOF mutants at equivalent depths in the bilayer	135

7.3.1	Effects of changing lipid chain length on emission maxima	148
7.3.2	Positions of the <i>cis</i> double bond in phosphatidylcholines of different chain lengths	151
7.3.3	Fluorescence quenching of I23W and F27W in brominated phospholipids as a function of lipid headgroup	161
7.3.4	Relative lipid binding constants of TbMscL mutants as a function of lipid head group	163
7.3.5	Fluorescence quenching of L30W and F34W in brominated phospholipids as a function of lipid headgroup	172
7.3.6	Relative lipid binding constants of TbMscL mutants on the cytoplasmic and periplasmic sides of TbMscL as a function of lipid head group	174
7.3.7	Effects of changing lipid headgroup on emission maxima	177

Acknowledgements

Firstly I would like to thank my supervisor Professor Tony Lee for all his help and support throughout my PhD, and for being an excellent boss to work for. Without his excellent supervision and willingness to sit for hours explaining the intricacies of biological membranes, I would not have been able to do it.

Thank you to Raj Gill, Alun Coker, and Simon Kolstoe for help with molecular modelling. Thank you to all the people who help in many other ways to keep the ball rolling (Lorraine, William, Malcom, Ray, Diane,).

A large chunk of thanks goes to my lab buddies in 4061, past and present, and anyone else who helped to corrupt my innocent little self!!! Special thanks go to Sanj, John (likewise-it has been a pleasure having you behind me for so long!) Nicki, Phedra, Andy, Jeab, Vicki and Jane. Thank you for being there for me for chats and for making my three years so damn funny and enjoyable. I will never have lab mates quite like it, of that I am certain and I am sure I will never laugh so much on such a constant basis. Thanks also to the rest of the bunch that started with me-again, some very good chuckles along the way (Glasgow sticks in my mind for some reason-Charlie!)

Thank you to Jo for talking me through the hard times and spurring me on. Thanks to Ian, Karen, Clare, Sue, Valerie, Ray, Stuart and various other people for keeping me going and providing other conversation that didn't revolve around science!

Thank you to my family for their support and words of encouragement over the last three years. I have tried to explain but now you can read my thesis!

Anyone I may have forgotten, you know who you are. Thank you.

I would like to dedicate this thesis to the memory of my mum.

1
2
3
4
5
6
7
8
9
10
11
12
13
14
15
16
17
18
19
20
21
22
23
24
25
26
27
28
29
30
31
32
33
34
35
36
37
38
39
40
41
42
43
44
45
46
47
48
49
50
51
52
53
54
55
56
57
58
59
60
61
62
63
64
65
66
67
68
69
70
71
72
73
74
75
76
77
78
79
80
81
82
83
84
85
86
87
88
89
90
91
92
93
94
95
96
97
98
99
100
101
102
103
104
105
106
107
108
109
110
111
112
113
114
115
116
117
118
119
120
121
122
123
124
125
126
127
128
129
130
131
132
133
134
135
136
137
138
139
140
141
142
143
144
145
146
147
148
149
150
151
152
153
154
155
156
157
158
159
160
161
162
163
164
165
166
167
168
169
170
171
172
173
174
175
176
177
178
179
180
181
182
183
184
185
186
187
188
189
190
191
192
193
194
195
196
197
198
199
200
201
202
203
204
205
206
207
208
209
210
211
212
213
214
215
216
217
218
219
220
221
222
223
224
225
226
227
228
229
230
231
232
233
234
235
236
237
238
239
240
241
242
243
244
245
246
247
248
249
250
251
252
253
254
255
256
257
258
259
260
261
262
263
264
265
266
267
268
269
270
271
272
273
274
275
276
277
278
279
280
281
282
283
284
285
286
287
288
289
290
291
292
293
294
295
296
297
298
299
300
301
302
303
304
305
306
307
308
309
310
311
312
313
314
315
316
317
318
319
320
321
322
323
324
325
326
327
328
329
330
331
332
333
334
335
336
337
338
339
340
341
342
343
344
345
346
347
348
349
350
351
352
353
354
355
356
357
358
359
360
361
362
363
364
365
366
367
368
369
370
371
372
373
374
375
376
377
378
379
380
381
382
383
384
385
386
387
388
389
390
391
392
393
394
395
396
397
398
399
400
401
402
403
404
405
406
407
408
409
410
411
412
413
414
415
416
417
418
419
420
421
422
423
424
425
426
427
428
429
430
431
432
433
434
435
436
437
438
439
440
441
442
443
444
445
446
447
448
449
450
451
452
453
454
455
456
457
458
459
460
461
462
463
464
465
466
467
468
469
470
471
472
473
474
475
476
477
478
479
480
481
482
483
484
485
486
487
488
489
490
491
492
493
494
495
496
497
498
499
500
501
502
503
504
505
506
507
508
509
510
511
512
513
514
515
516
517
518
519
520
521
522
523
524
525
526
527
528
529
530
531
532
533
534
535
536
537
538
539
540
541
542
543
544
545
546
547
548
549
550
551
552
553
554
555
556
557
558
559
560
561
562
563
564
565
566
567
568
569
570
571
572
573
574
575
576
577
578
579
580
581
582
583
584
585
586
587
588
589
590
591
592
593
594
595
596
597
598
599
600
601
602
603
604
605
606
607
608
609
610
611
612
613
614
615
616
617
618
619
620
621
622
623
624
625
626
627
628
629
630
631
632
633
634
635
636
637
638
639
640
641
642
643
644
645
646
647
648
649
650
651
652
653
654
655
656
657
658
659
660
661
662
663
664
665
666
667
668
669
670
671
672
673
674
675
676
677
678
679
680
681
682
683
684
685
686
687
688
689
690
691
692
693
694
695
696
697
698
699
700
701
702
703
704
705
706
707
708
709
710
711
712
713
714
715
716
717
718
719
720
721
722
723
724
725
726
727
728
729
730
731
732
733
734
735
736
737
738
739
740
741
742
743
744
745
746
747
748
749
750
751
752
753
754
755
756
757
758
759
760
761
762
763
764
765
766
767
768
769
770
771
772
773
774
775
776
777
778
779
780
781
782
783
784
785
786
787
788
789
790
791
792
793
794
795
796
797
798
799
800
801
802
803
804
805
806
807
808
809
810
811
812
813
814
815
816
817
818
819
820
821
822
823
824
825
826
827
828
829
830
831
832
833
834
835
836
837
838
839
840
841
842
843
844
845
846
847
848
849
850
851
852
853
854
855
856
857
858
859
860
861
862
863
864
865
866
867
868
869
870
871
872
873
874
875
876
877
878
879
880
881
882
883
884
885
886
887
888
889
890
891
892
893
894
895
896
897
898
899
900
901
902
903
904
905
906
907
908
909
910
911
912
913
914
915
916
917
918
919
920
921
922
923
924
925
926
927
928
929
930
931
932
933
934
935
936
937
938
939
940
941
942
943
944
945
946
947
948
949
950
951
952
953
954
955
956
957
958
959
960
961
962
963
964
965
966
967
968
969
970
971
972
973
974
975
976
977
978
979
980
981
982
983
984
985
986
987
988
989
990
991
992
993
994
995
996
997
998
999
1000

Abbreviations

APS	Ammonium persulphate
bp	base pair
CMC	Critical micelle concentration
di(C14:1)PC	dimyristoleoylphosphatidylcholine
di(C18:1)PA	dioleoylphosphatidic acid
di(C18:1)PC	dioleoylphosphatidylcholine
di(C18:1)PE	dioleoylphosphatidylethanolamine
di(C18:1)PG	dioleoylphosphatidylglycerol
di(C18:1)PS	dioleoylphosphatidylserine
di(C22:1)PC	dierucoylphosphatidylcholine
Eco	<i>E. coli</i>
EGTA	Ethyleneglycol-bis(β -aminoethylether)-N,N,N',N-tetraacetic acid
HEPES	N-(2-hydroxyethyl)piperazine-N'-(2-ethanesulphonic acid)
IPTG	Isopropyl- β ,D-thiogalactopyranoside
Kb	Kilobase
kDa	Kilo Dalton
MscL	Mechanosensitive channel of large conductance
OG	<i>n</i> -Octyl β -D-glucopyranoside
PA	Phosphatidic acid
PAGE	Polyacrylamide gel electrophoresis
PBS	Phosphate Buffered Saline
PC	Phosphatidylcholine
PCR	Polymerase chain reaction
PE	Phosphatidylethanolamine
PG	Phosphatidylglycerol
PS	Phosphatidylserine
SDS	Sodium dodecyl sulphate
TAE	Tris-acetate ethylenediamine tetraacetic acid
TEMED	N,N,N',N'-Tetramethylethylenediamine

Tb *Mycobacterium tuberculosis*
 TM Transmembrane
 Tris Tris(hydroxymethyl)aminomethane
 Trp Tryptophan
 Tyr Tyrosine

Chapter 1 – General Introduction

1.1 Biological Membranes

Biological membranes are physical barriers that fulfil vital functions as interfaces to the outside world, between cells, and as boundaries of intracellular compartments (Werten *et al.*, 2002). The main components of biological membranes are lipids and proteins. Because of their amphipathic nature, lipids in membranes are arranged as bilayers, forming a hydrophobic core consisting of the fatty acyl chains from each monolayer and a hydrophilic surface consisting of the lipid headgroups interacting with the aqueous phase on both sides of the membrane. Interspersed within the bilayer lipids are numerous membrane proteins, the weight ratio of lipid to protein varying from 1:4 to 4:1 (Stryer, 1996).

Membrane proteins carry out many basic cellular processes including respiration, photosynthesis, signal transduction and motility (Palsdottir and Hunte, 2004). Integral membrane proteins also play a pivotal role in the communication of cells with their environment (Bever *et al.*, 1999). Primary examples of such proteins are surface adhesion proteins such as integrins and cadherins which form binding sites on membranes for extracellular proteins or homophilic attachments with other cells respectively (Nelson and Cox, 2005).

Lipid bilayers exhibit selective permeability, allowing the rapid diffusion of small non-polar molecules such as O₂ and CO₂ and the slower diffusion of small uncharged polar molecules such as water and urea (Alberts *et al.*, 2002). Lipid bilayers are highly impermeable to charged molecules due to the hydrophobic nature of the hydrocarbon core of the bilayer. The movement of such molecules across the bilayer requires the presence of membrane proteins such as transporters and channels.

The specific function of a cell membrane has been suggested to be modulated by a variety of physical properties, including membrane fluidity, bilayer thickness, interfacial polarity, charge, and curvature strain (Epan, 1998). The structure of a lipid bilayer with the different classes of associated proteins is shown in Figure 1.1.

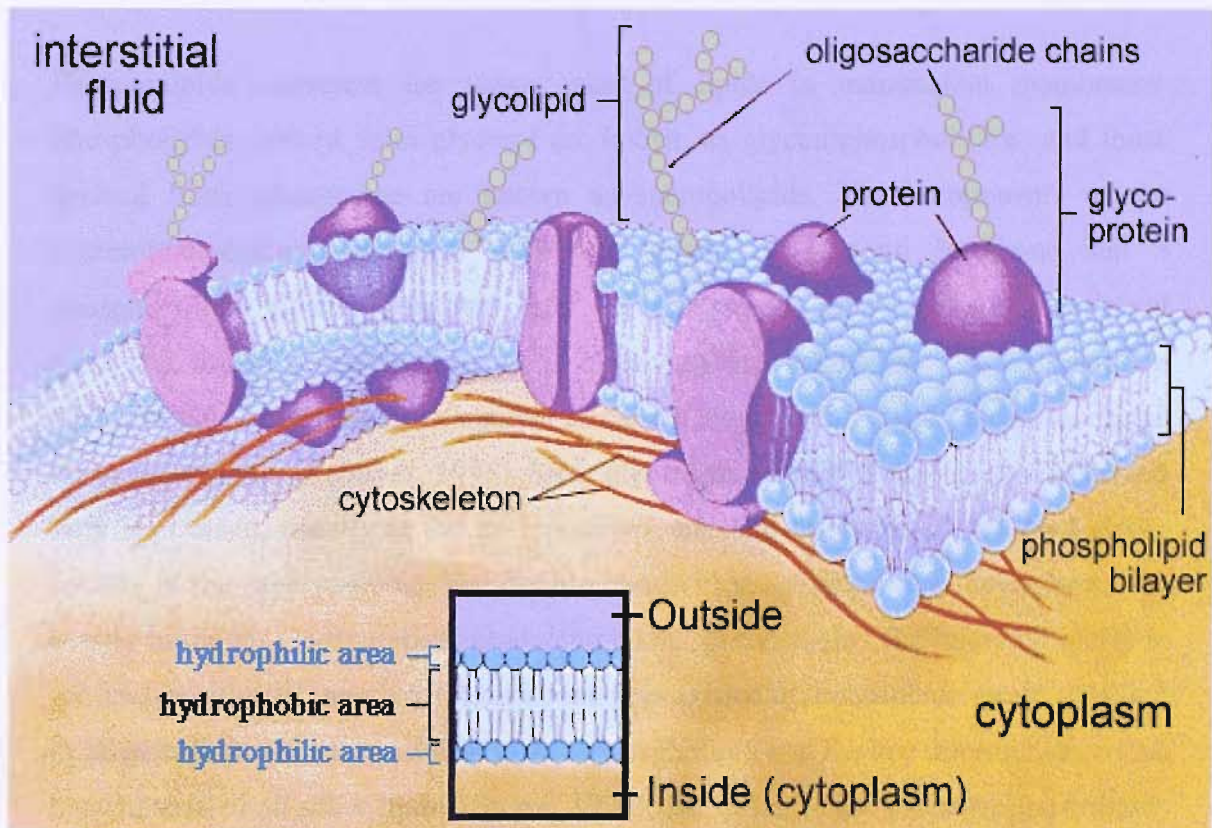


Figure 1.1 Structure of a phospholipid bilayer. Lipid headgroups are represented by blue circles and membrane proteins are represented in purple. Inset shows how the hydrophobic and hydrophilic regions of the lipids arrange themselves in order to form a lipid bilayer and the main picture shows various peripheral and integral membrane proteins and glycolipids associated with the bilayer (taken from www.bergen.org).

1.2 Lipids

Lipids are amphipathic water-insoluble molecules that can be readily dissolved in organic solvents such as chloroform and methanol. Lipids have several biological roles aside from providing structural integrity, serving as fuel molecules, as energy stores and as signalling molecules. Lipids can be classified as phospholipids, glycolipids and sterols. The basic structures of the main classes of lipid are shown in Figure 1.2.

1.2.1 Phospholipids

Phospholipids constitute the major class of lipids in mammalian membranes. Phospholipids derived from glycerol are known as glycerophospholipids, and those derived from sphingosine are known as sphingolipids. The components of the glycerophospholipids are two fatty acyl chains, a glycerol backbone and a phosphorylated alcohol. The two fatty acyl chains are esterified to the hydroxyl groups at the *sn*-1 and *sn*-2 positions of the glycerol backbone. The hydrocarbon chains usually contain an even number of carbon atoms with 16 and 18-carbon chains being most common (Stryer, 1996). Most glycerophospholipids contain one saturated fatty acyl chain, usually at the *sn*-1 position, and one unsaturated fatty acyl chain, usually at the *sn*-2 position. The double bonds in unsaturated fatty acyl chains are mostly in the *cis* configuration, producing a kink in the chain. The hydroxyl group at the *sn*-3 position of the glycerol backbone is esterified to a phosphate group resulting in phosphatidic acid, the simplest glycerophospholipid and the key intermediate in the biosynthesis of all other lipids (Stryer, 1996). All of the major glycerophospholipids are derived from phosphatidic acid via esterification of the phosphate group to the hydroxyl group of one of several alcohols. These are serine, ethanolamine, choline, glycerol and inositol, as shown in Figure 1.3. In the sphingomyelins the glycerol backbone is replaced by sphingosine, a long unsaturated hydrocarbon chain attached via its amino group to one fatty acyl chain. In sphingomyelin the headgroup is a phosphoryl choline group.

1.2.2 Glycolipids

Glycolipids are sugar-containing lipids that are found in the outer leaflet of the lipid bilayer although they may also be found in some intracellular membranes (Alberts *et al.*, 2002). Glycosphingolipids contain a sphingosine backbone, like sphingomyelin, but in this class of lipids, instead of being esterified to a phosphoryl choline headgroup, one or more sugars are attached to the primary hydroxyl group of the sphingosine backbone via a β -glycosidic bond forming a glycosphingolipid. Sphingolipids are found in the outer leaflet of the membrane and tend to interact with

cholesterol to form separate micro-domains in the bilayer known as lipid rafts. Lipid rafts are hard to solubilise with detergents at lower temperatures, making them relatively easy to isolate from the surrounding glycerophospholipids.

1.2.3 Sterols

The structure of cholesterol is shown in Figure 1.2. It is the most abundant example of the sterols found in many eukaryotic membranes. The structure of cholesterol is markedly different to that of the phospholipids and glycolipids in that the hydrophobic moiety is composed of four fused rings attached to an aliphatic carbon chain. The hydrophilic moiety is considerably smaller than that of phosphoglycerides, consisting of a single hydroxyl group, which orientates itself in a membrane close to the polar headgroups of the surrounding phospholipids. The rigid structure and the positioning of cholesterol in-between the phospholipid molecules decreases mobility and interaction between acyl chains and in most eukaryotic membranes, where the concentration of cholesterol is high, it serves to inhibit phospholipid phase transitions.

1.2.4 Prokaryotic Lipids

Whereas the membranes of most eukaryotic cells are composed of several types of glycerophospholipid, prokaryotic membranes are markedly different (Alberts, 2002). The plasma membrane contains predominantly one main type of glycerophospholipid, the most common lipids being phosphatidylethanolamine (PE), phosphatidylglycerol (PG), and cardiolipin, a four chain phosphoglyceride found only in the mitochondrial membranes in eukaryotes. Prokaryotes also contain a higher proportion of glycosphingolipids and phosphatidylinositol mannosides than eukaryotes and do not have cholesterol to maintain membrane fluidity like eukaryotic membranes, instead relying on the synthesis of short chain fatty acids and unsaturated lipid chains to increase fluidity when needed.

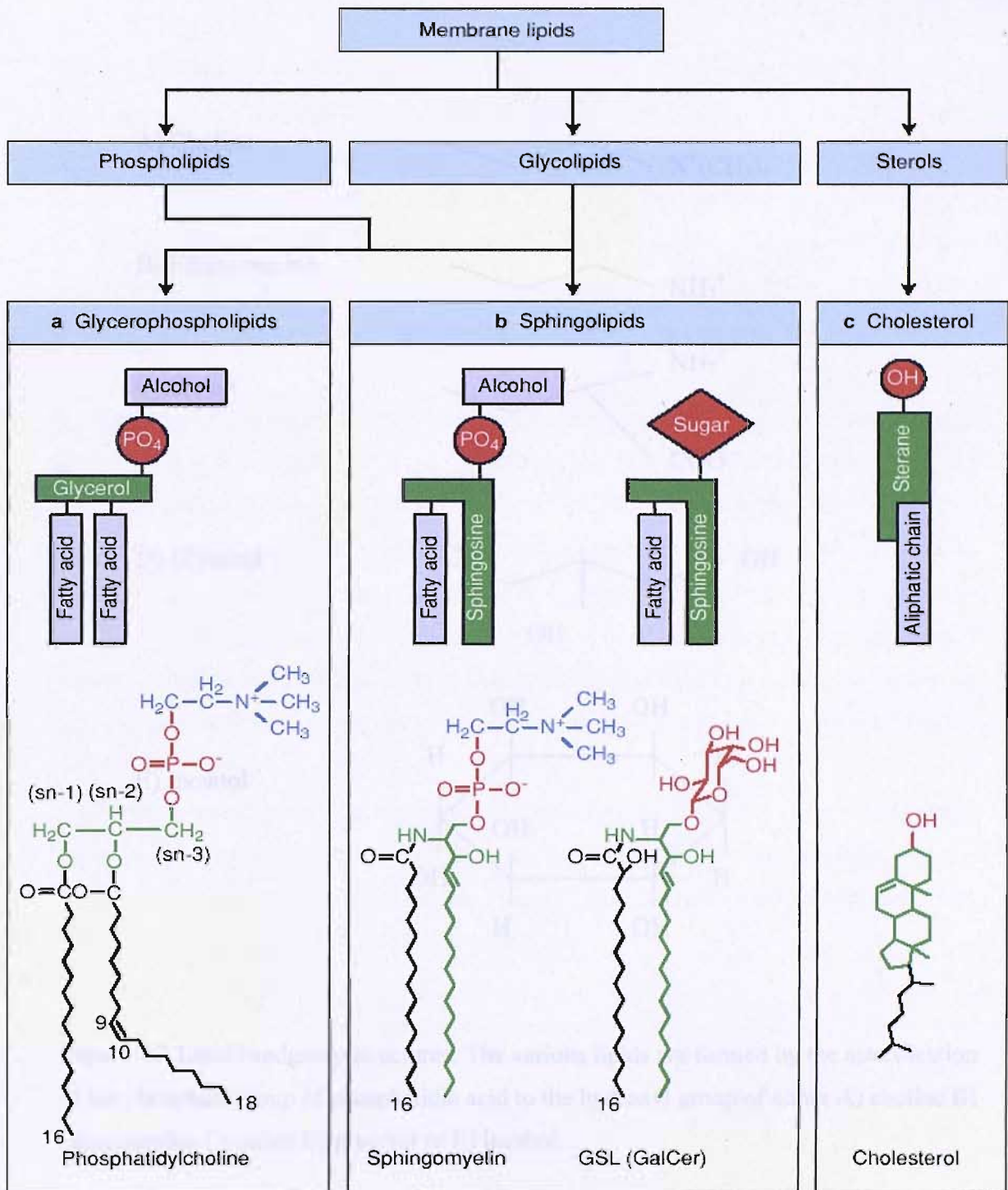


Figure 1.2 Structure-based classifications of membrane lipids representing a) glycerophospholipids, b) sphingolipids and c) the sterol cholesterol.

(Taken from www.expertreviews.com)

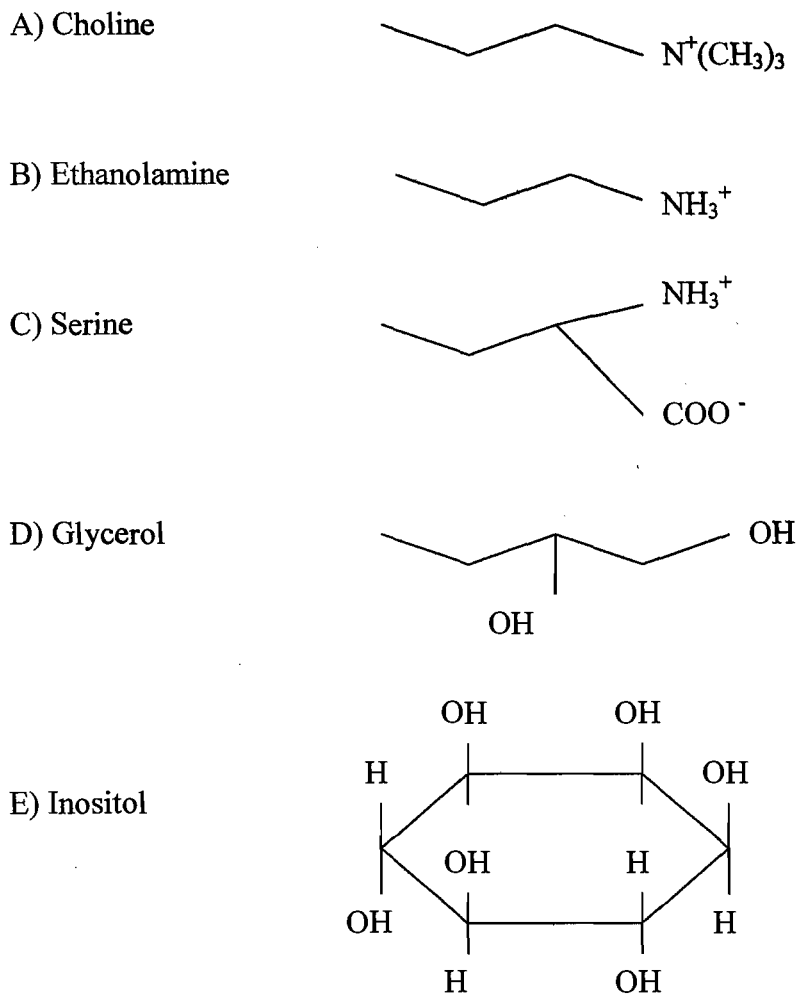


Figure 1.3 Lipid headgroup structures. The various lipids are formed by the esterification of the phosphate group of phosphatidic acid to the hydroxyl group of either A) choline B) ethanolamine C) serine D) glycerol or E) inositol.

1.3 Lipid Phases

When lipids are dispersed in water, they adopt a variety of different structures known as lipid phases. The spontaneous assembly of these phases is driven by the hydrophobic effect, sequestering the hydrophobic acyl chains away from the aqueous phase. Lipid phase is highly dependent on the properties of the lipid such as head group size, charge, hydrocarbon chain length and the solution the lipid is dispersed in although a bilayer arrangement is the dominant structural motif for membrane lipids. Other phases can be formed, of which the most important are the hexagonal and cubic phases (Lee, 2000).

Phospholipids such as phosphatidylcholine (PC) have a cylindrical shape, as shown in Figure 1.4, and therefore pack to form a bilayer. Phospholipids such as lysophosphatidylcholine (LPC) where the cross sectional area of the headgroup is greater than that of the acyl chains, form a micelle with the headgroups facing outwards towards the surrounding water molecules. Where the cross sectional area of the fatty acyl chains is greater than that of the headgroup, for example in phosphatidylethanolamine (PE), the structure formed is an hexagonal H_{II} phase with the hydrophilic moiety surrounding an aqueous pore with the acyl chains facing outward as shown in Figure 1.5 (Erand, 1998).

The most complex phases formed by non-bilayer forming lipids are cubic phases which exist as two main types: the micellar phase and the bicontinuous phase. In the bicontinuous phase (Figure 1.5) numerous aqueous channels interconnect with each other with a typical diameter of 50 Å (Erand, 1998).

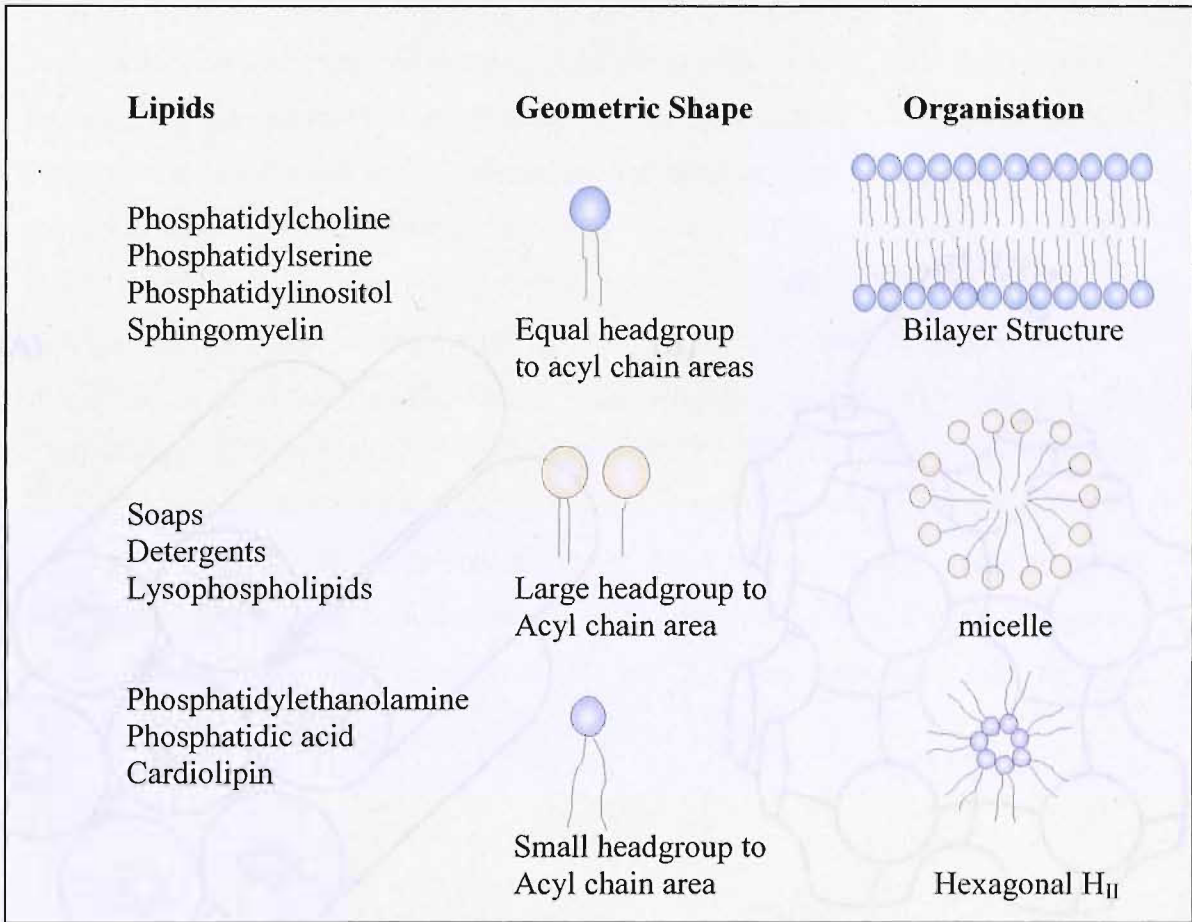


Figure 1.4 Cartoon illustration of the geometric shape of the different classes of lipids and the corresponding structures or phases adopted in aqueous solution. The phase formed depends on the physiochemical properties of the lipid and the solvent in which the lipid is dispersed.

1.4 Phase Transition of the Lipid Bilayer

At physiological temperatures the lipid bilayer components of biological membranes exist as fluid structures allowing rapid lateral movement of both heads and tails in the plane of the membrane. The fluidity of bilayer structure is dependent on many variables, temperature and length and saturation of the acyl chains. Studies of synthetic lipids have shown that different lipids have different phase transition temperatures between the liquid crystalline and gel states.

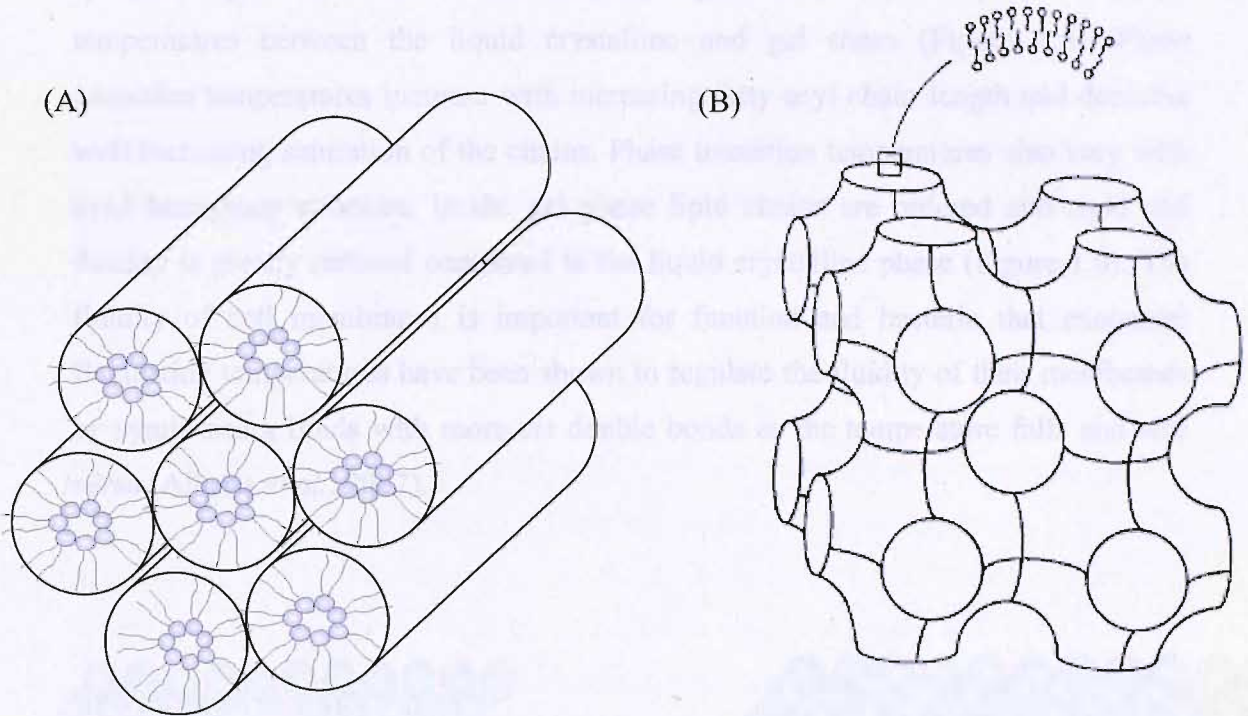


Figure 1.5 (A) Hexagonal H_{II} phase. Lipids with acyl chains that have a larger cross sectional area than the headgroup region arrange to form cylindrical structures with water trapped within the cylinders. (B) Bicontinuous cubic phase (Epan, 1998). Lipids are arranged in a continuous network with interconnecting aqueous channels where the water is able to exchange with the bulk aqueous phase.

Figure 1.4 illustrates the transition of a lipid bilayer. (A) A lipid bilayer in the liquid crystalline phase. The lipids are disordered and fluid. (B) A lipid bilayer in the gel phase with closely packed fatty acyl chains.

1.4 Phase Transition of the Lipid Bilayer

At physiological temperatures the lipid bilayer components of biological membranes exist as fluid structures allowing rapid lateral movement of both lipids and proteins in the plane of the membrane. The fluidity of bilayer structures is dependant on lipid composition, temperature and length and saturation of the fatty acyl chains. Studies of synthetic lipids have shown that different lipids have different phase transition temperatures between the liquid crystalline and gel states (Figure 1.6). Phase transition temperatures increase with increasing fatty acyl chain length and decrease with increasing saturation of the chains. Phase transition temperatures also vary with lipid headgroup structure. In the gel phase lipid chains are ordered and rigid and fluidity is greatly reduced compared to the liquid crystalline phase (Figure 1.6). The fluidity of cell membranes is important for function and bacteria that encounter fluctuating temperatures have been shown to regulate the fluidity of their membranes by synthesising lipids with more *cis* double bonds as the temperature falls and *vice versa* (Alberts *et al.*, 2002).

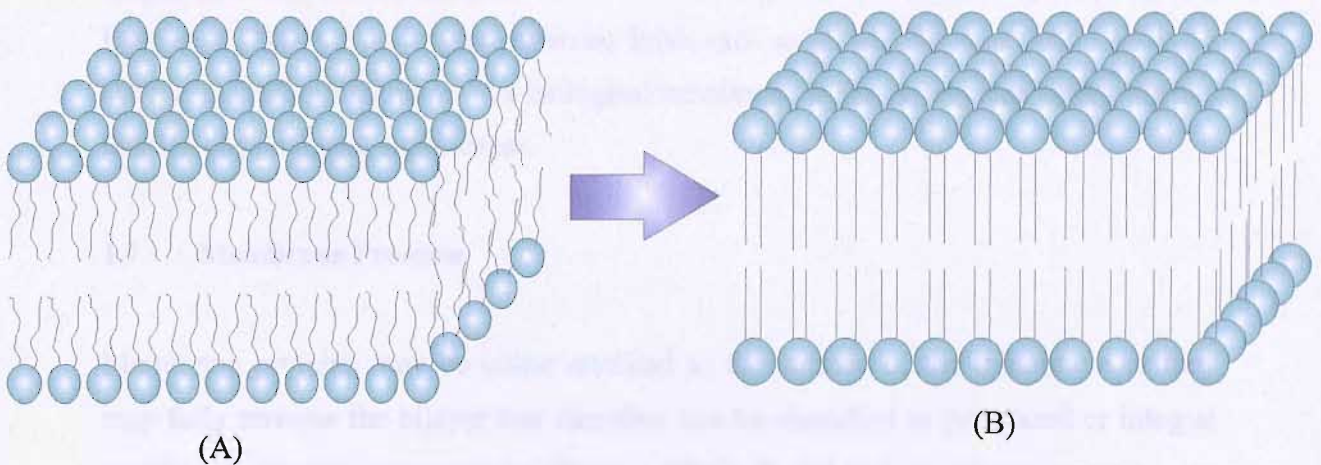


Figure 1.6 Cartoon diagram of a lipid bilayer. A) A lipid bilayer in the liquid crystalline phase. The lipids are disordered and fluid. B) A lipid bilayer in the gel phase with closely packed fatty acyl chains.

1.5 Lipid Composition

The various membranes of a eukaryotic cell differ markedly in their lipid compositions. For example, plasma membranes are enriched in sphingolipids, phosphatidylserine and cholesterol whereas the endoplasmic reticulum is depleted of these lipids (Pomorski *et al.*, 2001). In addition to differences between membranes, the distribution of lipids across a bilayer is asymmetric. In the plasma membrane the external leaflet contains predominantly glycosphingolipids and phosphatidylcholine whereas the cytoplasmic leaflet contains predominantly phosphatidylserine (PS) and phosphatidylethanolamine (PE) (Pomorski *et al.*, 2001). Anionic phospholipids such as phosphatidylserine and phosphatidic acid (PA) are thought to be involved in the membrane association of cytoplasmic proteins (Dowhan, 1997).

1.6 Lateral Pressure Profile

Nearly all cell membranes contain lipids that, when in isolation, adopt the hexagonal H_{II} phase at physiological temperatures. However, in the biological membrane these lipids are forced to adopt a bilayer structure by the presence of other lipid species that prefer a bilayer structure and by the presence of membrane proteins (Janes, 1996; Brink-van der Laan *et al.*, 2004). Non-bilayer preferring lipids such as PE are therefore said to exist in a state of curvature frustration in a biological membrane. It is not yet clear whether or not this has physiological significance.

1.7 Membrane Proteins

Membrane proteins may be either attached to the surface of the membrane or they may fully traverse the bilayer and therefore can be classified as peripheral or integral membrane proteins respectively (Stryer, 1996). Peripheral membrane proteins are attached to the membrane principally through charge or hydrophobic interactions, interacting either with integral membrane proteins or with the polar head groups of the lipids in the membrane. Many peripheral membrane proteins may be removed relatively easily with agents that disrupt ionic interactions.

Integral membrane proteins may be partially inserted in the bilayer or they may fully traverse the hydrophobic core of the bilayer. The resulting hydrophobic interactions between membrane lipids and membrane proteins make the removal of these proteins harder than peripheral proteins, requiring detergents to remove them from the membrane.

It is estimated that integral membrane proteins account for around 25-30% of all encoded proteins (Byrne and Iwata, 2002). The two structural motifs observed in the membrane spanning regions of integral membrane proteins are the α -helix and the β -pleated sheet, the former being the most predominant. The α -helix is a rod like structure with the main chain polypeptide backbone forming the inner core and the amino acid side chains extending outwards in a helical array. Formation and stabilisation of the α -helix is achieved through hydrogen bonding between a CO group and the NH groups of the fourth residue along in the structure.

The β -pleated sheet forms structures known as β -barrels. Proteins adopting this structure are usually found in the outer membranes of bacteria, chloroplasts, and mitochondria (Schulz, 2000) and are not as common as α -helical membrane proteins. All β -barrel proteins are anti-parallel and are held together by hydrogen bonding between peptide bonds in different strands (Alberts *et al.*, 2002). The number of β -strands in a β -barrel protein is always even with both the N and the C-termini on the periplasmic side of the membrane. In a manner similar to α -helical proteins aliphatic non-polar residues face the membrane interior and polar residues at every second position are sequestered in the inner pore of the β -barrel although some porins contain non-polar residues inside the β -barrel (Schulz, 2000).

1.8 Membrane Protein Topology

Membrane protein topology refers to the three-dimensional structure of the protein, the number of transmembrane segments, and how they orientate themselves in the membrane (Heijne, 1996). The thickness of the hydrophobic core of an average membrane is 30 Å and the length of an α -helix is 1.5 Å per residue therefore in order

for a transmembrane α -helix to span a bilayer more than 20 amino acids are needed and for β -sheets more than 10 amino acids are needed as the length of a β -sheet is 3.5 Å per residue (White and Wimley, 1999). For membrane proteins of unknown structure the use of hydropathy plots is a useful method for determining the topology of membrane proteins although knowing precisely where the ends of transmembrane helices are and how they interact with phospholipids is unclear.

1.9 Protein lipid interactions.

Membrane proteins and lipids must have co-evolved to allow membrane proteins to function in the environment which is provided by the lipid bilayer and to allow membrane proteins to be inserted into the bilayer without destroying it (Lee, 2003). As already discussed there are many interactions between phospholipids and proteins involved in maintaining a hydrophobic barrier between the inside and outside of the cell. Precisely how lipids interact with membrane proteins to ensure optimal functioning and where the lipid water interface is remains unclear as membrane proteins are normally crystallised in detergents and usually no lipids that are representative of the bulk phase are resolved in the x-ray structure of a membrane protein (Lee, 2003).

Under physiological conditions the lipid bilayer exists in a liquid-crystalline phase and is therefore highly fluid, making accurate predictions of how a protein sits in the bilayer even more difficult. Figure 1.7 shows the structure of a bilayer of phosphatidylcholine at 23°C and low hydration, as determined by x-ray crystallography. The positions of the peaks represent the locations of the various components of the lipid molecule and the width of the peak represents the degree of motion that each component is capable of. It can be seen that the acyl chains display the greatest motion and the glycerol backbone is the most rigid component.

Positive and negatively charged residues are often found at the extreme ends of transmembrane α -helices enabling ionic interactions between the protein and the lipids, further stabilising the protein within the lipid bilayer. Another feature of membrane proteins of known structure that allows us to predict how lipids interact with proteins is the presence of tryptophan and tyrosine residues at the lipid-water interface (Figure 1.8) (Lee, 2003). Due to the ability of these two amino acids to interact with both the aqueous and lipid phase, it is thought that they act as a 'floats' anchoring the protein to the membrane.

In a membrane, the integral membrane protein has to pack well with the lipid bilayer to prevent the formation of 'holes' at the protein-lipid interface which would prevent the lipid bilayer acting as a permeability barrier. Since the hydrophobic surface of a membrane protein is molecularly rough, lipid molecules in contact with the surface of a membrane protein would be expected to be disordered, with the chains distorted to pack closely with the protein surface. The presence of such disordered lipids was first detected using electron spin resonance (ESR) studying phospholipids with nitroxide spin labels at different positions on the acyl chains. Studies showed the presence of immobilised spin labelled lipids, corresponding to those lipids whose motion was impeded by interactions with the protein. (Lee, 2003) (Alberts *et al.*, 2002); these were referred to as boundary or annular lipids, to distinguish them from the lipids that make up the bulk of the lipid bilayer.

Lipid molecules have also been observed bound between transmembrane α -helices, either within a protein or at protein-protein interfaces in multi-subunit proteins, and have been termed non-annular lipid. The majority of non-annular lipids resolved in crystal structures are located between subunits of multi-subunit membrane proteins. One example of a membrane protein that contains non-annular lipids is the potassium channel KscA, where a phosphatidylglycerol (PG) lipid molecule is bound between transmembrane α -helices at monomer-monomer interfaces (Lee, 2004). These non-annular lipids are often required for activity of the membrane protein; they are therefore said to act as traditional co-factors (Lee, 2004).

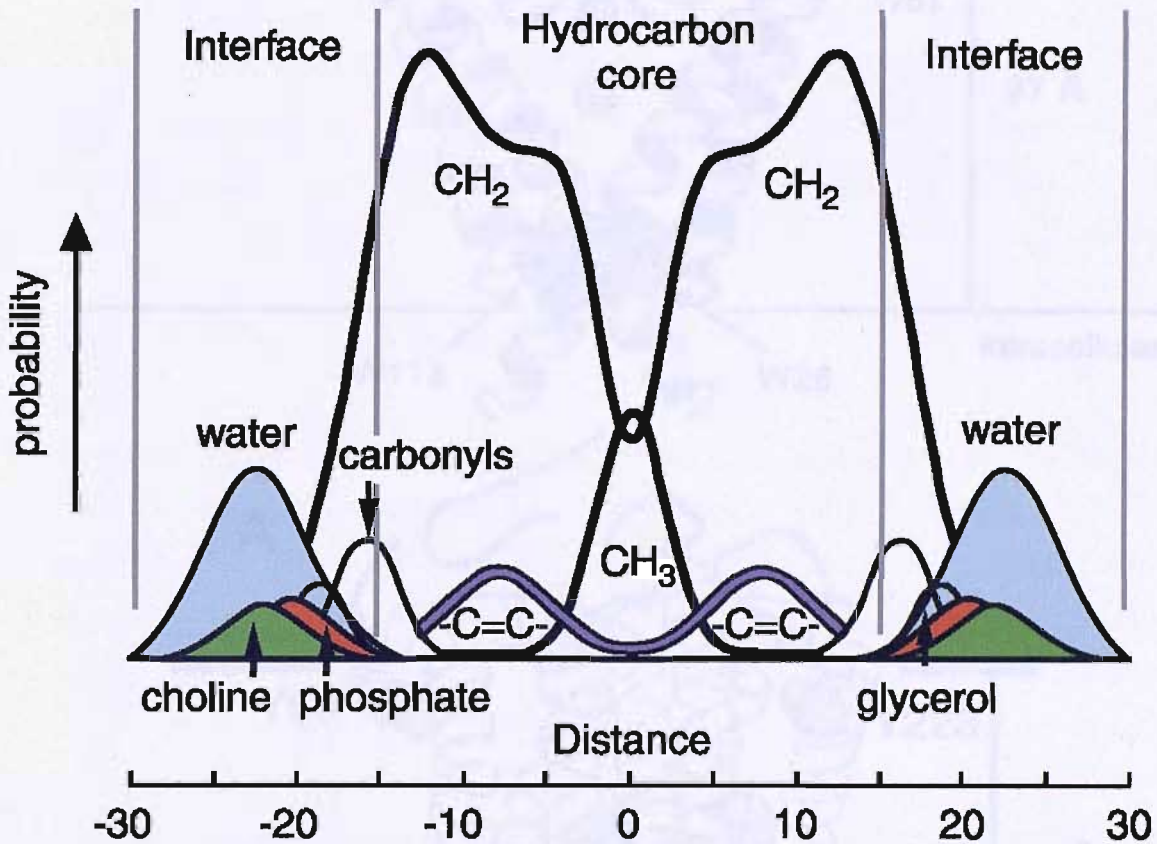


Figure 1.7 The structure of a bilayer of phosphatidylcholine at 23 °C and low hydration showing the projection onto the bilayer normal of each of the structural groups. The position of the peaks represents the position of each individual component. The width of the peak represents the degree of motion of each component. It can be seen that the hydrocarbon chains display the greatest degree of motional freedom and the glycerol backbone is the most rigid component of the bilayer. Vertical lines represent the hydrocarbon core (Lee, 2003).

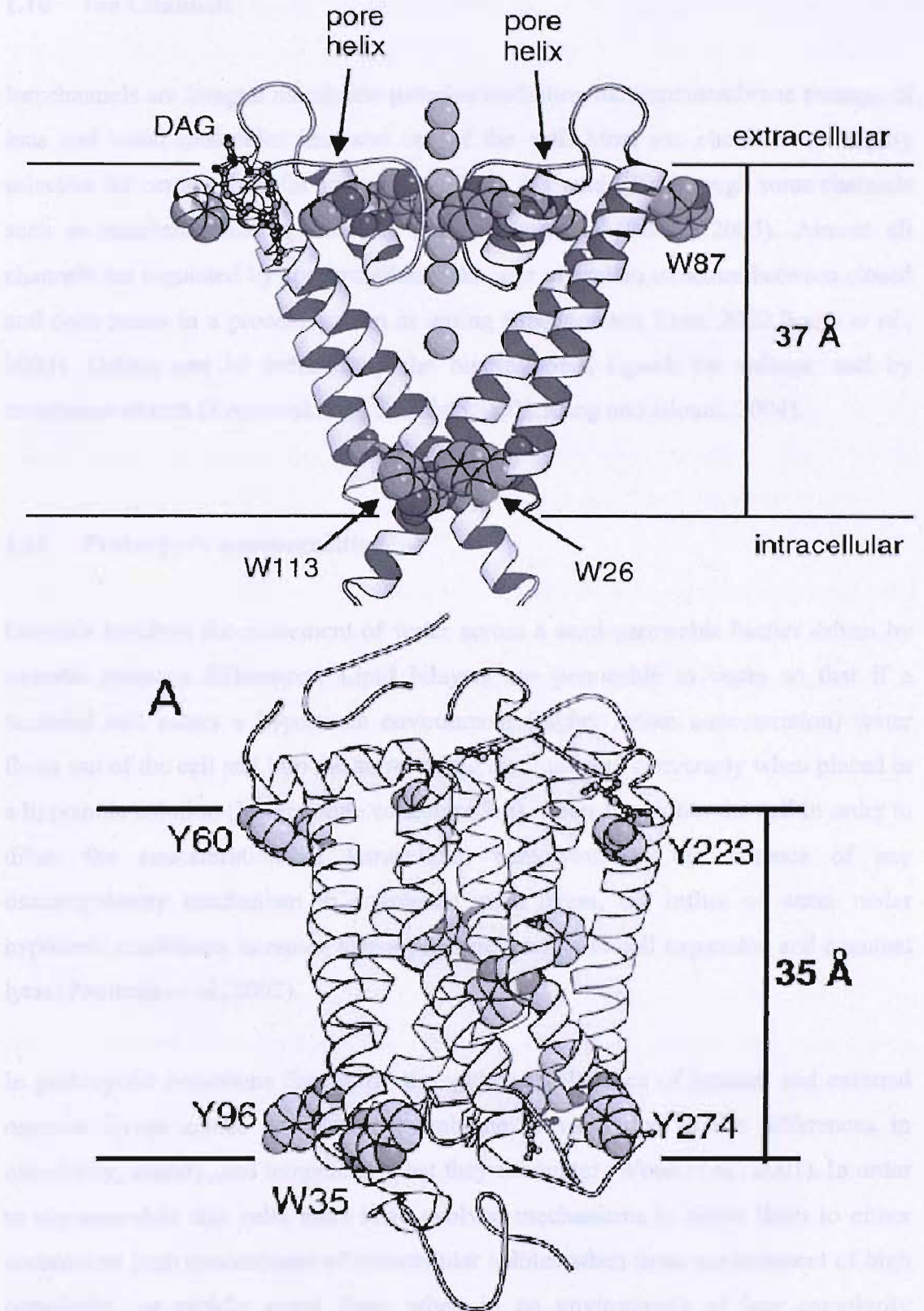


Figure 1.8 The structures of KcsA (top) and Rhodopsin (bottom) showing the position of aromatic residues at the ends of transmembrane helices (Lee, 2003). Tryptophan and tyrosine, shown in spacefill format, are thought to act as ‘floats’ capable of interacting with both the lipid and the aqueous phase.

1.10 Ion Channels

Ion channels are integral membrane proteins mediating the transmembrane passage of ions and small molecules into and out of the cell. Most ion channels are highly selective for certain ions, for example K^+ , Ca^{2+} , Na^+ and Cl^- , although some channels such as mechanosensitive channels are non-selective (Booth, 2005). Almost all channels are regulated by conformational changes of protein structure between closed and open states in a process known as gating (Spencer and Rees, 2002; Booth *et al.*, 2003). Gating can be induced by the binding of a ligand, by voltage, and by membrane stretch (Koprowski and Kubalski, 2001; Kung and Blount, 2004).

1.11 Prokaryotic osmoregulation

Osmosis involves the movement of water across a semi-permeable barrier driven by osmotic pressure differences. Lipid bilayers are permeable to water so that if a bacterial cell enters a hypertonic environment (higher solute concentration) water flows out of the cell and into the surrounding medium, and conversely when placed in a hypotonic solution (lower solute concentration), water flows into the cell in order to dilute the concentration of intracellular osmolytes. In the absence of any osmoregulatory mechanism to counteract such stress, the influx of water under hypotonic conditions increases turgor pressure leading to cell expansion and eventual lysis (Poolman *et al.*, 2002).

In prokaryotic organisms the ability to regulate the balance of internal and external osmotic forces across the plasma membrane is vital, due to the differences in osmolarity, salinity, and temperature that they encounter (Wood *et al.*, 2001). In order to accommodate this cells must have evolved mechanisms to allow them to either accumulate high concentrations of intracellular solutes when in an environment of high osmolarity, or rapidly expel them when in an environment of low osmolarity (Poolman *et al.*, 2002).

The internal solute concentration can be increased by either pumping inorganic ions into the cell from the surrounding environment or by direct synthesis or concentration

of organic solutes. Common osmoprotectants which bacteria may accumulate when the extracellular osmolarity rises differ between species although the zwitterionic osmoprotectants that are compatible with cell physiology (termed compatible solutes) are preferred as they are able to be accumulated within the cell to high molar concentrations without compromising macromolecular structure and function due to their high water solubility (Poolman *et al.*, 2002). Such osmoprotectants include the amino-acids glycine betaine, proline, and the proline derivative ectoine (Wood *et al.*, 2001), carbohydrates such as sucrose and trehalose, and alcohol-type solutes such as glycerol and mannitol (Madigan *et al.*, 2000). Glycine-betaine is the most widely distributed compatible solute amongst bacteria as replacement of protons on the amino group by three methyl groups produces a permanent positive charge on the nitrogen making this amino acid derivative highly soluble (Madigan *et al.*, 2000).

The concentration of compatible solutes within a cell is dependent on the extracellular solute concentration and different micro-organisms show diversity in the amounts of compatible solutes they are capable of accumulating, thus resulting in the various tolerance levels of micro-organisms for different ranges of water potential (Madigan *et al.*, 2000). For example, halophilic bacteria can inhabit salty environments, osmophiles can inhabit environments high in sugar, and xerophiles can grow in very dry environments (Madigan *et al.*, 2000).

In response to a decrease in external osmolarity, in addition to the expulsion of osmoprotectants, some cytoplasmic proteins including elongation factor Tu, thioredoxin, and DnaK have also been found to be excreted from *E. coli* cells (Ajouz *et al.*, 1998). The trigger which allows the rapid and unselective expulsion of intracellular solutes has been linked to specific physical changes in the cell bilayer—most importantly membrane stretch. As membrane proteins are embedded in, and surrounded by phospholipids, such deformations of the bilayer allow direct transduction of this signal into a mechanosensory response, a process known as mechanotransduction.

Mechanosensation mediates a variety of sensory functions encompassing both prokaryotes and eukaryotes, for examples touch and hearing in mammals. Mechanosensory responses have been found in more than 30 cell types including embryonic chick skeletal muscles and frog muscle and are ubiquitous amongst the bacterial kingdom (Moe *et al.*, 2000; Martinac, 2004). As well as providing a role as emergency release valves as a result of osmotic changes, mechanosensitive channels are also thought to act as sensors of turgor pressure to regulate cell division and cell growth as a slight outwardly directed turgor pressure of around 4 atm is required in order to for cell growth to occur (Wood *et al.*, 2001; Perozo and Rees, 2003).

Mechanosensitive (MS) channels were first detected following the observation that bacterial cells lacking these particular proteins lysed upon dilution into a hypo-osmotic medium. There are three classes of mechanosensitive channels found in prokaryotes and these can be distinguished by order of decreasing conductances. The smallest, MscM (mini conductance) is activated at low membrane tensions, followed by MscS (small conductance) and finally MscL which opens at membrane tensions close to the lytic limit of the bilayer, which for many bilayers is thought to be 8-12 dyne cm⁻¹ (Betanzos *et al.*, 2002) (Sukharev, 2000). MscS is also sensitive to changes in the transmembrane voltage (Martinac *et al.*, 1987; Biggin and Sansom, 1999). The conductances of MscM, MscS, and MscL are 100-200 pS, 1 nS and 3 nS respectively (Koprowski *et al.*, 2001); the tension sensitivities of the channels are thought to allow a graded response to osmotic pressure. The best studied of these MS channels is MscL, first identified, purified and cloned from *E. coli* in Kung's laboratory (Perozo *et al.*, 2003).

Prokaryotic mechanosensitive channels were first studied by patch clamp methods using giant *E. coli* spheroplasts (Perozo *et al.*, 2003) and were found to play a vital role in transducing physical stress into an electrochemical response (Chang *et al.*, 1998). Since the Mechanosensitive channel of large conductance (MscL) and its homologues are fully functional when reconstituted into lipid bilayers (Sukharev *et al.*, 1994), it is clear that their function does not require the association with cytoskeletal proteins, as in eukaryotic mechanosensitive channels.

1.12 TbMscL Structure

The structure of the mechanosensitive channel of large conductance isolated from *Mycobacterium tuberculosis* (TbMscL) has been solved by x-ray diffraction to a resolution of 3.5 Å (Chang *et al.*, 1998; Moe *et al.*, 2000). It is a homopentamer, each monomer containing 151, mostly hydrophobic, amino acids with an approximate mass of 18 kDa. It exhibits approximately 37% sequence homology to *E. coli* MscL (Chang *et al.*, 1998).

MscL is organised as a homopentamer with each monomer comprised of two transmembrane (TM) helices and one cytoplasmic helix (Figure 1.9). The channel structure can be divided into two distinct domains: the transmembrane spanning domain and the cytoplasmic domain. Both the N and the C termini are co-localised within the cytoplasm. The inner ring of TM1 helices run up through the centre of the channel and are tilted by approximately 30° with respect to the bilayer normal (Oakley *et al.*, 1999); (Chang *et al.*, 1998). This tilting results in an inverted ‘teepee’ shape with a hydrophobic constriction of around 3 Å at the cytoplasmic side formed by a ring of highly conserved valine residues and a further ring of highly conserved isoleucine residues (Figure 1.10). It is the TM1 helices that form the permeation pathway for solutes across the membrane as they are lined with several polar or charged residues (Thr-25, Thr-28, Thr-32, Lys-33). Linking the two TM helices is a periplasmic loop which forms the periplasmic face of the channel (Oakley *et al.*, 1999). The five TM2 helices form a peripheral skirt around the TM1 helices and run back down through the bilayer providing direct physical contact with the surrounding shell of phospholipids in the bilayer (Bilston and Mylvaganam, 2002).

The MscL channel is 85 Å in length. The transmembrane region is roughly 50 Å in length, including the head group regions on both sides of the membrane, and the cytoplasmic region is around 35 Å in length. The hydrophobic length of the transmembrane helices is thought to be around 25 Å which satisfies hydrophobic matching between the protein and the bilayer (Powl *et al.*, 2003).

Sequence alignments of some MscL homologues are shown in Figure 1.11. Higher sequence conservation can be seen in TM1 than TM2, with cytoplasmic S3 helices, shown in pink, also showing a good degree of sequence conservation. The highly conserved residues of the N-terminal S1 helical bundle can be seen between the S1 helices, shown in purple, and TM1 helices, further supporting their critical role in channel gating.

Analysis of helix-packing in membrane proteins shows that the most common packing angle is around 20° (Mall *et al.*, 2001; Lee, 2003) which would maximise the interfacial area between helices, as an angle of this degree gives almost parallel packing of helices. In MscL, however, each TM1 helix contacts 4 helices, two neighbouring TM1 helices and two TM2 helices, one from the same subunit with a crossing angle of 135° , and one from a neighbouring subunit, with a crossing angle of 169° . These steep packing angles minimise interfacial packing of helices which may help helix rearrangements during channel gating. The most extensive set of interactions occurs between TM1 and TM2 helices of adjacent subunits (Figure 1.12). The contact between TM1 and TM2 of the same subunit are less extensive (Sukharev *et al.*, 2001b). Packing of TM1 helices with each other is described as 4-4 ridges into grooves, a feature also observed in the potassium channel KcsA (LeMasurier *et al.*, 2001). During gating of the MscL channel, residues are thought to slide over each other to achieve the open state (Sukharev *et al.*, 2001b). Most of the residues on TM1 are hydrophobic therefore preventing the need to break hydrogen bonds during the gating process (Sukharev *et al.*, 2001b).

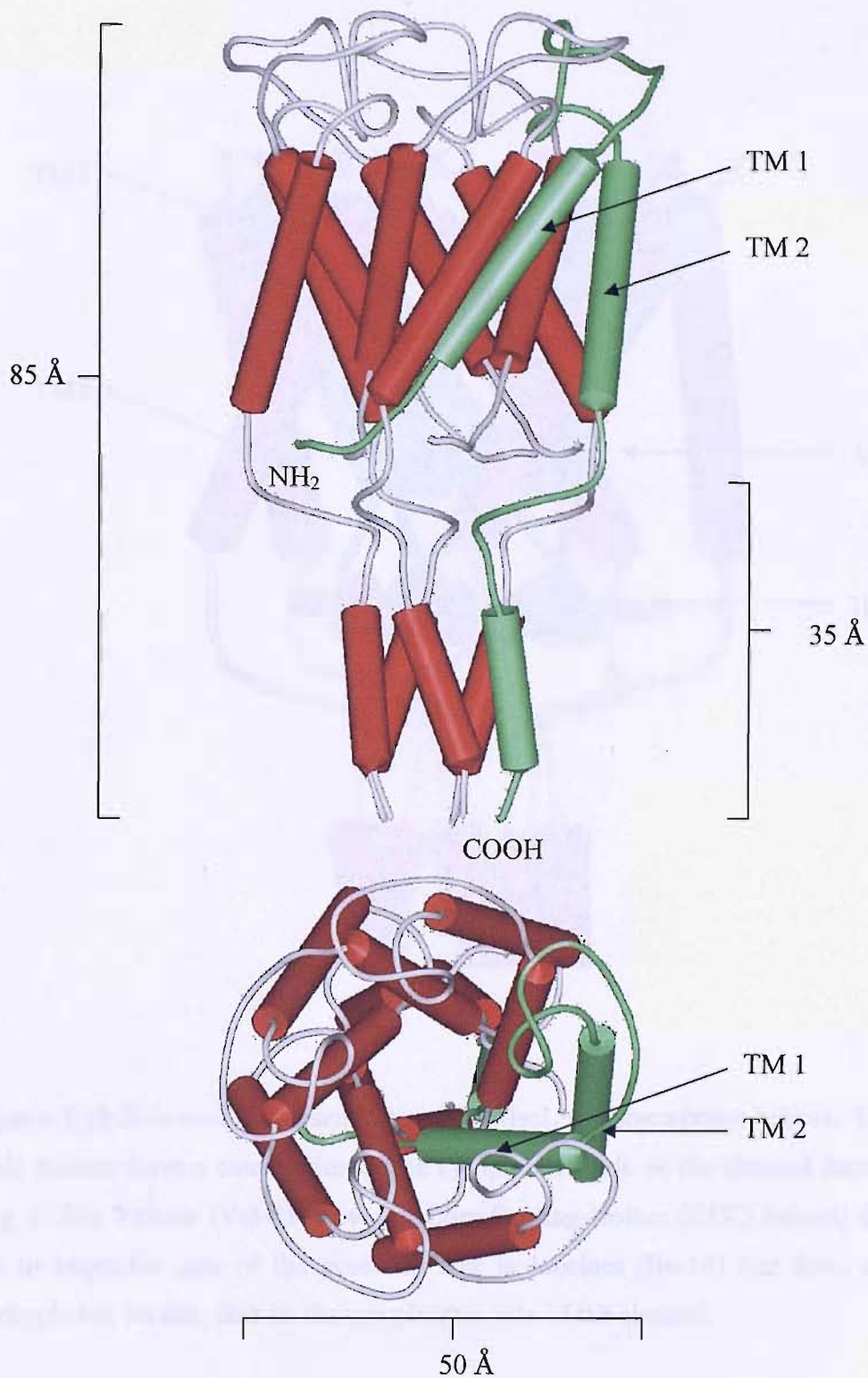


Figure 1.9 Structure of TbMscL. Transmembrane view (top) showing one monomer highlighted in green and periplasmic view (bottom) showing TM1 lining the permeation pathway and TM 2 forming a peripheral skirt around the TM1 helices.

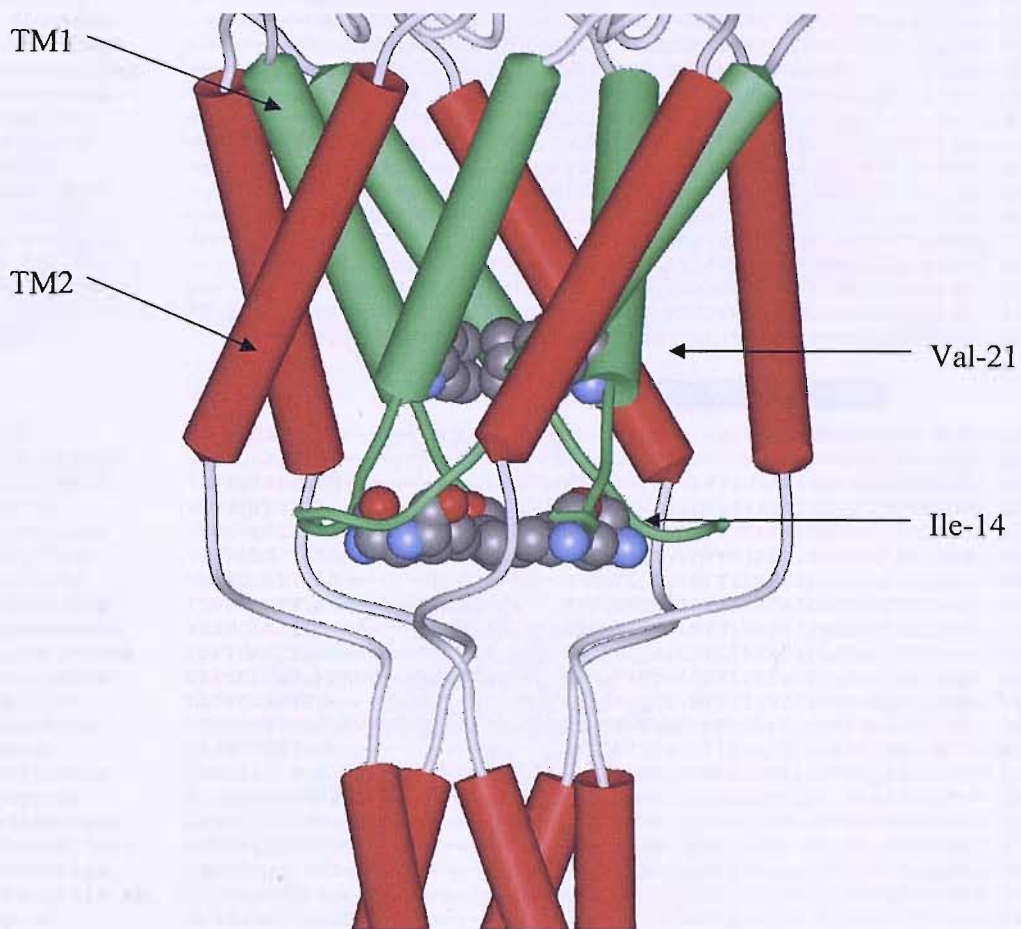





Figure 1.10 Schematic representation of TbMscL transmembrane helices. The inner TM1 helices form a constriction at the cytoplasmic side of the channel formed by a ring of five Valines (Val-21 shown in Cory-Pauling-Koltun (CPK) format) that form the hydrophobic gate of the pore and five isoleucines (Ile-14) that form a further hydrophobic barrier, also on the cytoplasmic side of the channel.

			
<i>E. coli</i>	-----MSI I KEFRE F AMRGNVVDLAVGVII GAAF GKIVSSLVADI IMPPLG-LLIGG-		51
<i>S. typhimurium</i>	-----MSFIKEFRE F AMRGNVVDLAVGVII GAAF GKIVSSLVADI IMPPLG-LLIGG-		51
<i>E. carotovora</i>	-----MSI I KEFRE F AMRGNVVDLAVGVII GALFGKIVSSLVSDI IMPPLG-LLIGG-		51
<i>Y. pestis</i>	-----MSFMKEFRE F AMRGNVVDLAVGVII GAAFGRIVSSLVADI IMPPLG-LLIGG-		51
<i>P. aeruginosa</i>	-----MGLLSEFKAF AVKGNVDMAVGII I GAAF GKIVSS FVGDVIMPPIG-LLIGG-		51
<i>P. multocida</i>	-----MSFVKEFRE F AMRGNVDMAVGVI I GGAF GKIVSSLVGDVIMPLG-ILTGG-		51
<i>V. cholerae</i>	-----MSLLKEFKAFAS RGNVIDMAVGII I GAAF GKIVSS FVADI IMPPIG-IILGG-		51
<i>H. influenzae</i>	-----MNF I KEFRE F AMRGNVDMAVGVI I GS AF GKIVSSLVSDI FTPLVIG-ILTGG-		51
<i>P. fluorescens</i>	-----MGLLSEFKAF AVKGNVDMAVGII I GAAF GKIVSS FVGDVIMPPIG-LLIGG-		51
<i>C. histolyticum</i>	-----MWKDFKE F AMRGNVVDLAVGVII GGAF GKIVTSLVNDVIMPLG-LILGG-		49
<i>C. crescentus</i>	-----MSVVKEFRE F IARGNVIDLAVGVII GAAFNGIVKSLVDQVIMPPIG-LLTGG-		51
<i>B. subtilis</i>	-----MWNEKFA F AMRGNIVDLAIGVVI GGAF GKIVTSLVNDI IMPLVG-LLLGG-		49
<i>B. japonicum</i>	-MSGVDEKGRRLK E FEFAMKGNVVDLAVGVII IRRAFGAI VTSLVGDVIMPLIG-AVTGG-		59
<i>S. aureus</i>	-----MLKEFKE F ALKGNVDLAIAVVMGA AFNKI ISSLVNDI IMPLIG-IFGG-		49
<i>C. perfringens</i>	-----MWKEFKE F AMKGNVIDLAIGVVI GGAF GKIVTSLVNDI IMPVVG-SLVGK-		49
<i>S. pyogenes</i>	-----MVKELKAF LFRGNII ELAVAVI GGAFGAI VTSFVNDI I TPLINLPALKA-		50
<i>D. radiodurans</i>	-----MLNGFRDF I LRGNVVDLAVGVVI GAAFNNVVA AFTKAFLDPLI-RLATGGH-		50
<i>M. tuberculosis</i>	-----MLKGFK EFLRGNVIDLAVAVVIGTAF TALVTKFTDSI I TPLINRIGVNAQ-		51
<i>S. pneumoniae</i>	-----MLKNLKS F LRGNVIDLAVGVVI ASAFGAI VTSFVNDI I TPLINRIGVNAQ-		50
<i>Synechocystis sp.</i>	MVKSARQ GAGGFWRDFKDF I LRGNVVDLAVAVVIGGAF TSIVNAFVAVLMAVLLQ-PVLDQ-		61
<i>M. leprae</i>	-----MFRGFKE FLSRGNIVDLAVAVVIGTAF TALIKFTDSI I TPLINRVGNVQ-		51

		
<i>E. coli</i>	IDFKQFAVTLRD-----A QGDIPAVVMHYGVFI QNVDFLIVAF AIFMAIKL INKLNK-	105
<i>S. typhimurium</i>	IDFKQFAVTLRE-----A QGDIPAVVMHYGVFI QNVDFVIVAF AIFVAIKL INRLNR-	105
<i>E. carotovora</i>	VDFKQFALFLRN-----A QGGIPAVVMNYGAFI QNIFDFI I VAF AIFIAIKL MNKMRCK-	105
<i>Y. pestis</i>	VDFKQFHFVLR A-----A EGTIPAVVMNYGT FFIQSIFDFVIVAL AIFS AVKLMNKL RRE-	105
<i>P. aeruginosa</i>	VDFSDLAITLKA-----A EGDVPAVVLAYGKFI QTVLDFVIVAF AIFMGVKAINRLKRE-	105
<i>P. multocida</i>	VDFKDL SIVLKE-----A AGEVPAVTLNYGAFI QTVDFV IIAFAIFLMIKALNKLKRE-	105
<i>V. cholerae</i>	VNFSDL SFLVLA-----A QGDAPAVVIA YGKFI QTVVDF TIIAFAIFMGLKAINSLKRR-	105
<i>H. influenzae</i>	IDFKDMKFVLAQ-----A QGDVPAVTLNYGLFI QNVDFI IIAFAIFMMIKVINKVRKP-	105
<i>P. fluorescens</i>	VDFSDLAITL K-----A EGDVPAVVLAYRKF I QTVLNFVIVAF AIFMGVKAINRLKRE-	104
<i>C. histolyticum</i>	INFSAKLT LHG-----I LNSEKPLTLNYGQFI QNILDFLI ISFSIFL FIRLINRFKRR-	102
<i>C. crescentus</i>	LDFSNLYINLSGQ QFNSLQEAQAAG AATINYLFLN LNINFLIIA FSI FIVIKQINKLNF-	110
<i>B. subtilis</i>	LDVSGLSFTFG-----D AVVKYGSFI QTVNFLI ISFSIFIVIR TLNGLRRK-	96
<i>B. japonicum</i>	LDFSNYFTPLSKAVTATNLADAKKQGA VLWGSF LTLTINFI IIAFVLFVIR AINTLKRK-	120
<i>S. aureus</i>	VDFAKESWFWG-----I KYGLFIQSVDFI IIAFALFI FVKIANTLMKK-	93
<i>C. perfringens</i>	VDFS NLYINLSGQQFNSLQEAQAAG AATINYLFLN LNINFLIIA FSI FIVIKQINKLNF-	110
<i>S. pyogenes</i>	ANVENITQLSWN-----G VKYGSF LGAVINFLI IGTSLFFVVKAAEKAMP--	95
<i>D. radiodurans</i>	GKVAGT-FAVNG-----I TFDWGT FVSTLINFL LTAAVLYFFVVM PMNAATE-	96
<i>M. tuberculosis</i>	SDVGI LRIGIGGG-----Q TIDLNVLLSAAINFFLI AFVYFLVLPYNTLRK-	97
<i>S. pneumoniae</i>	AKVERIAQLSWH-----G VYGNFLSALINFI FVGTALFFI IKGIEKAQKL-	96
<i>Synechocystis sp.</i>	AGVSQLQDLPLG-----L GELVIAIINFLI IAFVIFLI IKAIEKMQRK-	104
<i>M. leprae</i>	TNISPLRIDIGGD-----Q AIDLNIVLSAAINFL LIALVVYFLVLPYTTIRK-	99


		
<i>E. coli</i>	---K---EEPAAPAPTKEEVLLTEIRDLLKEQNNRS-----	136
<i>S. typhimurium</i>	---KA---EEPAAPPAPSKEEVLLGEIRDLLKEQNNRS-----	137
<i>E. carotovora</i>	---QE---DTPAAPPKPSAEKLLAEIRDLLKEQQT RQ-----	137
<i>Y. pestis</i>	---KA E---E E PATPPAPTTEE LLA EIRDL LKQAHTK-----	137
<i>P. aeruginosa</i>	---EA---VAPSEPPVPSAEETLLTEIRDLLKAQQNKS-----	137
<i>P. multocida</i>	---EPK---VEEPAEPKLSNEEVLLTEIRDLLK-----	133
<i>V. cholerae</i>	---EE---EAPKAPPAPTKDQELLSEIRDLLKAQQDK-----	136
<i>H. influenzae</i>	---EEK---KTAP-----KAETLLTEIRDLLK-----	128
<i>P. fluorescens</i>	---EA---VAPSEPPVPSAEETLLTEIRDLLKAQQNKS-----	136
<i>C. histolyticum</i>	---EE---AVEEAKIPEISREEELLGEIRDLLKEKNK-----	133
<i>C. crescentus</i>	---DAAEPAPAAPPAPTAETLLTEIRDLLAKG-----	139
<i>B. subtilis</i>	---KE---AEEEEAEVDAQEELLTEIRDLLKQQA KSP E-----	130
<i>B. japonicum</i>	---EE---AAP---AAPPKPSAEVELLTEIRDLLKKSCTRTL RPNC-----	157
<i>S. aureus</i>	---EE---EEEEAVVEENVLLTEIRDLLREKK-----	120
<i>C. perfringens</i>	---TK---KKEEVKVEATEKDCPYCYTKI DIKATRC PHCTSVLEEATN-----	152
<i>S. pyogenes</i>	---KKEK---EAAAPTQEELLTEIRDLLAQK-----	120
<i>D. radiodurans</i>	---RLKRSEKAAEA EPSNEEKLLAEIRD AVRSR-----PL-----	128
<i>M. tuberculosis</i>	---KGE---VEQPG---DTQVLLTEIRDLLAQ TNGDSPGRHGGRG---TPSPTDGPRASTESQ	151
<i>S. pneumoniae</i>	---TG---I KEEKTDEKKPTELEVLQEIKALLEKK-----	125
<i>Synechocystis sp.</i>	AVEEEIVAEAQDPVLEAQTNLDSINRLITDSINRLITLENQSSSQ-----	145
<i>M. leprae</i>	---HGE---VEQFD TDLIGNQVLLAEIRDLLAQSN GAPSGRHVD TADLTPTPNHEPRADT---	154

Figure 1.11 Sequence alignment of MscL homologues. Coloured cylinders represent S1 helices (purple), TM1 helices (yellow), TM2 helices (blue) and S3 helices (pink).

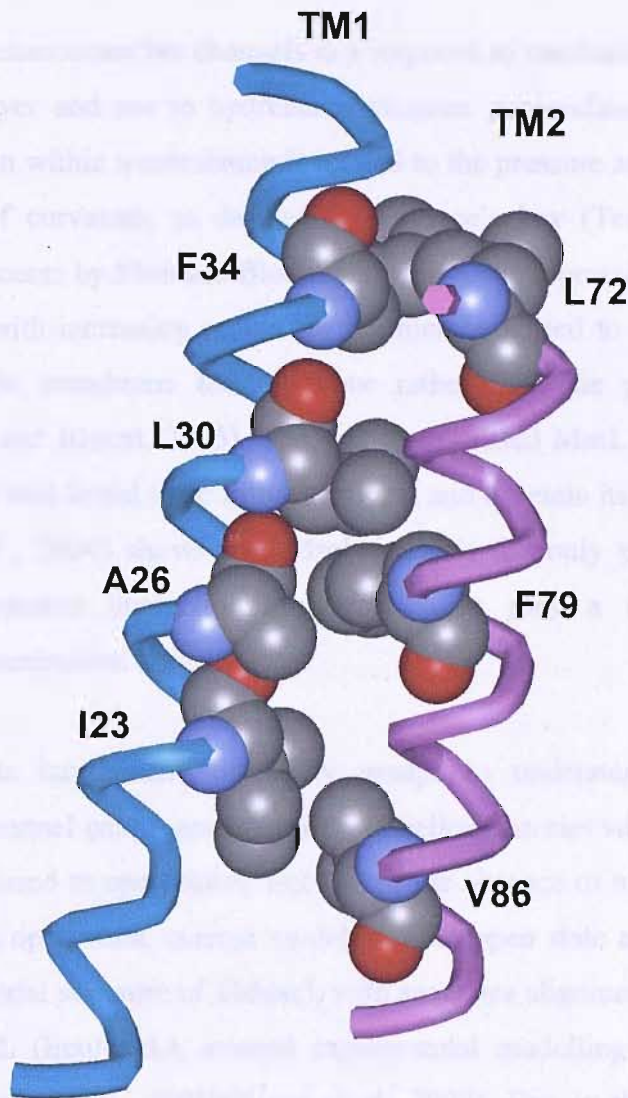


Figure 1.12 Representation of helix-helix interactions between TM1 and TM2 of an adjacent subunit. Modelled using WebLabViewer software and shown in CPK format. Relative position of TM1 and TM2 helices are thought to remain unchanged throughout the gating process.

1.13 Gating mechanism of TbMscL

The gating of mechanosensitive channels is a response to mechanical forces along the plane of the bilayer and not to hydrostatic pressure perpendicular to it (Martinac, 2004). The tension within a membrane is related to the pressure across the membrane and the radius of curvature, as defined by LaPlace's law (Tension = Pressure x radius/2). Experiments by Moe and Blount showing that the pressure required to open MscL increases with increasing radius for the membrane led to the conclusion that MscL responds to membrane tension alone rather than the pressure across the membrane (Moe and Blount, 2005). The fact that purified MscL when reconstituted into lipid vesicles was found to be fully functional and to retain its mechanosensitivity (Yoshimura *et al.*, 2004) shows that MscL itself is the only protein required for function. Lipid-protein interactions therefore must play a significant role in transducing this mechanical signal.

Significant efforts have been made by many groups to understand and define the mechanisms of channel gating and how the TM helices interact with each other in the transition from closed to open states, but due to the absence of a crystal structure of the channel in an open state, current models for the open state are hypothetical. By combining the crystal structure of TbMscL with sequence alignments of both TbMscL and *E. coli* MscL (EcoMscL), several experimental modelling studies have been published (Sukharev *et al.*, 2001b; Kong *et al.*, 2002). Due to the 'stiffness' of the TbMscL channel in comparison to the EcoMscL channel (TbMscL gates at tensions over twice as high than EcoMscL), many research groups have used EcoMscL in order to relate structural information to structural data (Betanzos *et al.*, 2002).

The large 3 nS conductance of MscL, which is roughly 100-fold greater than most eukaryotic channel conductances, and molecular sieving experiments (Cruickshank *et al.*, 1997; Ajouz *et al.*, 1998) suggest an open pore diameter of 30-40 Å for MscL. In order to achieve such dimensions there must be a large degree of structural rearrangement of the TM helices in order to accommodate such large effluxes of non-selective osmolytes upon osmotic downshock.

The limited points of contact between TM1 and TM2 helices may facilitate the large structural rearrangements that are required for channel gating. One other feature that

may have a role in allowing such extensive helix rearrangements is the positioning of aromatic residues on MscL. The general consensus is that aromatic residues commonly found at the ends of transmembrane α -helices are thought to anchor, and therefore stabilise, the protein in the membrane due to the preference of tyrosine (Tyr) and tryptophan (Trp) residues for the lipid bilayer interface (White *et al.*, 1999). Unusually for a membrane protein, MscL contains no Trp residues. Sequence alignments of mechanosensitive channels have shown that the positions of aromatic residues are highly conserved with phenylalanines found predominantly on TM2, and tyrosines in TbMscL and EcoMscL only at one end of transmembrane α -helices. Current opinion is that absence of ‘anchoring’ aromatic residues that are so characteristic of other membrane proteins may also play a role in facilitating such extensive helix tilting. Loss-of-function (LOF) mutations result in loss of channel activity and require greater tensions than wild type to open the channel. Recent studies by Chiang *et al.* have shown that ‘capping’ TM2 helices at both ends slows the gating kinetics and results in a partial loss-of-function (LOF) phenotype, while ‘capping’ of TM1 results in a total loss-of-function phenotype (Chiang *et al.*, 2005), leading to the conclusion that the presence of an aromatic ‘belt’ imposes restraints of transmembrane helix movements and severely compromises channel function.

The crystal structure of TbMscL shows the hydrophobic constriction narrowing to a pore of around 3 Å. This is formed by a ring of five valines and isoleucines (Val-21 and Ile-14) which are highly conserved (Figure 1.10). Separation of these tightly packed TM1 helices lining the channel pore is thought to be the initial step in channel opening (Anishkin *et al.*, 2005) so that this region is thought to be the primary gate. Random mutations in this region lead to two distinct phenotypes: LOF phenotypes, as already described (Yoshimura *et al.*, 2004), and hydrophilic substitutions which lead to gain-of-function (GOF) phenotypes that spontaneously open or open at lower tensions than the wild type (Ou *et al.*, 1998; Yoshimura *et al.*, 1999). The latter phenotype can be identified by a simple *in vivo* growth assay. Although GOF mutations dramatically altered the gating kinetics of MscL, the channel was still able to open and close completely suggesting the presence of a secondary gate that occludes the channel pore (Sukharev *et al.*, 2001a).

It is believed that gating is not an all or none response and it is currently proposed that there are at least five sub-conductance states for the MscL channel during the closed to open transition, although recent studies indicate the presence of several more intermediate states (Chiang *et al.*, 2004). Kinetic analysis of EcoMscL suggested that the kinetic barrier between the closed and open states occurs when the transmembrane in-plane area of the channel is two thirds that of the open state implying a considerable amount of protein expansion during the conformational changes prior to channel opening (Sukharev *et al.*, 1999). The following sequence of gating transitions has been proposed (Sukharev *et al.*, 2001b) based upon studies of EcoMscL, suggesting the presence of three defined transient sub-conductance states between the closed and open states.



The knowledge that MscL undergoes such radical in-plane expansion and the movement through transient sub-conducting states before achieving the fully open state, along with the results of random mutagenesis studies, as previously mentioned, strongly implicates the involvement of a secondary gate which is possibly broken between the last sub-conducting state and the fully open state; this been postulated to be the N-terminal S1 helical bundle (Sukharev *et al.*, 2001a). The S1-M1 linker that joins the S1 helices to the TM1 helices is highly conserved in sequence alignments for nearly all MscL homologues (Figure 1.11) and has been found to contain three highly conserved residues (Arg-13, Gly-14 and Asn-15 in TbMscL) (Kong *et al.*, 2002) indicating that it serves a critical role. Unfortunately this region was unresolved in the crystal structure for TbMscL but it has been reconstructed by modelling, supported by cross-linking and mutational studies (Sukharev *et al.*, 2001a; Anishkin *et al.*, 2005).

Cross-linking of cysteine residues on the S1 helices that are close to each other in the closed state (Ile-3, Phe-7 and Phe-10 in EcoMscL) prevented channel opening (Sukharev *et al.*, 2001a). When the channel is in an open state, the model proposed by Sukharev predicts that S1 helices dock next to TM1 and TM2 helices. Cross-linking of residues on S1 and TM2 (Ile-3 and Ile-96 respectively) prevented channel closure (Sukharev *et al.*, 2001a). These findings confirm that the amino-terminal S1 helices form a secondary gate which occlude the channel pore when closed and that they move into the transmembrane region upon sensing tension from the S1-M1 linker to compensate for shortening of TM1 and TM2 helices in the open state

Although several models have been suggested for the channel opening, the model in current favour is the 'tilting 5-helix pore' model (Sukharev *et al.*, 2001b). Upon expansion of the entire transmembrane complex, tension is conveyed through the S1-M1 linker causing it to stretch. Upon full stretching of the linker, the secondary gate formed by the S1 helical bundle senses the tension and completes the full transition from an intermediate substate to the fully open state (Sukharev *et al.*, 2001a). The 'tilting 5-helix pore' model is illustrated in Figure 1.13 showing how the S1 element may be involved in the transition from a closed state to an open state and how this may contribute to the formation of a second hydrophobic barrier at the cytoplasmic side of the channel. The 'tilting 5-helix pore' model relies on the assumption that TM1 and TM2 helices move together during channel gating and that the position of TM2 helices relative to TM1 helices remain the same in the closed and open states and that the open pore dimensions are achieved by extensive helix tilting of both TM1 and TM2 helices in unison. This model has also been supported by EPR studies (Betanzos *et al.*, 2002).

2.1. Membranes

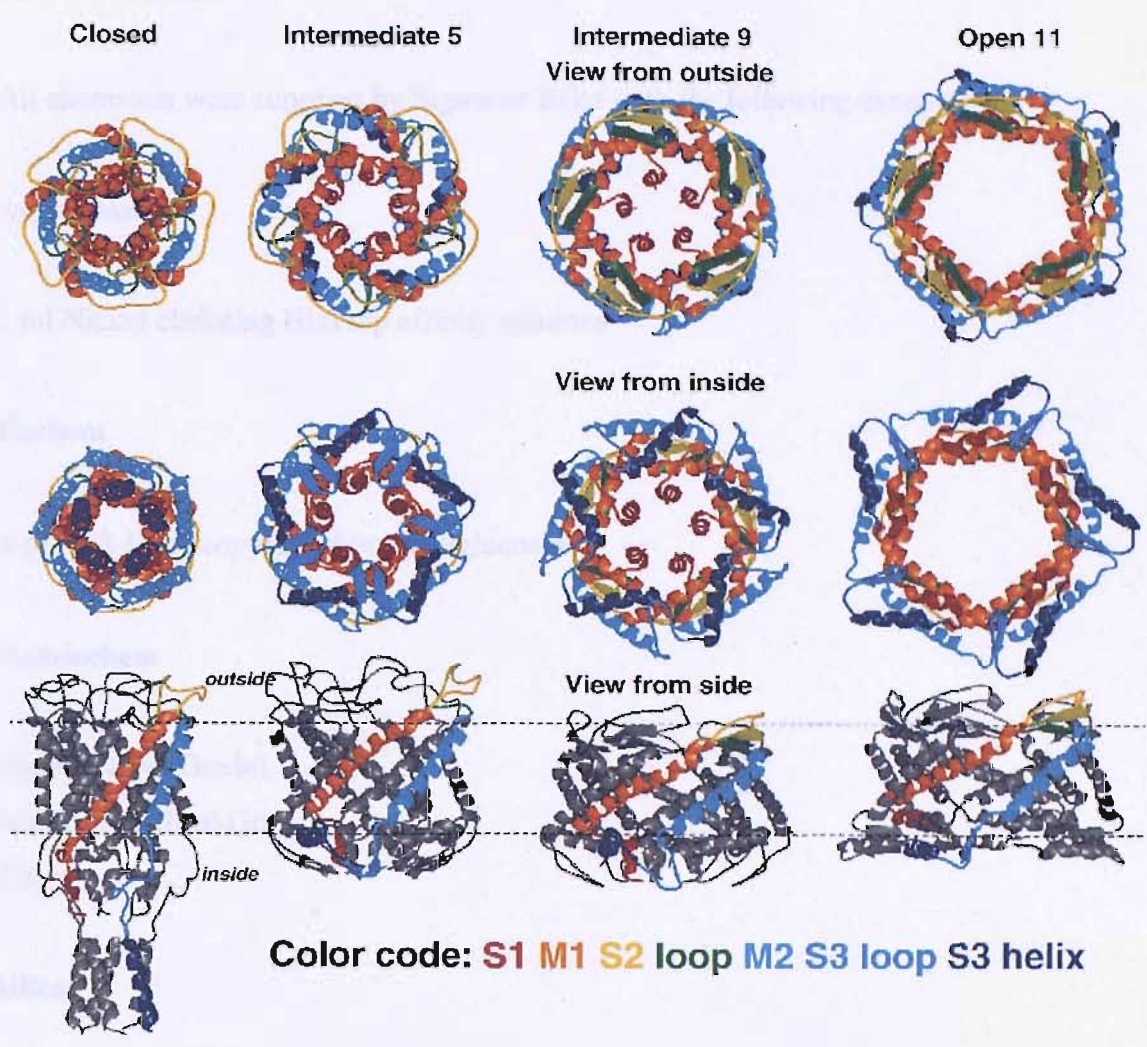


Figure 1.13 Ribbon representation of models of TbMscL in a closed, intermediate 5, intermediate 9, and an open conformation shown as viewed from outside the cell (top row), inside the cell (middle), and from the side (bottom). (Sukharev *et al.*, 2001b) They are currently thought to be nine sub-conducting states of MscL during channel gating which can be divided into the four main structures represented above (Chiang *et al.*, 2004).

Chapter 2. General Materials and methods

2.1 Materials

All chemicals were supplied by Sigma or BDH with the following exceptions

Amersham

1 ml Nickel chelating HisTrap affinity columns

Bachem

n-octyl- β -D-glucoopyranoside (octylglucoside)

Calbiochem

Hepes (Ultrol Grade)

Imidazole (Ultrol Grade)

Tris

Difco

Bacto-yeast agar

Bacto-agar

National Diagnostics

Protogel (30 % (w/v) acrylamide: 0.8 % (w/v) bis-acrylamide)

New England Biolabs

*Bam*H1

*Nde*1

Pharmacia

Agarose (NA Grade)

Promega

*Dpn*1

Pfu DNA polymerase

Wizard® *Plus* Minipreps DNA purification system

Sartorius

Sterile disposable 0.22 µm filters

2.2 General Methods

Microbiological Techniques

2.2.1 Sterilisation

Luria-broth (LB) growth medium, distilled water, pipette tips, and eppendorf tubes were sterilised by autoclaving at 121 °C, 15 lbs.sq.inch for 15 minutes.

2.2.2 Antibiotic stocks

Ampicillin at 100 mg ml⁻¹ and kanamycin 25 mg ml⁻¹ were prepared in sterile water. Chloramphenicol 25 mg ml⁻¹ was prepared in ethanol. Stocks were stored at -20 °C in 1 ml aliquots until use.

2.2.3 Luria Broth

Luria broth was made by adding 20.6 g EZ mix (Sigma) to 1 L distilled water and then autoclaved as described. When ready for use, antibiotic was added at the appropriate concentration and the pH adjusted to pH 7.2. Final concentrations of antibiotics were 100 µg ml⁻¹ ampicillin, 25 µg ml⁻¹ chloramphenicol and 25 µg ml⁻¹ kanamycin.

2.2.4 LB agar

4.5 g of Bacto-agar was added to 300 ml of luria broth and autoclaved as described. The appropriate antibiotic was added upon cooling to below 50 °C.

2.2.5 SOB Medium

Reagents Used

5 g Bacto Yeast Extract

20 g Bactotryptone

10 mM MgCl₂

10 mM MgSO₄

10 mM NaCl

10 ml of 250 mM KCl was added to 950 ml of analytical grade water and adjusted to pH 6.8. Water was added to a final volume of 1 L followed by autoclaving as previously described.

2.2.6 SOC Medium

Following autoclaving of SOB medium, 20 mls of 1 M sterile-filtered glucose was added and SOC medium was aliquoted and frozen at -20 °C until use.

2.2.7 Transformation Buffer

100 mM CaCl₂

The solution was made to a final volume of 50 mls and then autoclaved as previously described.

2.2.8 Escherichia Coli Strains

Strain	Genotype	Source
BL21(DE3)pLysS	F ⁻ <i>ompT hsdS</i> (r _B ⁻ , m _B ⁻) <i>gal dcm</i> λ(DE3) [pLysS Cam ^r]	Novagen
XL-1 Blue	<i>recA1 endA1 gyrA96 thi-1 hsdR17</i> <i>supE33 relA1 lac</i> [F' <i>proAB lac^q</i> ΔM15 Tn10(Tet ^r)]	Novagen

Escherichia coli strain BL21(DE3)pLysS was used for high level protein expression of TbMscL.

XL-1 Blue cells were transformed with *dpnI* digested PCR products carrying the desired mutation of TbMscL and used to repair and replicate TbMscL prior to sequencing of DNA.

2.2.9 Glycerol Stocks

10 ml overnight cultures containing the appropriate antibiotic were grown at 37 °C for 16 hours. 1 ml of culture was added to 500 μl of autoclaved glycerol in a 1.5 ml cryovial. Samples were mixed and stored at -80 °C.

DNA Techniques

2.2.10 Purification of Plasmid DNA

Reagents Used

Resuspension Buffer

50 mM Tris-HCl, pH 7.5

10 mM EDTA

100 µg/ml RNase A

Cell Lysis Buffer

0.2 M NaOH

1% SDS

Column Wash

80 mM potassium acetate pH 4.8

8.3 mM Tris-HCl

40 µM EDTA

55% ethanol (prior to use)

Neutralising Buffer

1.32 M potassium acetate

TbMscL DNA was obtained from XL-1 blue cells carrying the desired construct. A single colony of the wild type or mutant TbMscL was inoculated into 5 mls LB medium containing the appropriate antibiotic and incubated overnight in an orbital shaker at 37 °C at 220 rpm. The culture was centrifuged at maximum speed to pellet the cells. Cells were then resuspended in 300 µl resuspension buffer and transferred to a 1.5 ml eppendorf micro-centrifuge tube. 300 µl of cell lysis buffer was added and samples mixed by inversion until the solution cleared. 300 µl of neutralisation buffer was added and the samples mixed as previously described. Samples were spun at 13 000 rpm in a bench top centrifuge for 5 minutes and the supernatant transferred to a

new 1.5 ml eppendorf micro-centrifuge tube. To completely eliminate cell debris, samples were re-spun for 3 minutes at maximum speed and the supernatants transferred to new 1.9 ml eppendorf tubes. 1 ml of pre-warmed DNA purification resin was added to each sample and left at room temperature for at least 5 minutes with gentle inversion. The resin/DNA mixes were applied to assembled syringe barrels connected to a vacuum manifold and samples were pulled through by applying a vacuum. 2 mls of column wash solution were then applied to each sample to wash the resin and the vacuum was removed. The syringe barrel was removed and the minicolumn was transferred to a clean 1.5 ml eppendorf tube and centrifuged at maximum speed as before for 1 minute to remove any residual column wash solution. The minicolumn was transferred to a clean 1.5 ml eppendorf tube and the DNA eluted with 50 μ l sterile water, pre-warmed to 70 °C. Samples were left for 1 minute and then DNA eluted by centrifuging at maximum speed as previously detailed for 1 minute.

2.2.11 Restriction digests for linearization of DNA and for digestion of methylated DNA

In order to linearise and visualise the eluted DNA, restriction endonuclease BamH1 was used to carry out a single digest. The appropriate volume of DNA (~5 μ l) was added to 3 μ l of sterile water and 1 μ l of enzyme buffer 2. 1 μ l BamH1 was added to the eppendorf, the sample was briefly vortexed, centrifuged for 5 seconds and incubated at 37 °C for 1 hour to digest the DNA. Digested DNA was visualised on a 1 % agarose gel to check for size. For *dpn 1* digests of PCR products, 1 μ l of *dpn 1* was added to 50 μ l PCR product and left to digest at 37 °C for 1 hour.

2.2.12 Agarose Gel Electrophoresis

Reagents Used

Agarose

100 g (Pharmacia)

50 X TAE

242 g Tris

57.1 ml glacial acetic acid

1.9 g NaEDTA

Sterile water to 1 L pH 8.0

Stock Ethidium Bromide

100 mg ethidium bromide

10 mls sterile water

Gel Loading Buffer

3 ml glycerol

30 mg bromophenol blue

1 ml 10 X TAE buffer

Sterile water up to 10 ml

1 % agarose in 1 X Tris acetate EDTA (TAE) buffer was melted and ethidium bromide was added at a final concentration of $0.4 \mu\text{g ml}^{-1}$. Gels were poured and allowed to set before running in 1 X (TAE) buffer diluted from a 50 X stock solution. Gel loading buffer was added to the DNA samples and run on the agarose gel alongside a 1 Kb DNA ladder at 120 volts for 50 minutes. DNA was visualised using a Syngene imaging system.

2.2.13 Quick Change Site-directed mutagenesis of TbMscL

Reagents Used

41.4 µl sterile water

5 µl wild type template TbMscL DNA at 50 ng/µl

1 µl 10 x *pfu* DNA polymerase reaction buffer

1 µl deoxynucleotide triphosphates (dNTPs)

0.3 µl each of forward and reverse primers

1 µl *pfu* DNA polymerase (3U/µl)

To generate mutants of interest for study, wild type MscL DNA obtained from a DNA mini-prep was used as the template to carry out site-directed mutagenesis according to the QuikChange® site-directed mutagenesis protocol. Forward and reverse primers were designed incorporating the desired mutations. Reactions were carried out in thick-walled 0.5 µl eppendorfs with a final volume of 50 µl. Reagents were mixed and placed in a Peltier Thermal Cycler PTC-200. PCR products were then analysed on a 1 % agarose gel.

2.2.14 Ethanol precipitation of DNA for sequencing by MWG-Biotech

Around 7 µg of plasmid DNA, obtained from mini-preps of overnight cultures, was added to a 1.5 ml eppendorf tube and precipitation was carried out by addition of 10 µl of 3 M NaAc pH 5.1. 200 µl of ice cold ethanol was added and DNA samples were left on ice for 30 minutes. Samples were centrifuged at maximum speed in a bench top centrifuge and the supernatant was discarded. 1 ml of 70 % ethanol was added and the samples were then centrifuged at maximum speed in a bench top centrifuge for 10 minutes. Supernatants were discarded and samples were left to air dry before being sent to MWG for sequencing (section 2.2.15).

2.2.15 DNA Sequencing

Following TbMscL mutagenesis using the quick change PCR method and visualisation of the PCR product on an agarose gel, mutations were verified by DNA sequencing carried out by MWG Biotech. Plasmid DNA was precipitated as described in the ethanol precipitation section.

2.2.16 Sequence Analysis

Using the Blast program, sequences were checked against the wild type sequence to ensure the correct mutation had been generated.

Molecular Biology Techniques

2.2.17 Preparation of Ultra-competent cells

Competent cells were prepared fresh as required. The desired cell strain was inoculated from a glycerol stock into 10 ml of LB broth containing the appropriate antibiotic and grown at 37 °C overnight at 220 rpm in an orbital shaker. Cells were centrifuged at 3,000 rpm in a benchtop centrifuge for 10 minutes and the supernatant was poured off. Cells were resuspended in 5 ml ice cold sterile 100 mM CaCl₂ and left on ice for 30 minutes. Cells were centrifuged as before and resuspended in 1 ml ice cold CaCl₂. Aliquots of 200 µl were prepared and used for heat shock of DNA.

2.2.18 Transformation of DNA into ultra-competent cells

DNA was transformed into XL-1 blue ultra-competent cells for sequencing or BL21(DE3)pLysS cells for expression as required. 2 μl of DNA was added to 200 μl competent cells and incubated on ice for 30 minutes. Cells were heat shocked at 42 °C for 45 seconds and then placed on ice for 3 minutes. 500 μl of SOC media was immediately added and cells were recovered by incubating at 37 °C at 200 rpm for 1 hour. Cells were then spread onto LB plates supplemented with ampicillin at a final concentration of 100 $\mu\text{l ml}^{-1}$. Plates were then incubated at 37 °C overnight.

Expression and Purification of Tb MscL

2.2.19 Expression of TbMscL

Following sequencing, the pET-19b plasmid carrying the MscL gene, with the wild type or desired mutation, was transformed into BL21(DE3)pLysS expression cells, streaked onto LB amp plates and incubated overnight at 37 °C. A single colony was picked and inoculated into 10 mls Luria-Bertani (LB) media containing 100 $\mu\text{g/ml}$ ampicillin and incubated at 37 °C in an orbital shaker at 220 rpm overnight. The 10 ml overnight culture was inoculated into 1 L LB amp medium and grown to an OD_{600} of 0.6. A 1 ml pre-induction sample was taken and expression of the protein was induced by the addition of 1 mM isopropyl β ,D-thiogalactopyranoside (IPTG). Cells were left for an additional 4 hours, a 1 ml post-induction sample was taken and cells were pelleted by centrifugation at 7,000g for 20 minutes in a Beckman Avanti J-20 XPI at 4 °C. The cell pellet was stored at -20 °C until use.

2.2.20 Purification of TbMscL

Reagents Used

PBS

140 mM NaCl

2.7 mM KCl

10 mM Na₂HPO₄

pH 7.2 KOH

Made to 1L with sterile distilled water

To purify the protein, cell pellets were thawed and resuspended in 60 mls 1 x PBS and lysed by sonication on ice for 5 minutes (20 seconds on, 15 seconds off for 15 cycles) using an XL-2020 Misonix sonicator. Cells were then spun at 100,000 g for 40 minutes at 4 °C in a Beckman L7 Ultracentrifuge. The supernatant was discarded and the pellet was resuspended in 120 mls of PBS with the addition of 40 mM *n*-octyl- β -D-glucopyranoside (OG) (Bachem). The protein was left stirring at room temperature to solubilise for 1 hour. The insoluble material was collected by centrifugation at 8,000g for 20 minutes in a Beckman J2-HS at 4 °C. The supernatant was filtered through a 0.22 μ m filter and 30 mM imidazole (Calbiochem) was added to prevent non-specific binding of proteins to the nickel-agarose. Supernatant was loaded onto a 1 ml HisTrap nickel-chelating column (Amersham) pre-equilibrated with 5 column volumes of buffer A (PBS supplemented with 40 mM OG and 30 mM imidazole, pH 7.2). Protein was washed with 5 column volumes of buffer A and eluted from the column in 1 ml fractions with 2.5 column volumes of Buffer B (PBS supplemented with 40 mM OG and 400 mM imidazole). Fractions were analysed by SDS-PAGE and fractions containing the protein were pooled, aliquoted and stored at - 80 °C following flash-freezing in liquid nitrogen. Protein concentrations of aliquots were determined upon thawing by the Bradford Assay (Section 2.2.22).

2.2.21 Sodium dodecyl sulphate polyacrylamide gel electrophoresis (SDS-PAGE)

Reagents Used

Running Gel

3.5 mls Protogel
2.4 mls 1.5 M Tris pH 8.8
60 μ l 10 % SDS
30 μ l 25 % ammonium persulphate (APS)
10 μ l temed
3.13 mls sterile water

Stacking Gel

1.7 mls sterile water
600 μ l Protogel
1.6 mls 3.6 M Tris pH 9.3
20 μ l 25 % APS
40 μ l 10 % SDS
4 μ l temed

SDS sample buffer

1 ml 0.625 M Tris pH 6.8
2 ml 10 % SDS
1 ml glycerol
bromophenol blue
0.5 ml sterile water

SDS Running Buffer

75.75 g Tris

360.25 g Glycine

25 g SDS

Distilled water was added to 5 L and buffer was diluted 1:5 with distilled water prior to use.

Coomassie Blue

250 mg coomassie brilliant blue

450 ml methanol

460 ml water

90 ml acetic acid

Destain solution

1 L methanol

375 ml acetic acid

3.625 L distilled water

SDS-PAGE was carried out according to the method of Laemmli. As the MscL protein is only 18 kDa, 17.5 % gels were used. These were set and run using a BioRad mini-gel system. Samples were prepared and run in 1 x SDS running buffer diluted from stock at a constant current of 50 mAmps. Bromophenol blue was used as a dye front marker. Low range molecular weight markers were used to approximate the size of protein samples. The gels were stained with Coomassie blue and then destained in destain solution until bands became visible. Gels were then scanned using a Syngene gel imaging system.

2.2.22 Determination of Protein Concentration using Bradford Assay

The concentration of MscL protein was determined following affinity purification on a 1ml HisTrap column. Bovine serum albumin (BSA) standards ranging from 2 – 10 $\mu\text{g ml}^{-1}$ were prepared from a stock solution in sterile analytical grade water. 750 μl water was added to a cuvette in duplicate and 50 μl of the BSA standards were added. The volume was made up to 1 ml with 200 μl of Bio-rad dye. Samples were mixed and left for 5 minutes at room temperature. Absorbance was recorded at 595 nm using a U-2001 Spectrophotometer (Hitachi) at a constant temperature of 25 °C. A blank sample was prepared by adding 200 μl of Biorad dye to 800 μl sterile water.

Chapter 3: Mutagenesis of TbMscL

3.1 Introduction

Although progress has been made in recent years in understanding the conformational changes that occur in gating of MscL, the crystal structure of MscL has only been determined in the closed state and the structure of the open state is unknown. Each monomer of TbMscL contains 151, mostly hydrophobic, amino acids. A series of hydrophilic residues along TM1, mostly threonines, form the channel pore creating a distinct polar region of the protein (Chang *et al.*, 1998). Among the MscL proteins, the TM1 helix is the most highly conserved region with mutations in this region significantly altering channel gating (Ou *et al.*, 1998; Anishkin *et al.*, 2005). Wild type TbMscL lacks Trp residues. Here, single Trp residues were introduced into TM1 of TbMscL both to study functional effects and to allow the use of fluorescence spectroscopy to study lipid-protein interactions.

Figure 3.1.1 shows the wild type amino acid sequence of TbMscL with TM1 and TM2 highlighted in red and blue respectively. Residues along TM1 that were chosen for tryptophan substitution, seen in Figure 3.1.1, are underlined in red. Figure 3.1.2 shows the nucleotide sequence of TbMscL with the forward and backwards reading frames shown above and below respectively, and Figure 3.1.3 shows one monomer of TbMscL with the positions of the residues chosen for Trp substitution marked along TM1.

```
M L K G F K E F L A R G N I V D L A V A V V I G T A F T A
L V T K F T D S I I T P L I N R I G V N A Q S D V G I L R
I G I G G G Q T I D L N V L L S A A I N F F L I A F A V Y
F L V V L P Y N T L R K K G E V E Q P G D T Q V V L L T E
I R D L L A Q T N G D S P G R H G G R G T P S P T D G P R
A S T E S Q
```

Figure 3.1.1 Wild type amino acid sequence of TbMscL. Transmembrane helix 1 is highlighted in red and transmembrane helix 2 is highlighted in blue.


```

Met leu lys gly phe lys glu phe lys ala arg gly asn ile val asp leu ala
atg ctc aaa gga ttc aag gag ttt ctc gcg cgg ggt aat atc gtc gac ctg gct
tac gag ttt cct aag ttc ctc aaa gag cgc gcc cca tta tag cag ctg gac cga

val ala val val ile gly thr ala phe thr ala leu val thr lys phe thr asp
gtc gcg gtg gta atc ggc aca gcg ttc acg gcg ttg gtc acc aag ttc acc gac
cag cgc cac cat tag ccg tgt cgc aag tgc cgc aac cag tgg ttc aag tgg ctg

ser ile ile thr pro leu ile asn arg ile gly val asn ala gln ser asp val
agc atc att acg ccg ctg atc aac cgg atc ggc gtc aac gca cag tcc gac gtc
tcg tag taa tgc ggc gac tag ttg gcc tag ccg cag ttg cgt gtc agg ctg cag

gly ile leu arg ile gly ile gly gly gly gln the ile asp leu asn val leu
ggc atc ttg cgg atc ggt atc ggc ggt ggt cag acc att gac ttg aac gtc ttg
ccg tag aac gcc tag cca tag ccg cca cca gtc tgg taa ctg aac ttg cag aac

leu ser ala ala ile asn phe phe leu ile ala phe ala val tyr phe leu val
ttg tcg gca gcg atc aac ttt ttc ctg atc gcg ttc gcg gtg tac ttc cta gtc
aac agc cgt cgc tag ttg aaa aag gac tag cgc aag cgc cac atg aag gat cag

val leu pro tyr asn thr leu arg lys lys gly glu val glu gln pro gly asp
gtg ctg ccc tac aac aca cta cgc aag aag ggg gag gtc gag cag ccg ggc gac
cac gac ggg atg ttg tgt gat gcg ttc ttc ccc ctc cag ctc gtc ggc ccg ctg

thr gln val val leu leu thr glu ile arg asp leu leu ala gln thr asn gly
acc caa gtc gtg ctg ctc acc gaa atc cgc gat ctg ctc gcg caa acg aac ggg
tgg gtt cag cac gac gag tgg ctt tag gcg cta gac gag cgc gtt tgc ttg ccc

asp ser pro gly arg his gly gly arg gly thr pro ser pro ser asp gly pro
gac tcg ccg ggg agg cac ggc ggc cgt ggg aca cca tcg cca acc gac ggg cct
ctg agc ggc ecc tcc gtg ccg ccg gca ccc tgt ggt agc ggt tgg ctg ccc gga

arg ala ser thr glu ser gln
cgc gcg agc aca gaa tcg caa
gcg cgc tcg tgt ctt agc gtt

```

Figure 3.1.2 Wild type nucleotide sequence of TbMscL. The forward reading frame of TbMscL is shown in black with the corresponding complementary DNA sequence shown in red. Amino acids are written above the nucleotide sequence in blue.

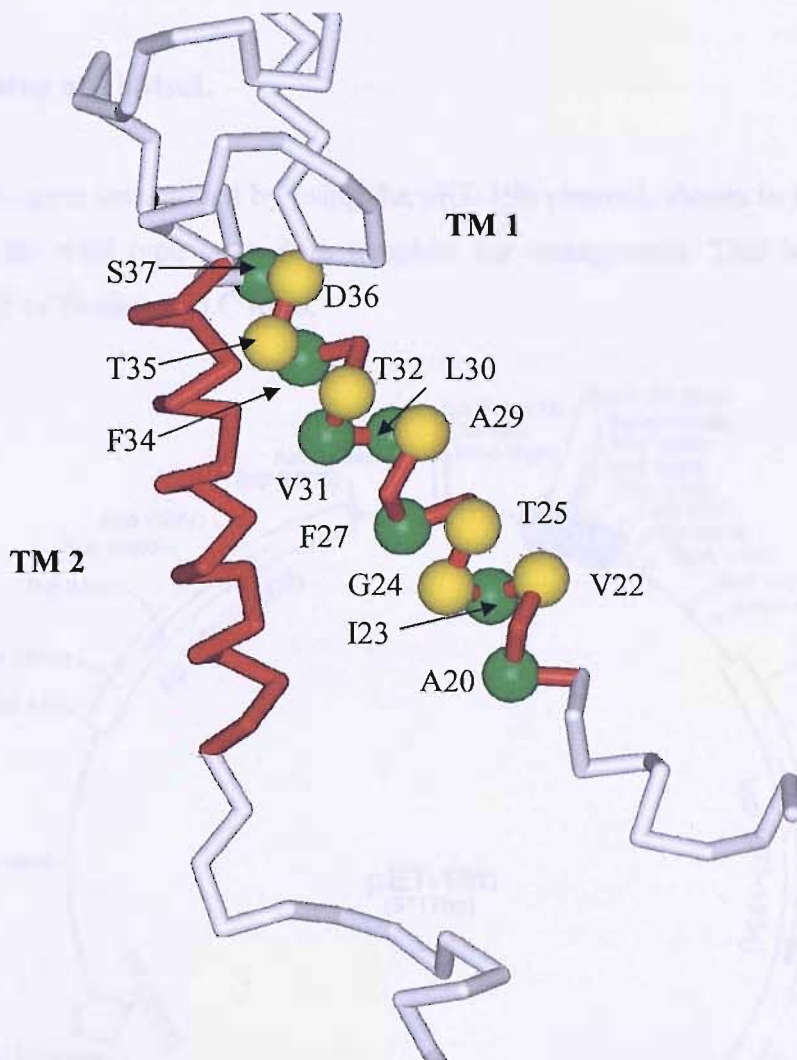


Figure 3.1.3 A monomer of TbMscL showing α -carbons of residues on TM1 that were mutated to Trp. Residues that face directly towards the lipid bilayer are coloured in green and residues that are buried within the protein structure or face the channel pore are coloured in yellow.

3.2 Methods

Molecular biological methods were carried out as detailed in the general methods section (Chapter Two).

3.2.1 Cloning of TbMscL

The TbMscL gene was cloned by using the pET-19b plasmid, shown in Figure 3.2.1, harbouring the wild type gene as a template for mutagenesis. This was the very generous gift of Professor D.C Rees.

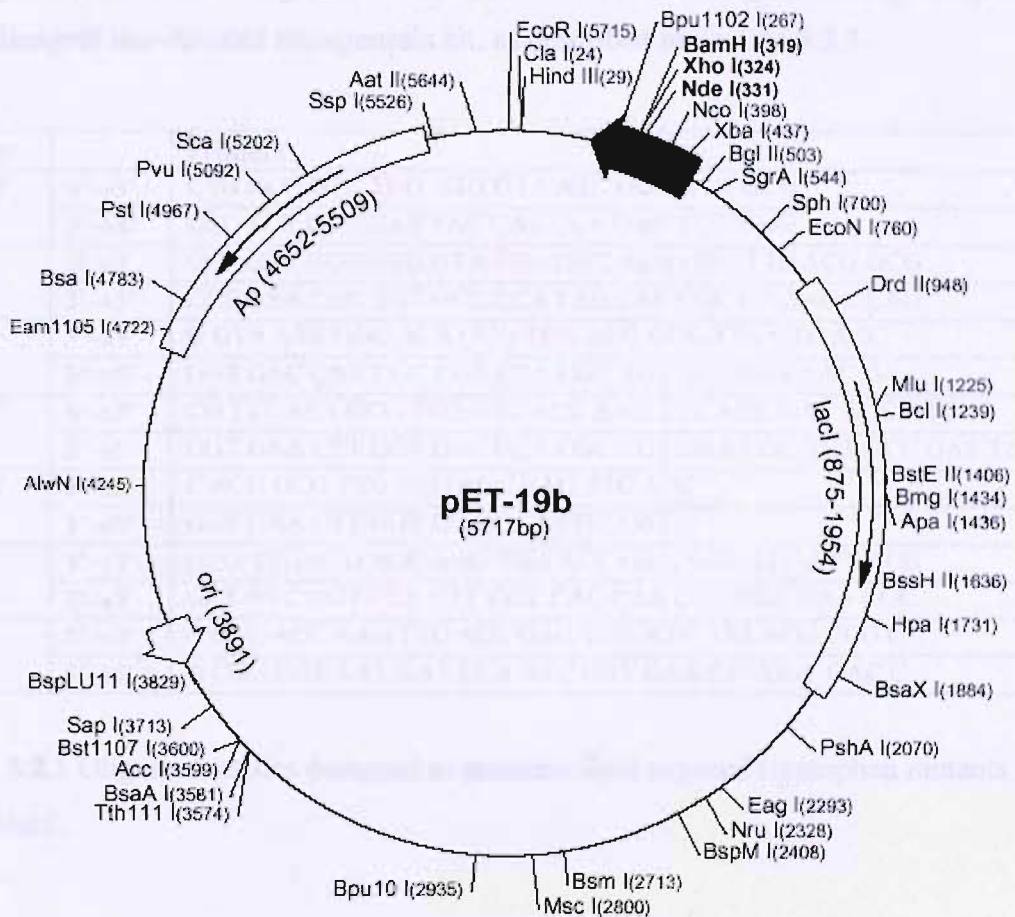


Figure 3.2.1 Vector map of pET-19b plasmid used to express TbMscL for cloning.

The pET-19b vector carries an N-terminal His-Tag sequence which makes the end protein product suitable for purification by affinity chromatography. Expression of the gene is under the control of a T7 inducible promoter.

3.2.2 Generation of Trp mutants of MscL

To generate MscL mutants expressing tryptophan in the region of interest for study, oligonucleotide primers incorporating the desired Trp mutation, complementary to opposite strands of the vector, were designed using the DNASTar software. Primers were ca. 36 bps in length with the Trp mutation in the middle. Primers used to generate tryptophan-mutated MscL species are shown in Tables 3.2.1. - 3.2.3. Trp mutations are underlined in red and silent mutations, incorporated to avoid hairpin formations, are shown in blue.

Once primers had been designed, mutant species of MscL were generated by using the Quikchange® site-directed mutagenesis kit, as described in Section 3.2.3.

Mutant		Primers
A20W	5'→3'	CTG GCG GTC <u>TGG</u> GTG GTA ATC GGC ACA GCG
	3'→5'	CGC TGT GCC GAT TAC CAC <u>CCA</u> GAC CGC CAG
I23W	5'→3'	GCT GTC GCG GTG GTA <u>TGG</u> GGC ACA GCG TTC ACG GCG
	3'→5'	CGT GAA CGC TGT GCC <u>CCA</u> TAC CAC CGC GAC AGC CAG
F27W	5'→3'	G GTA ATC GGC ACA GCG <u>TGG</u> ACG GCG TTG GTC ACC
	3'→5'	GGT GAC CAA CGC CGT <u>CCA</u> CGC TGT GCC GAT TAC C
L30W	5'→3'	CG TTC ACT GCG <u>TGG</u> GTC ACC AAG TTC ACC GAC AGC ATC
	3'→5'	GGT GAA CTT GGT GAC <u>CCA</u> CGC CGT GAA CGC TGT GCC GAT TAC C
V31W	5'→3'	C ACG GCG TTG <u>TGG</u> ACC AAG TTC ACC
	3'→5'	GGT GAA CTT GGT <u>CCA</u> CAA CGC CGT G
F34W	5'→3'	GCG TTG GTG ACC AAG <u>TGG</u> ACC GAC AGC ATC ATT ACG
	3'→5'	GCT GTC GGT <u>CCA</u> CTT GGT CAC CAA CGC CGT GAA CGC
S37W	5'→3'	G GTC ACC AAG TTC ACC GAC <u>TGG</u> ATC ATT ACG CCG C
	3'→5'	G CGG CGT AAT GAT <u>CCA</u> GTC GGT GAA CTT GGT GAC C

Table 3.2.1 Oligonucleotides designed to generate lipid exposed tryptophan mutants of TbMscL.

Mutant		Primers
V22W	5'→3'	CT GTC GCG GTT TGG ATC GGC ACA GCG TTC ACG GCG TTG
	3'→5'	GT GAA CGC TGT GCC GAT CCA AAC CGC GAC AGC CAG GTC
G24W	5'→3'	GCG GTG GTA ATC TGG ACA GCG TTC ACG GCG TTG GTC
	3'→5'	GT GAC CAA CGC CGT GAA CGC TGT CCA GAT TAC CAC C
T25W	5'→3'	GCG GTG GTA ATC GGC TGG GCG TTC ACG GCG TTG G
	3'→5'	C CAA CGC CGT GAA CGC CCA GCC GAT TAC CAC CGC
A29W	5'→3'	C GGC ACA GCG TTC ACG TGG TTG GTC ACC
	3'→5'	GGT GAC CAA CCA CGT GAA CGC TGT GCC G
T32W	5'→3'	GCG TTG GTC TGG AAG TTC ACC GAC AGC ATC ATT ACG
	3'→5'	CGT AAT GAT GCT GTC GGT GAA CTT CCA GAC CAA CGC
T35W	5'→3'	G GTC ACC AAG TTC TGG GAC AGC ATC ATT ACG CCG
	3'→5'	CGG CGT AAT GAT GCT GTC CCA GAA CTT GGT GAC C
D36W	5'→3'	ACC AAG TTC ACC TGG AGC ATC ATT ACG CCG CTG ATC
	3'→5'	GAT CAG CGG CGT AAT GAT GCT CCA GGT GAA CTT GGT GAC C

Table 3.2.2 Oligonucleotides designed to generate pore lining tryptophan mutants of TbMscL.

Mutant		Primers
V21K (mutant templates)	5'→3'	C CTG GCT GTC GCG AAG GTA ATC GGC ACA G
	3'→5'	GT GCC GAT TAC CTT CGC GAC AGC CAG

Table 3.2.3 Oligonucleotides designed to generate open channel tryptophan mutants of TbMscL. Primers were used with tryptophan mutated templates.

3.2.3 Quik-change® site-directed Mutagenesis

The use of the polymerase chain reaction to generate mutated forms of a chosen protein is a very powerful technique utilising small synthetic oligonucleotides containing the desired genetic mutation. The oligonucleotides anneal to the wild type template DNA and are extended by *pfu turbo* DNA polymerase. Successive rounds of DNA replication by thermal cycling produce mutated plasmid with staggered nicks.

Using the Quik-change® site-directed mutagenesis method allows direct mutagenesis of double stranded plasmid making it a relatively simple procedure requiring only the chosen plasmid carrying the gene of interest acquired from a plasmid mini-prep. A brief overview of the process is shown in Figure 3.2.2. pET-19b plasmid carrying the wild type template DNA was first obtained using the Promega-wizard® plus minipreps DNA purification system. Thermal cycling was carried out as described in Section 2.2.13. Cycle conditions used involved denaturation at 95 °C for 30 seconds, annealing at 55 °C for 1 minute and extension at 68 °C for 6 mins (1 min/Kb of plasmid length). Each cycle was repeated 16 times as suggested by the Stratagene Quik-change® manual. The final cycle was held at 4 °C.

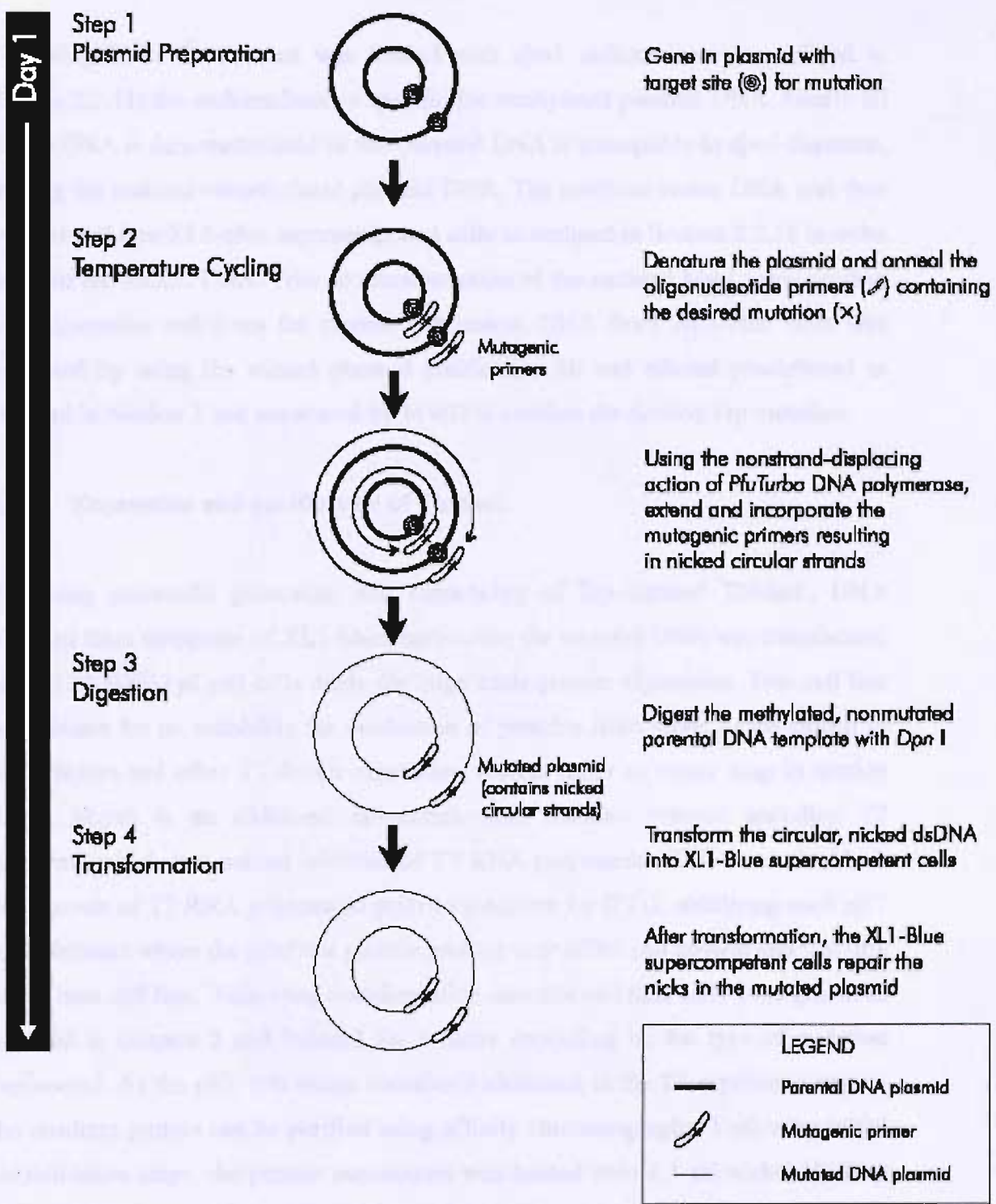


Figure 3.2.2 Overview of the QuikChange® site-directed mutagenesis method. Taken from the Stratagene manual

Following PCR, the product was treated with *dpn1* endonuclease as outlined in Section 2.2.11; the endonuclease is specific for methylated parental DNA. Nearly all *E. coli* DNA is dam-methylated so that parental DNA is susceptible to *dpn1* digestion, leaving the mutated unmethylated plasmid DNA. The resultant vector DNA was then transformed into XL1-blue supercompetent cells as outlined in Section 2.2.18 in order to repair the nicked DNA. Prior to transformation of the mutated MscL gene product into expression cell lines for protein expression, DNA from XL1-blue cells was harvested by using the wizard plasmid purification kit and ethanol precipitated as outlined in Section 2 and sequenced by MWG to confirm the desired Trp mutation.

3.2.4 Expression and purification of TbMscL

Following successful generation and sequencing of Trp-mutated TbMscL, DNA obtained from minipreps of XL1-blues harbouring the mutated DNA was transformed into BL21 (DE3) pLysS cells ready for large scale protein expression. This cell line was chosen for its suitability for production of proteins from target genes cloned in pET vectors and other T7-driven expression vectors (refer to vector map in section 3.2.1). pLysS is an additional chloramphenicol resistant plasmid encoding T7 lysozyme which is a natural inhibitor of T7 RNA polymerase. This serves to block basal levels of T7 RNA polymerase prior to induction by IPTG, stabilising such pET recombinants where the resultant protein product may affect cell growth and viability of the host cell line. Following transformation into this cell line, cells were grown as outlined in Chapter 2 and induced for 4 hours depending on the type of mutation engineered. As the pET 19b vector contains 9 histidines in the T7 expression region, the resultant protein can be purified using affinity chromatography. Following initial solubilisation steps, the protein supernatant was loaded onto a 1 ml nickel HisTrap column (Amersham). Flow through material containing non-bound and unspecific host cell proteins was removed prior to elution of pure MscL protein. Protein was eluted with addition of 400 mM imidazole and collected in 1 ml fractions so that the purity of small fractions could be ascertained prior to pooling and freezing of pure MscL protein. Purity was assessed by loading samples of eluted fractions on a 15 % SDS-polyacrylamide gel.

3.3 Results

3.3.1 Restriction Digests of TbMscL

Prior to generation of Trp mutants by PCR a single and double digest of the wild type construct was performed to check the plasmid and the gene are of the correct size (see methods in section 2.2.11). The DNA gel shown in Figure 3.3.1 shows a single digest in lane A and a double digest in lane B with the gene coding for MscL visible at 500 bp in lane B.

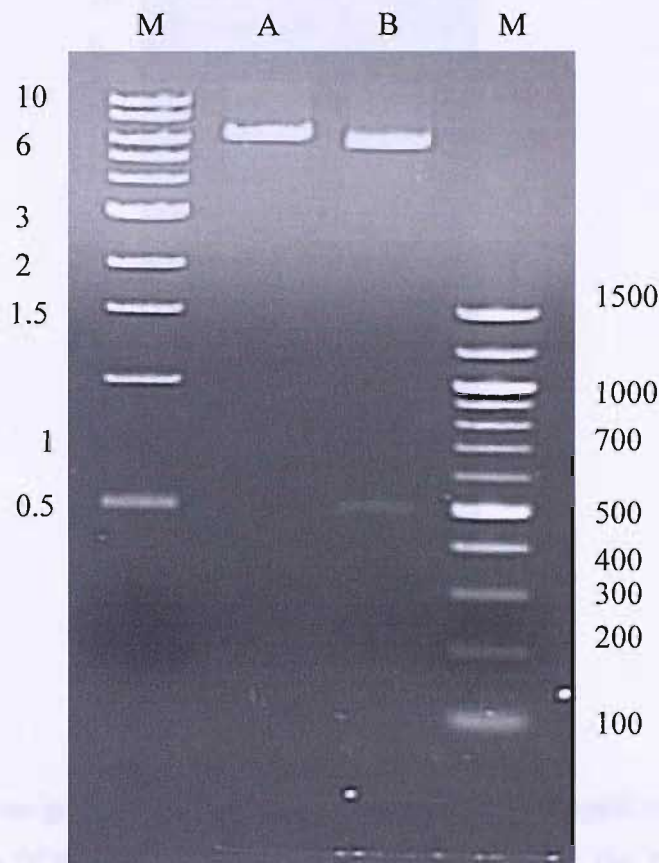


Figure 3.3.1 Agarose gel of TbMscL DNA. A single and a double digest of wild type DNA. Lane A shows a single digest with BamH1 producing linearised DNA. Lane B shows a double digest with BamH1 and Nde1 producing plasmid DNA and the 500 bp gene encoding MscL. The markers are: (left), 1Kb DNA ladder; (right), 100 bp DNA ladder.

3.3.2 Quik-change® site directed mutagenesis

Using the oligonucleotide primers listed in Tables 3.2.1-3.2.3, single tryptophan mutants were produced by Quik-change® site-directed mutagenesis. Following PCR, amplification of the product was checked by electrophoresis of 5 µl of the product on a 1 % agarose gel. Figure 3.3.2 shows the PCR products of V22W and F27W.

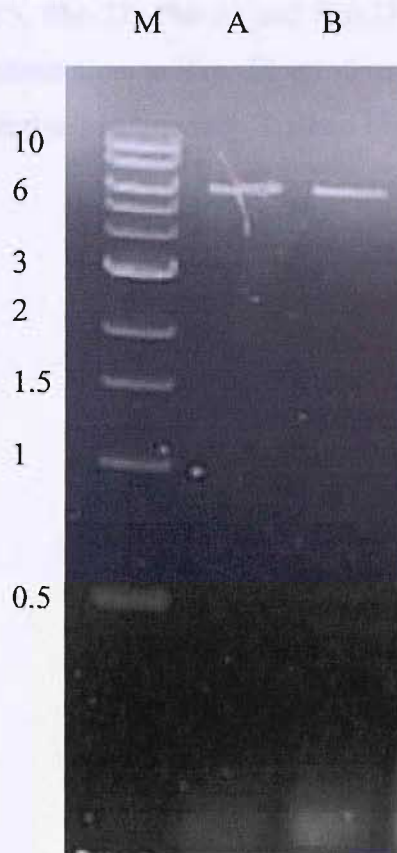


Figure 3.3.2 Agarose gel of PCR products following Quik-change® mutagenesis. Lane A shows the PCR product for V22W and lane B shows the PCR product for F27W. Both are at the expected position for TbMscL. The marker, M, is a 1 Kb DNA ladder.

3.3.3 Sequencing of TbMscL Trp constructs

Following Quik-change® mutagenesis and purification of plasmid DNA, samples were sent to MWG to confirm the correct mutation. Figure 3.3.3 shows an electroferragraph of V22W DNA. The nine His tag and the Met start codon are highlighted. The Val to Trp substitution is also shown. Partial electroferragraphs for the Val-22, Ile-23, Thr-25, Phe-27, Phe-34 and Ser-37 mutants are shown in Figure 3.3.4 highlighting the substitution to Trp. Electroferragraphs for all mutants shows that replacement of the original residue with Trp had been successful.

3.3.4. Expression and Purification of Mutants

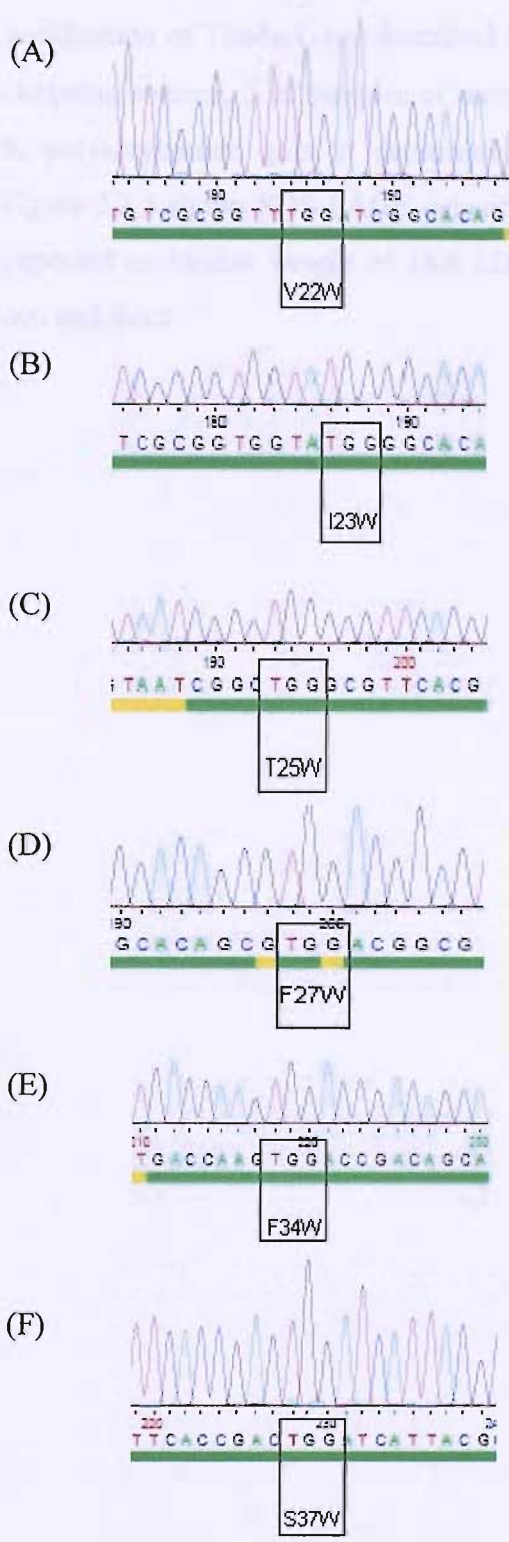


Figure 3.3.4 Electroferragrams of TbMscL mutants showing amino acid changes to Trp. (A) Val-22, (B) Ile-23, (C) Thr-25, (D) Phe-27, (E) Phe-34, and (F) Ser-37.

3.3.4 Expression and Purification of TbMscL

Following affinity purification of TbMscL (as described in Section 2.2.20) using a 1 ml HiTrap Nickel-chelating column, 5 μ l samples of each of the 1 ml eluted samples were run on 15 % polyacrylamide gels to determine which fractions contained purified TbMscL. Figure 3.3.5 shows SDS-PAGE gels of V22W and F27W showing the protein at the expected molecular weight of 18.6 kDa. Most of the protein was eluted in fractions two and three.



Figure 3.3.5 SDS-PAGE gels of V22W and F27W showing the protein at the expected molecular weight of 18.6 kDa. Most of the protein was eluted in fractions two and three.

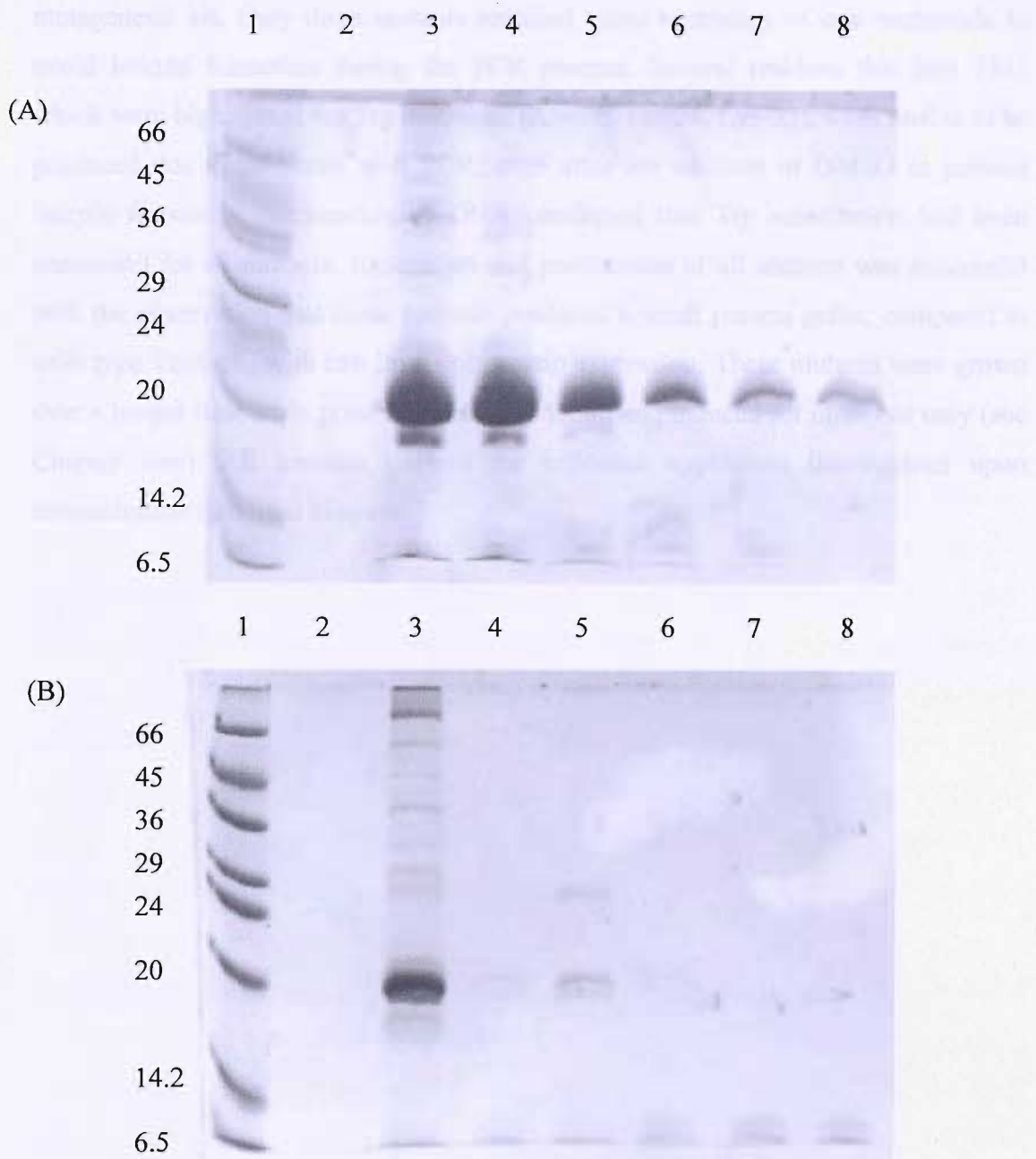


Figure 3.3.5 15 % SDS-polyacrylamide gel of (A) F27W and (B) the gain-of-function mutant V22W. Lane 1 contains *Sigma* low molecular weight markers (10 μ l) Lanes 2-8 show purified TbMscL monomer corresponding to different eluted fractions.

3.4 Discussion

Trp mutants of TbMscL on TM1 were generated using the Quick-change® mutagenesis kit. Only three mutants required silent mutations of one nucleotide to avoid hairpin formation during the PCR process. Several residues that line TM1 which were highlighted for Trp mutation, (Ala-26, Thr-28, Lys-33), were unable to be produced due to problems with PCR, even after the addition of DMSO to prevent hairpin formation. Sequencing of DNA confirmed that Trp substitution had been successful for all mutants. Expression and purification of all mutants was successful with the observation that some mutants produced a small protein pellet, compared to wild type TbMscL, with low levels of protein expression. These mutants were grown over a longer time scale prior to protein induction and induced for one hour only (see Chapter five). All mutants showed the expected tryptophan fluorescence upon reconstitution into lipid bilayers.

Chapter 4: Fluorescence Properties of Lipid Exposed mutants on TM1

4.1 Introduction

For clarity, results on the fluorescence properties of Trp mutants of TbMscL have been separated into different chapters based on whether the Trp residues face towards the centre of the channel, are involved in helix-helix contacts, or face outwards towards the lipid bilayer. The aim of the work in this chapter is to determine the accessibility of the inner ring of TM1 helices in TbMscL to the fatty acyl chains of the lipid molecules immediately surrounding the protein. The TM α -helices of TbMscL are arranged with the five TM1 helices lining the central pore within a ring of five TM2 helices. The major contacts with the surrounding lipid bilayer will be made by residues in TM2 (refer to Figure 1.9 in the general introduction) but several residues in TM1 also face directly towards the lipid bilayer. Figure 4.1.1 shows the transmembrane surface of TbMscL showing that some of the lipid-facing residues in TM1 are located within a cleft between TM2 helices. The figure also shows that, in general, lipid facing residues in TM2 are closer to the protein surface than those residues in TM1. Further, the way that the TM1 helices are tilted with respect to the bilayer normal means that lipid-facing residues towards the C-terminal end of TM1 are relatively close to the protein surface whereas those at the N-terminal end of TM1 are buried in crevices between the TM2 helices.

To determine differences between the fluorescence properties of tryptophan residues on TM1 and TM2, single Trp mutants of lipid facing residues were generated along TM1 and the emission maxima of residues were used to report changes in the local environment. Brominated lipids were used to assess differences in the accessibility of residues to the lipid phase and the water soluble quenchers acrylamide and iodide were used to assess accessibility of residues from the aqueous phase. Quenching of Trp fluorescence by phospholipids containing brominated fatty acyl chains provides a powerful technique for probing lipid-protein interactions (O'Keefe *et al.*, 2000; Alvis *et al.*, 2003; Williamson *et al.*, 2003; Lee, 2005; Powl *et al.*, 2005b). Quenching of Trp fluorescence by brominated phospholipids shows a sixth power dependence on distance between the bromine and Trp moieties with 50% quenching at a distance of

ca 8 Å (Bolen and Holloway, 1990). Thus efficient quenching of the fluorescence of a Trp residue located within a cavity by a brominated phospholipid would indicate that a phospholipid chain was able to penetrate into the cavity.

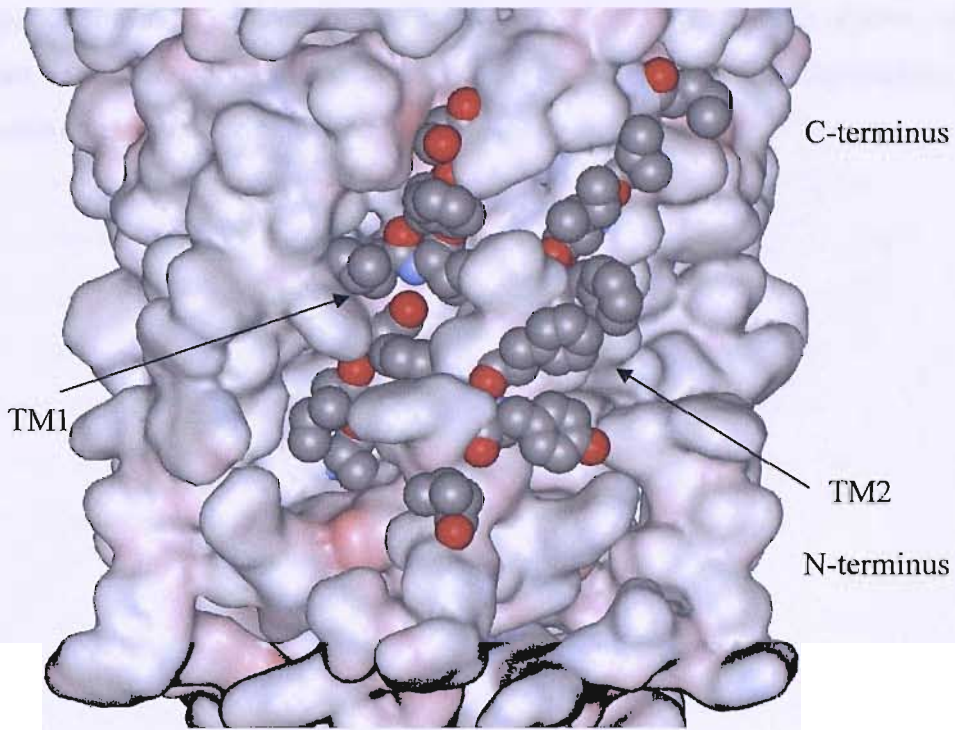


Figure 4.1.1 Surface representation of TbMscL with lipid facing residues on TM1 and TM2 shown in CPK format. A number of residues on TM1 face outwards towards the lipid bilayer. TM1 helices are tilted with respect to the bilayer normal so that lipid facing residues towards the C-terminal end of TM1 are relatively close to the protein surface whereas those at the N-terminal end are buried in crevices between the TM2 helices. The van der Waals surface of the protein is shown.

4.2 Fluorescence

The use of fluorescence as a tool for studying protein conformation and relating protein structure to function is an invaluable and widely used technique. The fluorescence of proteins can be attributed to the presence of several naturally occurring, or intrinsic, fluorophores and these are the aromatic amino acids tryptophan, tyrosine, and phenylalanine. Tryptophan normally dominates the fluorescence emission of proteins (Ladokhin, 2000).

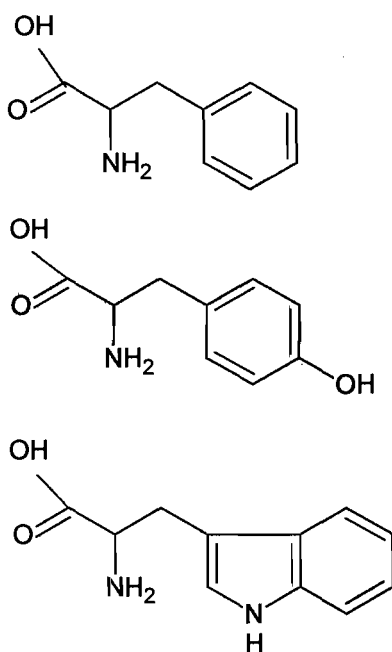


Figure 4.2.1 Structures of the three aromatic amino acids that contribute to the intrinsic fluorescence of proteins. A) Phenylalanine. B) Tyrosine and C) Tryptophan.

Fluorescence refers to the emission of light following excitation of electrons from of a ground state to an excited state following absorption of light. The process of absorption and emission of light is illustrated in the Jablonski diagram (Figure 4.2.2) where ground, first and second electronic states are depicted by S_0 , S_1 and S_2 respectively. The process of light absorption is almost instantaneous and takes approximately 10^{-15} seconds (Lakowicz, 1983). Almost all molecules occupy the lowest vibrational level of the ground electronic state at room temperature and during the excitation process electrons may occupy any one of the higher vibrational levels of the excited state, labelled 0, 1, and 2 in the diagram. Excitation is followed by relaxation of the molecule to the lowest vibrational level of S_1 in a process known as internal conversion, which takes around 10^{-12} seconds (Lakowicz, 1983). The molecule returns to the ground state from S_1 either by emitting heat or by emitting light, the latter being fluorescence. The light emitted from fluorescent molecules is at a longer wavelength than the exciting light due to the loss of energy during internal conversion, a phenomenon known as Stokes' shift.

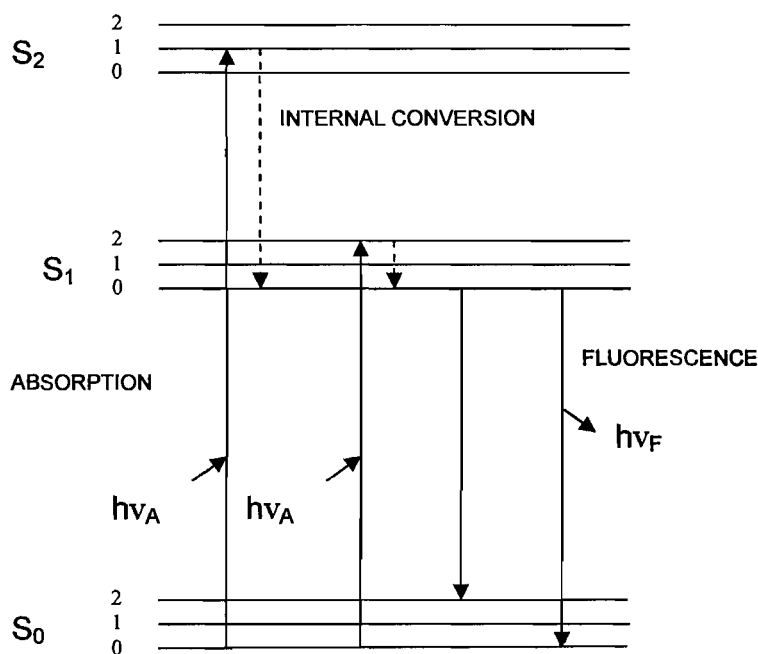


Figure 4.2.2 Jablonski diagram (Lakowicz, 1983). Illustration of the absorption and emission of light. S_0 , S_1 and S_2 represent the ground state and the first and second excited states respectively. Each electronic state has several different vibrational energy levels, depicted by the thinner lines.

4.2.1 Tryptophan Fluorescence

Absorbance of light by tryptophan is due to $\pi \rightarrow \pi^*$ transitions in the indole ring (Ladokhin, 2000). Due to the sensitivity of tryptophan emission to polarity and mobility of the surrounding environment, tryptophan is an important tool in looking at protein structure and conformation (Lakowicz, 1983). In aqueous solutions tryptophan displays a wide emission spectrum with a λ^{\max} centred around 350 nm with a peak width at half height of around 50 nm. In contrast, a Trp in a hydrophobic environment emits at around 320 nm thus tryptophan-scanning mutagenesis combined with fluorescence spectroscopy can provide information on the precise location of a Trp residue within a protein and its accessibility to the aqueous phase. Figure 4.2.3 shows the fluorescence emission spectra for free tryptophan in water and a Trp residue in MscL located in a hydrophobic environment.

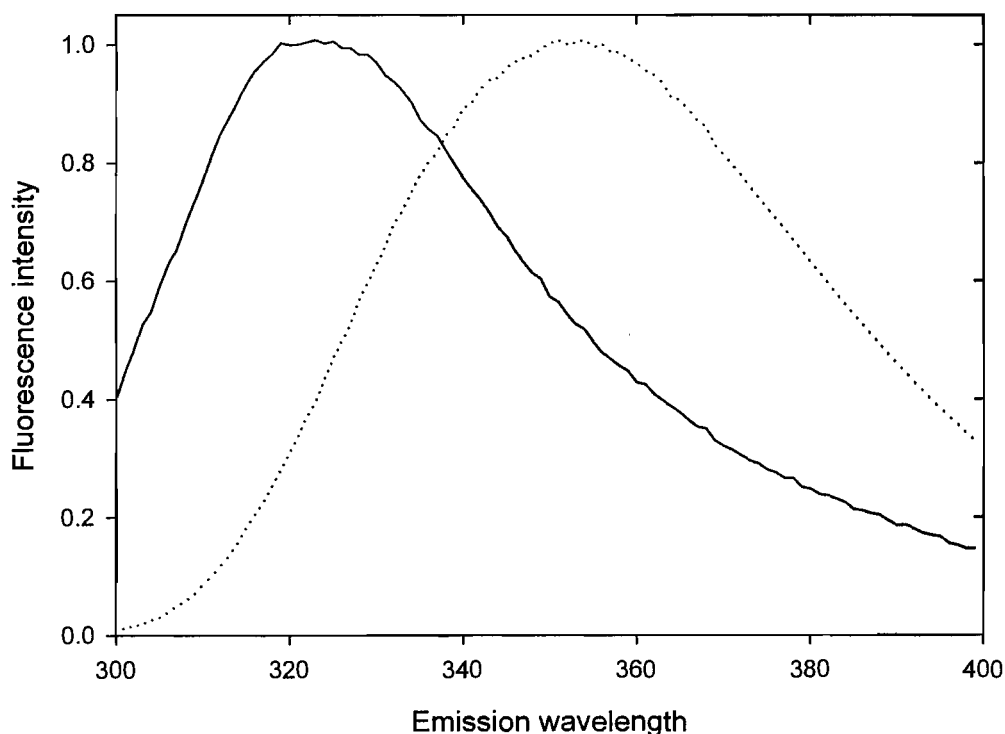


Figure 4.2.3 Fluorescence emission spectra of tryptophan indicating sensitivity to environment. The fluorescence emission spectrum, centred at 321 nm is shown for the TbMscL Trp-mutant F27W reconstituted into bilayers of di(C18:1)PC, indicating a very hydrophobic environment for the Trp (black line), and for free tryptophan in Hepes buffer with an emission spectrum centred at 352 nm (dotted line).

4.2.2 Quenching of Tryptophan Fluorescence

Fluorescence quenching refers to any process that decreases the fluorescence intensity of a given substance (Lakowicz, 1983). Quenchers of tryptophan fluorescence are used to assess the accessibility of tryptophan residues from either the aqueous or the lipid phase with different quenchers displaying particular sensitivities. Examples of quenchers include oxygen, iodide, bromide, and acrylamide. Brominated lipids can be used to assess the accessibility of a Trp residue to the lipid phase whereas molecules such as acrylamide or iodide can be used to assess the accessibility of a Trp residue from the aqueous phase.

Fluorescence quenching processes include collisional quenching, otherwise known as dynamic quenching, static quenching, and energy transfer. In collisional quenching the quencher must be able to diffuse to the fluorophore during the lifetime of the excited state in order to quench fluorescence. Collisional quenching of fluorescence may be described by the Stern-Volmer equation 4.1(Lakowicz, 1983).

$$F_0/F = 1 + k_q \tau_0 [Q] = 1 + K_{SV}[Q] \quad \text{Equation 4.1}$$

Here F_0 and F represent the fluorescence intensities in the absence and presence of quencher respectively, k_q is the bimolecular quenching constant, τ_0 is the lifetime of the fluorophore in the absence of quencher, and $[Q]$ is the quencher concentration. K_{SV} is the Stern-Volmer quenching constant.

In contrast to collisional quenching which is dependent on diffusion of the quencher, static quenching results from the formation of a complex between the quencher and the fluorophore when occupying a non-fluorescent ground state (Lakowicz, 1983). On absorption of light, the complex immediately returns to the ground state without photon emission.

Fluorescence energy transfer involves transfer of energy from the excited state of a donor fluorophore to an acceptor molecule. The extent of energy transfer is dependent upon several variables. These are the degree of overlap between the emission spectrum of the donor and the absorption spectrum of the acceptor, known as the overlap integral (J), the distance between the acceptor and donor, the relative orientation of the acceptor and donor dipoles, and the quantum yield of the fluorophore (Lakowicz, 1983). It is generally assumed that the dependence on orientation is averaged out by rapid thermal motion of the donor and acceptor so that the efficiency of energy transfer can then be used to calculate the distance between the donor and acceptor. The efficiency of energy transfer can be calculated simply from the intensity of fluorescence in the presence of acceptor (F_{da}) compared to that in the absence of acceptor (F_d) as given by Equation 4.2 (Ladokhin, 2000)

$$E = 1 - (F_{da}/F_d) \quad \text{Equation 4.2}$$

Efficiency of energy transfer can be related directly to the distance between the acceptor and donor according to Förster theory, as shown by Equation 4.3 (Lakowicz, 1983) (Ladokhin, 2000)

$$E = R_0^6 / (R_0^6 + r^6) \quad \text{Equation 4.3}$$

where r is the distance between donor and acceptor, and R_0 is the distance at which the efficiency of transfer is 50 %.

4.3 Materials and methods

4.3.1 Materials

All chemicals were obtained from Sigma or BDH unless otherwise stated.

Avanti Polar Lipids

di(C18:1)PC 1,2 dioleoyl-*sn*-glycero-3-phosphatidylcholine

Bachem

n-octyl β -D-glucopyranoside (OG)

4.3.2 Methods

4.3.2.1 In vivo cell viability assay for gain-of-function mutants

Gain of function mutants were identified using a liquid growth assay. *E.coli* BL21(DE3)pLyS transformants carrying the pET-19b plasmid with the Trp-mutated *TbMscL* gene were grown overnight at 37 °C in 10 mls LB containing ampicillin at 100 µg ml⁻¹ for 16 hours at 220 rpm. Overnight cultures (100 µl) were used to seed fresh LB (50 mL). Cultures were induced with 1 mM IPTG upon reaching an OD₆₀₀ of 0.2. Absorbance measurements were recorded every 30 minutes at 600 nm.

BL21(DE3)pLyS carrying the pET 19b vector with no MscL gene inserted were used as controls.

4.3.2.2 Preparation of lipid stocks

The appropriate lipid was dissolved in chloroform at a concentration of 20 mg ml⁻¹.

4.3.2.3 Preparation of brominated lipid stocks

A solution of lipid in chloroform was made at 20 mg ml⁻¹ and brominated by dropwise addition of bromine until a pale yellow colour could be seen. Excess bromine was removed by vacuum on a rotary evaporator and the dried lipid was dissolved in chloroform at 20 mg ml⁻¹, sealed under nitrogen and stored at -20 °C until use.

4.3.2.4 Hepes Buffer

Hepes buffer was prepared by making a solution of 20 mM Hepes, 100 mM KCl and 1 mM EGTA in distilled water. The pH was adjusted to pH 7.2 with KOH.

4.3.2.5 Preparation of Potassium Cholate

48.9 mmoles of cholic acid was dissolved in a minimal volume of methanol at 35 °C. Equimolar amounts of KOH were added to the cholic acid in methanol and incubation

was continued. The potassium cholate was precipitated from the methanol by the addition of an excess of diethyl ether. Solvent was filtered off using a Buchner funnel and the solid potassium cholate product was dried down under vacuum for at least 16 hours to ensure complete removal of diethyl ether.

To make cholate buffer 15 mM potassium cholate was dissolved in Hepes Buffer.

4.3.2.6 Reconstitution of TbMscL into lipid bilayers by dilution

Following purification of TbMscL, reconstitution into phospholipid bilayers was achieved by mixing lipid, in cholate, with protein already in Octyl Glucoside (OG) in the desired concentrations. This was followed by rapid dilution into buffer below the critical micelle concentration (CMC) of the detergent to reform membranes.

0.47 μ moles of lipid was dried down onto walls of a scintillation vial and 400 μ l of cholate buffer was added. This was sealed under nitrogen, warmed, vortexed and sonicated to clarity in a bath sonicator (Ultrawave). 4.7 nmoles of TbMscL was added to the lipid solution resulting in a 100:1 molar ratio of lipid: protein monomer. The sample was then incubated at 25 $^{\circ}$ C for 15 minutes. 250 μ l of the sample was then diluted into 2.75 mls Hepes buffer and incubated at 25 $^{\circ}$ C. Fluorescence measurements were recorded using the SLM-8000C fluorimeter.

4.3.2.7 Fluorescence Quenching of TbMscL by Acrylamide

Samples were prepared as detailed in section 4.3.2.6. A 1 M stock of acrylamide was prepared in Hepes buffer and added to the sample at a final concentration of 300 mM. The inner filter effect was minimised by exciting fluorescence at 295 nm. Corrections for the inner filter effect were made by applying the correction factor $10^{0.5c\epsilon}$ where ϵ is the molar extinction coefficient at 295 nm ($0.070 \text{ M}^{-1} \text{ cm}^{-1}$), and c is the concentration of quencher.

4.3.2.8 Fluorescence Quenching of TbMscL by Iodide

Samples were prepared as detailed in section 4.3.2.6. A 1 M stock of iodide (1M iodide and 100 mM potassium thiosulphate) was prepared in Hepes buffer and added to the sample at a final concentration 0.45 M using Hepes buffer containing 1 M KCl and 100 mM potassium thiosulphate to maintain a constant ionic strength for both F (KI) and F_0 (KCl) measurements of 0.91 M. The inner filter effect was minimised by exciting the fluorescence at 295 nm. Corrections for the inner filter effect were made by applying the correction factor $10^{0.5c\epsilon}$ where ϵ is the molar extinction coefficient at 295 nm ($0.032 \text{ M}^{-1} \text{ cm}^{-1}$), and c is the concentration of quencher.

4.3.2.9 Fluorescence Measurements

Tryptophan fluorescence intensities were measured at 330 nm with an excitation wavelength of 280 nm, for $0.98 \mu\text{M}$ TbMscL in Hepes buffer at 25°C , using an SLM-Aminco 8000C fluorimeter. 4 nm slit widths were used in all experiments with the emission slit at 8 nm. Fluorescence intensities were corrected for light scatter by the subtraction of a suitable phospholipid blank.

Fluorescence emission spectra were recorded between 300 nm and 400 nm. Spectra were then fitted to a skewed Gaussian using equation 4.4

$$F = F_{\max} \exp(-(\ln 2) [\ln(1 + 2b(\lambda - \lambda_{\max})/w_\lambda)/b]^2) \quad \text{Equation 4.4}$$

where F and F_{\max} are the fluorescence intensities at λ and λ_{\max} respectively, b is the skew parameter, and w_λ is the peak width at half height.

4.3.2.10 Statistical Analysis

Data were analysed, where appropriate, using the Kruskal-Wallis using a Dunn's multiple comparison test. Results were considered significant when $p < 0.05$ (*).

4.3 Results

In the studies reported here lipid-facing residues in TM1 were mutated to Trp. To see to what extent these residues were buried, Trp residues were introduced into the three dimensional structure of TbMscL using the MSI viewer programme and the Trp residues were rotated to remove any contacts between atoms that were within 70% of the sum of the covalent radii (Figure 4.4.1). Some mutants such as I23W are located within a cleft in the protein surface whereas others, such as that in the mutant F34W, are surface exposed, like the Trp residue in TM2 in the mutant Y87W.

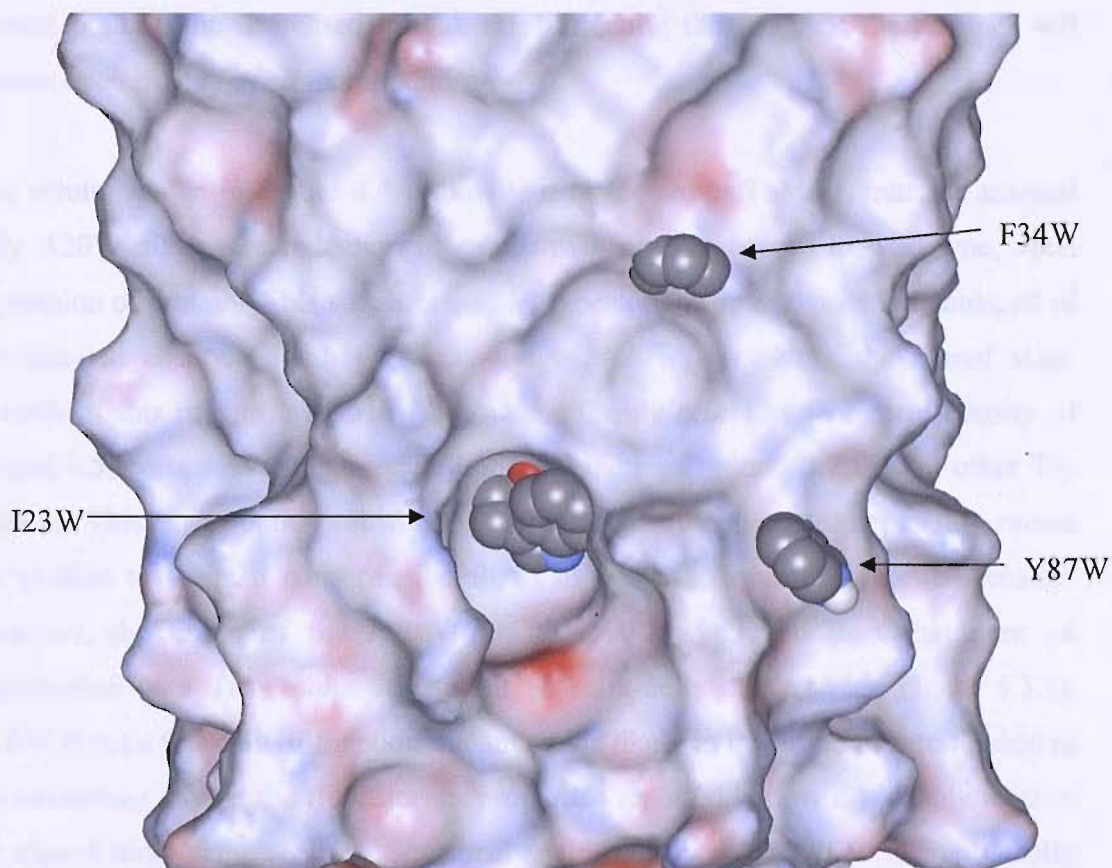


Figure 4.4 View of the lipid-exposed surface of TbMscL with Trp residues at positions 23 and 34 in TM1 and position 87 in TM2 shown in space-fill format. The surface is coloured according to electrostatic potential. I23 is located towards the N-terminus of TbMscL and is buried within a cleft in the protein surface between TM2 helices. F34 is located at the C-terminus of TbMscL and is at a position that is relatively close to the protein surface, similar to Y87. The solvent accessible surface is shown, with a solvent of radius 3Å

4.4.1 Functional Analysis of Trp-mutants of TbMscL

Mutation of TbMscL can lead to two phenotypes. Mutations that result in the channel opening at lower tensions are termed Gain-of-Function mutations (GOFs) and mutations that result in a loss of function or that need higher tension to cause opening are termed Loss-of-Function mutations. To ascertain whether substituting lipid exposed residues on TM1 with Trp resulted in GOF mutations, an *in vivo* cell viability assay for this phenotype was carried out as outlined in Section 4.3.2. In this assay, a GOF phenotype is recognised by a decrease in growth rate for *E. coli* expressing the mutant protein, the decreased growth rate reflecting the fact that the channel will remain open in the *E. coli* membrane.

The results shown in Figure 4.4.1 show that of the seven TbMscL mutants assayed only A20W displays a reduction in cell growth rate, compared to wild type, upon expression of protein. This suggests that, as expected for lipid-exposed mutants, all of the mutated channels, with the exception of A20W, remain in the closed state. Growth of this mutant appears to be impaired, only reaching an optical density of around 0.5, compared to an average optical density of around 0.7 for the other Trp mutants. This suggests that substituting alanine for tryptophan at this position causes the protein to adopt a conformation that can open at lower than normal tension. However, the effect of the A20W mutation is less marked than that seen on introduction of a Trp residue at a point of helix-helix contact (see Figure 6.3.1). A20W is not a full gain of function mutant and is likely to be closed at zero tension in the membrane so that the fluorescence properties reported here will probably refer to the closed state of the channel. Statistical analysis shows that A20W is significantly different to I23W but not the other mutants assayed. As I23W only has a slightly higher OD than the wild type absorbance at 300 minutes, this implies that there is no real difference and so it can therefore be concluded that A20W is probably in the closed state. The observation that all mutants, displayed a normal phenotype allowed further analysis and characterisation by fluorescence spectroscopy and fluorescence quenching.

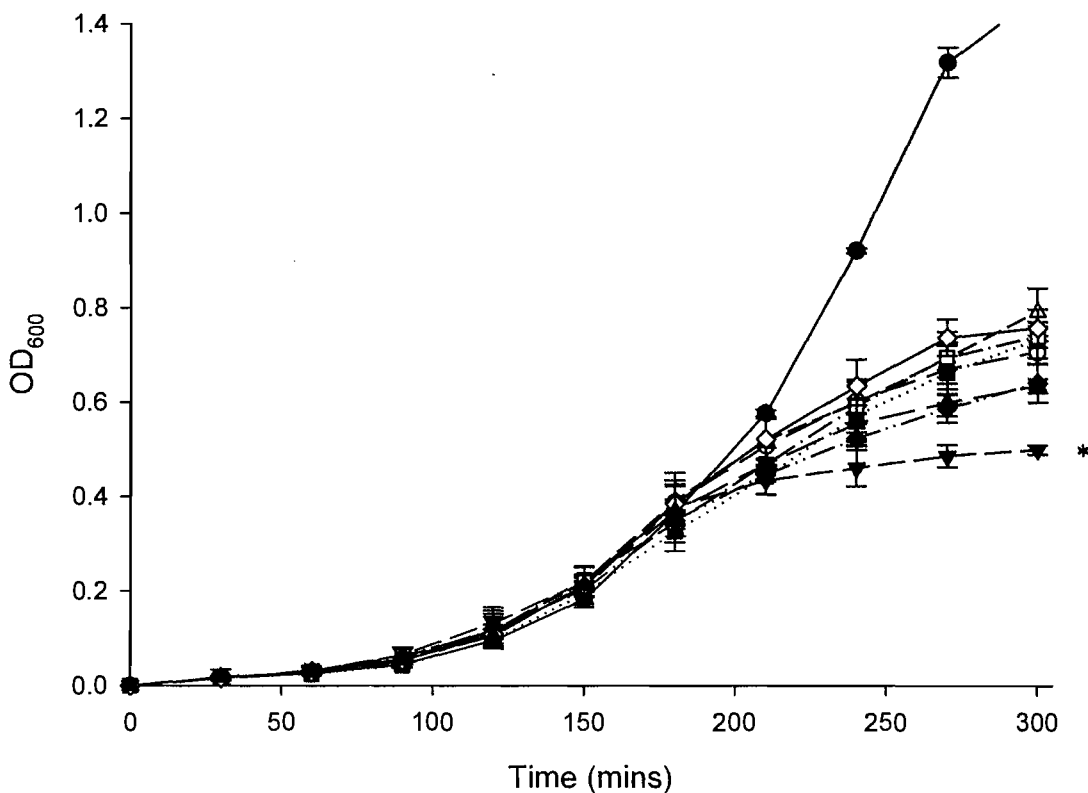


Figure 4.4.1 *In Vivo* assay for Gain of Function mutants. *E. coli* BL21(DE3)pLysS transformants carrying the pET-19b plasmid with the Trp-mutated *TbMscL* gene were grown in Luria both containing ampicillin ($100 \mu\text{g ml}^{-1}$) to an optical density of OD_{600} of 0.2 and expression was induced by addition of 1 mM IPTG. The optical density was measured every 30 minutes to determine which mutants produced a Gain-of-function (GOF) phenotype. *TbMscL* mutants expressed were: wild type, (○); A20W, (▼); I23W, (△); F27W, (■); L30W, (□); V31W, (◆); and F34W, (◇); S37W, (▲). BL21(DE3)pLysS cells with the pET 19b vector and with no *MscL* gene inserted were grown as a control (●). Error bars are standard deviations obtained from the average of three determinations.

4.4.2 Fluorescence emission spectra for Trp-mutants of TbMscL

Residues on TM1 that face outwards towards the lipid bilayer were mutated to Trp by site-directed mutagenesis. Mutants were then reconstituted into bilayers of di(C18:1)PC at a molar ratio of lipid: protein monomer of 100:1. The fluorescence emission spectra shown in Figure 4.4.2 were fitted to the equation for a skewed Gaussian (equation 4.4) to obtain accurate values for the wavelength of maximum fluorescence emission (Table 4.4.1). The emission width at half height varied from 50.4 for F27W to ca 66 nm for F34W (Table 4.4.1). These results are largely consistent with the relationship between fluorescence emission maxima and peak width established by Ladokhin *et al.* (Ladokhin, 2000) which showed that peak width increased with increasing fluorescence emission maximum. The fluorescence intensity varies markedly between the mutants shown in Figure 4.4.2. Various groups present in a protein are capable of quenching Trp fluorescence so that Trp fluorescence intensity is highly variable (Lakowicz, 1983).

The fluorescence emission maximum for tryptophan in water is 351 nm, whereas the fluorescence emission maximum for a Trp residue in a very hydrophobic environment is ca 320 nm, as shown in Figure 4.2.3. Experiments with KcsA, where the Trp residues are located at the ends of the transmembrane helices, show that a Trp residue located in the glycerol backbone region of the lipid bilayer has a fluorescence emission maximum at 332 nm (Alvis *et al.*, 2003). Results by Powl *et al.* showed the region of TM2, the outer lipid-facing helix, that spans the hydrocarbon core of the bilayer when reconstituted into bilayers of di(C18:1)PC runs from L69, with a fluorescence emission maximum of 332.8 nm, to L91, with a fluorescence emission maximum of 331.7 nm (Powl *et al.*, 2005b). A Trp residue in the middle of the helix, F80W, gave an emission maximum of 320 nm. The fluorescence emission maximum for F27W (321 nm) is blue shifted, consistent with a hydrophobic location towards the centre of the bilayer, similar to F80W, whereas the fluorescence emission maximum for A20W, which is located towards the cytoplasmic interface, is ca. 329 nm, similar to L91 on TM2. S37W has a red shifted emission spectrum of 336 nm, consistent with its location in the headgroup region, similar to that of L69.

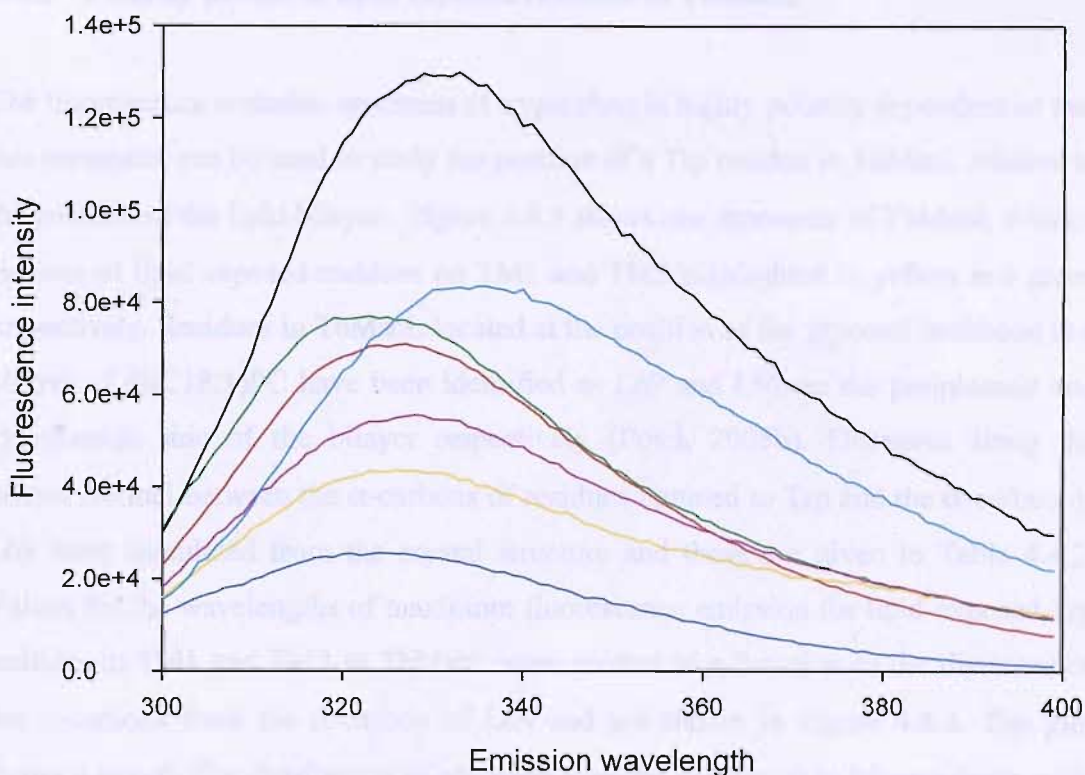


Figure 4.4.2 Fluorescence emission spectra of lipid exposed Trp-mutants of TbMscL. Purified TbMscL was reconstituted in di(C18:1)PC and fluorescence was excited at 280 nm. Samples were as follows: A20W, (-); I23W, (-); F27W, (-); L30W, (-); V31W, (-); F34W, (-); and S37W, (-). The concentration of TbMscL was 0.98 μ M and the molar ratio of lipid to protein monomer was 100:1.

Mutant	λ^{\max} (nm) in di(C18:1)PC	ω (nm)
A20W	329.3 \pm 0.3	58.4 \pm 0.3
I23W	325.2 \pm 0.1	50.9 \pm 0.2
F27W	321.0 \pm 0.2	50.4 \pm 0.4
L30W	327.6 \pm 0.1	57.8 \pm 0.2
V31W	323.1 \pm 0.3	61.5 \pm 0.7
F34W	326.2 \pm 0.4	66.6 \pm 0.9
S37W	335.9 \pm 0.1	58.4 \pm 0.2

Table 4.4.1 Fluorescence properties of lipid-exposed Trp-mutants of TbMscL reconstituted into bilayers of di(C18:1)PC and excited at 280 nm. The molar ratio of lipid to protein monomer was 100:1 and the concentration of TbMscL was 0.98 μ M.

4.4.3 Polarity profile of lipid exposed residues in TbMscL

The fluorescence emission spectrum of tryptophan is highly polarity dependent so that this parameter can be used to study the position of a Trp residue in TbMscL relative to the position of the lipid bilayer. Figure 4.4.3 shows one monomer of TbMscL with α -carbons of lipid exposed residues on TM1 and TM2 highlighted in yellow and green respectively. Residues in TbMscL located at the position of the glycerol backbone in a bilayer of di(C18:1)PC have been identified as L69 and L92 on the periplasmic and cytoplasmic side of the bilayer respectively (Powl, 2005b). Distances along the bilayer normal between the α -carbons of residues mutated to Trp and the α -carbon of L69 were calculated from the crystal structure and these are given in Table 4.4.2. Values for the wavelengths of maximum fluorescence emission for lipid-exposed Trp residues in TM1 and TM2 in TbMscL were plotted as a function of the distances of the α -carbons from the α -carbon of L69 and are shown in Figure 4.4.4. The plot shows a trough like distribution of emission maxima in relation to bilayer depth, with the exception of residues I77W and L30W. The fluorescence of residues located towards the centre of the bilayer is blue shifted relative to that of residues located towards either the periplasmic or cytoplasmic interfaces. It can be seen that the position of F27W in the bilayer is comparable to that for F80W with a fluorescence emission maximum of 321 nm. Finally, S37W has a relatively long wavelength emission, consistent with a location for S37 in the lipid headgroup region of the bilayer, as previously suggested for residues L69 in TM2.

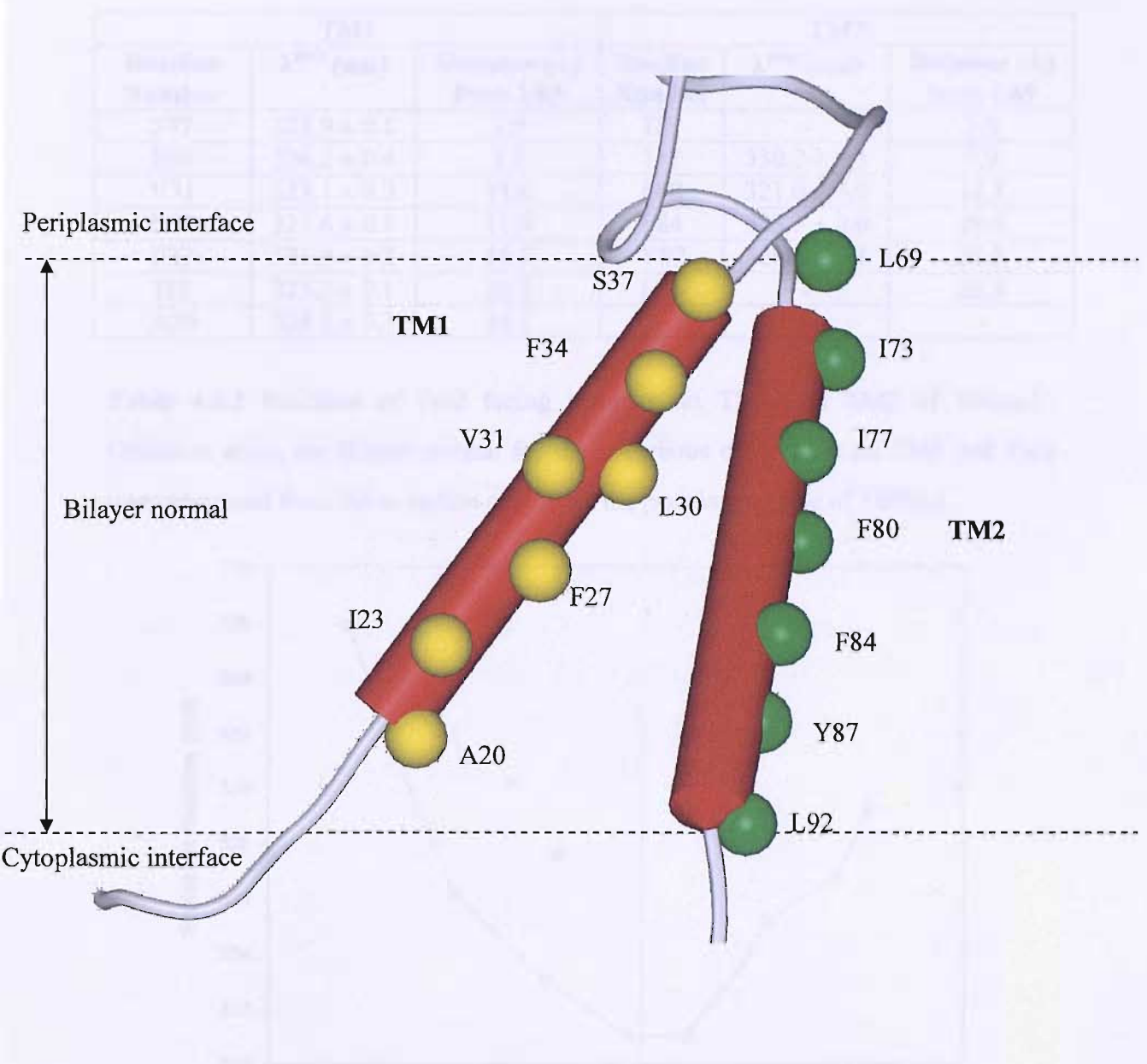


Figure 4.4.3 TbMscL monomer showing α -carbons of lipid facing residues on TM1 and TM2 in yellow and green respectively. Residues L69 and L92 are located at the periplasmic and cytoplasmic interfaces respectively. The direction of the bilayer normal is shown.

TM1			TM2		
Residue Number	λ^{\max} (nm)	Distance (Å) from L69	Residue Number	λ^{\max} (nm)	Distance (Å) from L69
S37	335.9 ± 0.1	2.9	I73	-	5.0
F34	326.2 ± 0.4	7.1	I77	330.2 ± 0.1	9.9
V31	323.1 ± 0.3	11.6	F80	321.0 ± 0.0	14.3
L30	327.6 ± 0.1	11.6	F84	323.5 ± 0.0	19.0
F27	321.0 ± 0.2	16.3	Y87	326.8 ± 0.1	23.5
I23	325.2 ± 0.1	20.1	L91	-	28.5
A20	329.3 ± 0.3	24.3	-	-	-

Table 4.4.2 Positions of lipid facing residues on TM1 and TM2 of TbMscL. Distances along the bilayer normal for the α -carbons of residues on TM1 and TM2 were measured from the α -carbon of L69 on the periplasmic side of TbMscL.

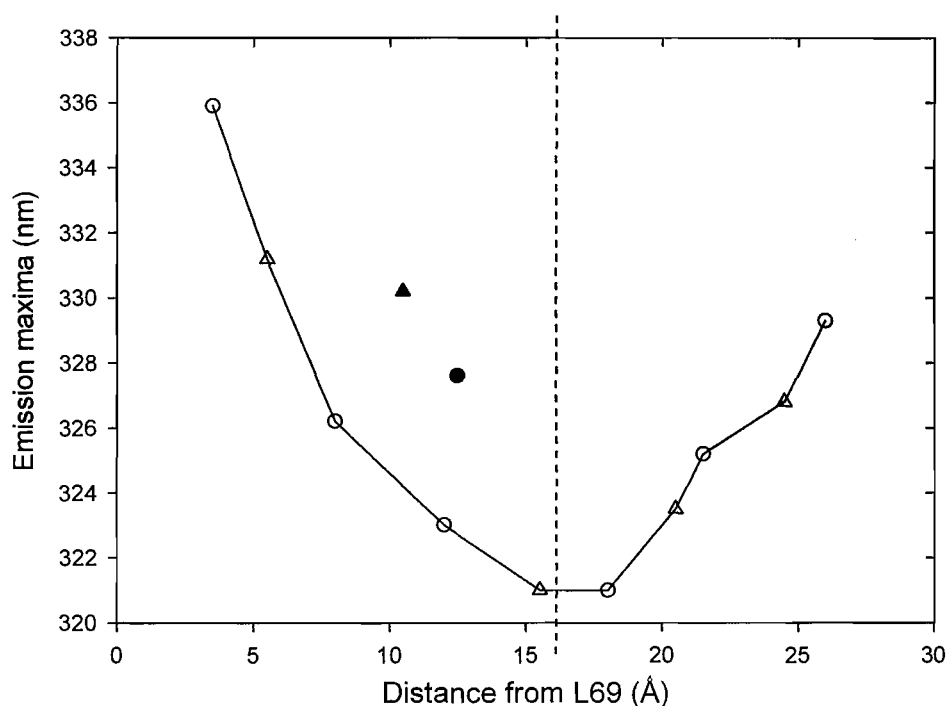


Figure 4.4.4 Polarity profile of lipid facing residues on TM1 and TM2 of TbMscL. Circles represent Trp residues on TM1 and triangles represent Trp residues on TM2. Emission maxima for residues on TM2 were obtained from previously published data (Powl *et al.*, 2005b). The dashed line denotes the centre of the bilayer. Wavelengths of maximum emission (nm) are plotted as a function of the distance (Å) along the bilayer normal of the α -carbon of the residue from that of L69. The filled symbols (▲; ●) are the results for I77W and L30W respectively.

4.4.4 Fluorescence quenching of TbMscL by brominated phospholipids

Fluorescence quenching by brominated phospholipids was used as a tool to assess the accessibility of Trp residues from the lipid phase. Purified TbMscL was reconstituted as described in Section 4.3.2.6 into bilayers of di(C18:1)PC and di(Br₂C18:0)PC at a 100:1 molar ratio of phospholipid to TbMscL monomer. Generation of large unsealed membrane fragments was achieved by a 12-fold dilution from cholate buffer into Hepes buffer to drop the concentration of cholate below its critical micelle concentration. The Trp fluorescence emission intensity was recorded at 330 nm and results were expressed as F/F_0 (Table 4.4.3) where F is the fluorescence intensity of TbMscL in brominated lipid and F_0 is the fluorescence intensity of TbMscL in non-brominated lipid. Figure 4.4.5 shows fluorescence quenching plotted as a function of the distance of the Trp residue from L69. It is clear from the results that residue L30W which is positioned towards the centre of the bilayer is quenched the most by brominated phospholipids and I23W, F34W, and S37W, which are located further away from the centre of the bilayer, are quenched by a lesser extent. A20W is quenched more than expected given its position towards the N-terminus of TbMscL and buried deep with the cavity between TM2 helices.

Mutant	Distance (Å) from L69	F/F_0 in di(Br ₂ C18:0)PC
S37W	2.9	0.54 ± 0.02
F34W	7.1	0.51 ± 0.02
V31W	11.6	0.63 ± 0.03
L30W	11.6	0.41 ± 0.04
F27W	16.3	0.45 ± 0.01
I23W	20.1	0.50 ± 0.01
A20W	24.3	0.42 ± 0.02

Table 4.4.3 Quenching of Trp fluorescence by brominated phospholipids. Mutants were reconstituted into bilayers of di(C18:1)PC and di(Br₂C18:0)PC. Fluorescence intensities were recorded at 330 nm and are expressed as F/F_0 where F and F_0 are fluorescence intensities for TbMscL reconstituted into di(C18:1)PC and di(Br₂C18:0)PC respectively. Values and standard deviations were obtained from the average of three determinations in duplicate.

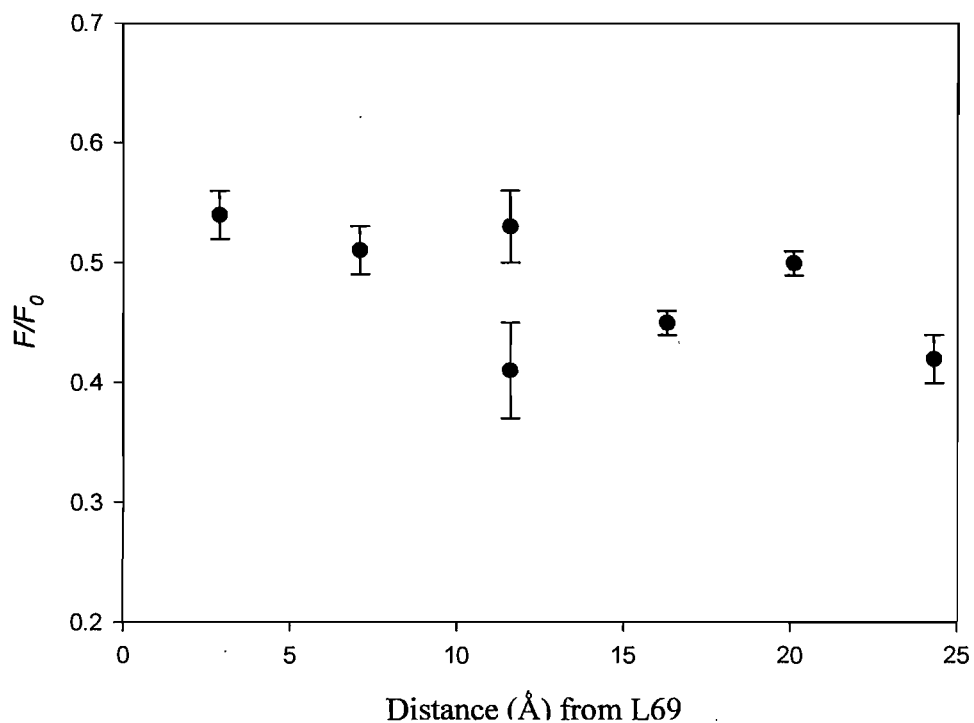


Figure 4.4.5 Fluorescence quenching of lipid facing residues on TM1 by brominated phospholipids. The fluorescence intensity was recorded at 330 nm and the results are expressed as F/F_0 plotted against distance of the Trp residue from L69.

4.4.5 Fluorescence quenching of TbMscL by acrylamide

Fluorescence quenching of lipid facing residues on TM1 by acrylamide was used to assess the accessibility of Trp residues in TbMscL from the aqueous phase in bilayers of di(C18:1)PC. TbMscL was reconstituted into bilayers of di(C18:1)PC at a 100:1 molar ratio of phospholipid to TbMscL monomer as previously described. To establish whether quenching by acrylamide fits to the Stern-Volmer equation, fluorescence intensities were plotted as a function of acrylamide concentration. As shown in Figure 4.4.6 a plot of fluorescence intensity versus acrylamide concentration was linear up to 300 mM for both I23W on TM1 and F80W on TM2, showing that the data fit to the Stern-Volmer equation.

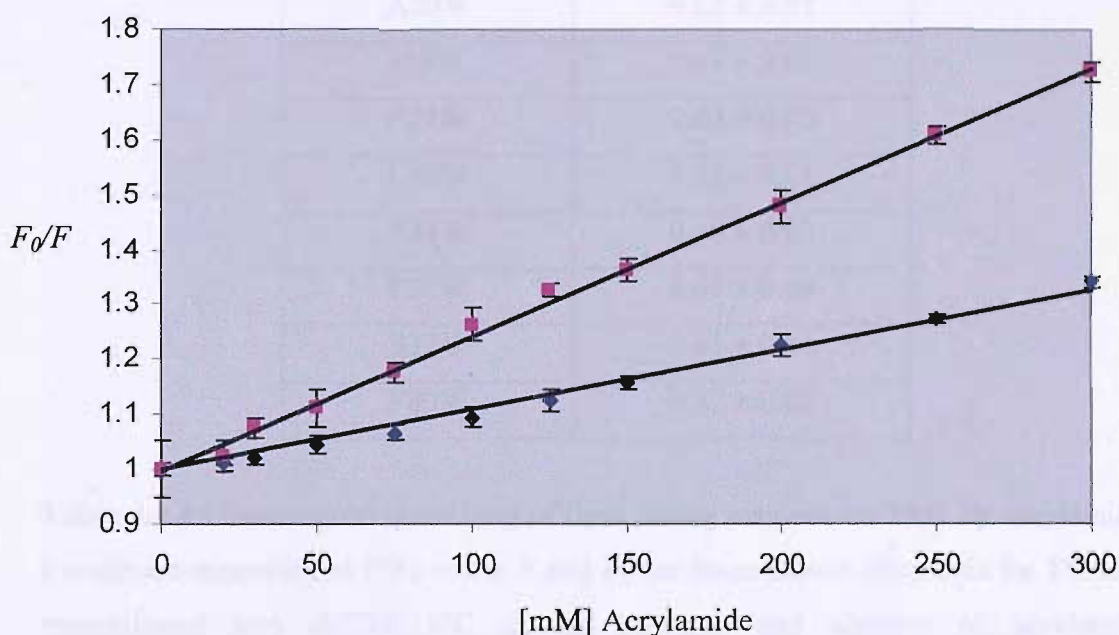


Figure 4.4.6 Stern-Volmer plots for quenching of the Trp fluorescence of TbMscL by acrylamide. Trp mutants were reconstituted into bilayers of di(C18:1)PC. Fluorescence intensities are expressed as a ratio of F_0/F where F_0 and F are the intensities in the absence and presence of acrylamide, respectively. Trp mutants are F80W (\blacklozenge) and I23W (\blacksquare).

Values of F/F_0 for the Trp mutants in di(C18:1)PC in the presence of 300 mM acrylamide are shown in Table 4.4.4. The results show a similar level of quenching for all mutants with the exception of V31W which shows a slightly reduced level of quenching. These results are surprising. Powl *et al.* (Powl *et al.*, 2005b) showed that levels of quenching for Trp mutants in TM2 varied between F/F_0 values of 0.75 and 0.45 for F80W and E103W respectively, for 250 mM acrylamide, a result repeated here for F80W (Table 4.4.4). The comparison with the results for Trp mutants in TM2 suggests that residues in TM1 are generally more accessible to acrylamide than those on TM2.

Mutant	F/F_0 in di(C18:1)PC
A20W	0.62 ± 0.03
I23W	0.61 ± 0.02
F27W	0.63 ± 0.05
L30W	0.63 ± 0.01
V31W	0.68 ± 0.02
F34W	0.61 ± 0.04
S37W	0.61 ± 0.03
F80W	0.72 ± 0.02

Table 4.4.4 Fluorescence quenching of lipid facing residues on TM1 by acrylamide. Results are expressed as F/F_0 where F and F_0 are fluorescence intensities for TbMscL reconstituted into di(C18:1)PC in the presence and absence of acrylamide respectively. Values and standard deviations were obtained from the average of three determinations in duplicate.

4.4.6 Fluorescence quenching of TbMscL by Iodide

The results obtained for fluorescence quenching by acrylamide show a similar level of quenching for all mutants. Whereas acrylamide is a neutral quencher, iodide is charged and so may show larger differences in accessibility. Values of F/F_0 for Trp mutants reconstituted into bilayers of di(C18:1)PC in the presence of 450 mM iodide are shown in Figure 4.4.7. The results show some differences in quenching between mutants with the Trp residues in A20W, I23W and S37W quenching the most. This is consistent with a location for these residues at the bilayer interface. Residues F27W and V31W are quenched the least by iodide suggesting that these residues are not as accessible to the aqueous phase. In this case, L30W, surprisingly, appears to be quenched by iodide to the same extent as residues located at the bilayer interface.

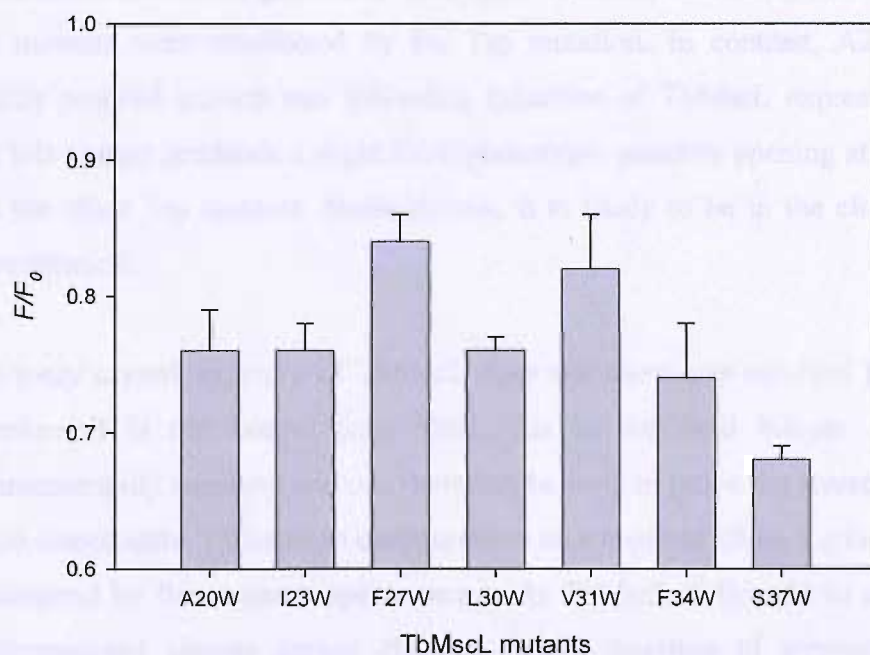


Figure 4.4.7 Fluorescence quenching of lipid facing residues on TM1 by iodide. Results are expressed as F/F_0 where F and F_0 are fluorescence intensities for TbMscL reconstituted into di(C18:1)PC in the presence and absence of iodide respectively. The ionic strength was kept constant at 0.91M. Bar charts show the average of three determinations and standard deviations in duplicate.

4.5 Discussion

4.5.1 Effects of Trp mutants of TbMscL on channel function

Residues on TM1 that were lipid facing were mutated to tryptophan using site-directed mutagenesis. In order to establish whether the insertion of a Trp residue affected function of TbMscL, an *in vivo* cell viability assay was carried out in order to screen for any gain-of function mutants. Gain-of-function mutations are characterised by decreased growth rates, presumably as a consequence of the open channel compromising membrane integrity. The results (Figure 4.4.1) show that the host cell, in the absence of the plasmid encoding *TbMscL* gene, grows to a high optical density and that expression of wild type TbMscL reduces the growth rate. The results with the lipid facing mutants of TbMscL show that all but one of the mutants, A20W, resulted in the same effects on growth as wild type TbMscL, indicating that function of the Trp mutants were unaffected by the Trp mutation. In contrast, A20W showed a slightly reduced growth rate following induction of TbMscL expression indicating that this mutant produces a slight GOF phenotype, possibly opening at lower tensions than the other Trp mutants. Nevertheless, it is likely to be in the closed state upon reconstitution.

The x-ray crystal structure of TbMscL does not show any resolved lipid molecules therefore it is not known how MscL sits in the lipid bilayer. Tryptophan is environmentally sensitive and can therefore be used to probe the structure of TbMscL in the closed state. Changes in conformation as a result of changing the lipid can also be detected by fluorescence spectroscopy. As TbMscL is thought to undergo a large conformational change during channel gating, insertion of tryptophans into key regions, thought to move between the closed and open states, can be used to detect any conformational changes of TbMscL as a result of movement of transmembrane α -helices. Upon channel opening, models show rotation of helices, resulting in thinning of the lipid bilayer surrounding TbMscL (Perozo *et al.*, 2002a) and movement of residues in and out of the bilayer. Rotation of helices during channel gating is thought to create a large pore with more pore-lining residues than in the closed state. To understand how the Trp fluorescence data is related to channel structure, it is important to understand what determines Trp fluorescence characteristics. Powl *et al.*

studied lipid-exposed Trp mutants in TM2 (Powl *et al.*, 2005b). The results showed that shifts in λ^{\max} were consistent with the crystal structure of TbMscL. This poses the question as to whether lipid-exposed Trp mutants in TM1 show the same consistency and whether buried residues share the same characteristics as lipid exposed residues. This may lead to an understanding of the solvation properties of TbMscL and whether lipid fatty acyl chains can penetrate into clefts present on the surface of TbMscL.

The Trp mutants of TbMscL were reconstituted into bilayers of di(C18:1)PC and their fluorescence emission maxima were determined. These are listed in Table 4.4.1. Most noticeable from this data is that F27W is the most blue shifted of the lipid facing mutants suggesting that F27 is located in the centre of the bilayer. As shown in Figures 4.4.3 and 4.5.1, residue 27 in TM1 is located at a similar distance from L69 along the bilayer normal to residue 80 in TM2. The Trp fluorescence emission maximum for F80W is also at 321 nm, suggesting that the Trp residues in F27W and F80W experience similar environments despite the fact that the Trp in F80W is surface exposed whereas that in F27W is buried below the protein surface (Figure 4.5.1).

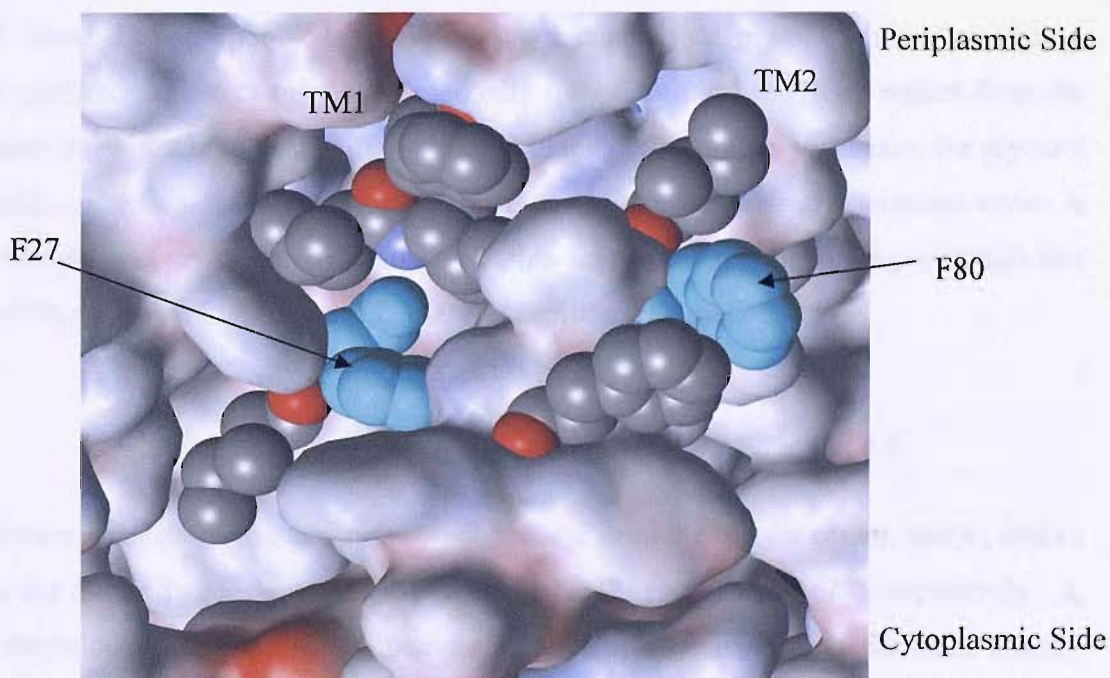


Figure 4.5.1 Surface representation of TbMscL with lipid facing residues on TM1 and TM2 shown in space-fill format. F27W and F80W (coloured in blue) are located in the centre of the bilayer on TM1 and TM2 respectively.

Moving in either direction from position 27 results in shifts in fluorescence emission maxima to longer wavelength, consistent with an increasingly polar environment for the Trp. From the crystal structure of TbMscL, the separation distance along the bilayer normal between the α -carbons of residues 69 and 92 is 31.8 Å which therefore defines the bilayer centre as 15.9 Å from L69. Table 4.4.2 lists and Figure 4.4.4 plots the fluorescence emission maxima as a distance of the separation from L69 along the bilayer normal for Trp residues in TM1 and TM2. Residues F27W and F80W have the most blue shifted emission maxima of 321 nm and are at the centre of the bilayer. Residues to the left of the plot represent residues on the periplasmic side of the membrane and residues on the right representing residues on the cytoplasmic side of the membrane. Immediately noticeable is the asymmetric distribution of fluorescence emission maxima with corresponding distance away from the centre of the bilayer on either side. The shape profile for the relationship between Trp fluorescence emission maxima and depth in the bilayer can be compared to models of how the dielectric constant is expected to change across a bilayer.

The dielectric constant of an aliphatic hydrocarbon is ca. 2 whereas that of water is ca. 78. Since the hydrophobic core of the bilayer consists mainly of hydrocarbon chains, the dielectric constant must vary markedly over the lipid headgroup region from the water molecules on one side of the bilayer to the hydrocarbons just below the glycerol backbone region. It has therefore been suggested that the dielectric constant varies in a smooth and continuous fashion over this interfacial region, giving a trough-like profile, as shown in Figure 4.5.2, that is described by equation 4.5

$$\varepsilon = \varepsilon_2 + \frac{\varepsilon_1 - \varepsilon_2}{1 + \exp(d - d_0)/\sigma)} \quad \text{Equation 4.5}$$

where ε is the dielectric constant at a distance d from the bilayer centre, and ε_1 and ε_2 are the dielectric constants in the bilayer centre (2) and in water (78) respectively. d_0 is the value of d at the point of maximum gradient, corresponding to the point where $\varepsilon = (\varepsilon_1 + \varepsilon_2)/2.0$, and σ is an exponential decay constant which reflects the width of the transition region (Flewellling and Hubbell, 1986). Figure 4.5.2 shows the dielectric constant profile calculated from the above equation with values for d_0 and σ of 12 and 2 Å, respectively, with values of ε_1 and ε_2 of 2 and 78 respectively.

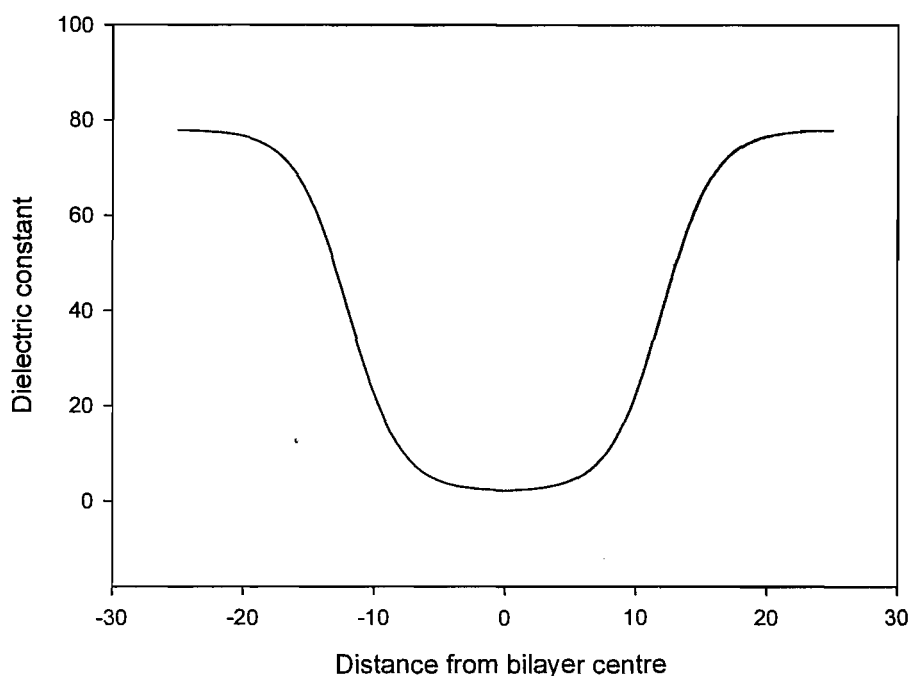


Figure 4.5.2 Dielectric profile of a bilayer. It is assumed that the dielectric constant varies in a smooth and continuous way over the interface, described by a sigmoidal dependence of dielectric constant over position in the interface region, giving a trough-like distribution across the membrane.

The shape of the polarity profile has been shown to be consistent with experimental data on ESR spectra obtained using spin-labelled phospholipids in lipid bilayers (Marsh, 2001). As Trp fluorescence emission is dependent on solvent polarity and the relationship between fluorescence emission maxima and solvent polarity is close to linear, Equation 4.5 can be used to describe the dependence of fluorescence emission maxima on position within a bilayer by substituting the dielectric constants in the bilayer centre and in water for the emission maxima of a Trp residue in the bilayer centre and in water (Equation 4.6).

$$\lambda = \lambda_2 + \frac{\lambda_1 - \lambda_2}{1 + \exp(d - d_0)/\sigma)} \quad \text{Equation 4.6}$$

Figure 4.5.3 shows how changing the values of d_0 and σ affect the calculated profile of fluorescence emission maxima. Increasing d_0 increases the length of the ‘flat’ central portion of the trough, increasing the separation between the regions where the dielectric constant increases steeply with distance. Increasing σ increases the width of the transition region and so decreases the steepness of the change in the dielectric constant in the interface region. As already described, the separation distances between the α -carbons of residues L69 and L92 in TbMscL is 31.8 Å, the centre of the bilayer being 15.9 Å from L69 (Figure 4.3.4). The wavelengths of maximum fluorescence emission for the lipid exposed residues on TM1 and TM2, plotted in Figure 4.3.4, were fitted to equation 4.6, for residues on the cytoplasmic and periplasmic sides of the protein, respectively. In Figure 4.5.4 wavelengths of fluorescence emission maxima are plotted for Trp residues between positions 27 to 37 and 69 to 80, and for residues between positions 20 to 27 and 80 to 91, as a function of distance from the centre of the bilayer, giving the parameters listed in Table 4.5.1. (Values were taken from the data in Table 4.4.1 and data previously published by Powl). (Powl *et al.*, 2005b) The data for residues on the periplasmic side of TbMscL fit well to Equation 4.6, falling on a smooth curve and giving the expected trough-like profile for solvent polarity as a function of distance. That residues L30W and I77W do not fit to this curve can be attributed to the free space surrounding these residues, allowing them a high degree of movement, and thus giving an inaccurate representation of their location in respect to the other residues on the periplasmic side of the membrane. In contrast the data for residues on the cytoplasmic side of TbMscL do not fit meaningfully to Equation 4.6 giving negative values for d_0 and large standard errors. Equation 4.6, therefore, provides a good model for the variation of emission maxima with distance from the centre of the bilayer on the periplasmic side but not on the cytoplasmic side. To achieve a trough-like profile on the cytoplasmic side of the membrane, lower values of fluorescence emission maximum would be needed for residues Y87W and I23W. One explanation for the lack of a trough-like profile on the cytoplasmic side could then be that these residues are free to move and have ‘snorkelled’ towards the interface so that their position is not well defined in terms of the α -carbon position. In fact the crystal structure shows that these residues are located in a region with free space surrounding them, in contrast to residues on the periplasmic side where Trp residues have less free space to move. In conclusion, if

Trp residues are buried within the structure of TbMscL then the data presented are in good agreement with the theory presented by Marsh (Marsh, 2001) but if Trp residues are free to move, then ‘snorkelling’ can distort the polarity profile.

The ESR measurements obtained by Marsh gave a value for d_0 in a bilayer of di(C18:1)PC of 13 Å giving a width of the region between the two points of maximum gradient of 26 Å, which is in agreement with the hydrophobic thickness of a bilayer of di(C18:1)PC which is 27 Å. The region of the bilayer defined by the values of d_0 corresponds, therefore, to the hydrophobic core of the bilayer. The value of d_0 obtained from fitting the data for the periplasmic side of TbMscL of 11.8 Å translates to a hydrophobic thickness for TbMscL of 23.6 ± 5.2 Å which is in good agreement with a previous estimate by Powl *et al.* of 25 Å (Powl *et al.*, 2005b). The value obtained for the width of the transition region (σ) is also in good agreement with the previous estimate by Marsh of 1-2 Å obtained from analysis of spin labelled phospholipids (Marsh, 2001).

Periplasmic side		Cytoplasmic side	
λ_1	321.7 ± 0.9	λ_1	278.9 ± 888.6
λ_2	344 ± 0.3	λ_2	334.1 ± 22.8
d_0	11.8 ± 2.6 Å	d_0	-9.4 ± 214.9 Å
σ	2.2 ± 1.2 Å	σ	8.37 ± 45.6 Å

Table 4.5.1 Calculated parameters obtained by fitting values of wavelengths for maximum fluorescence for lipid-exposed residues (Figure 4.3.4) to equation 4.6 for residues on the periplasmic and cytoplasmic sides of TbMscL (Figure 4.5.5).

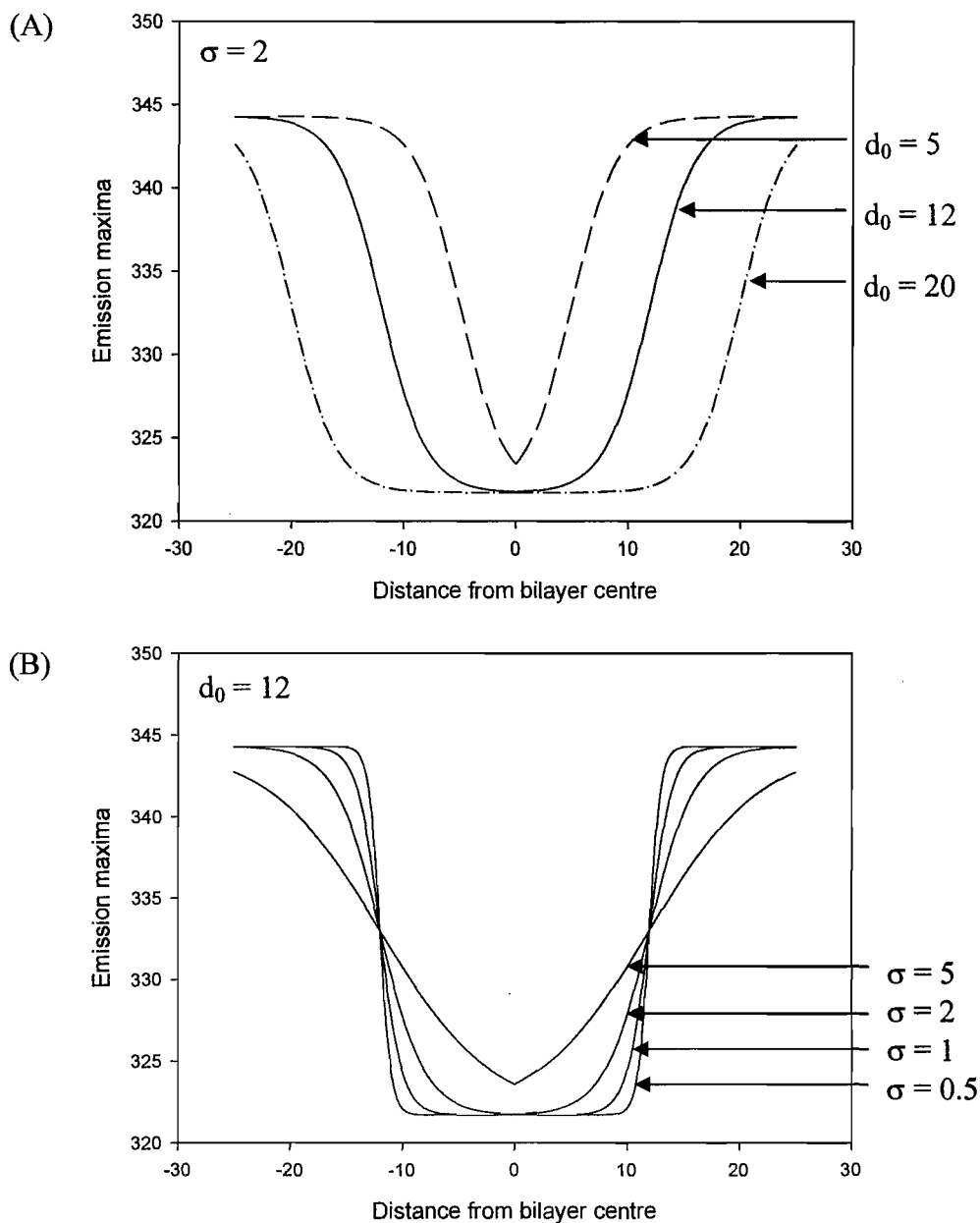


Figure 4.5.3 Dependence of fluorescence emission maxima on position within a bilayer. The simulations above demonstrate how changing the parameters in equation 4.6 affect the polarity profile. (A) shows how changing the bilayer thickness (d_0) affects the calculated polarity profile of emission maxima. Values of d_0 were 5, 12, and 20 Å with a fixed value for σ of 20. (B) shows how varying the width of the transition region (σ) affects the calculated profile of emission maxima. Values of σ were 0.5, 1, 2, and 5 Å with a fixed value for d_0 of 12 Å.

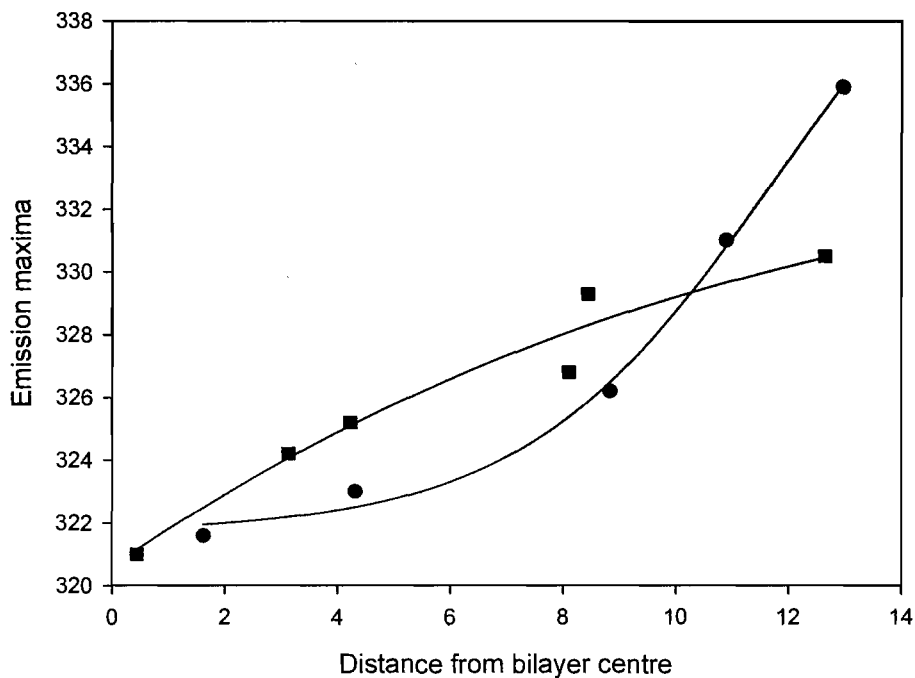


Figure 4.5.4 Fits of fluorescence emission maxima for Trp residues in TM1 and TM2 of TbMscL to Equation 4.6. Wavelengths of maximum emission were fitted to Equation 4.6, for residues on the cytoplasmic (■) and periplasmic (●) sides respectively. The data for residues on the periplasmic side of TbMscL fit well to equation 4.6, whereas residues on the cytoplasmic side do not. The parameters for the best fit are listed in Table 4.5.1.

4.5.2 Accessibility of Trp residues to acrylamide and iodide

In order to assess the accessibility of lipid facing Trp residues from the aqueous phase, effects of acrylamide and iodide were studied as quenchers of fluorescence. Acrylamide is a neutral molecule, and therefore is able to quench charged and uncharged amino acids with equal efficacy. Acrylamide is also known to be more sensitive to details of protein structure than other aqueous quenchers, acting as a 'ruler' to report the degree of exposure of particular tryptophan residues to solvent (Calhoun *et al.*, 1983). Previous studies by Powl *et al.* (Powl *et al.*, 2005b) revealed that the level of fluorescence quenching of lipid facing Trp residues on TM2 by acrylamide was almost the inverse of the level of fluorescence quenching observed with brominated phospholipids (Powl *et al.*, 2005b) with very low levels of quenching observed for residues in the middle of the bilayer. The results shown in Table 4.4.4 are unexpected as they do not follow this previously observed trend. A possible explanation for the similar levels of fluorescence quenching observed for all the residues in TM1 could be due to the fact that all Trp-residues chosen for study in TM1 are located at, or very close to the channel pore. Residues in TM2 depend on the extent of acrylamide penetration into the lipid bilayer, whereas quenching of Trp residues in TM1 could depend on penetration of acrylamide into the protein from the pore of the channel. In order to better establish any differences in the accessibility of Trp residues from the aqueous phase, the experiment was repeated using iodide as a quencher of fluorescence. Iodide is a charged quencher so the quenching profile would be expected to be different from that of acrylamide. The results shown in Figure 4.4.7 show that quenching by iodide is not the same for all the Trp residues, with residues located towards the centre of the bilayer generally quenching less than those located more towards either the periplasmic or the cytoplasmic interface. Figure 4.5.5 shows a plot of the levels of quenching of lipid facing Trp residues in TM1 and TM2 of TbMscL plotted as a function of the distance along the bilayer normal from L69. Fluorescence intensities for Trp residues in TM2 are taken from previously published data from Powl *et al.* (Powl *et al.*, 2005b). There does is a general trend for residues in the middle of the bilayer in both TM1 and TM2 to show lower levels of quenching than those at the interface. Further, levels of fluorescence quenching are higher for residues in TM1 than TM2 with smoother curves on the periplasmic side than the cytoplasmic side for both TM1 and TM2. The explanation for this could be the same

as for quenching by acrylamide, in that residues in TM1 are simply closer to, and therefore more accessible to, the channel pore of TbMscL, with iodide ions gaining access to the Trp residues via the pore.

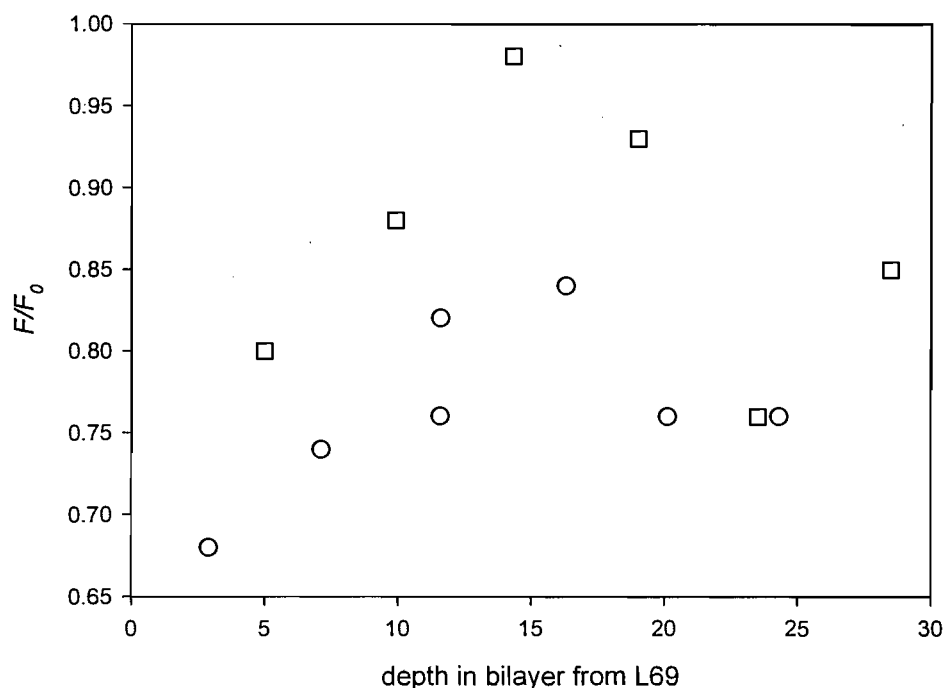


Figure 4.5.5 Fluorescence quenching of TbMscL by iodide. Fluorescence intensities for Trp residues in TM1 (○) and TM2 (□), for TbMscL reconstituted into di(C18:1)PC, are plotted as a function of the distance (Å) of the α -carbon of the residue from that of Leu-69, measured along the bilayer normal. Results are expressed as F/F_0 where F and F_0 are fluorescence intensities in the presence and absence of iodide respectively.

4.5.3 Penetration of lipid chains into the surface of TbMscL

To probe the accessibility of lipid facing residues on TM1 to the phospholipids in the surrounding lipid bilayer, Trp mutants were reconstituted into bilayers of di(Br₂C18:0)PC to obtain levels of fluorescence quenching. The levels of fluorescence quenching shown in Figure 4.4.5 indicate that residues in the centre of the bilayer are generally quenched more than those located away from the centre of

the bilayer. However, this is rather misleading as residues located towards the centre of the bilayer will be quenched by brominated lipid molecules in both halves of the bilayer, leading to an increased level of quenching. Figure 4.5.6 shows the efficiencies of fluorescence quenching for lipid exposed Trp residues in TM1 and TM2 as a function of distance from L69, leaving out the data for the Trp residues that can be quenched from both monolayers. Data for residues on TM2 are taken from previously published data by Powl *et al.* {Powl, 2005 150 /id}. The plot shows that levels of quenching for Trp residues in TM1 are similar to those for residues in TM2 at an equivalent depth in the bilayer. For example efficiencies of quenching for the Trp residues in A20W and I23W on the cytoplasmic side of the membrane are comparable to those for the Trp residues in I77W and L73W in TM2 at comparable depths in the membrane on the periplasmic side of TbMscL. This is important because whereas the Trp residues in I77W and L73W in TM2 are surface exposed, the Trp residues in A20W and I23W are quite deeply buried (Figure 4.5.7). This suggests that residues that are buried deep within the cleft between TM2 helices (Figure 4.1.2) are equally accessible to lipid fatty acyl chains as surface exposed residues on TM2, so that the lipid fatty acyl chains must be able to penetrate into the clefts on the protein surface.

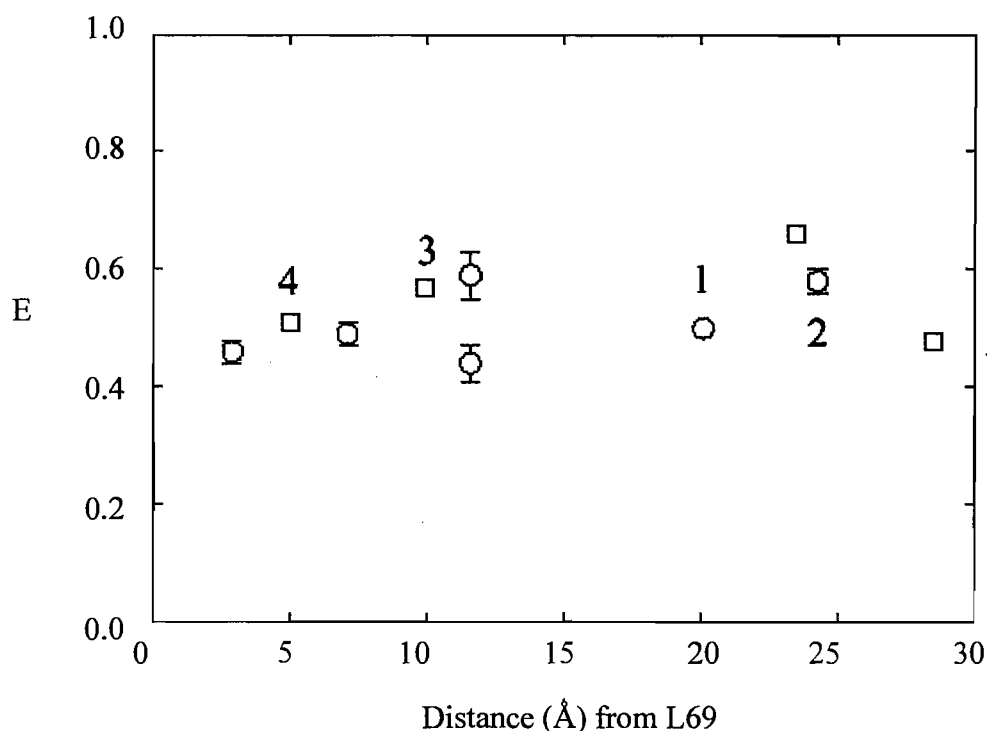


Figure 4.5.6 Quenching of Trp fluorescence in TbMscL by di(Br₂C18:0)PC. Efficiencies of fluorescence quenching are plotted for Trp residues in TM1 (○) and TM2 (□) as a function of the distance (Å) of the α-carbon of the residue from that of L69, measured along the bilayer normal. Efficiencies of quenching were calculated as $1-F/F_0$ where F and F_0 are fluorescence intensities in the di(Br₂C18:0)PC and di(C18:1)PC respectively. Data points labelled 1, 2, 3 and 4 correspond to I23W and A20W on TM1 and I77W and L73W on TM2 respectively.

In order to analyse the results in more quantitative terms fluorescence quenching was calculated in theoretical terms from calculated distances between Trp residues and Br atoms in the fatty acyl chains. Equation 4.3 shows how the effect of energy transfer between a donor and a single acceptor varies with the distance between them. The equation can be modified to give the efficiency E of energy transfer from Trp to x brominated fatty acyl chains all at the same distance r from the Trp:

$$E = x Ro^6 / (r^6 + x Ro^6) \quad \text{Equation 4.7}$$

The average number of lipid binding sites for residues on TM1 of TbMscL from which the fluorescence of a Trp residue can be quenched is 2.5 (see Chapter six) and given that there are two fatty acyl chains per lipid molecule, the value of x in Equation 4.7 is 5. The value of R_0 has been calculated to be 8 Å (Powl, 2003). Thus if distance r is known, then the efficiency of energy transfer can be calculated. Figure 4.5.9 shows how r can be calculated (r corresponds to d_1 in Figure 4.5.9). This requires a knowledge of the depth between the Trp residue and the bromine atoms along the bilayer normal (d_2) and the distances between the Trp residue and the bromine atom along the perpendicular to the bilayer normal (d_3). To calculate distances between Trp and bromine chains, Trp residues were first modelled into the crystal structure of TbMscL and positioned to remove any contacts between atoms that were within 70 % of the sum of the covalent radii. The depth of a Trp residue below the protein surface was then determined by docking a molecule of lipid with all *trans* fatty acyl chains onto the protein surface, with the lipid headgroups adjacent to the hydrophobic membrane-spanning region of TbMscL, defined by Leu-69 and Leu-92 on the periplasmic and cytoplasmic sides of the membrane, respectively. The lipid chosen, dilauroylphosphatidylethanolamine, seen in Figure 4.5.7, gives a bilayer with a hydrophobic thickness in the gel phase similar to that of TbMscL. The lipid molecule was located to minimise the distance between the outer edge of the Trp ring and the carbon backbone of a lipid fatty acyl chain, avoiding clashes between the protein and lipid molecules. These minimum contact distances are listed in Tables 4.5.2 and 4.5.3.

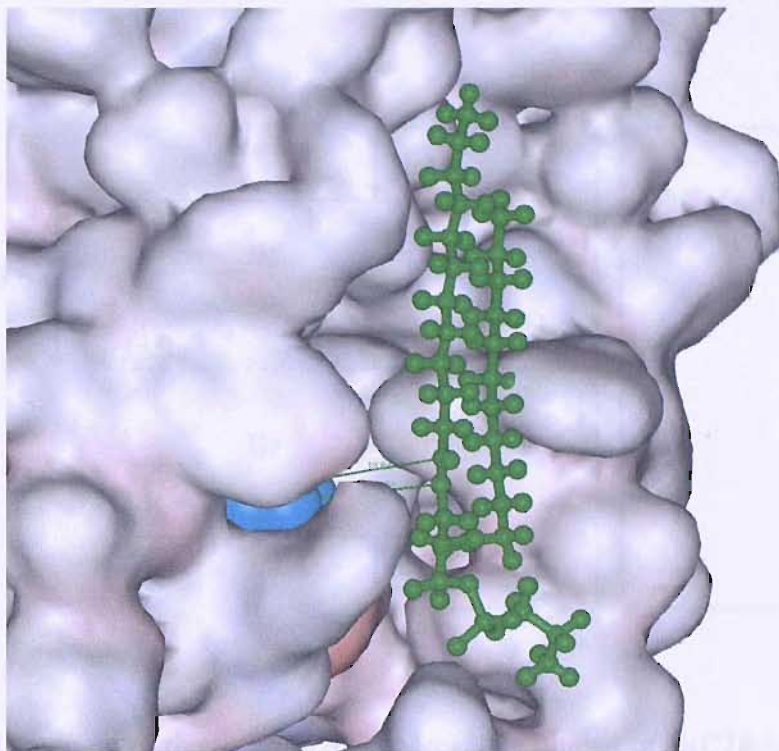


Figure 4.5.7 A Trp residue at position 20 is shown in blue in space-fill format with a dilauroylphosphatidylethanolamine molecule modelled on to the surface of TbMscL. The lipid molecule was located to minimise the distance between the outer edge of the Trp ring and the carbon backbone of the lipid molecule, avoiding clashes between the protein and lipid molecules.

The distance along the bilayer normal between the α -carbon of a residue and the bromine atoms of di(Br₂C18:0)PC was calculated assuming a symmetric location for TbMscL within the lipid bilayer, with a hydrophobic for TbMscL of 25 Å and a hydrophobic thickness for a bilayer of di(C18:1)PC of 27 Å with the two bromine atoms per chain, located between carbons 9 and 10, being located at an average distance of ca. 7.2 Å from the glycerol backbone region as seen in Figure 4.5.8.

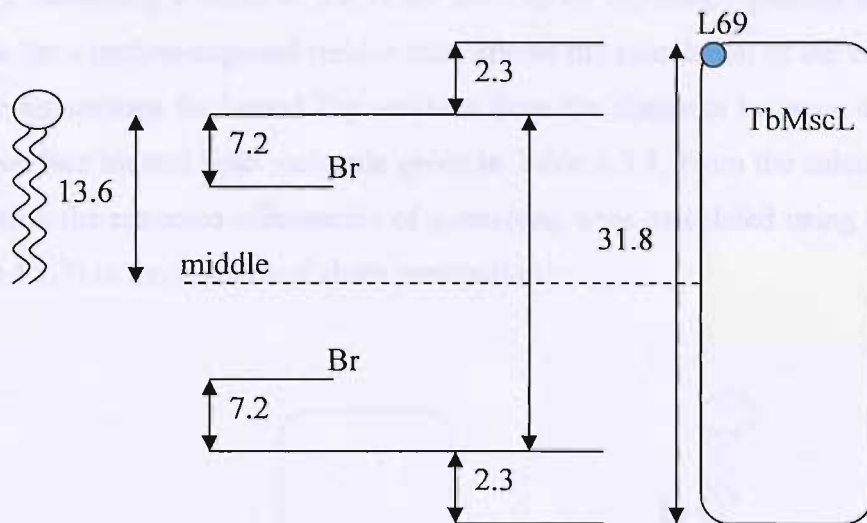


Figure 4.5.8 Diagram of the location of TbMscL in a bilayer of di(C18:1)PC.

TbMscL was positioned symmetrically in the bilayer. The middle of the bilayer is shown by the dotted line with the bromine atoms located ca. 7.2 Å from the glycerol backbone region on the periplasmic and cytoplasmic sides of the membrane.

Knowing the distances along the bilayer normal between the α -carbon of a residue and L69 from the crystal structure (Table 4.3.3), the distance along the bilayer normal between the α -carbon and the nearest bromines (Figure 4.5.9) can then be calculated (d_2 in Tables 4.5.2 and 4.5.3). The remaining distance to be calculated is d_3 (see Figure 4.5.9) which is related, in a way to be defined, to the distance between the edge of the Trp residue and the backbone of the nearest fatty acyl chain. The value of d_3 was determined experimentally, as follows. It was assumed that in the three surface-exposed mutants L73W, I77W, and Y87W in TM2, the Trp residues were in van der Waals contact with the neighbouring lipid fatty acyl chains. For the three Trp mutants, values of r (d_1 in Figure 4.5.9) were calculated from the experimentally determined value for F/F_0 in di(Br₂C18:0)PC using Equation 4.7 (Table 4.5.2). From r , together with the estimated values for the Trp-Br separations long the bilayer normal (d_2), the values for the Trp-Br separations parallel to the bilayer surface (d_3) can be calculated. As shown in Table 4.5.2, the values obtained are very similar for all three mutants, with an average value of 9.6 Å. This is very similar to the van der Waals contact

distance between the edge of a Trp ring and a bromine-containing alkyl chain (Figure 4.5.10). Assuming a value of 9.6 Å for the Trp-Br separation parallel to the bilayer surface for a surface-exposed residue then allows the calculation of the corresponding Trp-Br separations for buried Trp residues from the distances between a Trp residue and a surface located lipid molecule given in Table 4.5.3. From the calculated Trp-Br separation the expected efficiencies of quenching were calculated using Equation 4.7 (Table 4.5.3) in the absence of chain penetration.

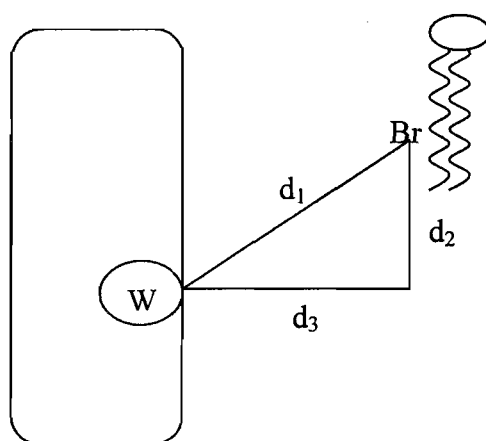


Figure 4.5.9 Parameters required to calculate expected efficiencies of quenching. Distance between quencher and Trp molecule (D_1), vertical distance of Trp residue from bromines (D_2), and depth of Trp residue from the surface of the protein (D_3).

Mutant	r (Å)	Trp-Br separation along bilayer normal (d_2)	Trp-Br separation parallel to bilayer surface (d_3)
L73W	10.4	4.5	9.4
I77W	9.9	0.4	9.9
Y87W	9.4	1.2	9.3

Table 4.5.2 Quenching data for Trp mutants in TM2. The value of r was calculated from experimental values of F/F_0 using equation 4.7 and the value of the Trp-Br separation distance along the bilayer normal was calculated as described from the structural data for TbMscL and for the lipid bilayer.

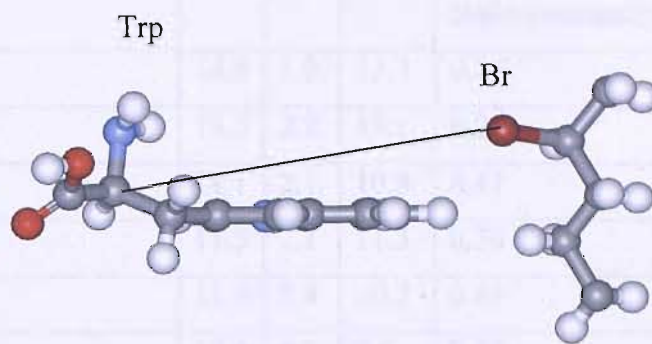


Figure 4.5.10 Minimum Trp to Br distance. The figure shows a Trp residue and a bromine-containing alkane with van der Waals contact between the edge of the Trp ring and the alkyl chain. The α -carbon to Br distance is marked.

For the two buried residues, A20W and I23W, the calculated efficiencies of fluorescence quenching assuming no chain penetration are very much smaller than the efficiencies of quenching observed experimentally, confirming that the observed levels of quenching must require penetration of the lipid fatty acyl chains into cavities in the protein surface. Modelling shows that the cavity around the buried Trp residues in A20W and I23W is large enough to accommodate small sections of alkyl chain with the chain being in van der Waals contact with the Trp residues. For example, Figure 4.5.11 shows I23W buried in the cavity, in van der Waals contact with hexane in the cavity, and F34W, a surface exposed residue, in contact with a molecule of PE modelled onto the protein surface.

Mutant	Distance between Trp edge and chain on surface (Å)	d ₁	d ₂	d ₃	Calculated efficiency of quenching with no chain penetration	Experimental efficiency of quenching
A20W	7.2	13.4	2.0	13.3	0.16	0.58
I23W	7.0	13.3	2.2	13.1	0.21	0.50
L30W	4.8	11.1	2.1	10.9	0.41	0.59
V31W	5.2	11.5	2.1	11.3	0.36	0.44
F34W	4.6	11.0	2.4	10.7	0.45	0.49
L73W	3.5	10.6	4.5	9.6	0.49	0.51
I77W	3.5	9.6	0.4	9.6	0.63	0.57
Y87W	3.5	9.7	1.2	9.6	0.61	0.66

Table 4.5.3 Distances of Trp residues from a lipid molecule docked onto the surface of the protein were calculated as described. The corresponding values of the efficiency of quenching in di(Br₂C18:0)PC in the absence of chain penetration were calculated.

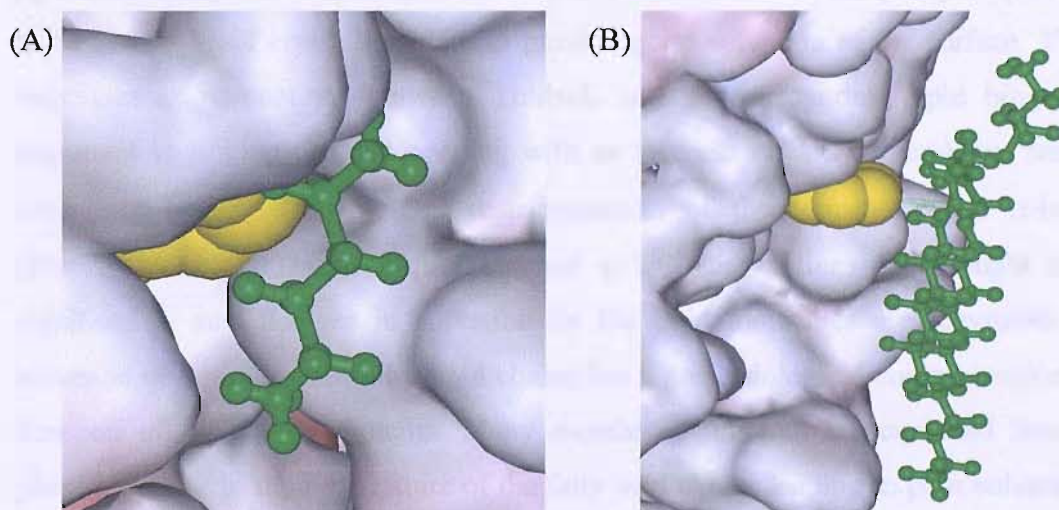


Figure 4.5.11 (A) A Trp residue at position 23 (yellow CPK format) is shown in van der Waals contact with hexane (green; ball-and-stick format) modelled into the cavity in the protein surface around position 23. (B) A Trp residue at position 34 (yellow) is shown with a molecule of Phosphatidylethanolamine modelled onto the protein surface (green) in close contact with the surface exposed Trp residue.

4.5.4 Conclusions

The results presented in this chapter give a greater insight into how TbMscL sits in the lipid bilayer and how it interacts with the surrounding phospholipids in the membrane. The fluorescence emission maxima for Trp residues in TM1 that are lipid facing give a polarity profile that is in good agreement with the fluorescence emission values previously obtained for lipid facing residues in TM2 (Powl *et al.*, 2005b), with residues at the two bilayer interfaces showing fluorescence emission at longer wavelengths than those residues located towards the centre of the bilayer. The levels of iodide quenching for Trp residues in TM1 also gave a profile that is comparable to levels of quenching for Trp residues in TM2, although levels of quenching were slightly increased probably due to the entry of iodide into the protein from the channel pore. Levels of fluorescence quenching for lipid-exposed residues in TM1 by brominated phospholipids were significantly higher than expected if the phospholipid chains could not penetrate into the protein surface, leading to the proposal that the fatty acyl chains are able to penetrate into the surface of TbMscL bringing the bromine atoms in close proximity to the Trp residues. Solvation of buried residues by lipid chains requires flexibility in the fatty acyl chains so that the phospholipids need to be in the liquid crystalline state to provide good solvation of the surface. This is important as interactions between TbMscL and the surrounding lipid bilayer are important in linking channel opening with an increase in lateral membrane tension, ultimately leading to structural rearrangements of the transmembrane α -helices (Perozo *et al.*, 2002a). During channel gating, the helices are thought to tilt significantly and changes in solvation by the lipid molecules are inevitable. The solvation of buried residues by lipid chains has a great biological consequence on the function of membrane proteins. Many membrane proteins are excluded from gel phase lipid due to the rigid nature of the fatty acyl chains leading to poor solvation of buried residues within the protein structure. For example, binding of gel phase lipid to the calcium-ATPase is a factor of 25 times weaker than binding of lipids in the liquid-crystalline phase {Lee, 2003} an effect which would greatly hinder optimal functioning of the Calcium ATPase.

Chapter 5: Fluorescence Properties of pore exposed residues on TM1

5.1 Introduction

Since the crystal structure of TbMscL was resolved to 3.5 Å resolution by Chang *et al.* (Chang *et al.*, 1998), mutagenesis studies and molecular dynamics simulations have provided a greater insight into how the transmembrane regions of mechanosensitive channels alter during channel gating. The results presented in Chapter four show how the polarity profile of lipid exposed residues on TM1 is similar to that of residues in TM2 and that fatty acyl chains of lipid molecules are able to penetrate the surface of TbMscL to provide full solvation of buried residues in TM1. The Trp residues in the mutants discussed in this chapter line the channel pore of TbMscL. Several Trp mutants that line the pore at the N-terminal end of TM1 resulted in gain-of-function mutants and these will be discussed in Chapter six. In the crystal structure of TbMscL residues Ile-14 and Val-21 form the pore constriction at the N-terminal end of TM1 and as the pore radius in this region is around 2 Å, the crystal structure of TbMscL is thought to be in the closed or nearly closed form. The channel pore is lined by a series of hydrophilic residues, (Thr-25, Thr-28, Thr-32, Lys-33, and Asp-36), making the interior surface very polar in nature. The crystal structure shows the central pore, with a radius of between ca. 2 Å at the constriction and ca. 18 Å at the periplasm, partially occluded at the cytoplasmic surface by Thr-25 (Chang *et al.*, 1998). In contrast to the crystal structure of MscL, the crystal structure of MscS, resolved to 3.9 Å resolution, is thought to be in a partially open state (Bass *et al.*, 2002). It was suggested by Bass *et al.* that MscS could have been crystallised in the open state because of the absence of the lipid bilayer, the lipid bilayer being required to keep the channel in the closed state. Since the crystal structure of TbMscL was also obtained in the absence of a lipid bilayer the question arises as to whether the crystal structure of MscL is representative of the fully closed form in a lipid bilayer. The aim of this chapter is therefore to characterise the environment of pore lining residues in TM1 for TbMscL in a lipid bilayer and to assess the accessibility of residues both from the aqueous and lipid phases in the closed channel. Figure 5.1 shows a periplasmic view of TbMscL with pore lining residues chosen for Trp substitution shown in CPK format.

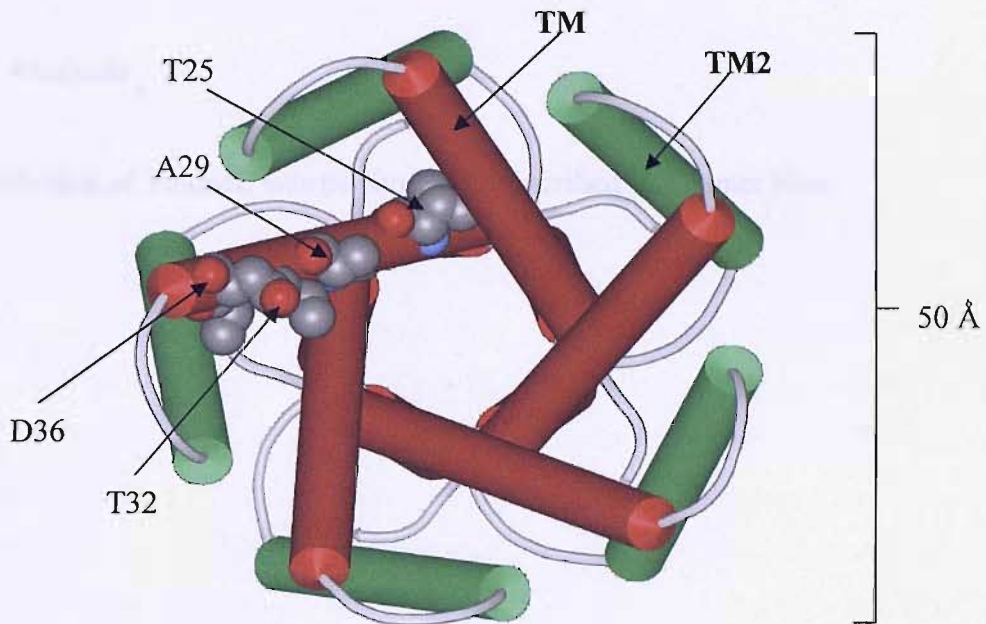


Figure 5.1 Periplasmic view of TbMscL showing pore lining residues chosen for Trp substitution in TM1 in CPK format. TM1 helices are shown in red and TM2 helices are shown in green.

5.2 Methods and Materials

5.2.1 Materials

All chemicals were obtained from Sigma or BDH unless otherwise stated.

5.2.2 Methods

Reconstitution of TbMscL was performed as described in Chapter Four.

[Faint, illegible text, likely bleed-through from the reverse side of the page]

5.3 Results

5.3.1 Functional Analysis of Trp-mutants of TbMscL

To ascertain whether substituting pore exposed residues on TM1 with Trp resulted in GOF mutations, an *in vivo* cell viability assay for this phenotype was carried out as outlined in Section 4.3.2.

The results shown in Figure 5.3.1 show that three of the four MscL mutants assayed (T25W, T32W, and D36W) had growth curves the same as wild type TbMscL. However, A29W has a slightly impaired growth rate when compared to the other Trp mutants, reaching an optical density after five hours of ca. 0.5. Thus none of the Trp mutants resulted in a full gain of function phenotype, unlike the severe gain of function mutant V21K, discussed in Chapter six. The reduced growth rate of A29W suggests that this mutant could open at lower tensions than wild type TbMscL but, nevertheless, is likely to be closed in reconstituted lipid bilayers at zero tension. Statistical analysis shows that this mutant is significantly different to wild type but none of the other mutants. As the optical density reached by wild type TbMscL is only very slightly above the other pore lining mutants, and the presence of protein on a coomassie stained SDS-PAGE gel indicates levels of protein expression comparable to wild type, it can be assumed this difference is not enough for the mutant A29W to be considered open.

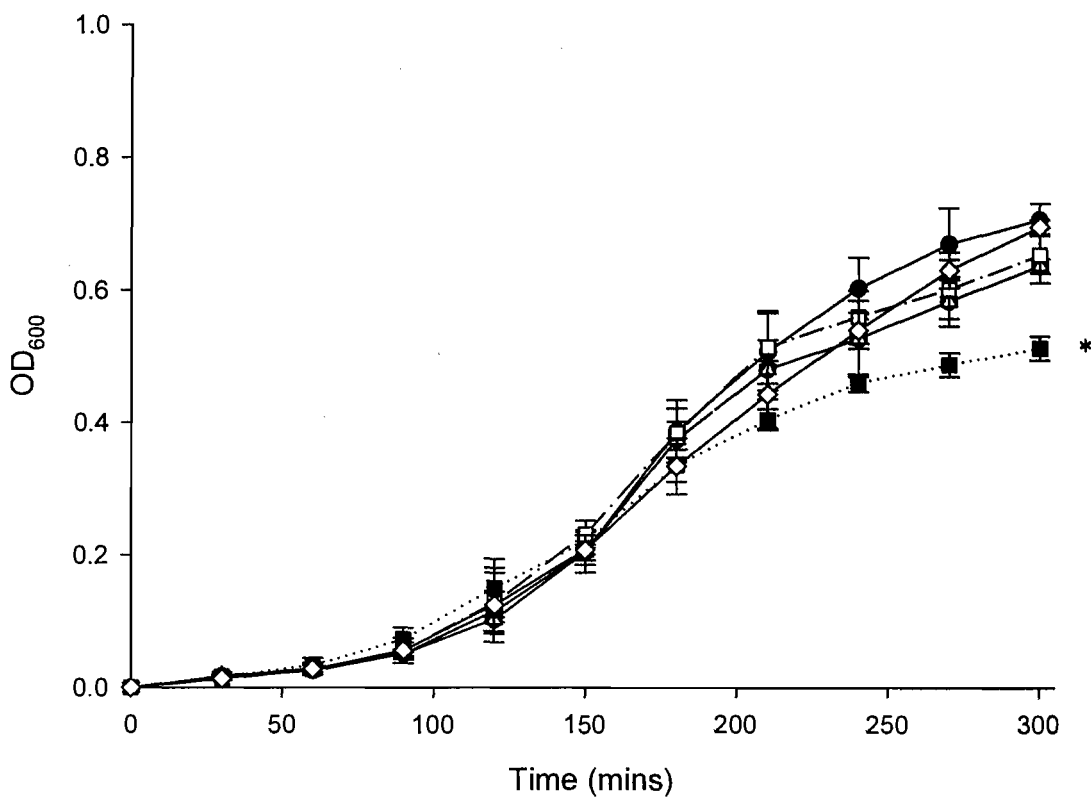


Figure 5.3.1 *In Vivo* assay for Gain of Function mutants. *E.coli* BL21(DE3)pLysS transformants carrying the pET-19b plasmid with the Trp-mutated *mscL* gene were grown in Luria both containing ampicillin ($100 \mu\text{g ml}^{-1}$) to an optical density of OD_{600} of 0.2 and expression was induced by addition of 1 mM IPTG. The optical density was measured every 30 minutes to determine which mutants produced a Gain-of-function (GOF) phenotype. TbMscL mutants expressed were: wild type, (●); T25W, (△); A29W, (■); T32W, (□); and D36W, (◇). Error bars are standard deviations obtained from the average of three determinations.

5.3.2 Fluorescence emission spectra of Trp-mutated TbMscL

Mutants were reconstituted into bilayers of di(C18:1)PC at a molar ratio of lipid: protein monomer of 100:1. The fluorescence emission spectra shown in Figure 5.3.2 were fitted to the equation for a skewed Gaussian (Equation 4.4) to obtain accurate values for the wavelength of maximum fluorescence emission (Table 5.3.1).

The fluorescence intensities of all the Trp mutants were similar, with fluorescence intensities similar to free Trp. Noticeable are the larger values obtained for the peak widths at half height (ω) than for lipid-exposed residues. As mentioned in Chapter Four, this is in agreement with the relationship between fluorescence emission maxima and peak width established by Ladokhin *et al.* (Ladokhin, 2000). Fluorescence emission maxima were greater than for lipid-exposed residues in TM1 at comparable depths in the bilayer. For example, the lipid-exposed residue F80W, located 14 Å from Leu-69 has an emission maximum of 321 nm showing that whereas the pore-exposed mutant T25W has an emission maximum of 331 nm (Table 5.3.1), the pore lining residues are in a more hydrophobic environment, as expected. Nevertheless, emission maxima for the pore lining residues are less than that for Trp in water (Figure 5.3.2) suggesting that the pore lining residues are not located in a totally water-exposed environment. Further, T32W and D36W, at the periplasmic end of TbMscL, show longer values for wavelengths of fluorescence emission than A29W and T25W, suggesting that residues towards the periplasmic end of TbMscL are in a more hydrophilic environment than those residues located towards the cytoplasmic end of the channel pore.

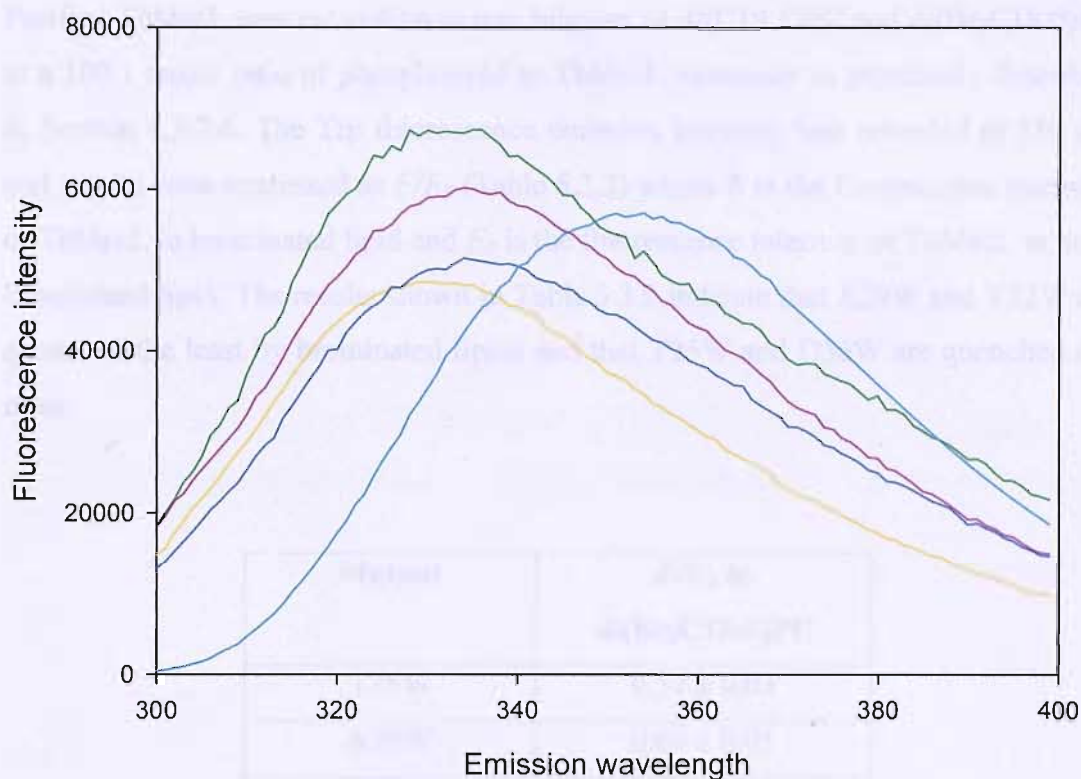


Figure 5.3.2 Fluorescence emission spectra of pore exposed Trp-mutants of MscL. Purified MscL was reconstituted in di(C18:1)PC and fluorescence was excited at 280 nm. Samples were as follows: T25W, (-); A29W, (-); T32W, (-) D36W, (-) and free Trp, (-). The concentration of MscL was 0.98 μM and the molar ratio of lipid to protein monomer was 100:1. The concentration of free Trp was 1 μM .

Mutant	λ^{max} (nm) in di(C18:1)PC	ω (nm)
T25W	331.2 ± 0.1	59.5 ± 0.2
A29W	331.2 ± 0.2	63.0 ± 0.3
T32W	337.2 ± 0.1	64.5 ± 0.2
D36W	335.2 ± 0.1	62.5 ± 0.2

Table 5.3.1 Fluorescence emission maxima for pore-exposed Trp-mutants of TbMscL reconstituted into bilayers of di(C18:1)PC and excited at 280 nm. The molar ratio of lipid to protein monomer was 100:1 and the concentration of MscL was 0.98 μM .

5.3.3 Fluorescence quenching of TbMscL by brominated phospholipids

Purified TbMscL was reconstituted into bilayers of di(C18:1)PC and di(Br₂C18:0)PC at a 100:1 molar ratio of phospholipid to TbMscL monomer as previously described in Section 4.3.2.6. The Trp fluorescence emission intensity was recorded at 330 nm and results were expressed as F/F_0 (Table 5.3.2) where F is the fluorescence intensity of TbMscL in brominated lipid and F_0 is the fluorescence intensity of TbMscL in non-brominated lipid. The results shown in Table 5.3.2 indicate that A29W and T32W are quenched the least by brominated lipids and that T25W and D36W are quenched the most.

Mutant	F/F_0 in di(Br₂C18:0)PC
T25W	0.57 ± 0.03
A29W	0.60 ± 0.01
T32W	0.70 ± 0.02
D36W	0.54 ± 0.04

Table 5.3.2 Quenching of Trp fluorescence by brominated phospholipids. Mutants were reconstituted into bilayers of di(C18:1)PC and di(Br₂C18:0)PC. Fluorescence intensities were recorded at 330 nm and are expressed as F/F_0 where F and F_0 are fluorescence intensities for TbMscL reconstituted into di(C18:1)PC and di(Br₂C18:0)PC respectively. Values and standard deviations were obtained from the average of three determinations in duplicate.

5.3.4 Fluorescence quenching of TbMscL by acrylamide

Fluorescence quenching of lipid facing residues on TM1 by acrylamide was used to assess the accessibility of Trp residues in TbMscL from the aqueous phase in bilayers of di(C18:1)PC. TbMscL was reconstituted into bilayers of di(C18:1)PC at a 100:1 molar ratio of phospholipid to TbMscL monomer as previously described. As observed for the lipid-exposed residues in Chapter 4 (Table 4.4.4) which also had an average value for F/F_0 of 0.6, the levels of fluorescence quenching listed in Table 5.3.3 are all the same, with an average value for F/F_0 of ca. 0.6 at 300 mM acrylamide. This suggests no difference in the accessibility of Trp residues to acrylamide regardless of a location facing towards the lipids or facing the channel pore.

Mutant	F/F_0 in di(C18:1)PC
T25W	0.61 ± 0.05
A29W	0.60 ± 0.04
T32W	0.58 ± 0.03
D36W	0.60 ± 0.03

Table 5.3.3 Fluorescence quenching of pore facing residues on TM1 by acrylamide. Results are expressed as F/F_0 where F and F_0 are fluorescence intensities for TbMscL reconstituted into di(C18:1)PC in the presence and absence of 300 mM acrylamide respectively. Values and standard deviations were obtained from the average of three determinations in duplicate.

5.3.5 Fluorescence quenching of TbMscL by Iodide

Values of F/F_0 for pore-lining Trp mutants of TbMscL reconstituted into bilayers of di(C18:1)PC in the presence of 450 mM KI are shown in Figure 5.3.3. Although the observed levels of fluorescence quenching are still fairly low, given the location of the Trp residues, the average value for F/F_0 ca. 0.7, is slightly higher than the average level of quenching observed for the lipid-facing residues in Chapter 4 (Figure 4.4.7), which was ca. 0.8. As the Trp mutants studied in this chapter face the pore, and residues D36 and T32 are located more towards the lipid headgroup region in TbMscL, it is a little surprising that these two residues appear to be quenched less than residues T25 and A29. Statistical analysis shows that A29W is significantly different to T25W and T32W, although the change in the level of fluorescence quenching is very small.

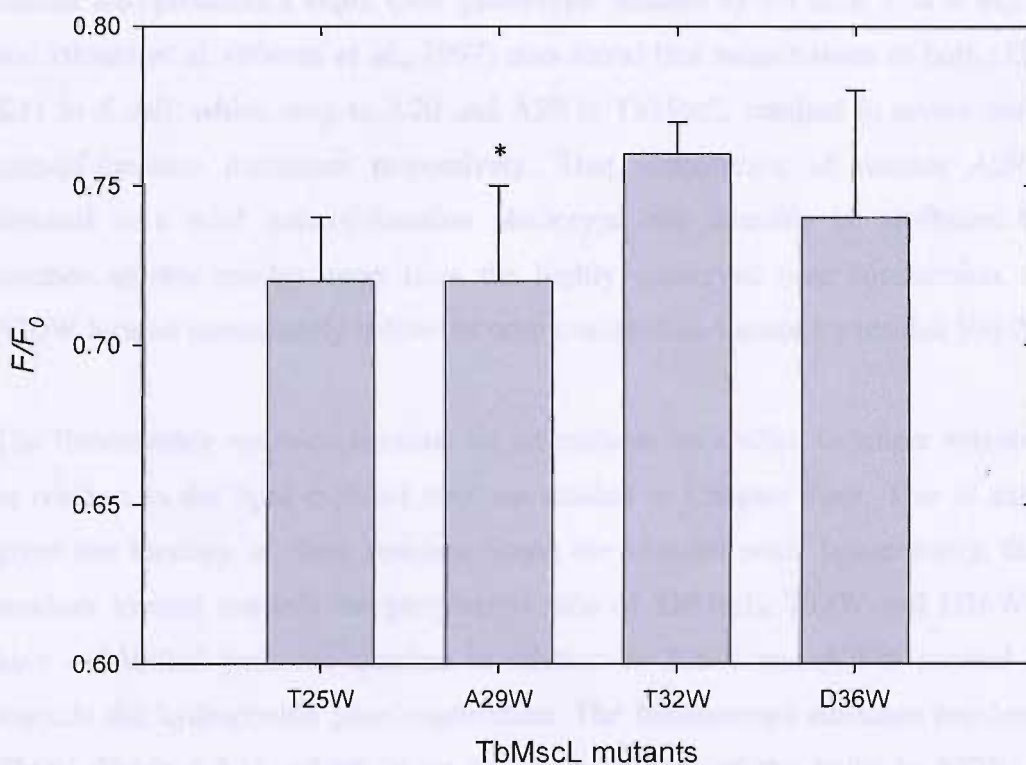


Figure 5.3.3 Fluorescence quenching of pore lining residues on TM1 by KI. Results are expressed as F/F_0 where F and F_0 are fluorescence intensities for TbMscL reconstituted into di(C18:1)PC in the presence and absence of iodide respectively. The ionic strength was kept constant at 0.91M. Bar charts show the average of three determinations and standard deviations in duplicate

5.4 Discussion

5.4.1 Properties of pore lining Trp mutants of TbMscL

Residues on TM1 that line the channel pore were mutated to tryptophan using site-directed mutagenesis. In order to establish whether the insertion of a Trp residue affected function of TbMscL, an *in vivo* cell viability assay was carried out in order to screen for any gain-of function mutants as in Chapter Four. The results (Figure 5.3.1) with pore lining Trp mutants of TbMscL show that all but one of the mutants, A29W, resulted in the same effects on growth as wild type TbMscL, indicating that function of the mutants was unaffected by insertion of the Trp residue. Similar to the lipid-exposed residue A20W (see Figure 4.3.1 in Chapter four) A29W showed a slightly reduced growth rate following induction of TbMscL expression indicating that this mutant also produces a slight GOF phenotype. Studies by Ou *et al.* (Ou *et al.*, 1998) and Blount *et al.* (Blount *et al.*, 1997) also found that substitutions of both G22 and K31 in *E.coli*, which map to A20 and A29 in TbMscL, resulted in severe and mild gain-of-function mutations respectively. That substitution of residue A29 only resulted in a mild gain-of-function phenotype can possibly be attributed to the location of this residue away from the highly conserved pore constriction, unlike A20W located immediately below the pore constriction formed by residue Val-21.

The fluorescence emission maxima for all mutants are shifted to longer wavelengths in relation to the lipid-exposed residues studied in Chapter Four. This is expected given the location of these residues lining the channel pore. Interestingly, the two residues located towards the periplasmic side of TbMscL, T32W and D36W, both have red-shifted emission maxima in relation to T25W and A29W located closer towards the hydrophobic pore constriction. The fluorescence emission maximum of T25W (Table 5.3.1), which is on the opposite side of the helix to F27W at an equivalent depth in the bilayer (see Table 4.4.1 in Chapter Four), shows a red-shifted value of 331.2 nm, in comparison to a value of 321 nm for F27W, indicating a hydrophilic environment for this residue even though it is located towards the middle of the membrane. The crystal structure of TbMscL shows that this residue is fully exposed to the channel pore, as shown in Figure 5.4.1. That the fluorescence of this residue is blue shifted in comparison to that of T32W and D36W is consistent with

the greater exposure of residues T32 and D36 to the aqueous phase both in relation to the channel pore and position in the lipid headgroup region. The central pore narrows from D36 at the periplasmic side to V21 at the pore constriction. Thus, T32 and D36 are more exposed to water than residue T25. Therefore, the fluorescence emission of T32W and D36W are consistent with the x-ray structure of TbMscL. D36 at the periplasmic end of the pore is close to S37, a lipid exposed residue which is located at the periplasmic interface. That the fluorescence emission spectra are very similar is consistent with the location of these residues being more exposed to water. The shift in λ^{\max} from 335 nm to 331 nm suggests that environmental polarity decreases from the surface to the central constriction at V21. In summary, the fluorescence emission spectra for TbMscL in a lipid bilayer are consistent with the x-ray structure crystallised from detergent micelles.

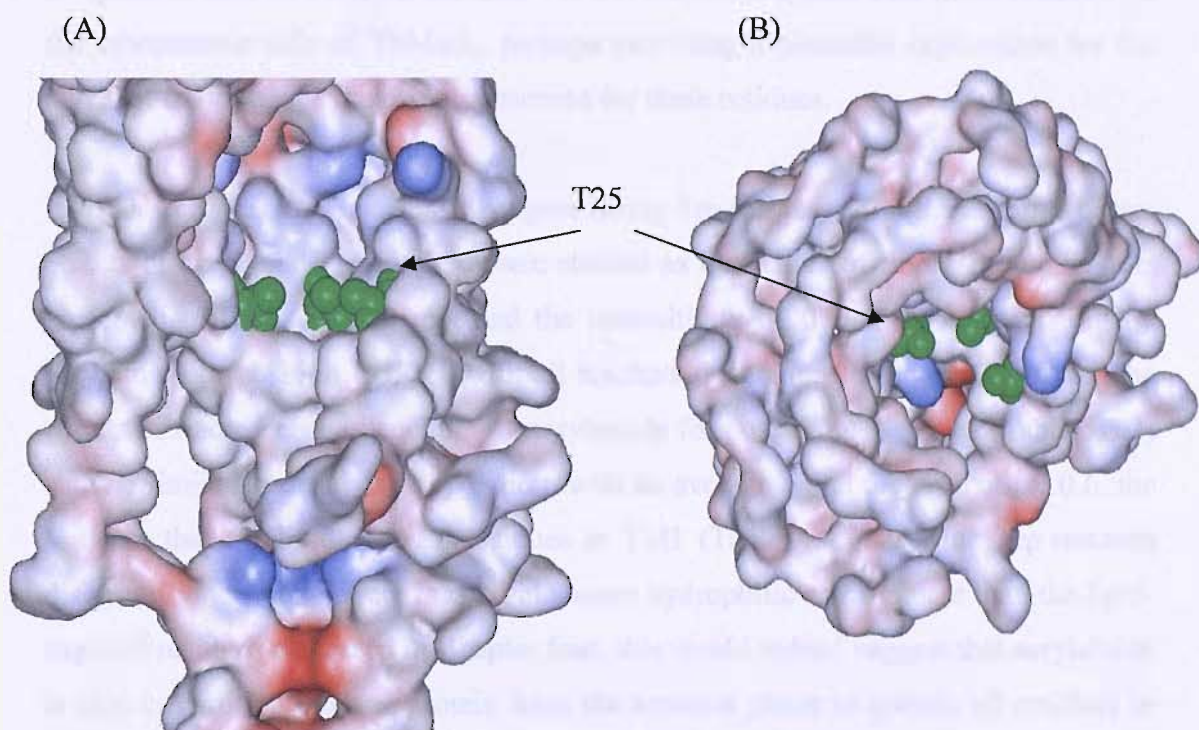


Figure 5.4.1 The inside surface of the MscL pentamer. The front two monomers have been removed to reveal the inside surface of the remaining three monomers. T25W is highlighted in green. This residue lines the pore of TbMscL and is in the middle of the membrane. (A) Transmembrane view and (B) Periplasmic view.

5.4.2 Accessibility of Trp residues from the lipid and aqueous phases.

Mutants of TbMscL with Trp mutants lining the pore were reconstituted into bilayers of di(Br₂C18:0)PC to probe their accessibility to the lipid phase. The results observed for quenching by brominated lipids are shown in Table 5.3.2. As expected, levels of fluorescence quenching are lower than those observed for lipid-exposed residues (Table 4.3.3). As T25 is located in the middle of the bilayer (Figure 5.4.1), as already mentioned, at an equivalent depth in the bilayer to that of F80W, the Trp residue in T25W can be quenched by brominated molecules in both halves of the bilayer, resulting in higher than expected values for the level of fluorescence quenching. Interestingly, the observed level of quenching for residue D36 is the same as for the lipid-exposed residue S37 (Figure 4.3.3). Due to the tilt angle of TM1, residues at the periplasmic side of TbMscL are closer to the fatty acyl chains than those residues on the cytoplasmic side of TbMscL, perhaps providing a plausible explanation for the levels of fluorescence quenching observed for these residues.

In order to assess the accessibility of pore lining Trp residues from the aqueous phase, effects of acrylamide and iodide were studied as quenchers of fluorescence. Results presented in Chapter Four revealed the insensitivity of fluorescence quenching by acrylamide to position in TM1 with all residues quenching to the same extent. The results of fluorescence quenching by acrylamide for pore lining residues (Table 5.3.3) show a similar insensitivity to position, with an average value for F/F_0 of ca. 0.6, the same as that for lipid-exposed residues in TM1 (Table 4.4.4). As the Trp mutants discussed in this chapter are located in a more hydrophilic environment than the lipid-exposed residues discussed in Chapter four, this would indeed suggest that acrylamide is able to partition into the protein from the aqueous phase to quench all residues in TM1 with equal efficacy. The results shown in Figure 5.3.3 for quenching by iodide show a slight increase in the levels of fluorescence quenching for the pore-exposed Trp residues compared to the lipid-exposed residues discussed in Chapter Four. The lower levels of quenching for Trp residues at positions 32 and 36 than positions 25 and 29 are rather surprising given their location at the widest part of the channel pore, where they would be expected to be more accessible to the aqueous phase. The differences in the levels of fluorescence quenching are, however, very small.

5.4.3 Conclusions

The results presented in this chapter focus on the channel pore and the question of how far water can penetrate into the pore. The TbMscL crystal structure indicates that a constriction in the cytoplasmic half of the TM1 pore poses a major hydrophobic barrier to ion permeation (Chang *et al.*, 1998; Spencer *et al.*, 1999). Pore lining residues below T25 were mutated to Trp (Val-22 and Gly-24) but these mutations resulted in severe gain-of-functions mutations and are thus discussed in Chapter Six. The crystal structure shows how T25 occludes the channel, possibly with ions only able to permeate into the pore as far as this residue. The more blue shifted fluorescence emission maximum obtained for a Trp residue at this position, in comparison to Trp residues located towards the periplasmic end of the pore, and the fact that mutations below this residue result on GOF phenotypes, is in good agreement with the idea that water molecules are able to penetrate down to T25, just above the pore constriction formed by residues Ile-14 and Val-21 (see Figure 1.10). Results in Chapter seven will show that the environment of the pore lining residues does not change on changing bilayer thickness. Thus any helix tilting involved in hydrophobic matching does not lead to any disruption of the pore.

Chapter 6: Gain-of-function mutants

6.1 Introduction

During channel opening, MscL moves from a closed conformation, through a series of closed intermediate states, to an open form. The proposed gating mechanism, outlining the predicted conformational changes, is discussed in Section 1.12. A key feature of the gating mechanism is the presence of closed-intermediate states, where the transmembrane region of MscL is involved in an iris-like expansion of helices away from the central pore, a process which occurs before the S1 helices (thought to comprise the secondary gate) pull apart to form the fully open form of the channel.

By inserting tryptophans into the transmembrane domain, in regions thought to be critical in the gating process, it may be possible to detect changes in conformation that are not seen in electrophysiology studies. Gain-of-function (GOF) mutants open at lower tension than wild type MscL and they may be closed in the lipid bilayer or, as in the case of severe GOF mutants, may open at zero tension and will therefore be open in the lipid bilayer. GOF mutations were first isolated in random mutagenesis studies and were localised to the cytoplasmic half of TM1 at the hydrophobic pore constriction (Ou *et al.*, 1998), postulated to be the primary gate. Leftward shifts in dose response curves, compared to wild type channels, were observed for hydrophilic substitutions of residues in this region indicating that channel gating occurred at lower membrane tensions (Yoshimura *et al.*, 1999). Further analysis of GOF mutants revealed the existence of prominent low-conducting substates at zero tensions, with further tension required to achieve the fully open state. The analysis of GOF mutants of different severity by Anishkin *et al.* revealed that closed conformations of GOF mutants are physically pre-expanded and that the most severe mutants are fully open (Anishkin *et al.*, 2005). Data obtained with GOF mutants adds weight to the two gate mechanism outlined in Section 1.12 which involves a primary gate formed by the hydrophobic pore constriction and a second gate formed by the S1 helices (see Figure 1.13). The first transition in channel gating is separation of TM1 helices resulting in a water-filled expanded conformation with transition to the fully open conformation requiring opening of the S1 helical bundle (Sukharev *et al.*, 2001a; Kong *et al.*, 2002;

Anishkin *et al.*, 2005). In the ‘tilting five-helix pore’ model proposed by Sukharev (Sukharev *et al.*, 2001b) the inner portion of the pore is lined by the five TM1 helices in all intermediate substates so that changes in environment remain small. Residues that form the hydrophobic pore constriction would experience the greatest change in environment, moving from a hydrophobic environment when closed to a hydrophilic environment upon hydration of the channel pore and subsequent channel opening.

Residues discussed in Chapter Five line the channel pore of TbMscL and upon substitution with a Trp residue, display a normal phenotype, as determined by growth curves. Residues discussed in this chapter also line the channel pore in the native structure. However, upon substitution with Trp, these residues show a gain-of-function phenotype, detectable by reduced cell growth. These GOF mutants are located in narrow regions of the channel, where introduction of a Trp residue would be expected to change the conformational structure of TbMscL. However, do these GOF mutants produce a modified conformation that is a distorted closed channel or an open form of the channel like that seen upon insertion of a positive charge at the pore constriction. In this chapter GOF mutants have been reconstituted into bilayers of di(C18:1)PC and their accessibility to both the lipid and aqueous phases assessed to try and determine whether these mutants occupy an open form of the channel or one of the closed intermediate substates.

6.2 Materials and methods

6.2.1 Materials

All chemicals were obtained from Sigma or BDH unless otherwise stated.

6.2.2 Methods

Reconstitution of TbMscL was performed as described in Chapter Four.

6.2.2.1 Small scale expression of TbMscL.

BL21(DE3)pLysS expression cells, containing the pET-19b plasmid harbouring the Trp-mutated TbMscL gene, were streaked onto LB amp plates and incubated overnight at 37 °C. A single colony was picked and inoculated into 10 mls Luria-Bertani (LB) media containing 100 µg/ml ampicillin and incubated at 37 °C in an orbital shaker at 220 rpm overnight. 500 µl of overnight culture was inoculated into fresh 10 mls LB and grown to an OD₆₀₀ of 0.6. A 1 ml pre-induction sample was taken and expression of the protein was induced by the addition of 1 mM isopropyl β,D-thiogalactopyranoside (IPTG). Cells were left for an additional 4 hours with 1 ml post-induction samples taken every hour. Samples were pelleted by centrifugation in a benchtop centrifuge at maximum speed for 5 minutes and resuspended in 60 µl 1 X sample buffer. To prepare samples for SDS-PAGE 7 µl of resuspended sample were added to 3 µl dH₂O and 5 µl 3 X SDS buffer and samples were boiled for 5 minutes prior to gel loading.

6.2.2.2 Expression of TbMscL GOF mutants

The pET-19b plasmid carrying the TbMscL gene, with the desired mutation, was transformed into BL21(DE3)pLysS expression cells as detailed in Section 2.2.19. Overnight cultures were prepared as listed in Section 2.2.19. 10 mls of overnight culture was inoculated into 1L LB amp medium and grown to an OD₆₀₀ of 1.0. Expression of protein was induced by addition of 1 mM IPTG and cells were left for one hour. Cells were pelleted by centrifugation as detailed in Section 2.2.19. 12 L of growth medium was typically used for expression of GOF mutants.

6.2.2.3 Production of charge mutants of TbMscL

Quickchange mutagenesis of TbMscL was performed as detailed in Section 3.2.2. For charge mutants of TbMscL, primers incorporating a lysine residue at position 21 were designed using DNASTar and are listed in Table 3.2.3. DNA from minipreps was obtained for Trp mutants chosen for study and used as template DNA in the PCR process.

6.3 Results

6.3.1 Functional Analysis of Trp-mutated TbmScL

Some pore-exposed residues in TM1 of TbmScL were non gain-of-function mutants and are discussed in Chapter Five. Some residues, which were also pore lining residues, produced strong GOF phenotypes as shown in the growth curves in Figure 6.3.1.

The results (Figure 6.3.1) show that cell growth was severely impaired for all three mutants (V22W, G24W, and T35W) with a maximum optical density of ca. 0.4 after three hours post induction. This is presumably a result of leakage of intracellular osmolytes from the *E.coli* cells. Statistical analysis shows that T35W and V22W are significantly different to wild type but G24W is not. That G24W does not yield large amounts of protein upon induction (comparable to wild type and non-GOF mutants), and the optical density reached is only slightly higher than the other two GOF mutants, however, it can be concluded that this mutant may not be as severe a GOF mutant as V22W and T35W but can still be considered to be in an open state. This indicates that all three Trp mutants open at lower than normal tensions and are, possibly, in the open state in the absence of membrane tension, comparable to the charge mutant V21K (Powl et al, 2005).

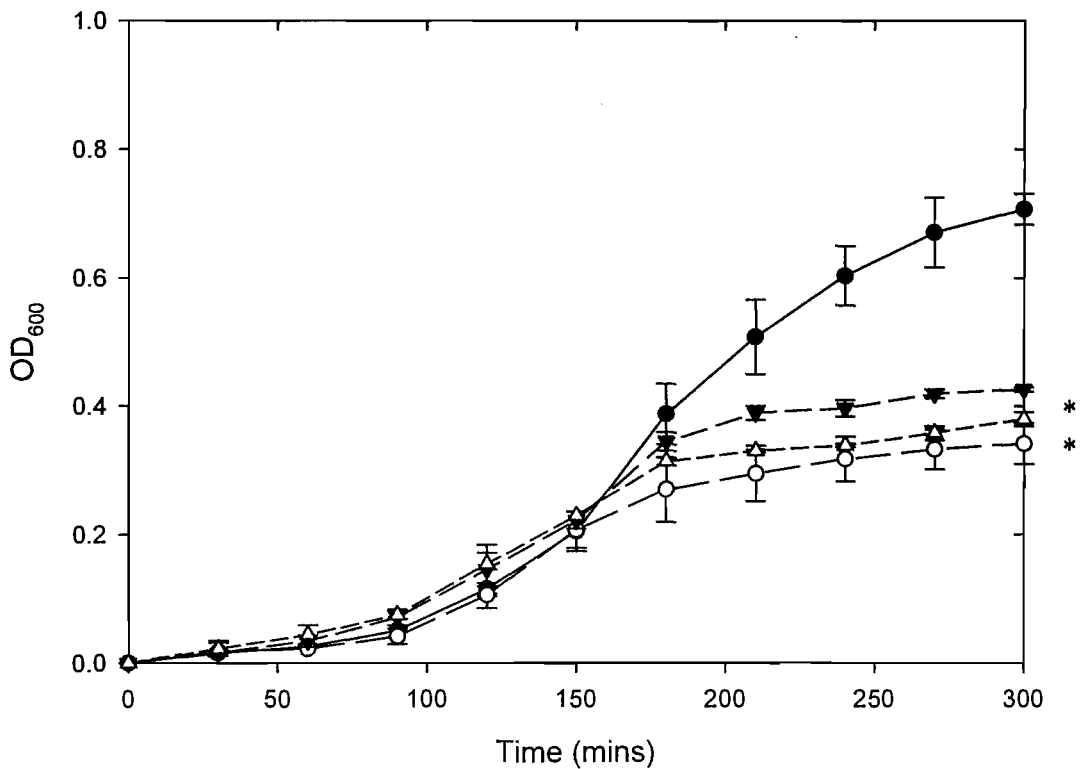


Figure 6.3.1 *In Vivo* assay for Gain of Function mutants. *E.coli* BL21(DE3)pLysS transformants carrying the pET-19b plasmid with the Trp-mutated *mscL* gene were grown in Luria both containing ampicillin ($100 \mu\text{g ml}^{-1}$) to an optical density of OD_{600} of 0.2 and expression was induced by addition of 1 mM IPTG. The optical density was measured every 30 minutes to determine which mutants produced a Gain-of-function (GOF) phenotype. TbMscL mutants expressed were: wild type, (●); V22W, (○); G24W, (▼); and T35W, (△). Error bars are standard deviations obtained from the average of three determinations.

6.3.2 Fluorescence emission spectra of Trp-mutated TbMscL.

The Trp-containing GOF mutants were reconstituted into bilayers of di(C18:1)PC at a molar ratio of lipid: protein monomer of 100:1. The fluorescence emission spectra shown in Figure 6.3.2 were fitted to the equation for a skewed Gaussian (Equation 4.4) to obtain accurate values for the wavelength of maximum fluorescence emission (Table 6.3.1). Similar to the pore-exposed mutants in Chapter five, the values obtained for the peak widths at half height (ω) are fairly large, consistent with the relationship between fluorescence emission maxima and peak width established by Ladokhin *et al.* (Ladokhin, 2000). The values for wavelengths of fluorescence emission maxima indicate a hydrophilic environment for all three residues, centred at ca. 330 nm. This is a surprising result given the location of V22 and G24 at the hydrophobic pore constriction in the closed channel. In the GOF mutants, therefore, the environment is likely to have changed so that residues at positions 22 and 24 are exposed to a more hydrophilic environment, with the channels being open at zero tension. The fluorescence emission spectrum for T35W is also characteristic of a hydrophilic environment for the Trp residue, but in this case this could be simply because residue 35 is located closer to the channel pore at the periplasmic side of TbMscL even in the closed channel.

Together with the results obtained from the growth curves (Figure 6.3.1), the data suggest that replacement of residues at positions 22, 24, and 35 with Trp results in a structure of TbMscL that is not the closed form of the channel.

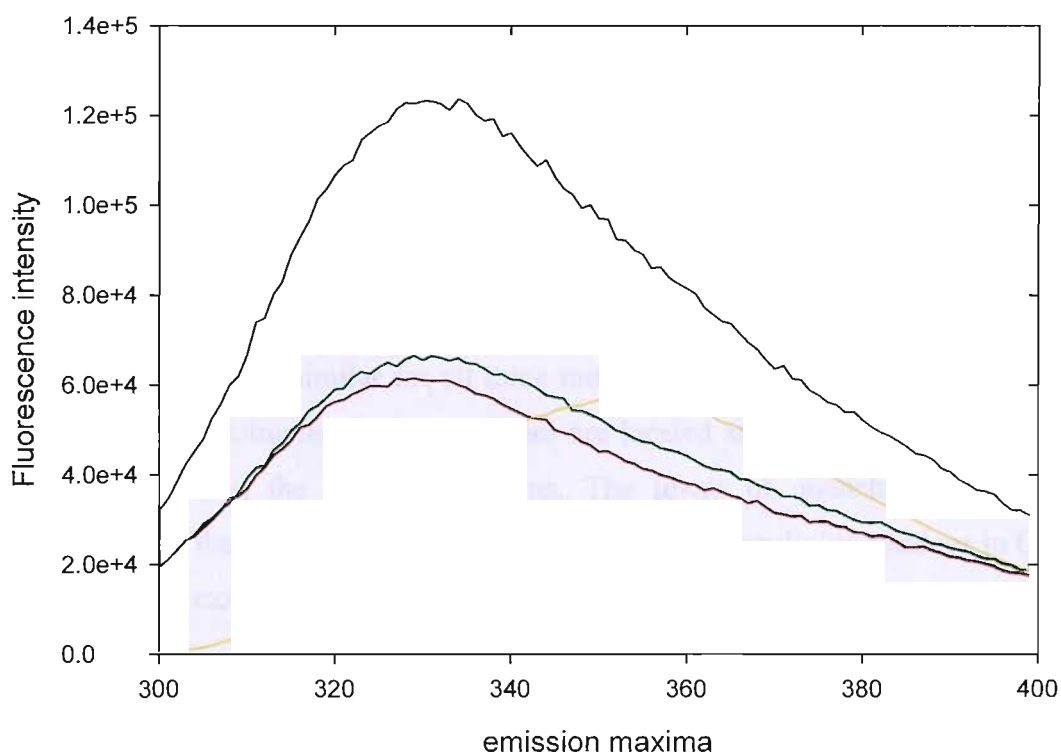


Figure 6.3.2 Fluorescence emission spectra of pore exposed GOF Trp-mutants of TbMscL. Purified TbMscL was reconstituted in di(C18:1)PC and fluorescence was excited at 280 nm. Samples were as follows: V22W, (-); G24W, (-); T35W, (-) and free Trp, (). The concentration of MscL was 0.98 μ M and the molar ratio of lipid to protein monomer was 100:1.

Mutant	λ^{\max} (nm) in di(C18:1)PC	ω (nm)
V22W	329.2 \pm 0.1	56.2 \pm 0.2
G24W	327.5 \pm 0.3	66.6 \pm 0.6
T35W	330.6 \pm 0.4	66.6 \pm 0.4

Table 6.3.1 Fluorescence emission maxima for pore-exposed GOF Trp-mutants of TbMscL reconstituted into bilayers of di(C18:1)PC and excited at 280 nm. The molar ratio of lipid to protein monomer was 100:1 and the concentration of TbMscL was 0.98 μ M.

6.3.3 Fluorescence quenching of TbMscL by brominated phospholipids

Purified TbMscL was reconstituted as described in Section 4.3.2.6 into bilayers of di(C18:1)PC and di(Br₂C18:0)PC at a 100:1 molar ratio of phospholipid to TbMscL monomer. The Trp fluorescence emission intensity was recorded at 330 nm and results were expressed as F/F_0 (Table 6.3.2) where F is the fluorescence intensity of TbMscL in brominated lipid and F_0 is the fluorescence intensity of TbMscL in non-brominated lipid.

The results shown in Table 6.3.2 indicate that levels of fluorescence quenching by brominated lipids are similar for all three mutants with an average value for F/F_0 of 0.6. This is surprising as all three residues are located at different distances from the bromine atoms in the fatty acyl chains. The levels of quenching observed are comparable to the levels of quenching obtained for the pore lining residues in Chapter five, with the exception of T32W, which showed an average level of quenching of 0.70.

Mutant	F/F_0 in di(Br₂C18:0)PC
V22W	0.56 ± 0.02
G24W	0.62 ± 0.04
T35W	0.62 ± 0.03

Table 6.3.2 Quenching of Trp fluorescence by brominated phospholipids. Mutants were reconstituted into bilayers of di(C18:1)PC and di(Br₂C18:0)PC. Fluorescence intensities were recorded at 330 nm and are expressed as F/F_0 . Values and standard deviations were obtained from the average of three determinations in duplicate.

6.3.4 Fluorescence quenching of TbMscL by acrylamide and iodide

Fluorescence quenching of lipid facing residues on TM1 by acrylamide and iodide was used to assess the accessibility of Trp residues in TbMscL from the aqueous phase in bilayers of di(C18:1)PC. TbMscL was reconstituted into bilayers of di(C18:1)PC at a 100:1 molar ratio of phospholipid to TbMscL monomer as previously described.

Values of F/F_0 for Trp mutants reconstituted into bilayers of di(C18:1)PC in the presence of 300 mM acrylamide or 450 mM iodide are shown in Table 6.3.3. As previously observed for all Trp mutants, the levels of fluorescence quenching observed with acrylamide are very similar, with an average value for F/F_0 of 0.6. Although only two mutants were assessed for their accessibility to iodide, due to the inability to purify more protein for T35W, the levels of fluorescence quenching observed are quite different for the two mutants assayed. The level of quenching observed for G24W is considerably lower than levels of quenching observed for the pore-exposed residues in Chapter five, indicating that the Trp residue in this GOF mutant is not as accessible to the channel pore as the other pore exposed residues and may be facing towards a more buried environment. The level of quenching observed for V22W is similar to the levels of quenching seen for the pore lining residues in Chapter five.

	Acrylamide	Iodide
Mutant	F/F_0 in di(C18:1)PC	F/F_0 in di(C18:1)PC
V22W	0.62 ± 0.03	0.71 ± 0.03
G24W	0.63 ± 0.03	0.83 ± 0.02
T35W	0.58 ± 0.03	-

Table 6.3.3 Fluorescence quenching of pore facing GOF mutants on TM1 by the aqueous quenchers acrylamide and iodide. Results are expressed as F/F_0 where F and F_0 are fluorescence intensities for TbMscL reconstituted into di(C18:1)PC in the presence and absence of 300 mM acrylamide and 450 mM iodide respectively. Bar charts show the average of three determinations and standard deviations in duplicate.

6.3.5 V21K mutants of TbMscL

In the previous section Trp mutants were made which resulted in GOF phenotypes. A limitation of this approach is that the Trp residue both triggers a change underlying the GOF phenotype and acts as the reporter group. It is not therefore possible to compare the Trp fluorescence spectrum in an open state with that for the Trp residue in a closed state. In this section, an alternative procedure was adopted, in which the Trp residue served as a reporter group alone, with a separate mutation resulting in the GOF phenotype. Gly-22 in EcoMscL forms the narrowest part of the channel at the hydrophobic constriction. Val-21 in TbMscL is equivalent to Gly-22 in EcoMscL. By substituting Val-21 at the pore constriction of TbMscL with a lysine residue, Powl *et al.* found that the insertion of a positive charge resulted in a severe GOF phenotype, and that there was a significant shift in Trp fluorescence emission to longer wavelength, from 321 nm for F80W to 331 nm, for the double mutant V21K:F80W (Powl *et al.*, 2005a). This indicates that residue F80 moves from a hydrophobic environment to a hydrophilic environment on introducing a lysine residue at position 21, presumably upon moving from a closed form of the channel to an open form of the channel in the GOF phenotype. This suggests that the GOF phenotype is associated with a major change in conformation, affecting the location of the Trp residue. In order to determine how TM1 helices change during channel opening, mutants that display a normal phenotype upon Trp substitution were chosen for study with the addition of the lysine mutation at position 21. Trp emission spectra could then be compared for TbMscL in the closed and open states. Trp residues chosen for study were the lipid-exposed mutants L30W, V31W, and F34W, discussed in Chapter four, and the pore-exposed mutant T32W, discussed in Chapter five. An *in vivo* cell viability assay was carried out to ensure the addition of a lysine residue at position 21 did result in a GOF phenotype. The results shown in Figure 6.3.3 show that growth was severely impaired for all four V21K mutants reaching an optical density of ca. 0.4 after three hours post induction, a result seen by Powl *et al.* for V21K:F80W (Powl *et al.*, 2005a).

Unfortunately, with these GOF mutants, amounts of TbMscL that could be purified were very small, with levels that were undetectable on a coomassie stained SDS gel. In an attempt to increase the amount of protein, growth was tried in the presence of

gadolinium since at submillimolar concentrations, gadolinium ions have been shown to prevent release of intracellular metabolites by inhibiting stretch-activated channels (Ewis and Lu, 2005). Studies by Ewis also revealed that gadolinium was able to block the release of cytoplasmic proteins such as Elongation factor Tu (EF-Tu) and carboxylesterase (Est55) as a result of osmotic shock (Ewis *et al.*, 2005) in EcoMscL. To see whether gadolinium could increase the amount of TbMscL expressed from BL21 cells, by blocking the channel, small scale expression assays were carried out using 0.3 mM and 3 mM gadolinium over a four hour period. The results shown in Figure 6.3.4 show a normal level of protein expression for wild type TbMscL but no detectable expression for V21K:F34W in the presence of gadolinium, although it must be being expressed at least at a lower level as it produces a GOF phenotype.

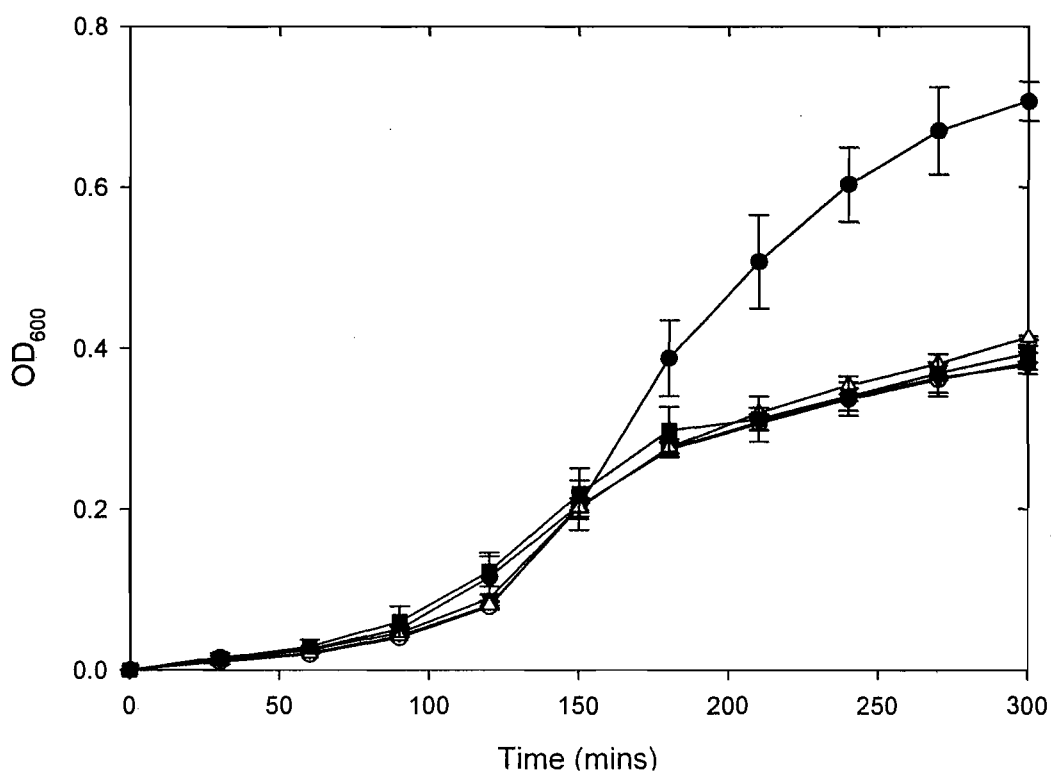


Figure 6.3.3 *In Vivo* assay for V21K Gain of Function mutants. *E.coli* BL21(DE3)pLysS transformants carrying the pET-19b plasmid with the Trp-mutated *mscL* gene were grown in Luria both containing ampicillin ($100 \mu\text{g ml}^{-1}$) to an optical density of OD_{600} of 0.2 and expression was induced by addition of 1 mM IPTG. The optical density was measured every 30 minutes to determine which mutants produced a Gain-of-function (GOF) phenotype. TbMscL mutants expressed were: wild type, (●); V21K:L30W, (○); V21K:V31W, (▼); and V21K:T32W; (△), and V21K:F34W; (■). Error bars are standard deviations obtained from the average of three determinations.

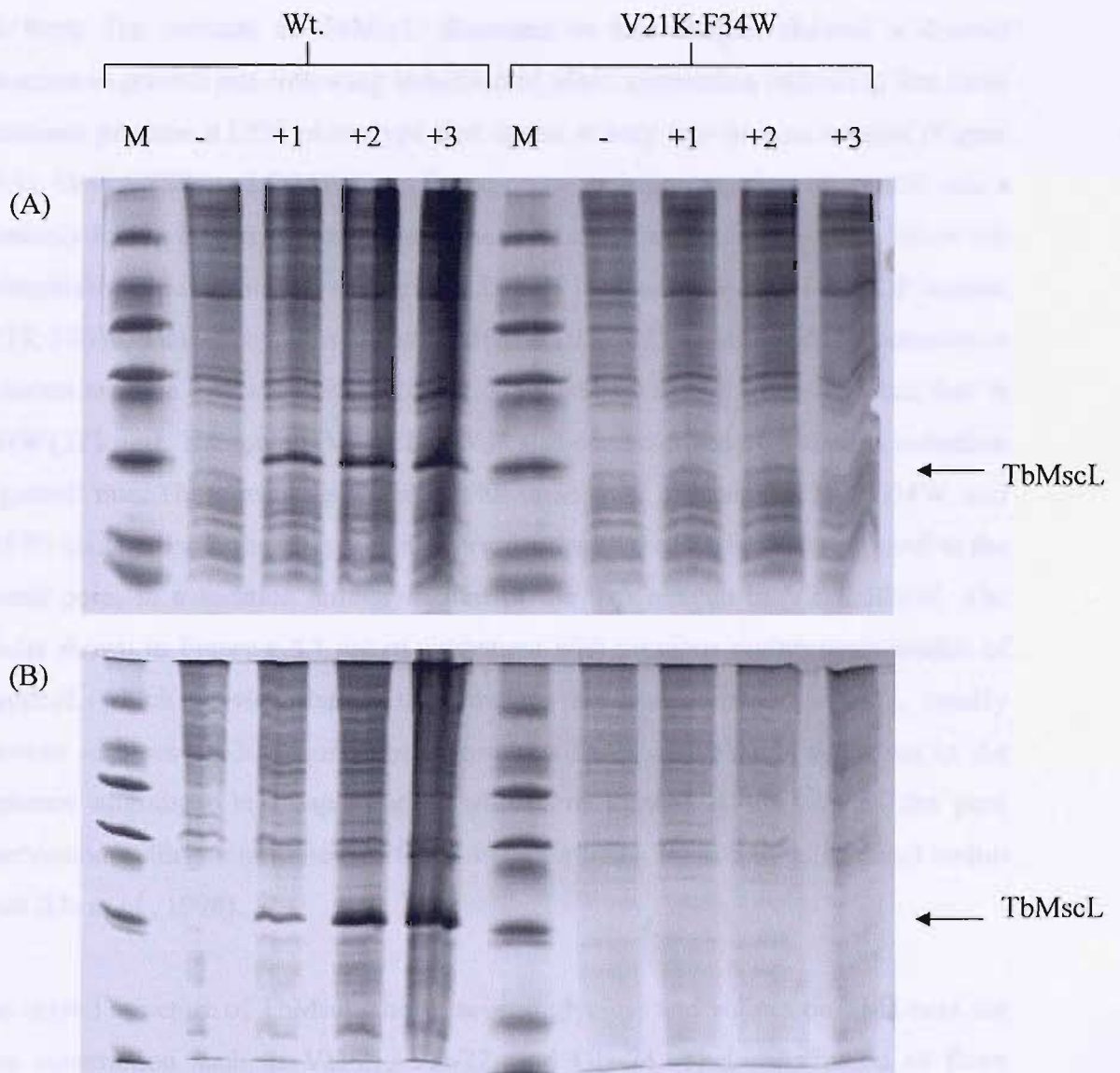


Figure 6.3.4 Effects of gadolinium on expression of TbMscL. Small scale expression of wild type TbMscL and V21K:F34W was assayed in the absence and presence of (A) 0.3 mM and (B) 3 mM gadolinium. Molecular weight markers are shown (M), and sample pre-induction (-), and one to four hours post induction (+1, +2, +3, and +4). The position of the TbMscL monomer is shown.

6.4 Discussion

All three Trp mutants of TbMscL discussed in this chapter showed a distinct reduction in growth rate following induction of MscL expression indicating that these mutations produce a GOF phenotype that opens at very low or zero tension (Figure 6.3.1). Both V22W and G24W have fluorescence emission maxima of ca. 330 nm, a relatively long wavelength considering the location of these Trp residues below the hydrophobic pore constriction (Figure 6.3.2). It is interesting that the GOF mutant V21K:F80W, studied by Powl *et al.* (Powl *et al.*, 2005a), also had a fluorescence emission maxima that was shifted to a much longer wavelength (331 nm) than that in F80W (321 nm). The mutant V21K:F80W is also characterised by a distinct reduction in growth rate. These results suggest that all three GOF mutants (V22W, G24W, and T35W) could exist in the bilayer in an open form with the Trp residues exposed to the central pore, in a location similar to that of the Trp residue in V21K:F80W. The results shown in Figure 6.3.1 are in agreement with previous mutagenesis studies of EcoMscL which showed that GOF mutations are concentrated on TM1, mostly between residues 13-30 (equivalent to residues 11-28 in TbMscL as shown in the sequence alignment in Chapter one), which are located at the rim of the pore constriction, with the most severe GOF mutation being substitutions of small amino acids (Ou *et al.*, 1998).

The crystal structure of TbMscL shows several glycines and valines on TM1 near the pore constriction such as Val-21, Val-22, and Gly-24. That substitution of these residues to larger or charged amino acids lead to GOF mutations, identified by bacterial growth assays, highlights the importance of these small polar amino acids for the gating process (Ou *et al.*, 1998). Results with EcoMscL have also shown that when G22 (equivalent to V21 in TbMscL) on TM1 was substituted with all other 19 amino acids, LOF and GOF phenotypes were observed depending on the hydrophilicity of the substituted residue, with substitutions for hydrophilic residues resulting in GOF phenotypes showing a decrease in the threshold pressure required to open the channel, whereas substitutions for hydrophobic residues increased the threshold pressure to open the channel (Yoshimura *et al.*, 1999).

The results obtained for fluorescence quenching by brominated lipids (Table 6.3.2) shows an appreciable level of fluorescence quenching still occurs with these GOF

mutants. The charge mutant V21K:F80W gave an F/F_0 value of 0.52 for fluorescence quenching in bilayers of di(Br₂C18:0)PC (Powl *et al.*, 2005a), (the Trp residue in this mutant being thought to face inwards towards the channel pore similar to the GOF mutants shown in Table 6.3.2). The Trp residue in the mutant F80W is a lipid-exposed residue in TM2, as shown by its fluorescence emission maxima of 321 nm and the high level of quenching by di(Br₂C18:0)PC observed for this mutant. The fluorescence emission maximum observed for the charge mutant of F80W (V21K:F80W) shows a more polar environment for the Trp residue of 331 nm, along with a lower level of fluorescence quenching with di(Br₂C18:0)PC. This suggests that a large change in conformation is observed upon channel opening with F80W upon moving from a hydrophobic environment when closed to a more hydrophilic environment when open. In Chapter five, the pore exposed Trp residues had fluorescence emission maxima centred at around 330 nm with values for F/F_0 in di(Br₂C18:0)PC of ca. 0.52. The values for F/F_0 for GOF mutants in this chapter were compared with values for F/F_0 obtained for lipid-exposed residues at similar depths in the lipid bilayer.

Mutant	Distance (Å) from L69	F/F_0	Mutant	Distance (Å) from L69	F/F_0
F84W	19.0	0.13	V22W	19.0	0.56 ± 0.02
F84W	19.0	0.13	G24W	19.0	0.62 ± 0.04
S37W	2.9	0.54	T35W	2.6	0.62 ± 0.03

Table 6.4.1 Fluorescence quenching by brominated phospholipids for lipid-exposed residues and GOF mutants at equivalent depths in the bilayer. Results are expressed as F/F_0 where F and F_0 are fluorescence intensities for TbMscL reconstituted into di(Br₂C18:0)PC and di(C18:1)PC respectively. Values and standard deviations were obtained from the average of three determinations in duplicate.

As can be seen in Table 6.4.1, fluorescence emission maxima and F/F_0 values were different to those obtained for lipid-exposed residues, suggesting that Trp residues in the GOF mutants V22W, G24W, and T35W are pore exposed. That the level of quenching is slightly higher in V21K:F80W than the GOF mutants on TM1 (Table 6.3.2) could simply be due to the location of F80W on TM2, closer to the lipids and located in the centre of the bilayer, so that the Trp residue can be quenched by bromine atoms on both sides of the membrane.

The results obtained for quenching by acrylamide are, again, very similar to those observed in previous chapters for lipid-exposed and pore-exposed mutants with values for F/F_0 of ca. 0.60 at 300 mM acrylamide (Table 6.3.3). The results obtained for quenching by iodide are interesting with a value for F/F_0 for G24W of 0.83 at 450 mM iodide (Table 6.3.3) compared to a value of 0.71 for V22W. This suggests that G24W could be located away from the channel pore, inaccessible to the aqueous phase. G24W also has the most blue-shifted spectrum of the GOF mutants, with a fluorescence emission maximum of 327 nm. The value of F/F_0 obtained for V22W in 450 mM iodide, of 0.71 (Table 6.3.3) is consistent with a location for this residue facing into the channel pore.

That the GOF mutants obtained from Trp mutation alone were expressed with a close to normal protein yield suggest that these channels are not in the fully open state but may simply be in one of the intermediate substates. The ‘tilting five-helix pore model’ suggests that TM1 and TM2 helices retain their relative positions during channel gating and that pore lining residues remain facing the pore in all conformations (Sukharev *et al.*, 2001b). The longer wavelengths observed for these mutants can be attributed to hydration of the channel pore during the first conformational change in channel gating leading to the first closed intermediate substate.

By modelling Trp residues into the crystal structure of TbMscL, steric clashes were observed for all three GOF mutants. Figure 6.4.1 shows G24 and V22 in direct contact. Modelling a Trp residue into position 24 results in extreme clashes, as expected. G24 can be rotated to minimise clashes, which results in a location for G24W pointing away from the pore towards the lipid bilayer (Figure 6.4.1). However, the structure of TbMscL in 6.4.1b is in the closed form. If the Trp residue in G24W is

displaced, then this would be the expected position. The alternative, however, is for the Trp residue to force the channel open to create more space. The fluorescence emission maximum obtained for G24W is rather more polar than expected if the Trp residue was simply displaced, therefore the channel is more likely to be in the open form.

The Trp residue in T35W on TM1, located on the periplasmic side of MscL, is located at the periplasmic side of TbMscL where the tilt angle of TM1 helices is greatest but also where TM1 is closest to TM2. It has been proposed that TM1 and TM2 helices of adjacent subunits stay together and change their tilt together during expansion of the transmembrane region during the gating process (Sukharev *et al.*, 2001b) and adjacent TM1 helices exhibit 4-4 ridges-into-grooves packing, a feature also seen in the potassium channel KcsA (valiyaveetil *et al.*, 2002). Insertion of a bulky Trp residue at position 35 could therefore interfere with helix packing requirements. What is interesting is that this particular mutation results in a GOF channel rather than a distorted version of the closed channel.

The growth curves for all three Trp mutants discussed in this chapter strongly suggest that these mutants cause TbMscL to adopt an open form of the channel. As these mutants are located below the pore constriction in the closed state, the fluorescence emission maxima for these residues would perhaps be expected to be quite blue-shifted. That the values of fluorescence emission maxima obtained are rather different to those obtained for lipid-exposed residues at equivalent depths in the bilayer, and are quite red-shifted with values similar to the Trp mutant in the charge mutant V21K:F80W, it can be concluded that these residues are indicative of TbMscL in the open form. V22W and G24W, in particular, quench a lot less than the equivalent lipid-exposed residue (Table 6.4.1), indicating that these residues may face inwards towards the channel pore.

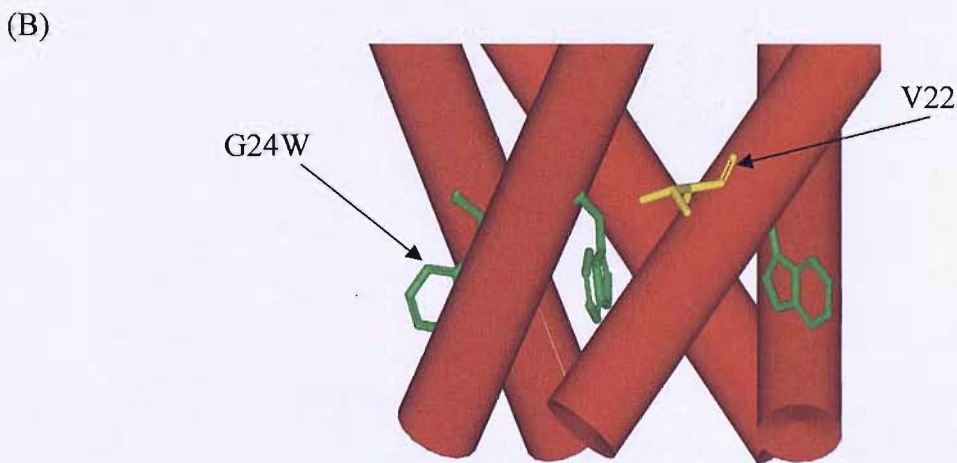
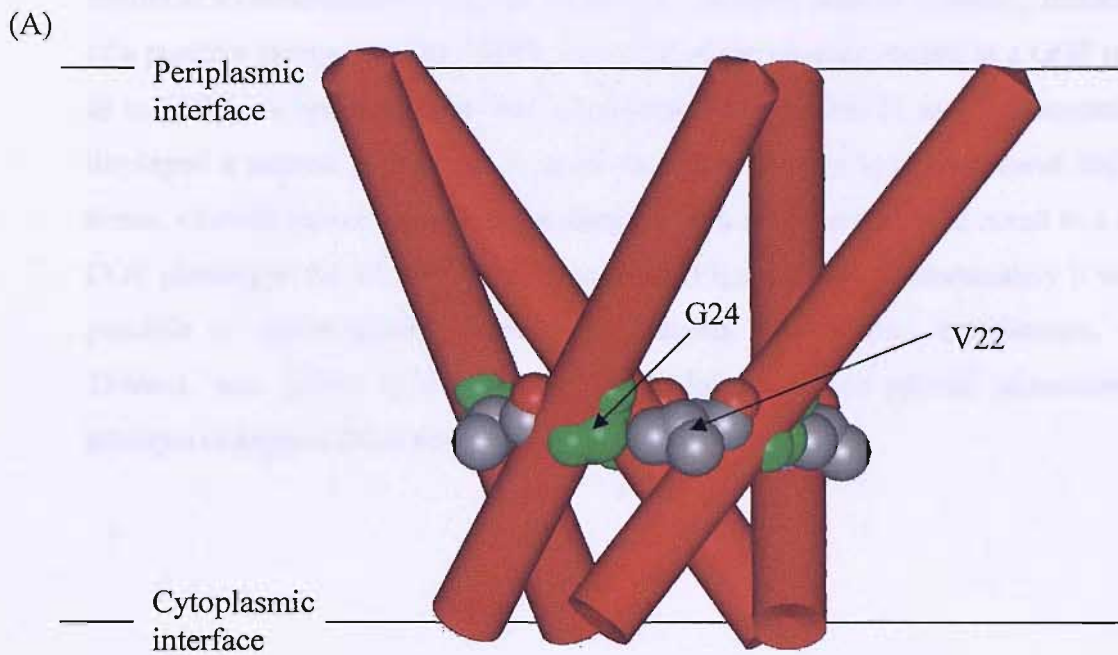


Figure 6.4.1 Schematic representation of TbMscL showing contacts between Gly-24 and Val-22 on neighbouring TM1 helices. (A) shows Gly-24 (green) in direct contact with Val-22 in a ring of residues facing into the core of the protein structure. (B) shows a Trp residue modelled into the crystal structure at position 24 and shown in stick format. The residue is facing outwards towards TM2 and the lipid bilayer.

Fluorescence properties of the V21K:F80W charge mutant suggests that the mutation results in a conformational change, leading to the open state of TbMscL. Introduction of a positive charge into the narrowest region of the channel results in a GOF mutant, as in V21K. A lysine residue was incorporated at position 21 into Trp mutants that displayed a normal phenotype in order to obtain data in both the closed and open forms. Growth curves show that the insertion of a lysine residue did result in a severe GOF phenotype for all four mutants assayed (Figure 6.3.3). Unfortunately it was not possible to obtain protein from these mutants. Small scale experiments, where TbMscL was grown in the presence of gadolinium, also proved unsuccessful in attempts to express these severe GOF mutants.

Chapter 7: Effects of lipid headgroup and chain length on TbMscL

7.1 Introduction

Although there are many questions that still need answering regarding protein-lipid interactions one important feature of the interaction is hydrophobic matching between the hydrophobic regions of the membrane protein and the lipid bilayer. During channel gating of TbMscL, the entire transmembrane complex expands dramatically, believed to result in extensive tilting and rotation of helices. Although several experiments have reported on the effects of lipid chain length on MscL gating (Hamill and Martinac, 2001; Kloda and Martinac, 2001), studies by Perozo *et al.* (Perozo *et al.*, 2002a) showed that reconstitution of EcMscL into short chain length lipids lowered the gating threshold required for opening and conversely, reconstitution into longer chain length lipids increased the gating threshold required to open the channel (Perozo *et al.*, 2002a; Perozo *et al.*, 2002b). By changing the lipid chain length conformational changes were seen upon changing from long chain to short chain lipid, in particular narrowing of the channel pore. Also, lipids immediately surrounding the protein were observed to be thinner than the bulk lipid upon reconstitution into short chain lipid, indicating the importance of hydrophobic matching between lipids and proteins (Elmore and Dougherty, 2003). This suggests that in short chain length lipids, EcMscL is likely to occupy one of the several sub-conducting states, in which the transmembrane α -helices have undergone some degree of tilting and rotation to achieve a thinner cross section, matching better a thin lipid bilayer. The predicted movements of transmembrane α -helices are shown in Figure 7.1.1.

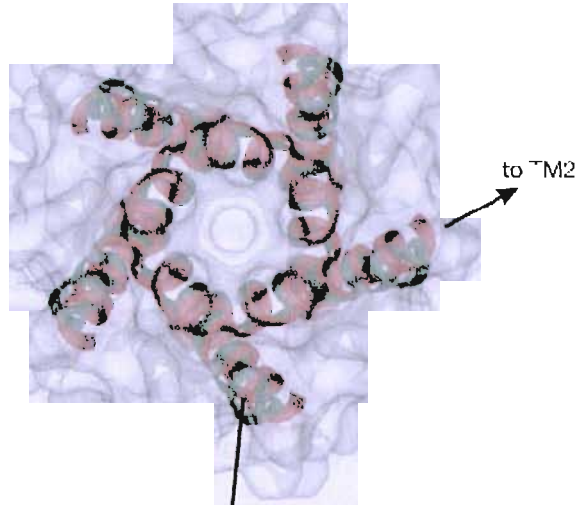
In addition to lipid chain length, lipid headgroups have been shown to be important for protein function. As gating of MscL is driven by an increase in lateral tension in the lipid bilayer, interactions between MscL and surrounding lipids are paramount to the gating process. Changes in lipid composition are therefore, likely to have an effect on the gating process. Previous molecular dynamics simulations have shown how different lipid head groups effect MscL structure and dynamics on the molecular level using molecular dynamics simulations, (Elmore and Dougherty, 2001; Gullingsrud, 2001). However previous MD simulations only considered one type of lipid with no

direct comparisons between structures in different lipids. As a result Elmore and Dougherty directly compared the effects of lipid chain length and lipid headgroup on the structure of TbMscL embedded in bilayers of PC and PE. The most noticeable changes upon changing headgroup from bilayers of PE to PC were seen in the C-terminal region of TbMscL, with a significant conformational change bringing the upper portion of this region closer to the membrane, and in the extracellular loop region. This result has been attributed to the decrease in protein-lipid hydrogen bonding interactions moving from PC to PE (Elmore *et al.*, 2003). The presence of nonbilayer forming lipids such as PE have been shown to have a direct effect on function by for many proteins, (Brink-van der Laan *et al.*, 2004) by either causing curvature stress in the membrane or by having a direct effect as a result of differences in hydrogen bonding and solvation properties of the protein, in particular peripheral proteins such as protein kinase C (Stubbs and Slater, 1996) and phospholipase A₂ (Cornell and Arnold, 1996). Conformational changes at the ends of α -helices can also be observed as a consequence of hydrogen bonding interactions as hydrogen bonding partners can be found in the glycerol backbone and headgroup regions of bilayer (Lee, 2004), different interactions being achieved with different lipid headgroups. Specific species of lipids can also have a direct influence on membrane protein function and are often co-crystallised with the protein. These lipids are termed co-factor lipids or non-annular lipids, since they interact with much greater specificity with the protein than annular lipids (Lee, 2004). An example of a lipid of this type is the phosphatidylglycerol (PG) molecule bound between α -helices at monomer-monomer interfaces in KcsA. PG or other anionic lipids are required for function of KcsA, acting as a co-factor for the protein (Heginbotham *et al.*, 1998;valiyaveetil *et al.*, 2002).

Changing lipids can often lead to conformational changes in protein structure and this can be detected by Trp fluorescence spectroscopy. For example, if helices in MscL rotate during conformational changes, a Trp residue exposed to the pore, in a hydrophilic environment, could change its position to be located facing the surrounding lipids, in a hydrophobic environment, hence resulting in a large change in tryptophan fluorescence. In this chapter, the effects of changing lipid headgroup and lipid chain length are studied for all the Trp mutants studied in previous chapters. Previous studies by Powl *et al.* reported the presence of hot spots for binding of

anionic phospholipids on the cytoplasmic side of the membrane. Binding constants for phospholipids to MscL from determined by the levels of Trp fluorescence quenching caused by brominated phospholipids will be used to assess whether residues on TM1 report any selectivity in binding of phospholipids and whether there are binding sites on the periplasmic side of MscL for a particular class of phospholipids.

(A)



(B)

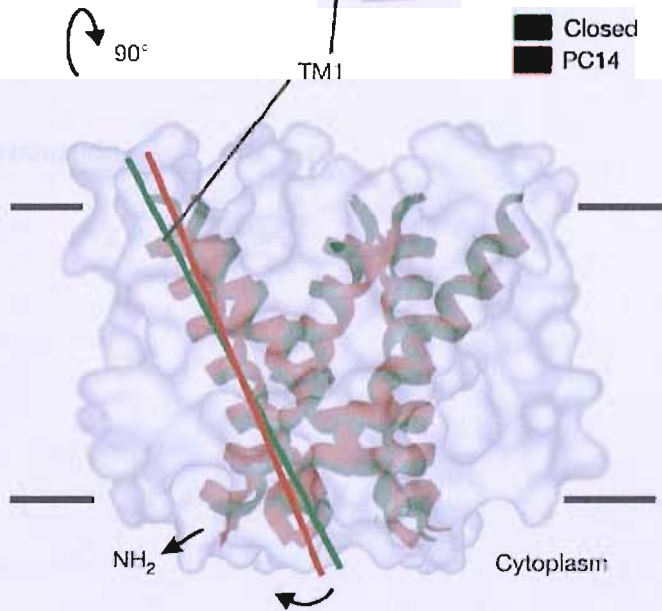


Figure 7.1.1 Ribbon diagram of EcoMscL showing predicted positions of TM1 helices in the closed-intermediate state (red; di(14:1)PC) and the closed state (green) as modelled in the crystal structure (Perozo *et al.*, 2002a). Helices are seen to rotate clockwise about the central helical axis by about 30° with a slight tilt towards the plane of the bilayer. (A) periplasmic view and (B) lateral view.

7.2 Methods and Materials

7.2.1 Materials

All chemicals were obtained from Sigma or BDH unless otherwise stated.

Avanti Polar Lipids

di(C14:1)PC	1,2 dimyristoleoyl- <i>sn</i> -glycero-3-phosphatidylcholine
di(C18:1)PC	1,2 dioleoyl- <i>sn</i> -glycero-3-phosphatidylcholine
di(C18:1)PE	1,2 dioleoyl- <i>sn</i> -glycero-3-phosphatidylethanolamine
di(C18:1)PG	1,2 dioleoyl- <i>sn</i> -glycero-3-phosphatidylglycerol
di(C18:1)PA	1,2 dioleoyl- <i>sn</i> -glycero-3-phosphatidic acid
di(C18:1)PS	1,2 dioleoyl- <i>sn</i> -glycero-3-phosphatidylserine
di(C22:1)PC	1,2 dierucoyl- <i>sn</i> -glycero-3-phosphatidylcholine

Bachem

n-octyl β -D-glucopyranoside

7.2.2 Methods

7.2.2.1 Reconstitution into mixed lipid Bilayers

Reconstitution into lipid bilayers was performed as described in Chapter Four.

For reconstitution of TbMscL into bilayers composed of two different phospholipids, separate lipid stocks were dried down and re-hydrated in cholate buffer as described in Section 4.3.2.6. Aliquots of the two lipid stocks in cholate were then mixed to achieve the desired mole ratios and incubated for 30 minutes at 70 °C to ensure mixing of lipids. TbMscL was added once the lipid mixtures had cooled to below 37 °C. Further steps were carried out as detailed above.

7.2.2.2 Reconstitution of Trp analogue into mixed bilayers

The Trp analogue NPTH (N-palmityl-Trp-Hexyl) was made upto 1 mg/ml in methanol. The appropriate mixtures of lipid and NPTH were dried down in sonication vials to give a mole ratio of lipid to NPTH of 100:1. The lipid and NPTH mixtures were resuspended in Hepes buffer and the sample was diluted into Hepes buffer to give a final concentration of NPTH of 1 µM.

7.2.2.3 Analysis of Fluorescence Measurements

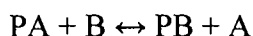
Quenching of Trp fluorescence by brominated phospholipids in mixtures of brominated phospholipid and the equivalent non-brominated phospholipid was fitted to a lattice model of quenching (Equation 7.1)

$$F = F_{\min} + (F_0 - F_{\min})(1 - x_{\text{Br}})^n \quad \text{Equation 7.1}$$

where F_0 and F_{\min} are the fluorescence intensities in non-brominated and brominated lipid respectively, F is the fluorescence intensity in the phospholipid mixture when the mole fraction of brominated lipid is x_{Br} , and n is the number of lipid binding sites

from which the fluorescence of the tryptophan residue can be quenched (Powl *et al.*, 2005a).

Reconstitution of TbMscL into mixtures of non-brominated lipid A and brominated lipid B allows the determination of the binding constant of A relative to B. An equilibrium between the lipids at each lattice site, as shown in Figure 7.2.1, will be reached, described by the following equation.



where PA and PB are protein bound to lipid A and lipid B respectively. The relative association constant (K) of lipid B relative to lipid A is given by equation 7.2 where square brackets denote the concentrations of various lipid species

$$K = ([PB][A])/([PA][B]) \quad \text{Equation 7.2}$$

The fraction of annular sites on TbMscL occupied by lipid B (brominated lipid, f_{Br}) is given by Equation 7.3

$$f_{Br} = [PB]/([PB] + [PA]) \quad \text{Equation 7.3}$$

which can be expanded from Equation 4.7 to give Equation 7.4.

$$f_{Br} = Kx_{Br}/(Kx_{Br} + [1 - x_{Br}]) \quad \text{Equation 7.4}$$

Fluorescence quenching in the lipid mixtures is then given by an equation analogous to equation 7.1:

$$F = F_{min} + (F_0 - F_{min})(1-f_{Br})^n \quad \text{Equation 7.5}$$

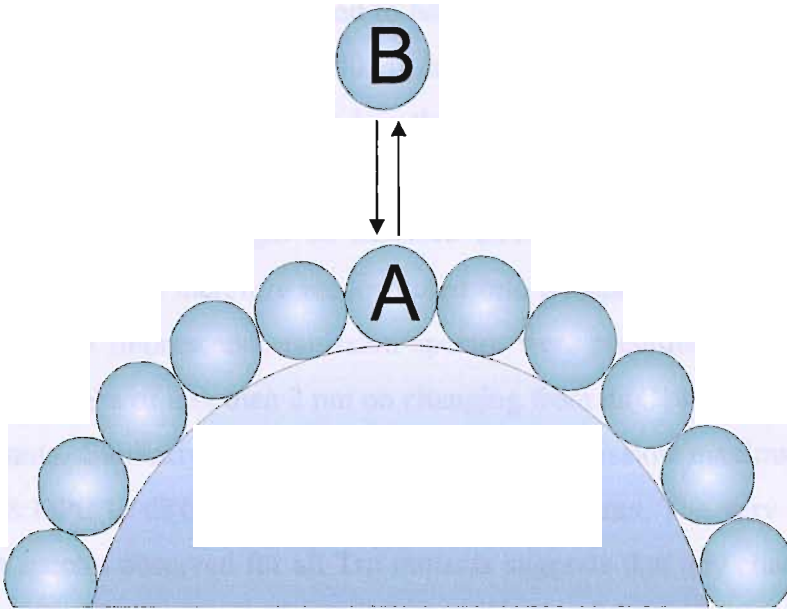


Figure 7.2.1 Cartoon showing lipid binding sites on the transmembrane surface of a membrane protein. The exchange of two phospholipids, A and B, at one site on the surface of the protein is shown. The exchange of lipid A and B is described by the relative binding constant K (modified from Lee, 2003).

7.3 Results

7.3.1 Effects of lipid chain length on emission maxima

The open form of TbMscL is predicted to have a hydrophobic thickness less than that of the closed form (Perozo *et al.*, 2002a) and Perozo *et al.* showed that the tension required to open the channel was less in a thin bilayer than in a thicker bilayer. These results suggested that MscL might adopt a different conformation in short or long chain lipids that, in turn, might be detected through changes in Trp fluorescence emission. TbMscL was therefore reconstituted into phosphatidylcholines of different chain lengths and fluorescence emission spectra were recorded. The results (Table 7.3.1) show changes of less than 2 nm on changing from di(C18:1)PC to di(C22:1)PC for all mutants. Similarly, changes in fluorescence emission maxima on changing from di(C18:1)PC to di(C14:1)PC are small for all mutants. The very small changes in emission spectra observed for all Trp mutants suggests that any changes in the tilt or rotation of α -helices upon reconstitution into long or short chain lipids are likely to be small.

Mutant	di(C14:1)PC		di(C18:1)PC		di(C22:1)PC	
	λ^{\max}	Peak width (ω)	λ^{\max}	Peak width (ω)	λ^{\max}	Peak width (ω)
A20W	330.1 ± 0.2	58.1 ± 0.3	329.3 ± 0.2	58.4 ± 0.3	329.4 ± 0.2	61.3 ± 0.3
V22W	328.7 ± 0.1	55.5 ± 0.2	329.2 ± 0.1	56.2 ± 0.2	330.7 ± 0.1	56.6 ± 0.2
I23W	325.0 ± 0.1	50.6 ± 0.2	325.2 ± 0.1	50.9 ± 0.2	326.5 ± 0.1	51.9 ± 0.2
G24W	326.9 ± 0.3	65.7 ± 0.6	327.5 ± 0.3	66.6 ± 0.6	328.8 ± 0.3	66.6 ± 0.6
T25W	331.9 ± 0.1	59.0 ± 0.2	331.2 ± 0.1	59.5 ± 0.2	332.5 ± 0.1	59.7 ± 0.2
F27W	321.7 ± 0.2	49.8 ± 0.4	321.0 ± 0.2	50.4 ± 0.4	322.4 ± 0.2	52.4 ± 0.4
A29W	330.7 ± 0.2	63.0 ± 0.3	331.2 ± 0.2	63.0 ± 0.3	331.3 ± 0.2	62.0 ± 0.3
L30W	327.7 ± 0.1	55.3 ± 0.2	327.6 ± 0.1	57.8 ± 0.2	329.1 ± 0.1	57.0 ± 0.2
V31W	322.0 ± 0.1	53.8 ± 0.3	323.9 ± 0.1	53.3 ± 0.3	324.7 ± 0.1	54.1 ± 0.2
T32W	335.9 ± 0.1	62.2 ± 0.2	337.2 ± 0.1	64.5 ± 0.2	338.0 ± 0.1	65.0 ± 0.2
F34W	325.3 ± 0.2	58.5 ± 0.5	326.2 ± 0.4	66.6 ± 0.9	326.9 ± 0.1	65.8 ± 0.7
T35W	330.6 ± 0.2	64.9 ± 0.4	330.6 ± 0.4	66.0 ± 0.4	331.4 ± 0.2	64.5 ± 0.4
D36W	335.3 ± 0.1	62.9 ± 0.2	335.2 ± 0.1	62.5 ± 0.2	335.8 ± 0.1	65.4 ± 0.2
S37W	335.6 ± 0.0	58.0 ± 0.1	335.9 ± 0.1	58.4 ± 0.2	336.3 ± 0.1	58.5 ± 0.1

Table 7.3.1 Fluorescence emission maxima for Trp mutants of TbMscL as a function of phospholipid chain length. Mutants were reconstituted into bilayers of di(C14:1)PC, di(C18:1)PC, and di(C22:1)PC. Fluorescence emission spectra were recorded between 300 nm and 400 nm. Emission spectra were fitted to a skewed Gaussian using Equation 4.4 (Chapter 4).

7.3.2 Fluorescence Quenching of TbMscL by brominated phospholipids

Fluorescence quenching by brominated phospholipids was used as a tool to assess the accessibility of Trp residues from the lipid phase.

Purified TbMscL was reconstituted as described in Section 4.2.2.5 into bilayers of di(C14:1)PC, di(C18:1)PC, di(C22:1)PC and the corresponding brominated phospholipid at a 100:1 molar ratio of phospholipid to TbMscL monomer. Generation of large un-sealed membrane fragments was achieved by a 12-fold dilution from cholate solution into Hepes buffer to drop the concentration of cholate below its critical micelle concentration. The Trp fluorescence emission intensity was recorded at 330 nm and results are expressed as F/F_0 (Figure 7.3.1) where F is the fluorescence intensity of TbMscL in brominated lipid and F_0 is the fluorescence intensity of TbMscL in non-brominated lipid. The results shown in Figure 7.3.1 show that for all the mutants, the level of quenching decreases with increasing fatty acyl chain length. The interpretation of this observation is not obvious. The positions of the *cis* double bonds in di(C14:1)PC and di(C18:1)PC are the same (Table 7.3.2) so that the two bromines per chain will be located at similar distances from the glycerol backbone region in bilayers of di(Br₂C14:1)PC and di(Br₂C18:1)PC, although the distance from the bilayer centre to the two bromines per chain will be less in bilayers of di(Br₂C14:1)PC than in bilayers of di(Br₂C18:1)PC. However, the *cis* double bond is located at the 13-14 position in di(C22:1)PC, whereas it is at the 9-10 position in di(C14:1)PC and di(C18:1)PC (Table 7.3.2). Analysis of the data is complicated by possible tilting of the helices which would result in shorter distances between a particular residue and the glycerol backbone region in bilayers of di(Br₂C14:1)PC than in bilayers of di(Br₂C18:1)PC. The lower levels of quenching in long chain lipids could also simply reflect the lower density of bromine atoms in the longer chain lipids than in the short chain lipids.

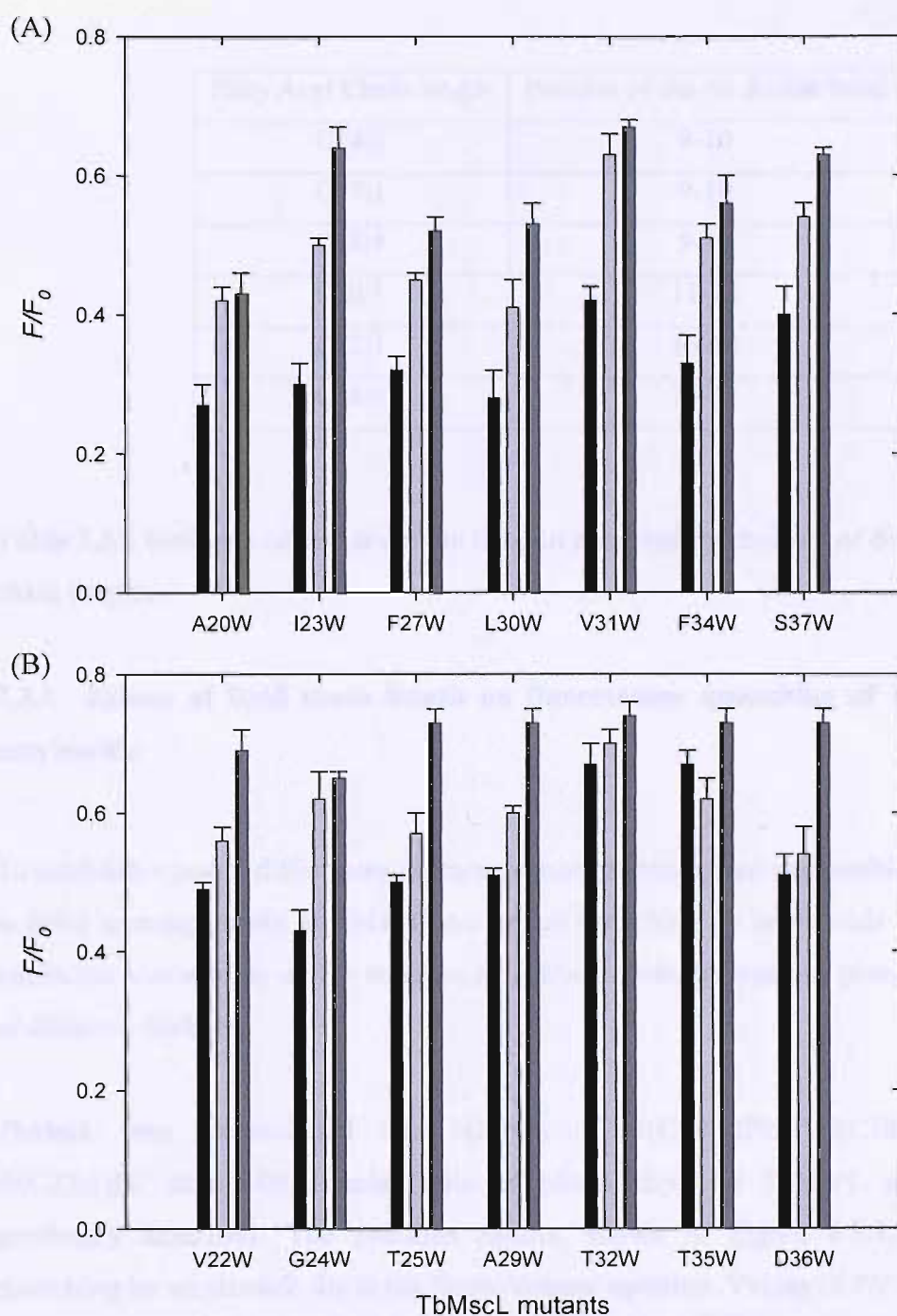


Figure 7.3.1 Quenching of Trp fluorescence by brominated phospholipids. Mutants were reconstituted into di(C14:1)PC and di(Br₂C14:0)PC (■), di(C18:1)PC and di(Br₂C18:0)PC (▨) and di(C22:1)PC and di(Br₂C22:0)PC (▩) at a lipid to protein ratio of 100:1. Fluorescence intensities of Trp-mutants excited at 280 nm in brominated phospholipids (F) were compared to the fluorescence intensities in non-brominated lipid (F_0). Bar charts show the average of three determinations and standard deviations in duplicate for: (A) lipid exposed mutants and (B) pore exposed mutants.

Fatty Acyl Chain length	Position of the <i>cis</i> double bond
C14:1	9-10
C17:1	9-10
C18:1	9-10
C20:1	11-12
C22:1	13-14
C24:1	15-17

Table 7.3.2 Positions of the *cis* double bond in phosphatidylcholines of different chain lengths.

7.3.3 Effects of lipid chain length on fluorescence quenching of TbMscL by acrylamide

To establish whether differences in fluorescence quenching are attributable to changes in helix rearrangements of TM1, fluorescence quenching by acrylamide was used to assess the accessibility of Trp residues in TbMscL from the aqueous phase in bilayers of different thickness.

TbMscL was reconstituted into bilayers of di(C14:1)PC, di(C18:1)PC, and di(C22:1)PC at a 100:1 molar ratio of phospholipid to TbMscL monomer as previously described. The previous results, shown in Figure 4.3.7, show that quenching by acrylamide fits to the Stern-Volmer equation. Values of F/F_0 for the Trp mutants in di(C14:1)PC, di(C18:1)PC, and di(C22:1)PC in the presence of 300 mM acrylamide are shown in Figure 7.3.2. Graph A shows the results for lipid exposed residues and graph B shows results for pore exposed residues. The results show a similar level of quenching for all mutants and for all three fatty acyl chain lengths with the largest difference in the levels of fluorescence quenching between di(C18:1)PC and di(C22:1)PC observed for F27W. This suggests that no large changes in environment are experienced by any of the Trp residues in TM1 on changing lipid fatty acyl chain length from C14 to C22.

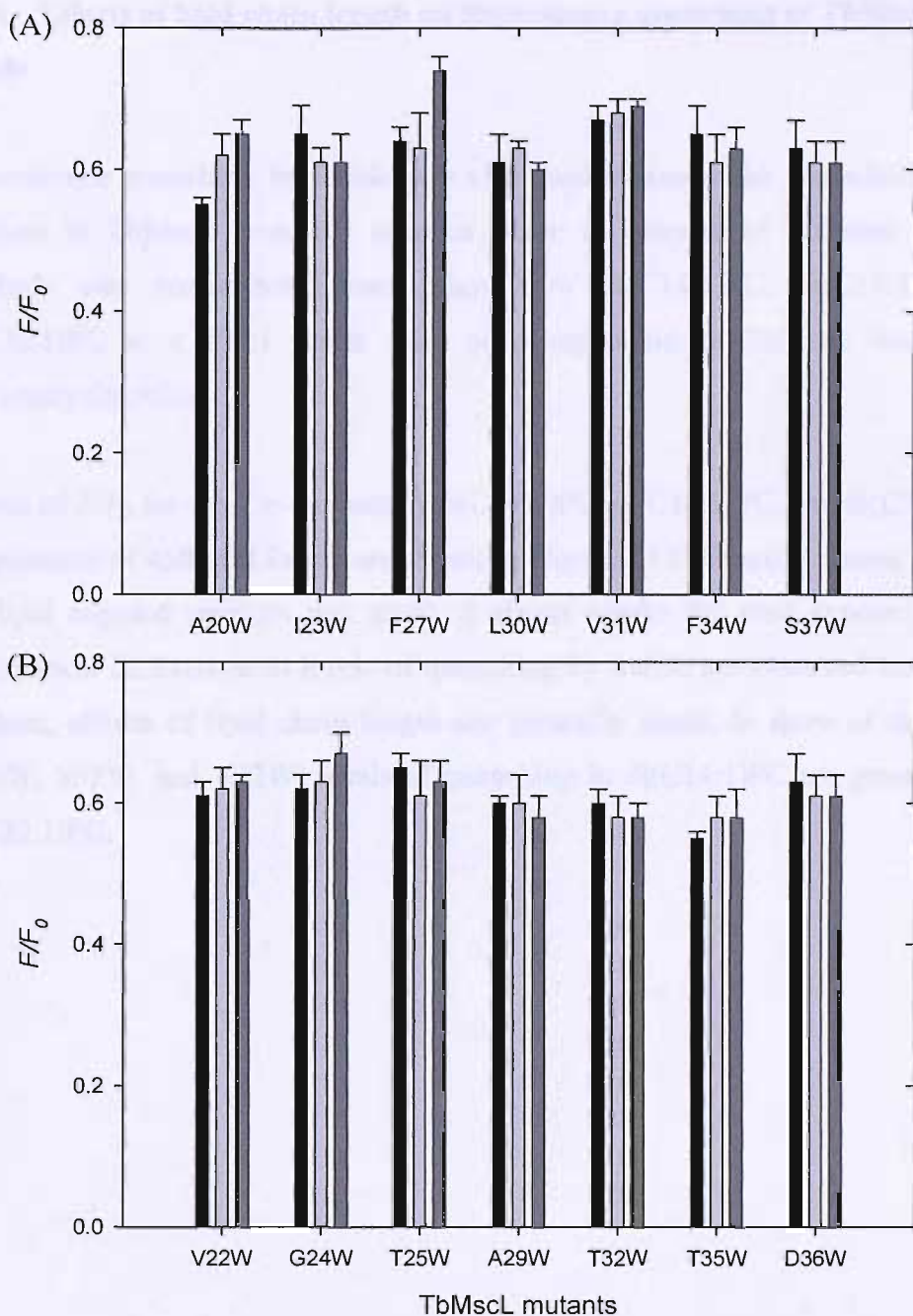


Figure 7.3.2. Quenching of Trp fluorescence by acrylamide. Trp-mutants of TbMscL were reconstituted into di(C14:1)PC, (■); di(C18:1)PC, (□); and di(C22:1)PC, (▣) at a lipid to protein ratio of 100:1. Fluorescence intensities in the presence of 300 mM acrylamide (F) were compared to fluorescence intensities in the absence of acrylamide (F_0). The data shown are the average and standard deviation of three determinations in duplicate for: (A) lipid exposed mutants and (B) pore exposed mutants.

7.3.4 Effects of lipid chain length on fluorescence quenching of TbMscL by Iodide

Fluorescence quenching by iodide was also used to assess the accessibility of Trp residues in TbMscL from the aqueous phase in bilayers of different thickness. TbMscL was reconstituted into bilayers of di(C14:1)PC, di(C18:1)PC, and di(C22:1)PC at a 100:1 molar ratio of phospholipid to TbMscL monomer as previously described.

Values of F/F_0 for the Trp mutants in di(C14:1)PC, di(C18:1)PC, and di(C22:1)PC in the presence of 450 mM iodide are shown in Figure 7.3.3. Graph A shows the results for lipid exposed residues and graph B shows results for pore exposed residues. Whilst clear differences in levels of quenching by iodide are observed between Trp residues, effects of lipid chain length are generally small. In three of the mutants (L30W, S37W, and V22W) levels of quenching in di(C14:1)PC are greater than in di(C22:1)PC.

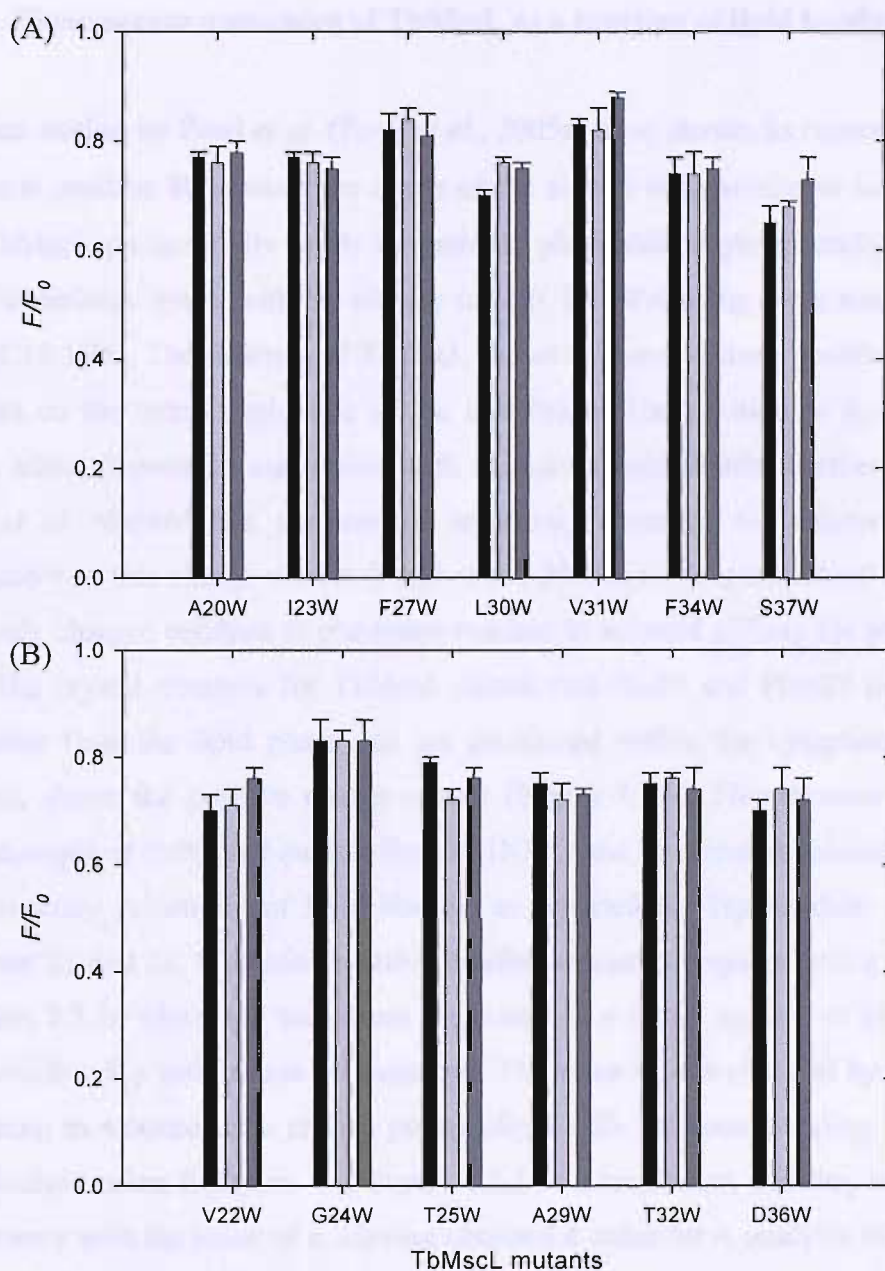


Figure 7.3.3. Quenching of Trp fluorescence by iodide. Trp-mutants of TbMscL were reconstituted into di(C14:1)PC, (■); di(C18:1)PC, (▒); and di(C22:1)PC, (□) at a lipid to protein ratio of 100:1. Fluorescence intensities in the presence of 450 mM iodide (F) were compared to fluorescence intensities in the absence of iodide (F_0). The data shown are the average and standard deviation of three determinations in duplicate for: (A) lipid exposed mutants and (B) pore exposed mutants.

7.3.5 Fluorescence quenching of TbMscL as a function of lipid headgroup

Previous studies by Powl *et al.* (Powl *et al.*, 2005a) have shown, as reported by a Trp residue at position 80 towards the centre of the second transmembrane α -helix TM2, that TbMscL preferentially binds the anionic phospholipid phosphatidic acid (PA) over zwitterionic lipids, with the affinity for di(C18:1)PA being about four times that for di(C18:1)PC. The structure of TbMscL shows a cluster of three positively charged residues on the cytoplasmic side of the membrane. The position of these residues would allow favourable interaction with anionic phospholipids. Further studies by Powl *et al.* showed that the marked selectivity observed for anionic lipid was attributable to this charge cluster (Powl *et al.*, 2005a) since mutation of each of the positively charged residues to glutamine resulted in reduced affinity for phosphatidic acid. The crystal structure for TbMscL shows that Ile-23 and Phe-27 on TM1 are accessible from the lipid phase and are positioned within the cytoplasmic half of TbMscL above the positive charge cluster (Figure 7.3.4). Fluorescence quenching with mixtures of BrPC and anionic lipid in DOPC and brominated anionic lipid were used to study selectivity of lipid binding as reported by Trp residues in TM1 at positions 23 and 27. Obtaining relative binding constants requires fitting the data to Equation 7.5 in which the unknowns are n and K . n is the number of binding sites from which a Trp residue can be quenched. The value of n is obtained by analysis of quenching in mixtures of a chosen phospholipid with the corresponding brominated phospholipid using Equation 7.1. Figure 7.3.5 is a simulation showing how quench curves vary with the value of n . Having obtained a value for n , analysis of quenching in mixtures of phospholipids, with different lipid headgroups, gives a value for the relative binding constant K . Figure 7.3.6 shows the effect of K on fluorescence quench curves for a fixed value of n of 2.

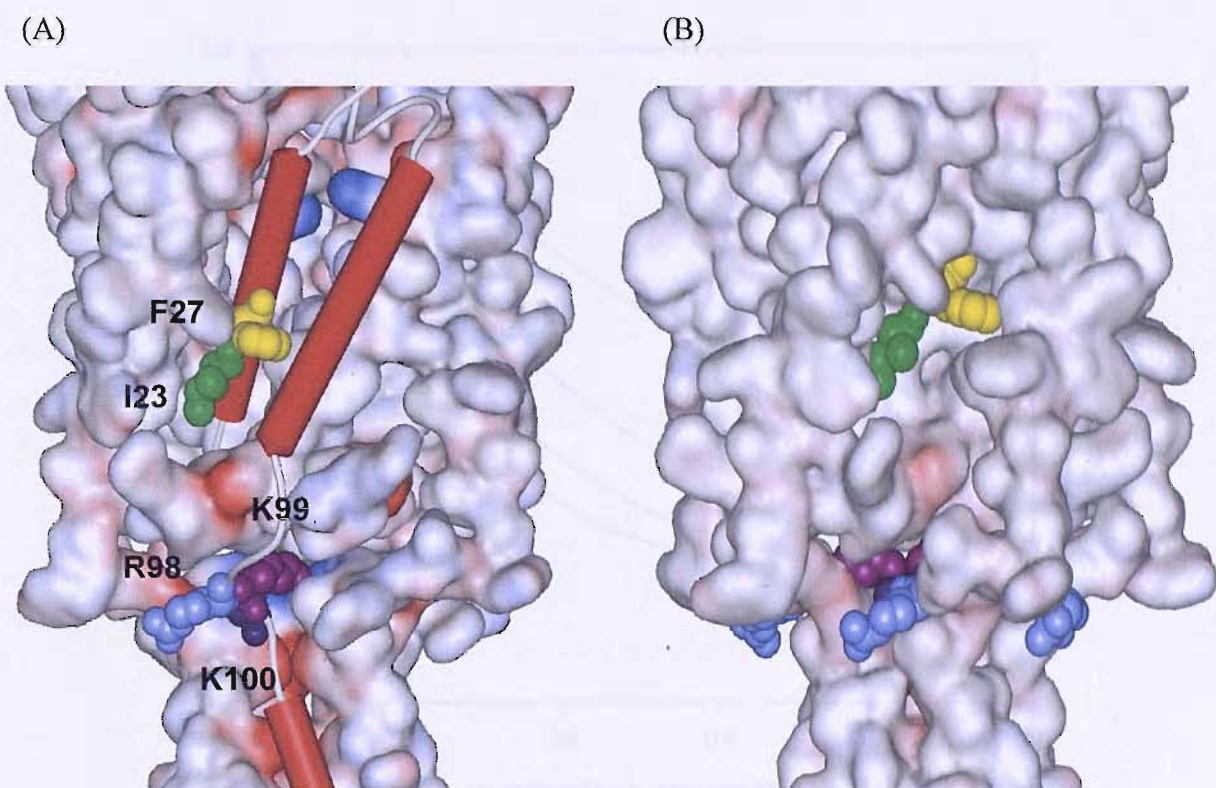


Figure 7.3.4 The structure of TbMscL. (A) One monomer is highlighted showing the positions of the two lipid exposed residues Ile-23 and Phe-27 relative to the positive charge cluster of Lys-98, Lys-99 and Arg-100. (B) Surface representation of TbMscL showing how Ile-23 and Phe-27 are accessible to the lipid phase, positioned above the positive charge cluster on the cytoplasmic side of the membrane.

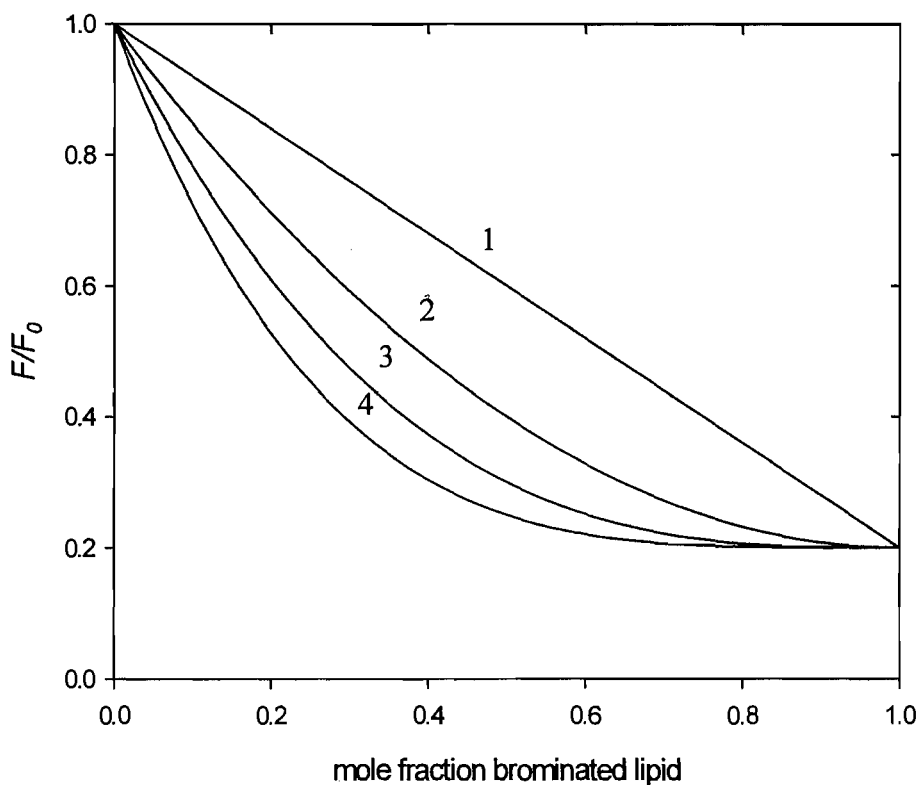


Figure 7.3.5 Effect of n , the number of lipid binding sites on a protein from which a bound BrPC molecule can quench the fluorescence of a given Trp residue in a protein. The figure shows a set of quench curves for a membrane protein reconstituted into bilayers containing mixtures of DOPC and BrPC showing values of F/F_0 calculated from Equation 7.1 with the given values of n , for a value of F/F_0 in BrPC of 0.2.

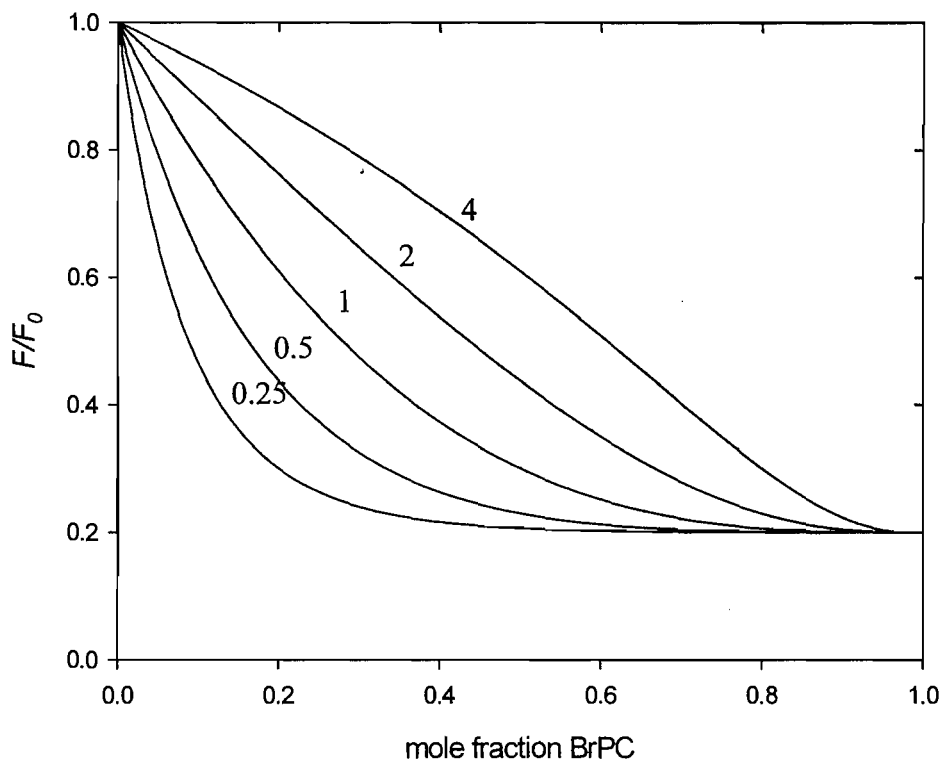


Figure 7.3.6 Effect of K . The level of fluorescence quenching of a Trp residue is dependent on the relative lipid binding constant (K) of the protein for the non-brominated lipid. The figure shows a set of quench curves for a membrane protein reconstituted into bilayers containing mixtures of lipid x and BrPC showing values of F/F_0 calculated from equation 7.5 with the given values of K , for a value of F/F_0 in BrPC of 0.2. The value of n was 2.

Fluorescence quenching curves of I23W and F27W reconstituted into mixtures of PC, PE, PS, PG and PA with the corresponding brominated lipids are shown in Figure 7.3.7. Fluorescence intensities are expressed as F/F_0 where F represents the fluorescence intensity at intermediate fractions of brominated phospholipid and F_0 is the fluorescence intensity where the mole fraction of non-brominated phospholipid is 1. The data were fitted to Equation 7.1 using the non-linear least-squares program in SigmaPlot to give the values of n listed in Table 7.3.3. The n values obtained for all phospholipid headgroups are very similar for both TbMscL mutants. Noticeable, however, is the fact that whereas the level of quenching by the brominated zwitterionic phospholipids PC and PE are the same, the level of quenching caused by brominated anionic lipid is greater than that of the zwitterionic lipids for both I23W and F27W.



Figure 7.3.7. Fluorescence quenching curves of I23W and F27W reconstituted into mixtures of PC, PE, PS, PG and PA with the corresponding brominated lipids. The curves show a decrease in fluorescence intensity as the mole fraction of brominated phospholipid increases, with the anionic lipids showing a steeper decline compared to zwitterionic lipids.

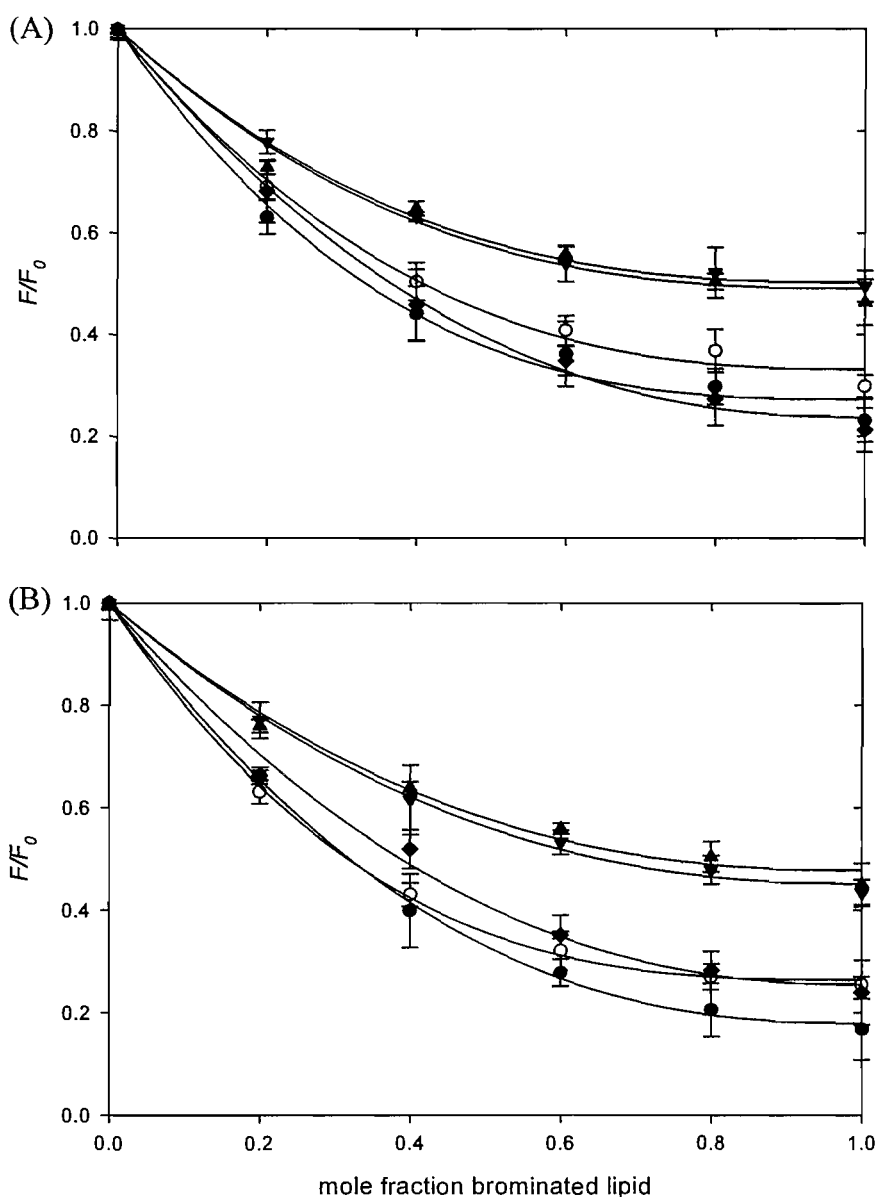


Figure 7.3.7 Quenching of Trp fluorescence of I23W and F27W by brominated phospholipids. I23W (A) and F27W (B) were reconstituted into bilayers containing mixtures of brominated lipid and the corresponding non-brominated lipid. Fluorescence intensities are expressed as a fraction of the fluorescence for TbMscL reconstituted in mixtures of non-brominated lipid. Lipid headgroups were as follows: di(C18:1)PC, (▼); di(C18:1)PE, (▲); di(C18:1)PS, (○); di(C18:1)PG, (◆) and di(C18:1)PA, (●). Error bars are standard deviations obtained from the average of three determinations. The solid lines show fits to Equation 7.1 giving the values of n listed in Table 7.3.3.

Phospholipid	F/F_0	n
I23W		
di(Br ₂ C18:0)PC	0.50 ± 0.01	2.65 ± 0.1
di(Br ₂ C18:0)PE	0.49 ± 0.02	2.75 ± 0.4
di(Br ₂ C18:0)PG	0.24 ± 0.01	2.33 ± 0.1
di(Br ₂ C18:0)PS	0.33 ± 0.02	2.73 ± 0.2
di(Br ₂ C18:0)PA	0.27 ± 0.02	2.88 ± 0.3
F27W		
di(Br ₂ C18:0)PC	0.45 ± 0.01	2.30 ± 0.1
di(Br ₂ C18:0)PE	0.48 ± 0.07	2.35 ± 0.2
di(Br ₂ C18:0)PG	0.25 ± 0.02	2.27 ± 0.2
di(Br ₂ C18:0)PS	0.27 ± 0.01	2.98 ± 0.1
di(Br ₂ C18:0)PA	0.18 ± 0.01	2.44 ± 0.1

Table 7.3.3 Fluorescence quenching of I23W and F27W in brominated phospholipids as a function of lipid headgroup. F and F_0 are fluorescence intensities for TbMscL reconstituted into brominated phospholipid and non-brominated phospholipid respectively, measured in Hepes buffer at pH 7.2. The value of n is the value obtained from fitting the data in Figure 7.3.7 to Equation 7.1.

In order to ascertain whether these residues report any selective binding of anionic phospholipid, I23W and F27W were reconstituted into mixtures of di(Br₂C18:0)PC and phosphatidylethanolamine or anionic lipid, or di(C18:1)PC and brominated phosphatidylethanolamine or brominated anionic lipid. Figures 7.3.8 - 7.3.11 show fluorescence intensities in these mixtures as a function of the mole fraction of brominated lipid. Relative phospholipid binding constants listed in Table 7.3.4 were obtained by fitting the data to Equation 7.5. Fluorescence quench curves for I23W and F27W in mixtures of phosphatidylcholine and phosphatidylethanolamine are shown in Figure 7.3.8. Relative binding constants obtained using di(Br₂C18:0)PC or di(Br₂C18:0)PE agree within experimental error, and are all close to 1, suggesting simple competitive binding of PC and PE to TbMscL, with no specificity. For PG relative binding constants for F27W obtained with BrPC or BrPG are equal, suggesting simple competitive binding to MscL, with an affinity for PG slightly greater than that for PC. For PG, the relative binding constant observed with I23W and BrPG is equal to that obtained with F27W. However, that obtained for I23W with BrPC is greater than that observed with BrPG, but this difference is probably not real. Figure 7.3.12 compares fluorescence quenching plots for I23W and F27W in BrPC and PG mixtures and it is clear that the data points are the same for the two mutants except at 40 % BrPC. Thus it is likely that PG binds with a slightly higher affinity than PC to MscL, as detected by Trp residues at positions 23 and 27. For phosphatidic acid I23W detects a slightly higher affinity for PA than PC, with identical binding constants determined with either BrPC or BrPA. For F27W a slightly higher binding constant is observed with BrPA than with BrPC. The difference here is somewhat greater than that observed with I23W and PG, and so could be real. The difference could be attributed to the presence of two binding sites close to the quenched residue, at one of which PA binds with higher affinity than PC, explaining the high relative binding constant obtained from experiments with di(Br₂C18:0)PA, the other site showing little selectivity between PA and PC, explaining the relative binding constant of ca. 1 obtained from experiments with di(Br₂C18:0)PC. The binding site of high affinity observed here from the experiments with F27W presumably corresponds to that detected by Powl *et al.* using Y87W and F80W. The higher levels of quenching obtained when I23W and F27W are reconstituted into brominated anionic lipids compared to brominated zwitterionic lipids will be discussed in Section 7.3.6.

Phospholipid	Relative binding constant measured using di(C18:1)PC	Relative binding constant measured using di(Br₂C18:0)PC
	I23W	
di(C18:1)PE	0.79 ± 0.2	0.94 ± 0.1
di(C18:1)PA	1.70 ± 0.3	1.79 ± 0.3
di(C18:1)PS	0.97 ± 0.1	0.92 ± 0.1
di(C18:1)PG	1.42 ± 0.1	2.33 ± 0.1
	F27W	
di(C18:1)PE	1.00 ± 0.1	1.03 ± 0.2
di(C18:1)PA	2.37 ± 0.2	1.07 ± 0.2
di(C18:1)PS	1.29 ± 0.1	1.23 ± 0.1
di(C18:1)PG	1.53 ± 0.1	1.49 ± 0.2

Table 7.3.4 Relative lipid binding constants of TbMscL mutants as a function of lipid head group. Binding constants relative to PC were obtained by fitting the quenching data for Trp mutants of TbMscL mutants reconstituted into mixtures of di(Br₂C18:0)PC with non-brominated lipid or di(C18:1)PC with brominated lipid to Equation 7.5 using the values of *n* listed in Table 7.3.3.

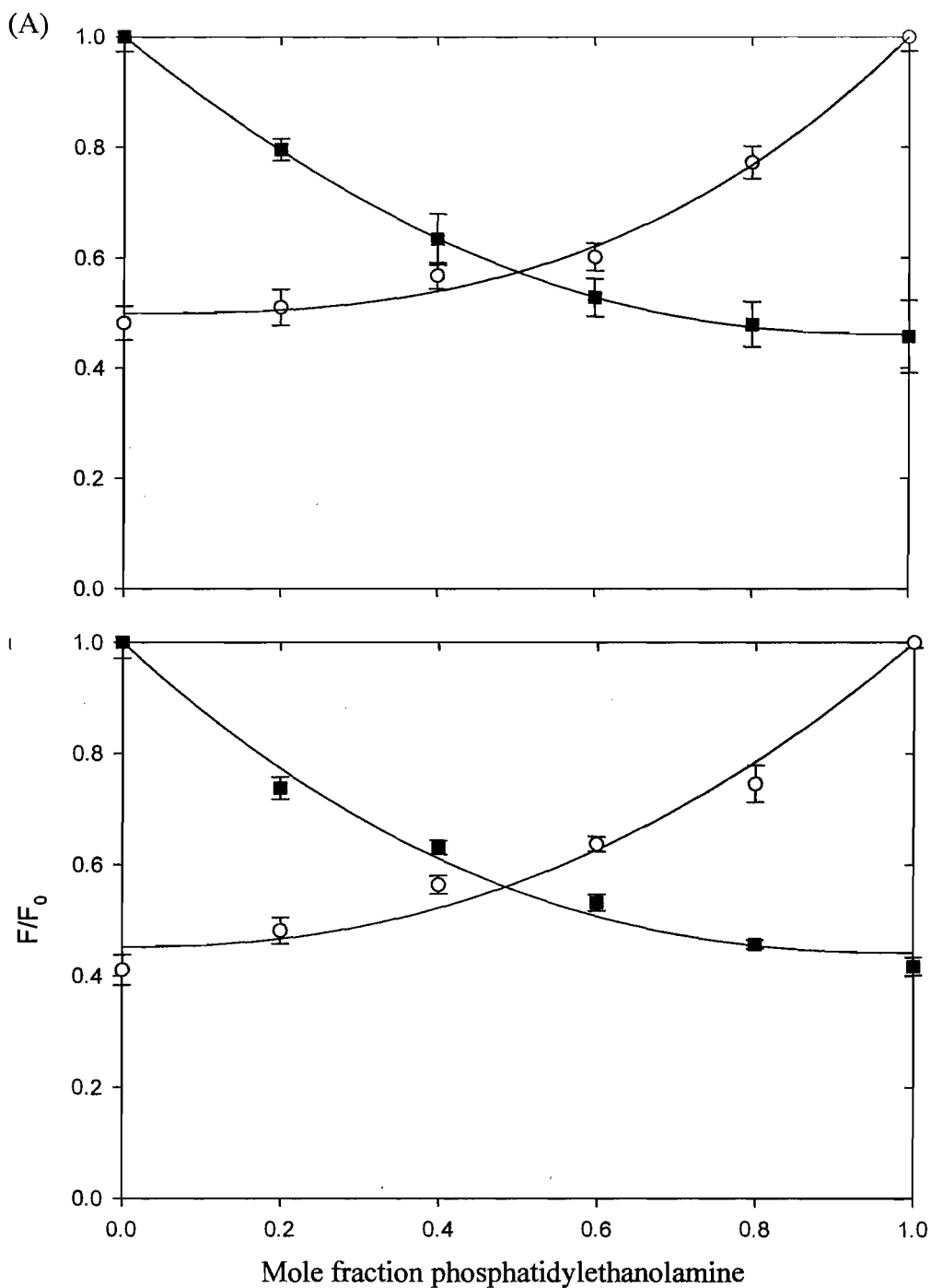


Figure 7.3.8 Fluorescence quenching of I23W and F27W in mixtures of zwitterionic phospholipids. I23W (A) and F27W (B) were reconstituted into mixtures of di(C18:1)PC with di(Br₂C18:0)PE, (■); or di(Br₂C18:0)PC with di(C18:1)PE, (○). Error bars are standard deviations obtained from the average of three determinations in duplicate. The solid lines show fits to Equation 7.5 giving the binding constants listed in Table 7.3.4.

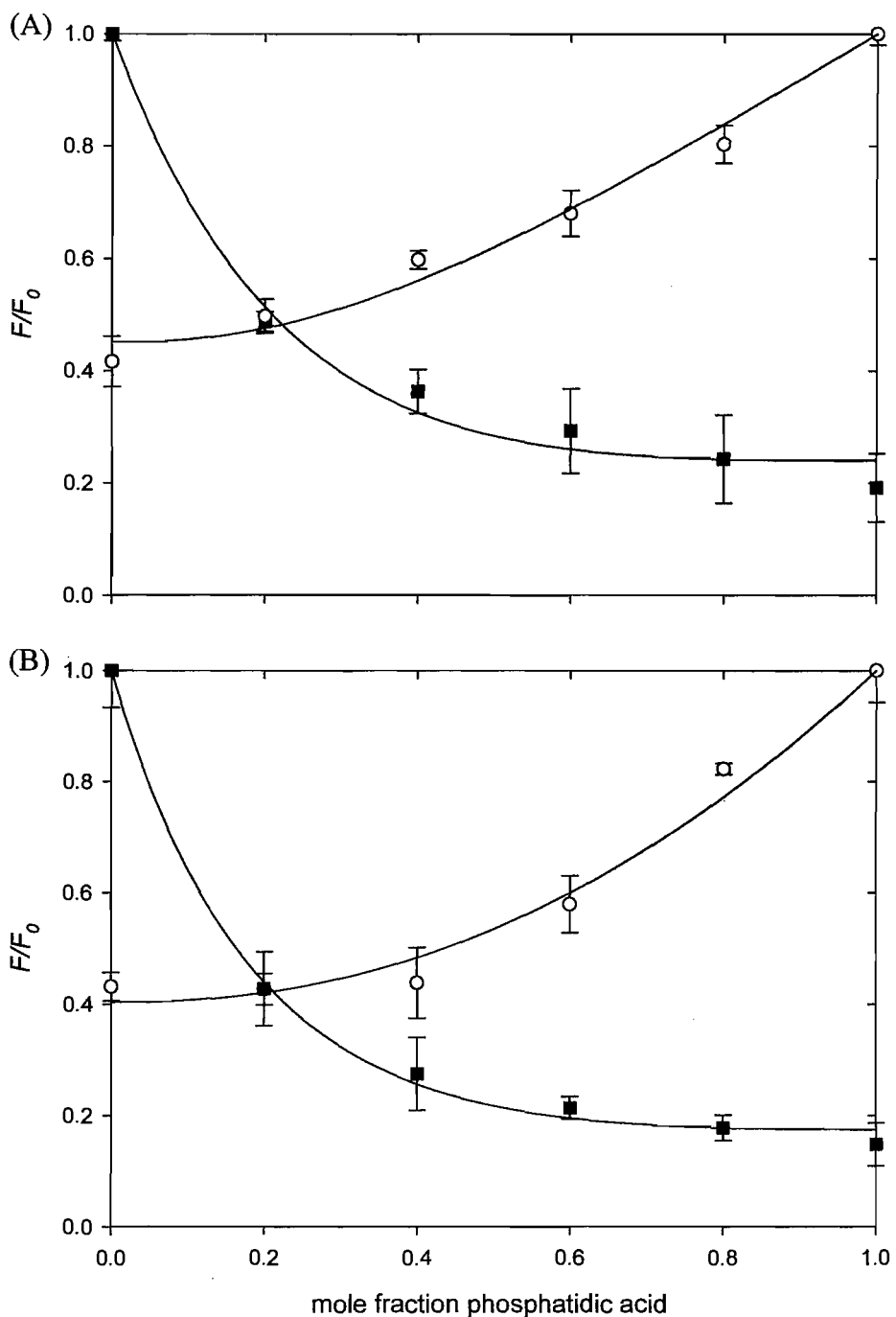


Figure 7.3.9. Fluorescence quenching of I23W and F27W in mixtures of anionic phospholipids. I23W (A) and F27W (B) were reconstituted into mixtures of di(C18:1)PC with di(Br₂C18:0)PA, (■); or di(Br₂C18:0)PC with di(C18:1)PA, (○). Error bars are standard deviations obtained from the average of three determinations in duplicate. The solid lines show fits to Equation 7.5 giving the binding constants listed in Table 7.3.4.

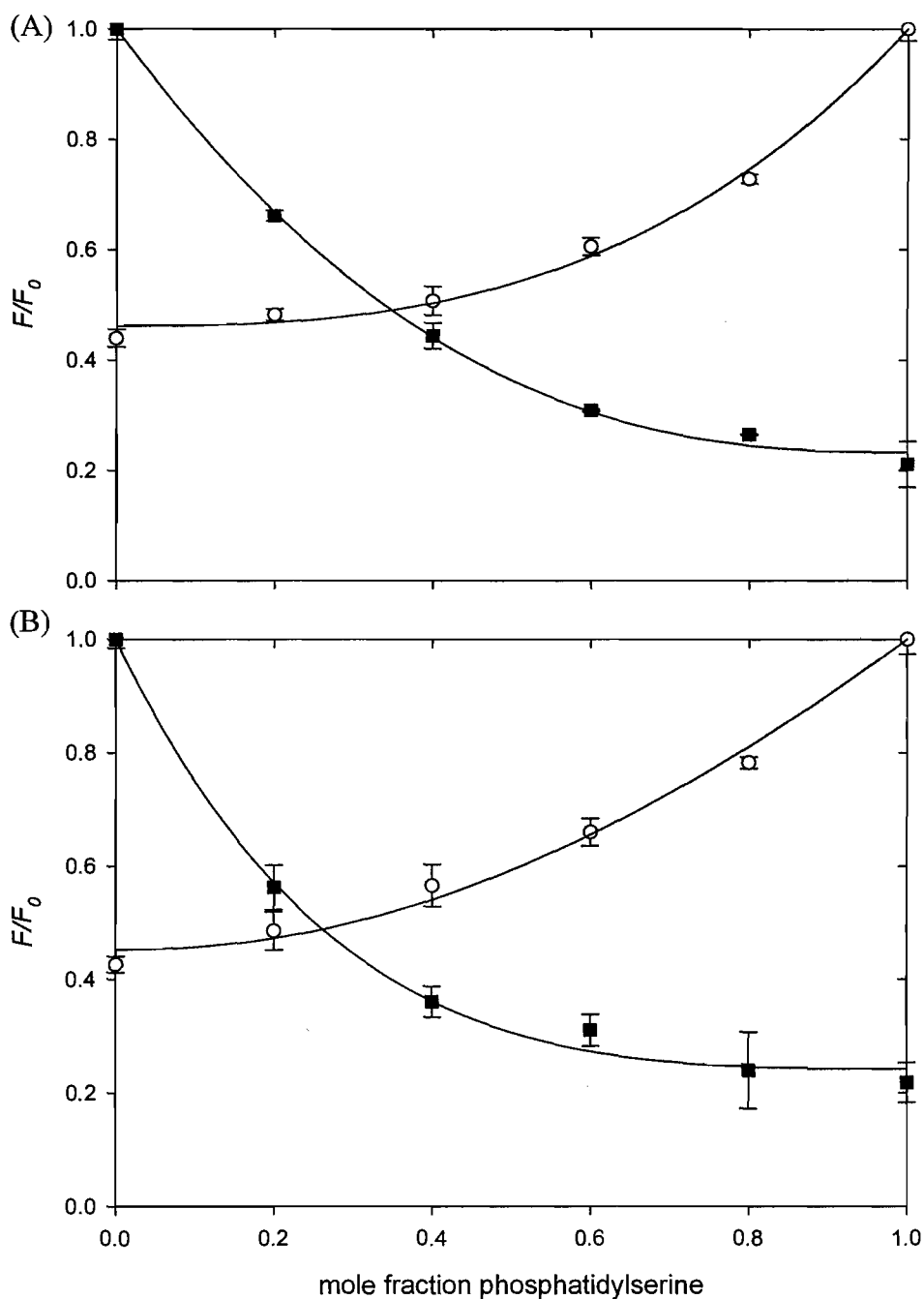


Figure 7.3.10 Fluorescence quenching of I23W and F27W in mixtures of anionic phospholipids. I23W (A) and F27W (B) were reconstituted into mixtures of di(C18:1)PC with di(Br₂C18:0)PS, (■); or di(Br₂C18:0)PC with di(C18:1)PS, (○). Error bars are standard deviations obtained from the average of three determinations in duplicate. The solid lines show fits to Equation 7.5 giving the binding constants listed in Table 7.3.4.

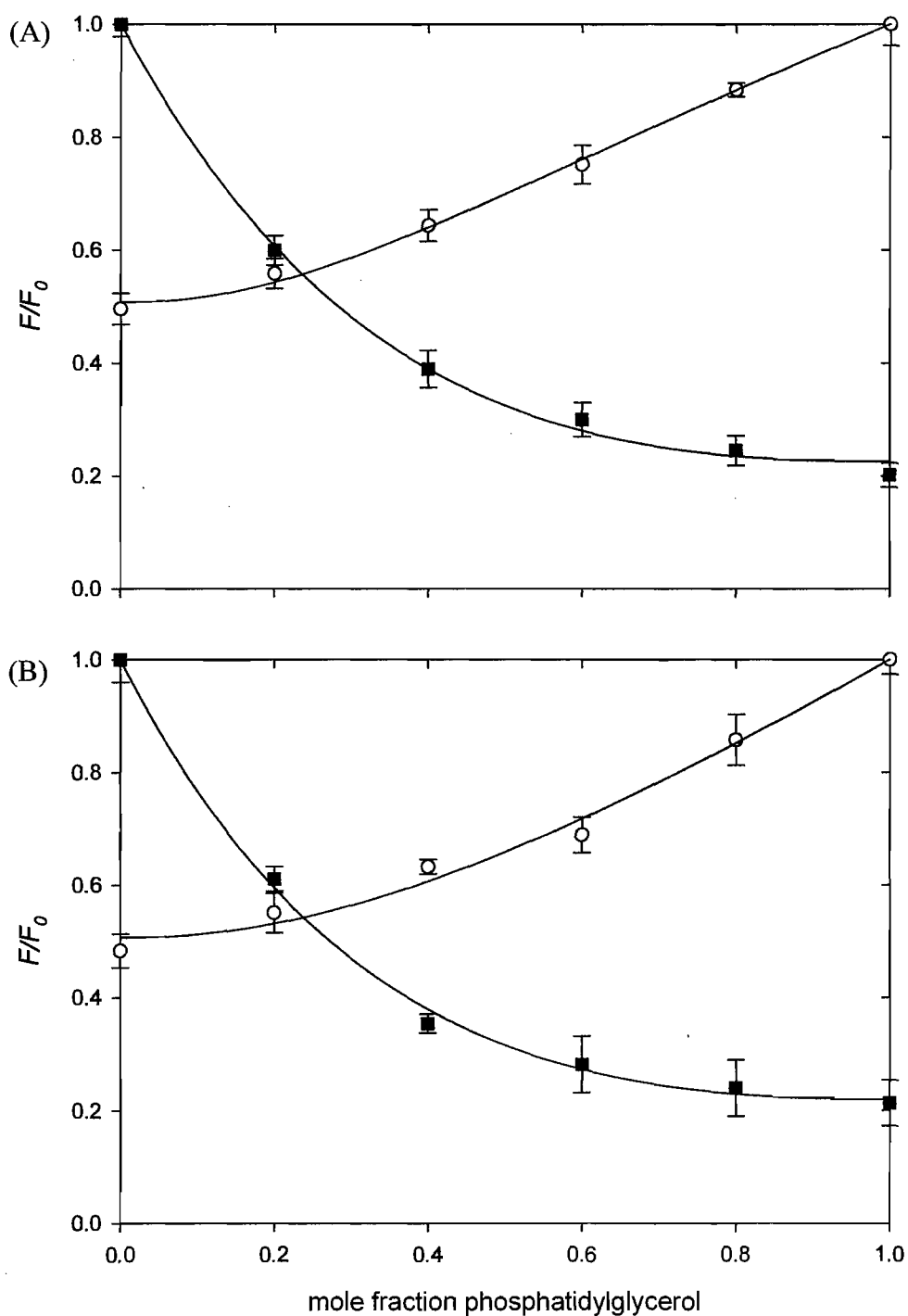


Figure 7.3.11 Fluorescence quenching of I23W and F27W in mixtures of anionic phospholipid. I23W (A) and F27W (B) were reconstituted into mixtures of di(C18:1)PC with di(Br₂C18:0)PG, (■); or di(Br₂C18:0)PC with di(C18:1)PG, (○). Error bars are standard deviations obtained from the average of three determinations in duplicate. The solid lines show fits to Equation 7.5 giving the binding constants listed in Table 7.3.4.

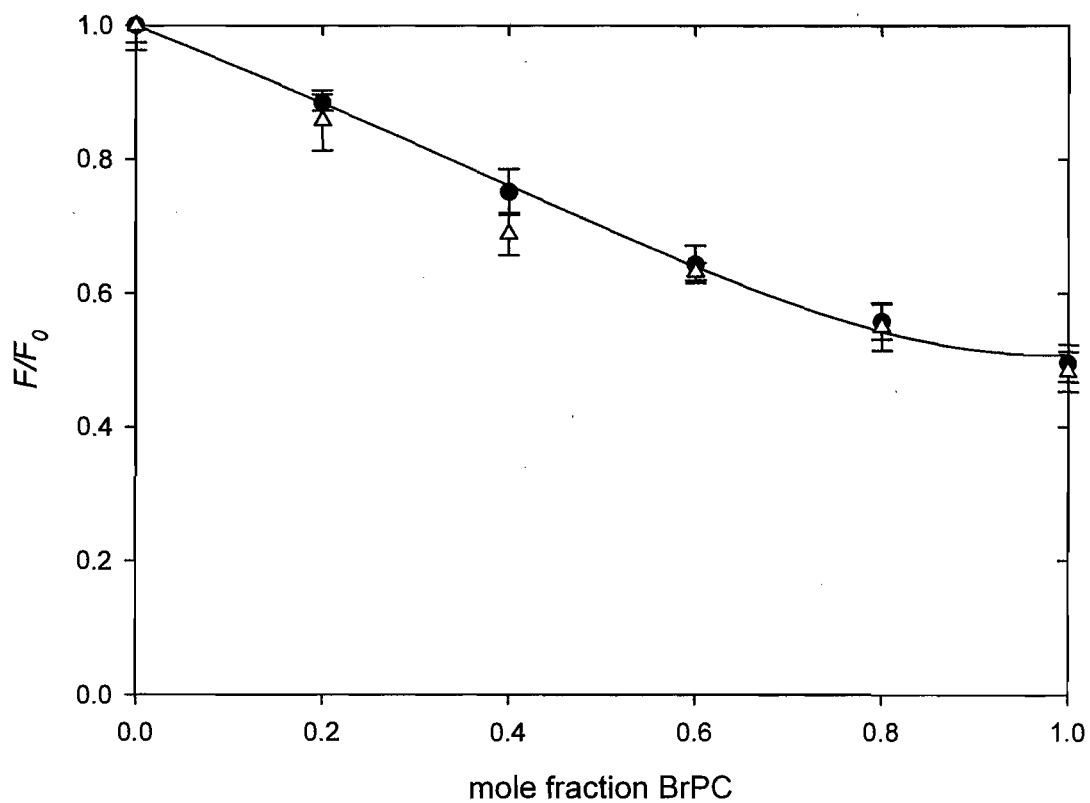


Figure 7.3.12 Fluorescence quenching of I23W and F27W in mixtures of anionic phospholipids. I23W (●) and F27W (△) were reconstituted into mixtures of di(Br₂C18:0)PC and di(C18:0)PG. Error bars are standard deviations obtained from the average of three determinations. Data points for both I23W and F27W are the same with the exception of that at 40% BrPC.

7.3.6 Fluorescence quenching for Trp residues on the periplasmic side of TbMscL

Residue 27 is in the middle of the membrane and so could be quenched by brominated lipids on either the cytoplasmic or periplasmic side of the membrane. Residue 23 is, however, on the cytoplasmic side of the membrane and so will only be affected by lipid binding on the cytoplasmic side of MscL (Figure 7.3.13). Leu-30 and Phe-34 on TM1 are accessible from the lipid phase and are positioned within the periplasmic half of TbMscL (Figure 7.3.13). Fluorescence quenching curves for L30W and F34W reconstituted into mixtures of PC or PA with the corresponding brominated lipid are shown in Figure 7.3.14. Fluorescence intensities are expressed as F/F_0 where F represents the fluorescence intensity at intermediate fractions of brominated phospholipid and F_0 is the fluorescence intensity when the mole fraction of non-brominated phospholipid is 1. The data were fitted to Equation 7.1 using the non-linear least-squares program in SigmaPlot to give the values of n listed in Table 7.3.5. The n values obtained for both phospholipid headgroups are similar for both TbMscL mutants. As previously observed with I23W and F27W the level of fluorescence quenching by the brominated anionic phospholipid PA is noticeably greater than the level of fluorescence quenching caused by the brominated zwitterionic phospholipid PC, for both L30W and F34W. This would then suggest that the higher levels of fluorescence quenching observed with brominated anionic lipids is a property of the anionic lipids themselves and does not reflect a different mode of binding to the protein. As described later, it has been observed that anionic lipid headgroups can themselves result in some quenching of Trp fluorescence (Figure 7.3.16).

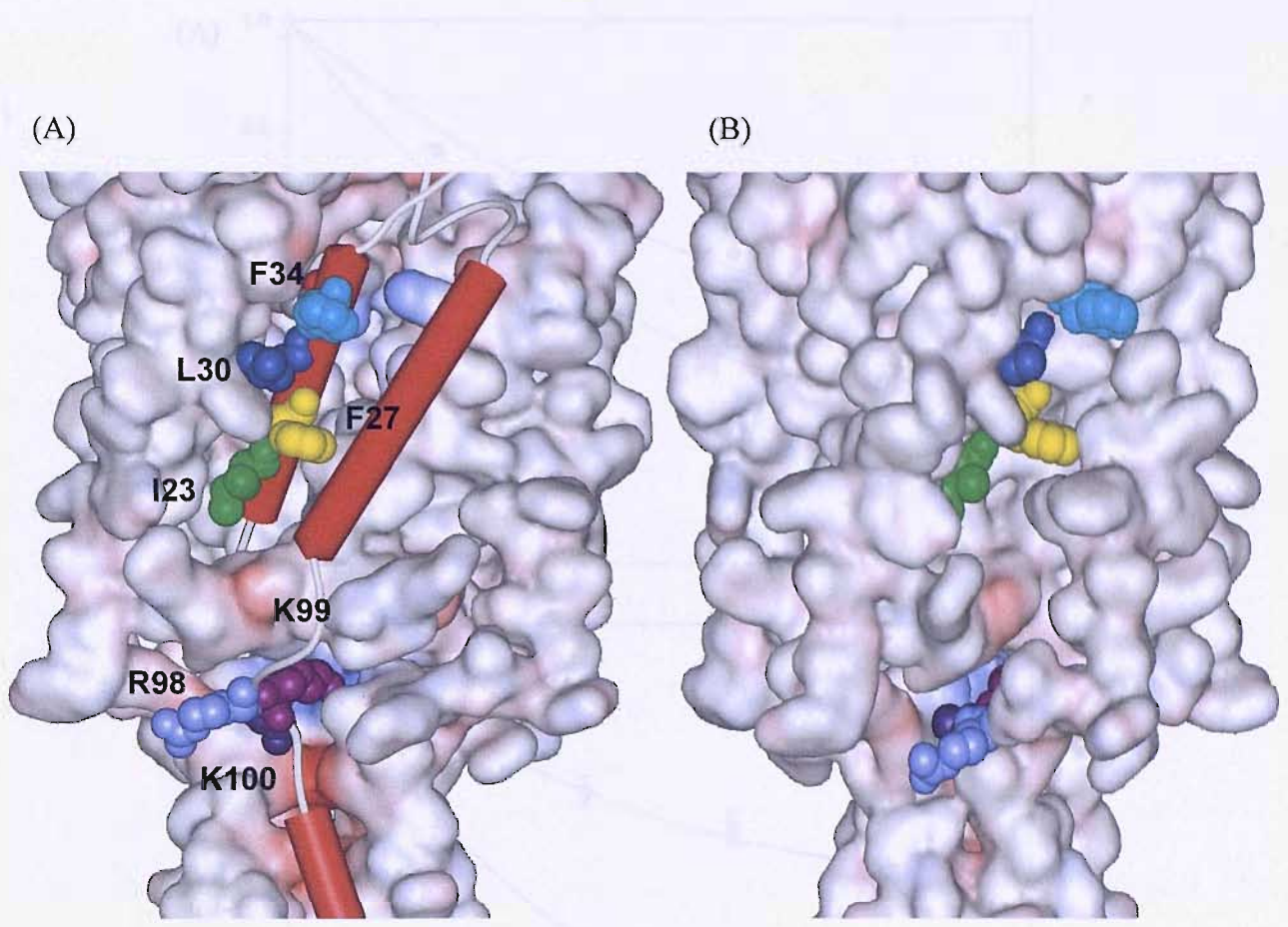


Figure 7.3.13 This diagram is the same as that shown in Figure 7.3.4. In this diagram, however, the positions of L30 (blue) and F34 (turquoise) are shown on the periplasmic side of the membrane.

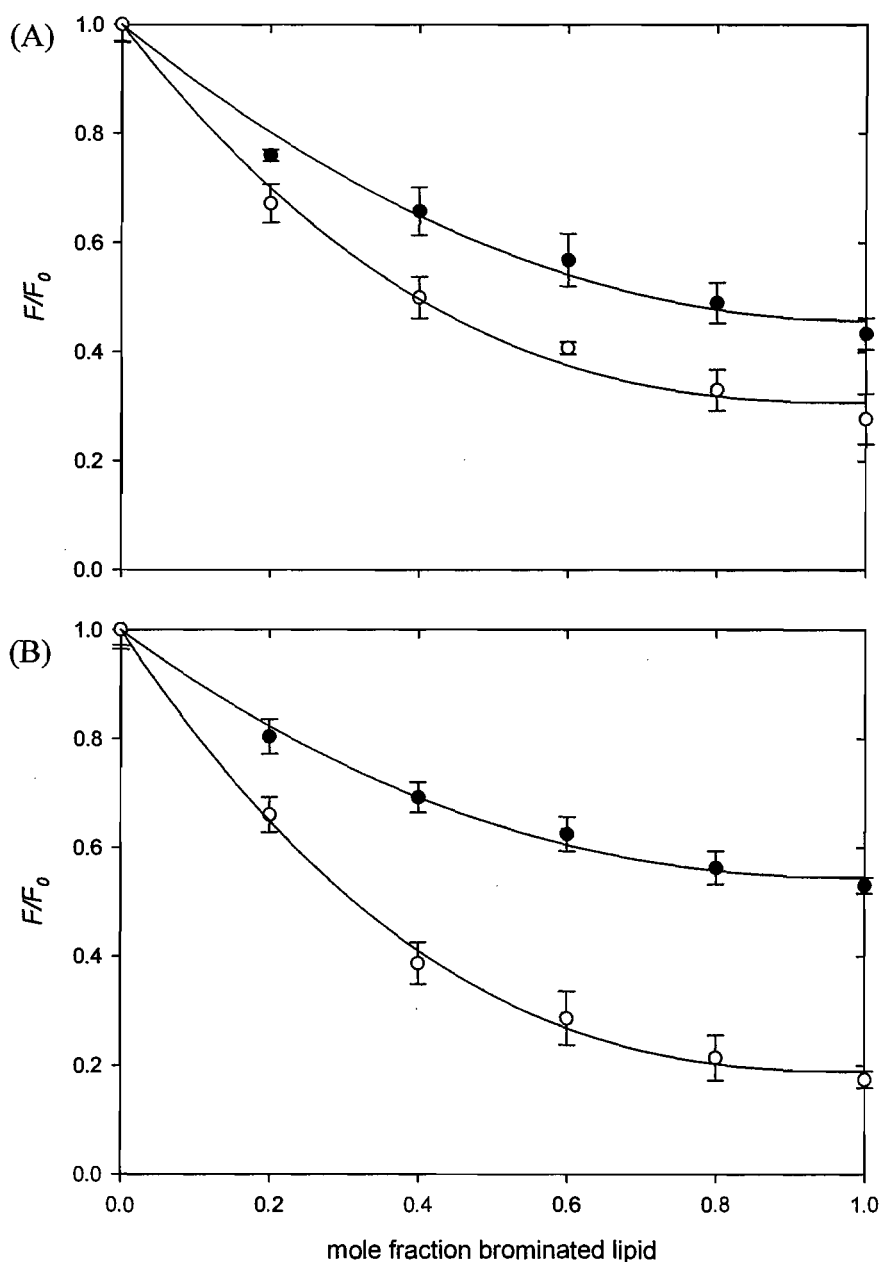


Figure 7.3.14 Quenching of Trp fluorescence of L30W and F34W by brominated phospholipids. L30W (A) and F34W (B) were reconstituted into bilayers containing mixtures of brominated lipid and the corresponding non-brominated lipid. Fluorescence intensities are expressed as a fraction of the fluorescence for TbMscL reconstituted in mixtures of non-brominated lipid. Lipid headgroups were as follows: PC, (●); and PA, (○). Error bars are standard deviations obtained from the average of three determinations in duplicate. The solid lines show fits to Equation 7.1 giving the values of n listed in Table 7.3.5.

Phospholipid	F/F_0	n
L30W		
di(Br ₂ C18:0)PC	0.45 ± 0.02	2.03 ± 0.3
di(Br ₂ C18:0)PA	0.31 ± 0.02	2.54 ± 0.2
F34W		
di(Br ₂ C18:0)PC	0.54 ± 0.01	2.20 ± 0.2
di(Br ₂ C18:0)PA	0.19 ± 0.01	2.54 ± 0.1

Table 7.3.5 Fluorescence quenching of L30W and F34W in brominated phospholipids as a function of lipid headgroup. F and F_0 are fluorescence intensities for TbMscL reconstituted into brominated phospholipid and non-brominated phospholipid respectively, measured in Hepes buffer at pH 7.2. The values of n are the values obtained from fitting the data in Figure 7.3.13 to Equation 7.1.

Binding constants for PA on the periplasmic side of MscL were determined by reconstituting L30W and F34W into mixtures of brominated phosphatidylcholine and phosphatidic acid or brominated phosphatidic acid and phosphatidylcholine. Figure 7.3.15 shows fluorescence intensities in these mixtures as a function of the mole fraction of brominated lipid. Relative phospholipid binding constants listed in Table 7.3.6 were obtained by fitting the data to Equation 7.5.

For F34W, comparable binding constants for PA were obtained using BrPC and BrPA suggesting simple competitive binding with a higher affinity for PA than for PC. Binding constants are very similar to those observed using I23W on the cytoplasmic side of the membrane. For L30W a higher relative binding constant was observed using BrPA than using BrPC, as for F27W. As previously described this would be consistent with the presence of two sites, one with a slightly higher affinity for PA than for PC and one with an equal affinity for PA and PC.

Phospholipid	Relative binding constant measured using di(C18:1)PC	Relative binding constant measured using di(Br ₂ C18:0)PC
Cytoplasmic side		
I23W	1.70 ± 0.3	1.79 ± 0.3
Middle of membrane		
F27W	2.37 ± 0.2	1.07 ± 0.2
Periplasmic side		
L30W	1.77 ± 0.2	1.08 ± 0.1
F34W	1.71 ± 0.3	2.01 ± 0.3

Table 7.3.6 Relative lipid binding constants of TbMscL mutants on the cytoplasmic and periplasmic sides of TbMscL as a function of lipid head group. Binding constants relative to PC for L30W and F34W were obtained by fitting the quenching data for Trp mutants of TbMscL reconstituted into mixtures of di(Br₂C18:0)PC with non-brominated anionic lipid or di(C18:1)PC with brominated anionic lipid to Equation 7.5 using the values of n listed in Table 7.3.5.

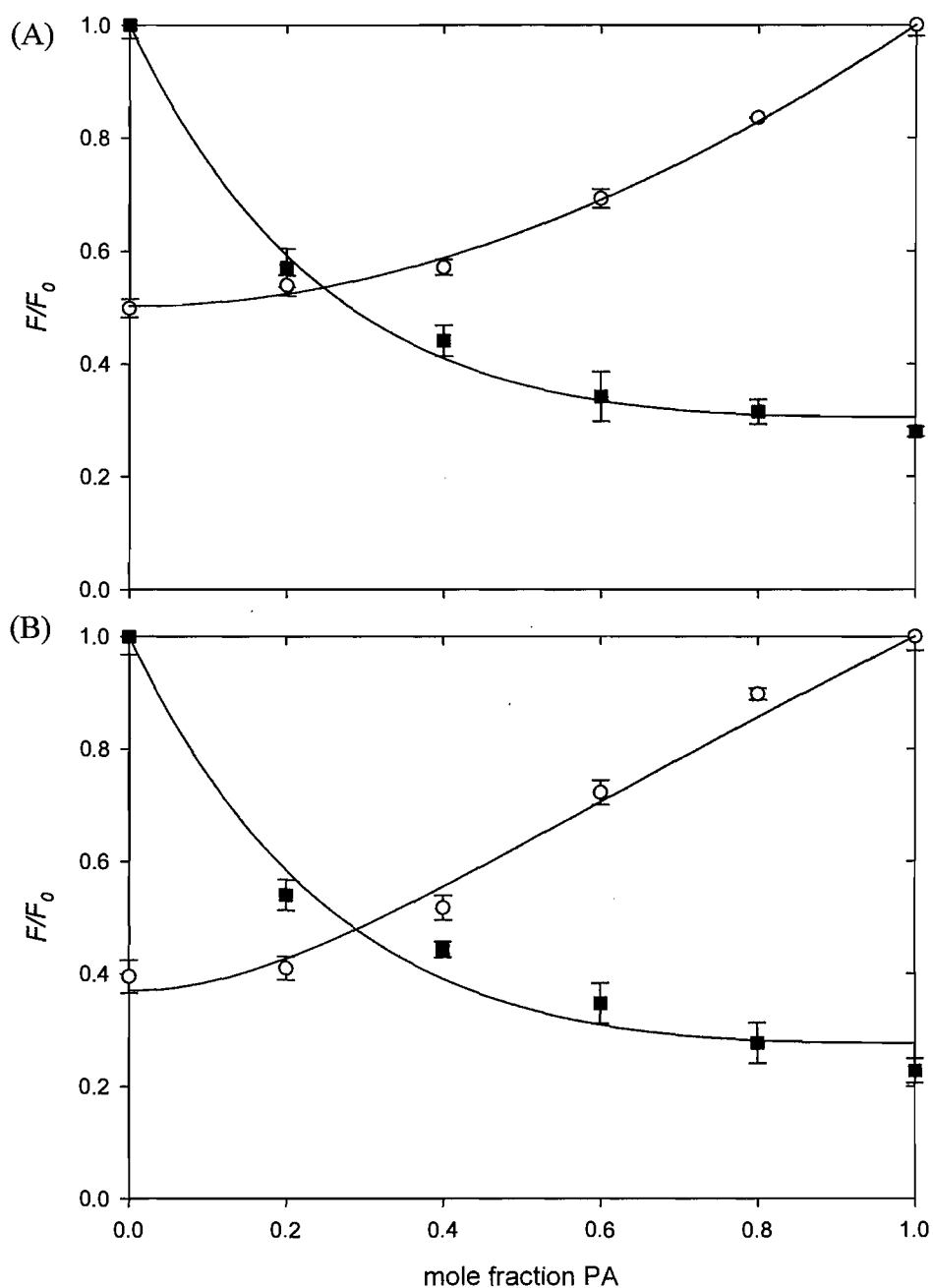


Figure 7.3.15 Fluorescence quenching of L30W and F34W in mixtures of phosphatidic acid and phosphatidylcholine. L30W (A) and F34W (B) were reconstituted into mixtures of di(C18:1)PC with di(Br₂C18:0)PA, (■); or di(Br₂C18:0)PC with di(C18:1)PA, (○). Error bars are standard deviations obtained from the average of three determinations in duplicate. The solid lines show fits to Equation 7.5 giving the binding constants listed in Table 7.3.7.

7.3.7 Effects of lipid headgroup on fluorescence emission maxima

Trp mutants of TbMscL were reconstituted into bilayers of di(C18:1)PE, di(C18:1)PA, di(C18:1)PS and di(C18:1)PG and fluorescence emission spectra were recorded and fitted to a skewed Gaussian peak using Equation 4.4 (see Chapter 4). I23W displays blue-shifts of 2 nm from 325 nm in di(C18:1)PC (Table 7.3.1) to 322 nm in di(C18:1)PA (Table 7.3.7). F34W also displays a blue shift similar to I23W of 326.2 nm in di(C18:1)PC (Table 7.3.7) to 321 nm in di(C18:1)PA and V31W displays shifts to shorter wavelengths of ca. 5 nm when reconstituted into all anionic phospholipids. This would suggest that the three lipid-exposed residues I23, V31, and F34 experience changes in environment in going from zwitterionic to anionic lipid headgroups. The pore lining residues G24W, which is a gain-of-function mutant, and A29W, a pore lining residue, also display shifts of ca. 3 nm when reconstituted into the anionic phospholipid PA. Interestingly, G24W displays a shift of 3 nm to a longer wavelength whereas A29W displays a shift of 3 nm to shorter wavelengths. One observation upon reconstituting TbMscL into anionic phospholipids is the noticeable decrease in fluorescence intensity for all mutants. Figure 7.3.16 shows the fluorescence intensities of TbMscL mutants at a concentration of 1 μ M. Lipid-exposed residues located near to the centre of the bilayer also show a marked decrease in fluorescence intensity in relation to those residues located at the lipid headgroup region on both sides of the membrane, a result not observed for pore-lining residues (Figure 7.3.16 B) which all have around the same fluorescence intensity in the zwitterionic phospholipids PC and PE.

Figures 7.3.17 and 7.3.18 show the effects of the anionic phospholipids PA and PS on the fluorescence intensity of the Trp analogue NPTH (N-palmityl-Trp-hexyl). This molecule is thought to partition into the membrane with the Trp residue at the glycerol backbone region with the palmityl and hexyl groups traversing the hydrophobic region of the membrane. It is clear to see how fluorescence intensity decreases as the mole fraction of anionic lipid is increased in bilayers of phosphatidylcholine.

Mutant	di(C18:1)PE		di(C18:1)PA		di(C18:1)PS		di(C18:1)PG	
	λ^{\max} (nm)	ω (nm)	λ^{\max} (nm)	ω (nm)	λ^{\max} (nm)	ω (nm)	λ^{\max} (nm)	ω (nm)
A20W	328.5 ± 0.2	57.3 ± 0.4	328.9 ± 0.3	60.3 ± 0.4	328.7 ± 0.3	60.3 ± 0.4	328.8 ± 0.2	60.2 ± 0.4
V22W	329.8 ± 0.1	57.3 ± 0.2	331.9 ± 0.1	60.0 ± 0.2	330.9 ± 0.1	60.3 ± 0.2	331.5 ± 0.1	62.9 ± 0.2
I23W	324.2 ± 0.1	49.6 ± 0.2	322.2 ± 0.1	47.3 ± 0.2	323.5 ± 0.1	50.0 ± 0.2	323.3 ± 0.1	50.6 ± 0.2
G24W	327.9 ± 0.3	63.9 ± 0.6	330.5 ± 0.4	77.7 ± 0.7	326.4 ± 0.4	71.3 ± 0.8	327.7 ± 0.5	73.9 ± 0.9
T25W	331.2 ± 0.1	59.1 ± 0.2	329.4 ± 0.2	59.7 ± 0.2	330.6 ± 0.2	62.0 ± 0.3	330.4 ± 0.1	62.8 ± 0.2
F27W	321.6 ± 0.2	51.2 ± 0.4	321.0 ± 0.2	49.7 ± 0.5	319.7 ± 0.2	49.7 ± 0.5	318.8 ± 0.2	50.3 ± 0.5
A29W	329.9 ± 0.2	60.5 ± 0.3	322.2 ± 0.2	52.1 ± 0.4	326.7 ± 0.2	62.3 ± 0.4	328.8 ± 0.2	66.9 ± 0.4
L30W	327.7 ± 0.1	55.2 ± 0.2	328.7 ± 0.1	56.7 ± 0.2	327.6 ± 0.1	57.1 ± 0.2	327.3 ± 0.1	57.5 ± 0.2
V31W	323.8 ± 0.1	54.7 ± 0.3	318.2 ± 0.1	51.2 ± 0.4	319.8 ± 0.1	55.6 ± 0.3	318.9 ± 0.8	54.5 ± 0.3
T32W	335.4 ± 0.1	62.6 ± 0.2	335.9 ± 0.2	65.3 ± 0.2	336.5 ± 0.2	66.7 ± 0.2	335.8 ± 0.1	71.0 ± 0.2
F34W	326.2 ± 0.2	58.1 ± 0.4	321.0 ± 0.2	50.1 ± 0.5	324.5 ± 0.2	55.6 ± 0.4	323.0 ± 0.2	56.1 ± 0.5
T35W	330.8 ± 0.2	65.4 ± 0.4	330.9 ± 0.3	68.8 ± 0.4	329.9 ± 0.3	69.4 ± 0.5	329.5 ± 0.3	69.3 ± 0.5
D36W	334.5 ± 0.1	60.4 ± 0.2	337.8 ± 0.1	63.5 ± 0.2	334.8 ± 0.1	65.7 ± 0.2	334.2 ± 0.1	67.5 ± 0.2
S37W	335.7 ± 0.1	58.7 ± 0.1	335.4 ± 0.1	63.8 ± 0.2	334.1 ± 0.1	61.4 ± 0.2	334.0 ± 0.1	63.1 ± 0.2

Table 7.3.7 Fluorescence emission maxima for Trp mutants of TbMscL as a function of phospholipid headgroup. Mutants were reconstituted into bilayers of di(C18:1)PE, di(C18:1)PA, di(C18:1)PS, or di(C18:1)PG and fluorescence emission spectra were recorded between 300 nm and 400 nm. Emission spectra were fitted to a skewed Gaussian using Equation 4.4 (Chapter 4).

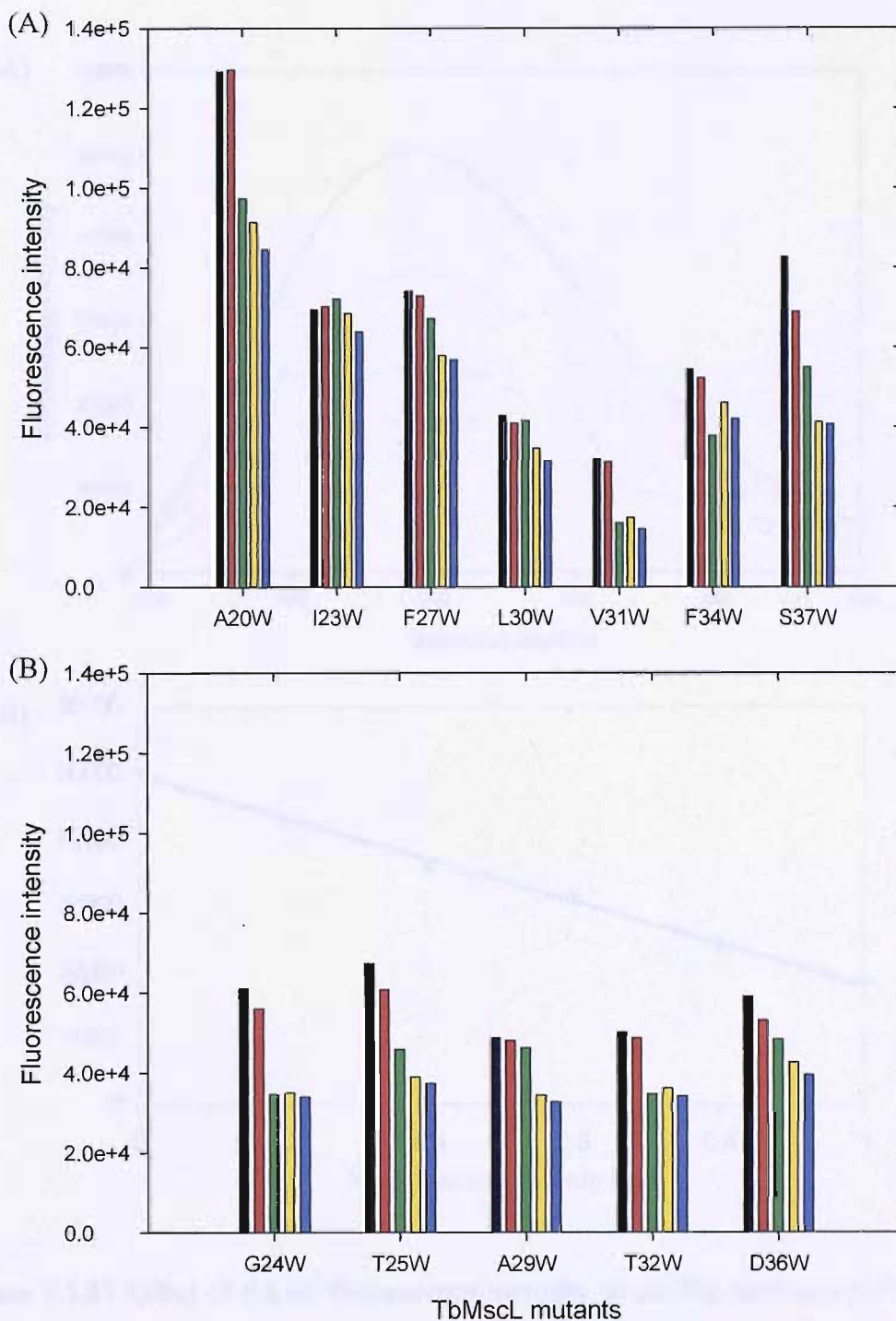


Figure 7.3.16 Relative fluorescence intensity for Trp mutants of TbMscL as a function of phospholipid headgroup. Mutants were reconstituted into bilayers of di(C18:1)PC, (■); di(C18:1)PE, (■); di(C18:1)PA, (■); di(C18:1)PS, (■); or di(C18:1)PG, (■) and fluorescence intensities were plotted as a function of lipid headgroup for (A) lipid-exposed residues and (B) pore-lining residues. The concentration of TbMscL was 0.98 μM and the ratio of lipid to protein monomer was 100:1.

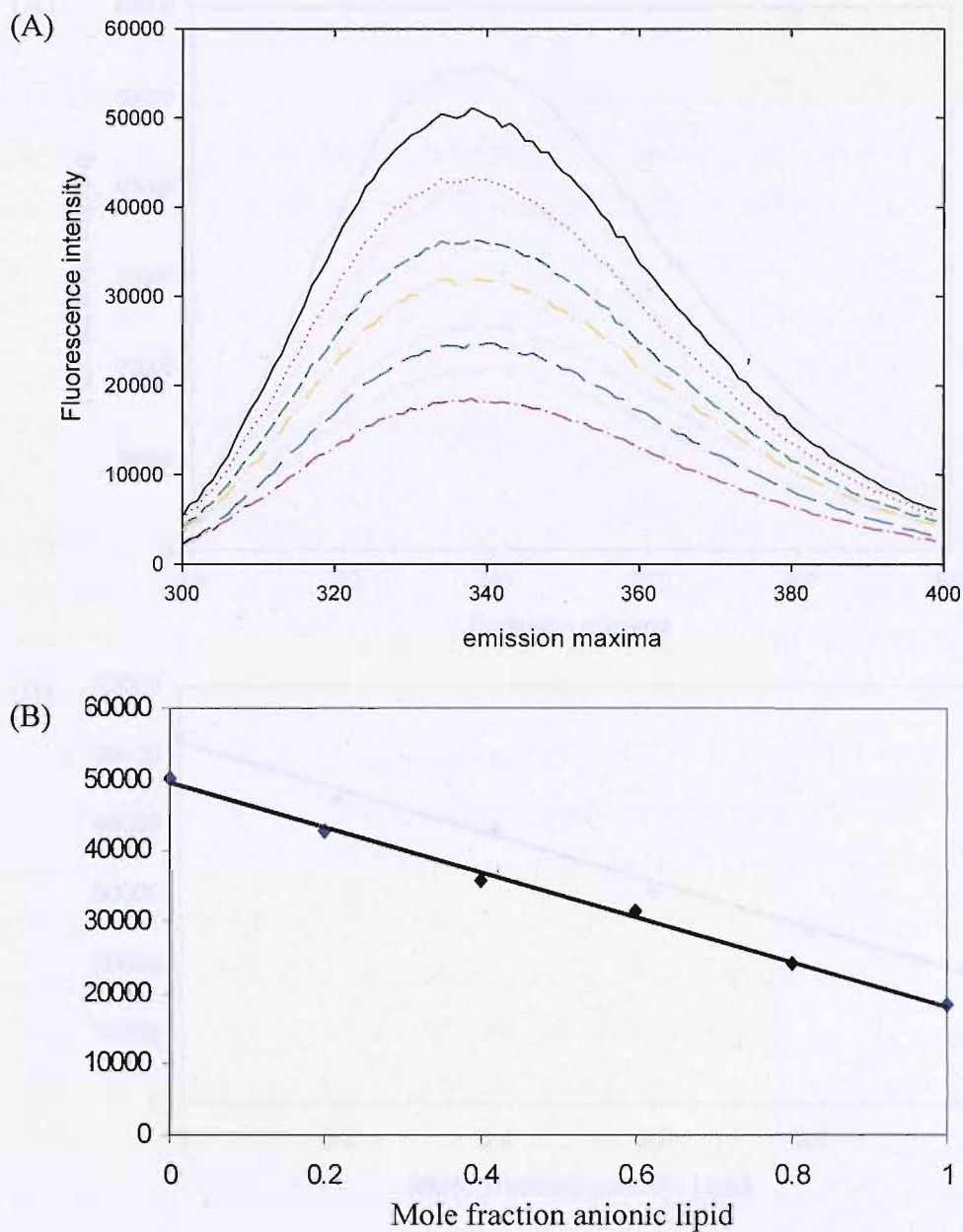


Figure 7.3.17 Effect of PA on fluorescence intensity of the Trp analogue NPTH (N-palmitoyl-Trp-hexyl). (A) Fluorescence emission spectra of NPTH showing decrease in fluorescence intensity with increasing mole fractions of PA. (B) Graphical representation showing the linear relationship between fluorescence intensity and the mole fraction of PA. The concentration of NPTH was 1 μM .

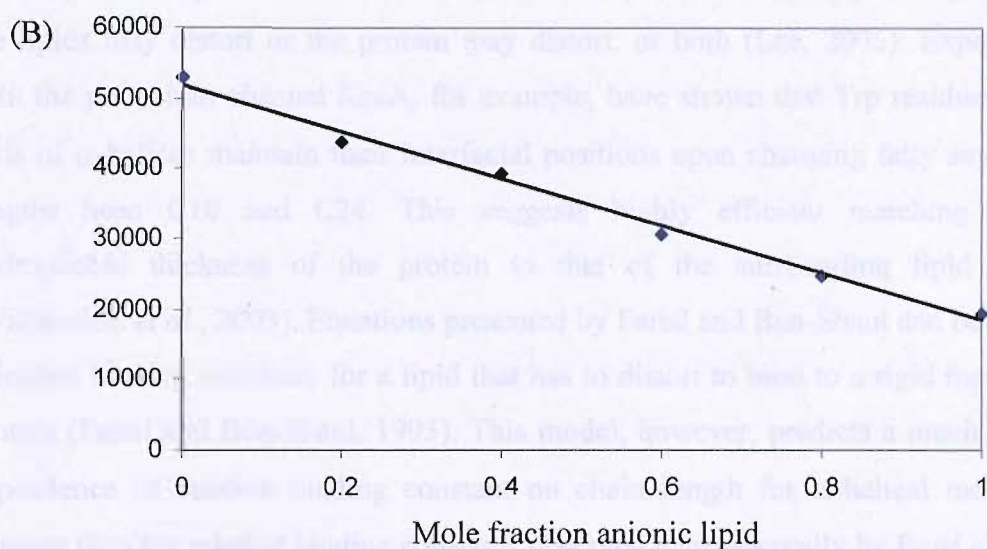
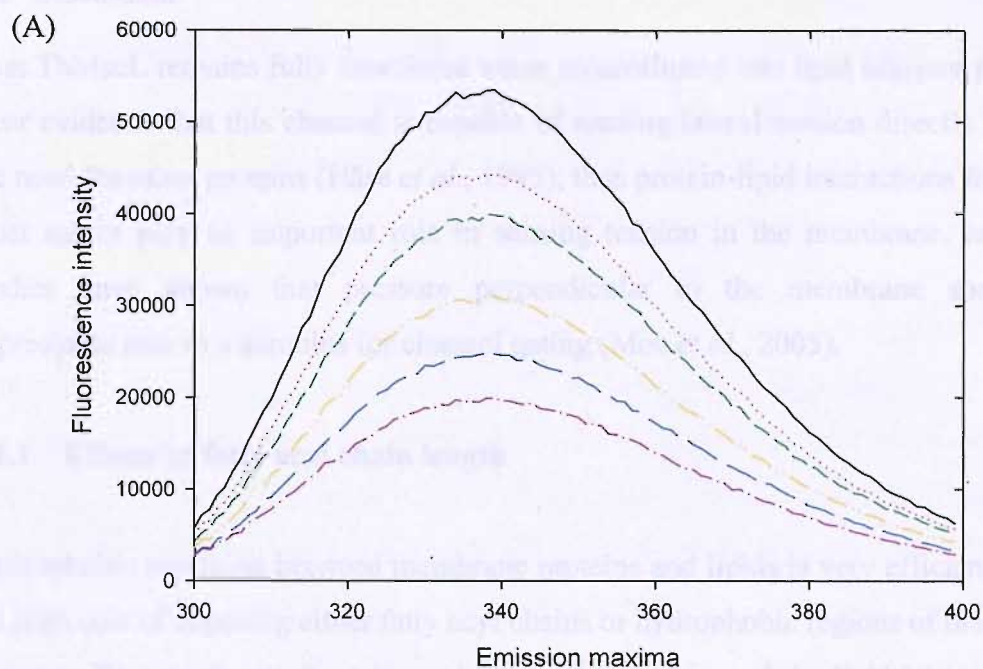


Figure 7.3.18 Effect of PS on fluorescence intensity of the Trp analogue NPTH (N-palmitoyl-Trp-hexyl). (A) Fluorescence emission spectra of NPTH showing decrease in fluorescence intensity with increasing mole fractions of PS. (B) Graphical representation showing the linear relationship between fluorescence intensity and the mole fraction of PS. The concentration of NPTH was 1 μM .

7.4 Discussion

That TbMscL remains fully functional when reconstituted into lipid bilayers provides clear evidence that this channel is capable of sensing lateral tension directly without the need for other proteins (Häse *et al.*, 1995), thus protein-lipid interactions for MscL must surely play an important role in sensing tension in the membrane, as recent studies have shown that pressure perpendicular to the membrane shows no appreciable role as a stimulus for channel gating (Moe *et al.*, 2005).

7.4.1 Effects of fatty acyl chain length

Hydrophobic matching between membrane proteins and lipids is very efficient due to the high cost of exposing either fatty acyl chains or hydrophobic regions of the protein to water. To compensate for mismatch between a protein and the lipid bilayer, either the lipids may distort or the protein may distort, or both (Lee, 2005). Experiments with the potassium channel KcsA, for example, have shown that Trp residues at the ends of α -helices maintain their interfacial positions upon changing fatty acyl chain lengths between C10 and C24. This suggests highly efficient matching of the hydrophobic thickness of the protein to that of the surrounding lipid bilayer (Williamson *et al.*, 2003). Equations presented by Fattal and Ben-Shaul can be used to calculate binding constants for a lipid that has to distort to bind to a rigid membrane protein (Fattal and Ben-Shaul, 1993). This model, however, predicts a much steeper dependence of relative binding constant on chain length for α -helical membrane proteins than the relative binding constants observed experimentally by Powl *et al.* for TbMscL (Powl *et al.*, 2003). Studies showed that relative binding constants of TbMscL for phosphatidylcholines with chain lengths between di(C12:0)PC and di(C24:1)PC vary only by a factor of 1.5, with the greatest affinity being for di(C16:1)PC (Powl *et al.*, 2003), with weaker binding observed for phosphatidylcholines with shorter or longer fatty acyl chains. This suggests that hydrophobic matching is not achieved just by distorting the lipid, but could also involve distorting the protein. One possibility is tilting of the transmembrane helices, consistent with the observation that the activities of many α -helical membrane proteins change with changing bilayer thickness (East and Lee, 1982; Pilot *et al.*, 2001). For TbMscL tilting of the transmembrane α -helices could be involved in the

channel opening process. Figure 7.1.1 shows the suggested changes in structure for TbMscL from the closed state to a closed-intermediate state, as modelled by Perozo *et al.* (Perozo *et al.*, 2002a). Most noticeable is the larger degree of movement of residues at both the cytoplasmic and periplasmic ends of TM1 α -helices than residues at the centre of the bilayer with little or no movement seen in this region of the helix.

Table 7.3.1 shows only a very small change in fluorescence emission maxima for all mutants on changing from di(C18:1)PC to di(C14:1)PC. Tryptophans close to the interface show no change in emission maxima therefore exposed residues above the glycerol backbone are not being buried in long chain lipids and buried residues below the glycerol backbone are not being exposed in short chain lipids; this provides a further example of the efficiency of hydrophobic matching. For residues towards the centre of TM1, lack of any change in emission maxima suggests that any tilting of helices is not associated with a large rotation, as a rotation of the helix would move a pore lining residue into the hydrophobic core of the bilayer, resulting in a blue-shift which is not seen for any of these mutants. Similarly, a rotation of a lipid-exposed residue to a pore-lining location would result in a red-shift in emission maxima, again, a result not seen for these residues. Hydrophobic matching, therefore, does not involve a large rotation of TM1 unlike the model proposed by Perozo *et al.* for channel opening (Perozo *et al.*, 2002a). Small rotations not involving a large environmental change would not be detected by changes in fluorescence emission spectra.

The accessibility of Trp residues for all mutants in di(C18:1)PC to brominated lipid and to aqueous quenchers was assessed in the respective chapters for each class of TbMscL mutants. Changes in accessibility of Trp residues from both the lipid phase and aqueous phase were monitored for mutants reconstituted into lipids with chains of different lengths. The level of quenching by brominated lipid is difficult to interpret in detail due to the different position of the *cis* double bonds in di(C22:1)PC compared to di(C14:1)PC and di(C18:1)PC (Table 7.3.2). The results shown in Figure 7.3.1 show that all Trp mutants are quenched the most in di(C14:1)PC and the least in di(C22:1)PC. This might simply reflect the fact that the proportion of atoms that are bromine is greater in a bilayer of di(Br₂C14:0)PC than the proportion of atoms that

are bromine in a bilayer of di(Br₂C22:0)PC. The results also show that the lipid exposed mutants were quenched the most by brominated phospholipids, a result not unexpected given the accessibility of these residues from the lipid bilayer, shown in Figure 4.1.1 (Chapter 4). That all pore exposed mutants were quenched the least by brominated phospholipids in all fatty acyl chain lengths is consistent with positions for these residues exposed to the channel pore rather than to the lipid bilayer. The results obtained for both acrylamide and iodide quenching for all mutants are as expected with pore exposed mutants showing a higher level of quenching than lipid exposed mutants (Figures 7.3.2 and 7.3.3). The lack of any significant change in the level of fluorescence quenching by acrylamide or iodide for all mutants upon reconstitution into different chain length lipids also suggests that no large scale tilt or rotation of α -helices has occurred, suggesting that TbMscL remains in the closed state in all three chain length lipids.

7.4.2 Effects of lipid headgroup

In membrane proteins, charged residues are normally located at the ends of transmembrane α -helices. In TbMscL, positive charges are found at both ends of TM1 and TM2, predominantly at the cytoplasmic side of the protein. Therefore, some interaction with anionic phospholipids would be expected to be observed. Interactions with anionic phospholipids could be due to either a general 'smeared-out' effect over the whole surface of the protein or due to the presence of distinct binding sites on the protein. The cationic charge cluster on the cytoplasmic side of TbMscL could make up a site for such interactions with anionic lipids. Previous experiments by Powl used Y87W, at the cytoplasmic side, and observed strong lipid binding to this cationic cluster (Powl *et al.*, 2005a). Using the average width of a lipid molecule and the dimensions of TbMscL, calculations show that there are around 3 lipid binding sites per monomer of TbMscL on each side of the membrane. The observation of 'hot-spots' for anionic lipids on the cytoplasmic side of MscL poses the questions as to whether there are distinct binding sites for anionic lipids on the periplasmic side of TbMscL and do all three cytoplasmic sites show high affinity for anionic lipids. As reported by I23W on the cytoplasmic side (Figure 7.3.4), higher affinities for PA and PG were observed, but not for PS. For PA at least, evidence suggests simple

competitive binding to the 2.5 sites from which fluorescence can be quenched. (n number, see Table 7.3.3). As reported by F27W, in the middle of the bilayer, again PG binds better than PS but binding of PA is more complex. The data obtained with F27W suggests the presence of one site with higher affinity for PA than PC and one site where the affinity for PA is equal to that of PC. On the periplasmic side of TbMscL, similar affinities for PA over PC were observed. Thus relative to the high binding constants detected by studies with Y87W, effects seen here are rather modest, pointing to a more generalised interaction with anionic lipids.

Figure 7.3.4 shows how residues I23W and F27W are positioned above a positive charge cluster on the cytoplasmic side of TbMscL. Previous studies show that some sites on TbMscL preferentially bind anionic phospholipid over zwitterionic phospholipids (Powl *et al.*, 2005a). The crystal structure of TbMscL highlights a distinct groove on the surface of the protein (Figure 7.3.4b) which would allow the close interaction of fatty acyl chains with I23W and F27W. Table 7.3.3 lists the values of n , the number of lipid sites from which the fluorescence of a Trp residue can be quenched. That the n numbers listed in Table 7.3.3 are very similar indicates that both I23W and F27W are equally accessible to all phospholipids.

The relative binding constants listed in Table 7.3.4 show no selectivity between PC and PE for either I23W or F27W. Similar results were seen for F80W (Powl *et al.*, 2003). Given that PE is a non-bilayer forming lipid (Dowhan, 1997), with significantly different physiochemical properties to PC, it is surprising that TbMscL binds PE and PC with equal affinity. Molecular dynamics simulations by Elmore and Dougherty (Elmore *et al.*, 2003) suggested that the structures of TbMscL in PE and PC were significantly different. The structure in PE was suggested to be very similar to the crystal structure but that in PC the number of protein-lipid hydrogen bonds was reduced, resulting in structural changes in the C-terminal domain of TbMscL (Elmore *et al.*, 2003). However, no changes in fluorescence emission maxima were observed for any of the Trp mutants when reconstituted into PC and PE (see Tables 7.3.1 and 7.3.8) suggesting that any changes in conformational between PC and PE are likely to be small.

To establish whether anionic lipid headgroups have any effect on the conformation of TbMscL, Trp mutants were reconstituted into bilayers of di(C18:1)PA, di(C18:1)PS and di(C18:1)PG and fluorescence emission maxima were recorded. The results shown in Table 7.3.7 indicate no significant changes in Trp emission spectra for many of the mutants, but with some showing small changes, particularly in PA. Largest fluorescence changes in PA are seen for the lipid exposed residues I23W, V31W, and F34W with blue shifts of 3 nm and 5 nm respectively and the pore exposed residues G24W and A29W. Although this might suggest a conformational change in PA, Moe *et al.* (Moe *et al.*, 2005) found that the membrane tension required to gate the channel was unchanged by the presence of anionic lipid, and therefore proposed that anionic lipids play no detectable role in the ability of TbMscL to sense membrane tension, or as a stimulus for channel gating.

Chapter 8-General Discussion

The selective permeability of lipid bilayers allows the continual passage of water and small hydrophobic molecules into a cell but requires the presence of specialised classes of membrane proteins, such as transporters and channels, to allow the passage of hydrophilic molecules such as ions and sugars. The passage of water across the membrane is driven by osmotic pressure differences and is therefore dependent on the intra and extracellular solute concentration of the surrounding medium. In the absence of any osmoregulatory mechanism to counteract osmotic stress, the influx of water under hypotonic conditions increases turgor pressure leading to cell expansion and eventual cell lysis (Poolman *et al.*, 2002). In bacteria, the ability to protect themselves against osmotic down shock (the influx of water) comes from the presence of mechanosensitive channels (MS) present in the inner membrane, which work as pressure release valves. Of the three types of MS channels present in bacteria, (MscM, MscS, and MscL), MscL has been the most extensively studied. Since MscL and its homologues are fully functional when reconstituted into lipid bilayers (Sukharev *et al.*, 1994), it is clear that their function does not require any association with cytoskeletal proteins, as in eukaryotic mechanosensitive channels.

Molecular modelling studies have predicted large structural changes during mechanosensitive channel gating (Sukharev *et al.*, 2001b; Bilston *et al.*, 2002; Betanzos *et al.*, 2002; Perozo *et al.*, 2002a) and mutagenesis studies have revealed residues that are critical in channel gating, producing either a loss-of-function phenotype or a gain-of-function phenotype (Ou *et al.*, 1998; Yoshimura *et al.*, 1999; Yoshimura *et al.*, 2004; Anishkin *et al.*, 2005).

TbMscL has no Trp residues allowing the introduction of single Trp residues into defined positions in TbMscL. Tryptophan scanning mutagenesis has been used to characterise the environment of residues in TM1 of TbMscL. Tryptophan fluorescence has the characteristic of being sensitive to the polarity of the surrounding environment and fluorescence emission maxima report on whether Trp residues are located in a hydrophilic or a hydrophobic environment.

Primers were designed to generate Trp mutants of TbMscL for pore lining residues and lipid exposed residues (see Tables 3.2.1 and 3.2.2). Residues in TM1 that are thought to form the permeation pathway for solutes consist of a series of threonines, a lysine and an aspartate, however, due to problems with primer design such as hairpin formations, not all Trp mutants of these polar residues were able to be produced.

Chapter four reports on lipid-exposed residues in TM1, and growth curves showed that insertion of Trp residues into lipid-binding sites on TM1 did not result in GOF mutants, although the mutant A20W showed a slightly reduced growth rate (Figure 4.4.1) upon expression of protein. The crystal structure of the closed channel shows lipid-exposed residues in TM1 to be buried in the surface of TbMscL (Figure 4.1.1) and so values for fluorescence emission maxima were obtained to determine whether buried residues in TM1 share the same fluorescence characteristics as lipid exposed residues in TM2. Previous work by Powl (Powl *et al.*, 2005b) in which TbMscL was reconstituted into bilayers of di(C18:1)PC gave a hydrophobic thickness of ca. 25 Å for TbMscL with the region of TM2 that spans the hydrophobic core of the bilayer running from Leu-69 at the periplasmic side, to Leu-92 on the cytoplasmic side. Fluorescence emission maxima for lipid-exposed residues in TM1 were obtained by reconstituting Trp mutants of TbMscL into bilayers of di(C18:1)PC and the values obtained were compared to those obtained for Trp residues in TM2 (Table 4.4.1 and Figure 4.4.4) and plotted as a function of the distances along the bilayer normal of the α -carbons of residues from the α -carbon of L69 (Figure 4.4.4). With the exception of Leu-30 in TM1 and Ile-77 in TM2, a trough-like profile was observed for fluorescence emission maxima as a function of distance from Leu-69 on the periplasmic side of the membrane. This trough-like profile was not observed for fluorescence emission maxima obtained for residues on the cytoplasmic side of TbMscL as a function of distance from Leu-69 (Figure 4.4.4). An equation describing how the dielectric constant varies across a bilayer was used to describe the dependence of fluorescence emission maxima on position within the bilayer. The data for residues on the periplasmic side of TbMscL fit well to this model, falling on a smooth curve and giving the expected trough-like profile for solvent polarity as a function of distance. In contrast the data for residues on the cytoplasmic side of TbMscL do not fit meaningfully to this model. It was suggested that residues on the

cytoplasmic side of TbMscL are less constrained than those on the periplasmic side and have 'snorkelled' towards the interface so that their position is not well defined in terms of the α -carbon position. The value obtained for the hydrophobic thickness of TbMscL of $23.6 \pm 5.2 \text{ \AA}$ is in good agreement with the previous estimate given by Powl *et al.* of 25 \AA (Powl *et al.*, 2005b).

The extent of lipid penetration into the MscL surface was determined. Trp residues were modelled into the structure. The surface of the transmembrane region of MscL was determined by locating a lipid with all trans chains onto the surface. From the calculated distances between the Trp residues and bromines in the fatty acyl chains the efficiencies of fluorescence quenching were calculated if the lipid molecule could not penetrate into the protein surface (Figure 4.5.7 and Table 4.5.3). Experimental levels of fluorescence quenching of lipid-exposed residues by brominated phospholipids were significantly higher than calculated using the model, leading to the proposal that the lipid fatty acyl chains are able to penetrate into the surface of TbMscL, bringing the chains into close proximity to the Trp residues. Thus the lipid fatty acyl chains of phospholipids can penetrate into the surface of TbMscL to provide full solvation of residues in TM1. As TbMscL senses tension directly from the lipids in the bilayer, such protein-lipid interactions are vital for channel function. Helices are thought to tilt significantly during the gating process, and the resulting changes in helix packing will lead to changes in solvation by the lipid molecules; these changes in solvation will be part of the energetics of channel opening.

Having characterised residues that were exposed to the lipid phase, the results presented in Chapter five characterise the pore lining residues. The crystal structure of the closed channel shows that a hydrophobic constriction is formed by residue Val-21 at the cytoplasmic side of TbMscL and that Thr-25 forms a partial occlusion (Chang *et al.*, 1998). The fluorescence emission maxima for all mutants were shifted to longer wavelengths in relation to the lipid-exposed residues (Table 5.3.1) and so are assumed to line the pore, as in the crystal structure. This suggests that the structure of TbMscL in the crystal is the same as that in a lipid bilayer. MscS is partially open in the crystal structure (Bass *et al.*, 2002) thought to be a result of the crystals being in detergent, with lipids no longer present to keep the channel closed. This is therefore not the case

with TbMscL, the presence of lipids not being required to keep the channel in a closed state.

Due to the tilt angle of TM1, pore-lining residues at the periplasmic side of TbMscL are closer to the fatty acyl chains than those residues on the cytoplasmic side of TbMscL and were quenched by brominated phospholipids to a greater extent than cytoplasmic residues, although overall levels were less than those observed for lipid exposed residues, as expected. The levels of quenching obtained for acrylamide for all residues in TM1 were not very informative as acrylamide appeared to be able to partition into the membrane, quenching residues with equal efficacy whether they were pore lining or lipid exposed. That the levels of fluorescence quenching by iodide observed for pore lining residues were slightly higher than those observed for the lipid exposed residues (Figure 5.3.3) suggests that water does penetrate down to T25W and that the channel of pore of TbMscL must be quite hydrated even in the closed state.

That mutation of pore lining residues located beneath T25 (A20, V22) to Trp resulted in gain-of-function mutants is consistent with previous observations (Anishkin *et al.*, 2005) that GOF mutations are centred at the pore constriction and that small amino acids are important in channel gating and maintaining close helix-helix contacts in this region of the protein. All three Trp mutants of TbMscL discussed in Chapter 6 showed a distinct reduction in growth rate following induction of MscL expression indicating that those mutations produce a GOF phenotype that opens at very low or zero tension (Figure 6.3.1). Values for fluorescence emission maxima obtained (Table 6.3.1) indicated that the Trp residues in all three GOF mutants were probably in a hydrophilic environment, in a location facing the channel pore. The levels of fluorescence quenching obtained for these mutants were very similar to the values obtained for the GOF mutant V21K:F80W, studied by Powl (Powl *et al.*, 2005a) adding weight to this suggestion. That T35W, at the periplasmic side of TbMscL, resulted in a GOF mutation can be attributed to alterations in helix-helix packing in this region of the protein, this mutation being located at the point where TM1 and TM2 come together.

The positive charge mutation V21K produces an open form of TbMscL (Powl *et al.*, 2005a). Trp mutants that displayed a normal phenotype were chosen to try to produce

Trp mutants of V21K to study properties of the open channel. However the protein failed to express at levels sufficient for purification. Small scale expression studies using gadolinium as a channel blocker were also tried (Figure 6.3.4) without success.

The results presented in Chapter 7 look at the effects of changing lipid headgroup and lipid chain length on the fluorescence properties of TbMscL, previous studies suggesting significant changes in structure when the lipid headgroup structure was changed (Perozo *et al.*, 2002a; Elmore *et al.*, 2003). Molecular dynamics simulations predicted changes in the conformation of TbMscL in PE compared to that in PC. It has also been shown that in thin bilayers, MscL is easier to open therefore conformational changes will be detected upon moving from a closed or intermediate state to an open state (Perozo *et al.*, 2002a; Elmore *et al.*, 2003). Fluorescence spectroscopy was used to detect any changes for TbMscL in bilayers of different lipid chain lengths and different lipid headgroups. The results presented indicated no significant change in structure when reconstituted into different fatty acyl chain length lipids or different headgroups (Tables 7.3.1 and 7.3.7). Explanations for this could be that conformational changes are restricted to small areas of the protein, in regions that were not chosen for Trp-scanning mutagenesis, or that changes were such that no change in Trp fluorescence could be detected. For example, rotation of a helix as in the model of Perozo *et al.* for channel opening (Perozo *et al.*, 2002a), would only result in a change in Trp fluorescence if the rotation resulted in a large change in environmental polarity for the Trp residue.

Membrane proteins, such as KcsA and rhodopsin, usually contain charged residues at the ends of transmembrane helices, anchoring the protein within the lipid bilayer and enabling charge interactions between the protein and lipids in the membrane. Previous experiments by Powl showed that strong binding of anionic phospholipids was observed on the cytoplasmic side of TbMscL, attributable to a cationic charge cluster (Powl *et al.*, 2005a). Results presented in Chapter 7 reported on whether there are distinct binding sites for anionic lipids on the periplasmic side of TbMscL (Table 7.3.4). Results suggested that there was no specificity for binding of anionic lipids on the periplasmic side of TbMscL and that the selectivity for anionic lipids on the

cytoplasmic side of TbMscL, determined using I23W and F27W as reporters, were rather modest in comparison to the studies by Powl.

Copyright Clearance Center, Inc.

100 Brook Hill Drive, West Nyack, NY 10994-2133

www.copyright.com

0000-0000-0000-0000

0000-0000-0000-0000

0000-0000-0000-0000

0000-0000-0000-0000

0000-0000-0000-0000

0000-0000-0000-0000

0000-0000-0000-0000

0000-0000-0000-0000

0000-0000-0000-0000

0000-0000-0000-0000

0000-0000-0000-0000

0000-0000-0000-0000

0000-0000-0000-0000

0000-0000-0000-0000

0000-0000-0000-0000

0000-0000-0000-0000

0000-0000-0000-0000

0000-0000-0000-0000

0000-0000-0000-0000

0000-0000-0000-0000

REFERENCES

- Ajouz B, Berrier C, Garrigues A, Besnard M, and Ghazi E (1998) Release of thioredoxin via the mechanosensitive channel MscL during osmotic downshock of *Escherichia coli* cells. *J Biol Chem*, **273**, 26670-26674.
- Alberts B, Johnson A, Lewis J, Raff M, Roberts K, and Walter P (2002). *Molecular biology of the cell*. Garland Science, New York.
- Alvis SJ, Williamson IM, East JM, and Lee AG (2003) Interactions of anionic phospholipids and phosphatidylethanolamines with the potassium channel KcsA. *Biophys J*.
- Anishkin A, Chiang CS, and Sukharev S (2005) Gain-of-function mutations reveal expanded intermediate states and a sequential action of two gates in MscL. *Journal of General Physiology*, **125**, 155-170.
- Bass RB, Strop P, Barclay MT, and Rees DC. crystal structure of *Escherichia coli* MscS, a Voltage-Modulated and Mechanosensitive Channel. *Science* **298**, 1582-1587. 2002.
- Betanzos M, Chiang CS, Guy HR, and Sukharev S (2002) A large iris-like expansion of a mechanosensitive channel protein induced by membrane tension. *Nature Structural Biology*, **9**, 704-710.
- Bevers E, Comfurius P, Dekkers DWC, and Zwaal RFA (1999) Lipid translocation across the plasma membrane of mammalian cells. *Biochimica et Biophysica Acta-Biomembranes*, **1439**, 317-330.
- Biggin PC and Sansom MSP (1999) Interactions of alpha-helices with lipid bilayers: a review of simulation studies. *Biophysical Chemistry*, **76**, 161-183.
- Bilston LE and Mylvaganam K (2002) Molecular simulations of the large conductance mechanosensitive (MscL) channel under mechanical loading. *Febs Letters*, **512**, 185-190.

Blount P, Schoeder M, and Kung C (1997) Mutations in a bacterial mechanosensitive channel change the cellular response to osmotic stress. *J Biol Chem*, **272**, 32150-32157.

Bolen EJ and Holloway PW (1990) Quenching of tryptophan fluorescence by brominated phospholipid. *Biochemistry*, **29**, 9638-9643.

Booth IR, Edwards MD, and Miller S (2003) Bacterial ion channels. *Biochemistry*, **42**, 10045-10053.

Booth PJ (2005) Sane in the membrane: designing systems to modulate membrane proteins. *Current Opinion in Structural Biology*, **15**, 435-440.

Brink-van der Laan E, Killian JA, and de Kruijff B (2004) Nonbilayer lipids affect peripheral and integral membrane proteins via changes in the lateral pressure profile. *Biochimica et Biophysica Acta-Biomembranes*, **1666**, 275-288.

Byrne B and Iwata S (2002) Membrane protein complexes. *Current Opinion in Structural Biology*, **12**, 239-243.

Calhoun DB, Vanderkooi JM, and Englander SW (1983) Penetration of small molecules into proteins studied by quenching of phosphorescence and fluorescence. *Biochemistry*, **22**, 1533-1539.

Chang G, Spencer RH, Lee AT, Barclay MT, and Rees DC (1998) Structure of the MscL homolog from *Mycobacterium tuberculosis*: A gated mechanosensitive ion channel. *Science*, **282**, 2220-2226.

Chiang CS, Anishkin A, and Sukharev S (2004) Gating of the large mechanosensitive channel in Situ: Estimation of the spatial scale of the transition from channel population responses. *biophysical journal*, **86**, 2846-2861.

Chiang CS, Shirinian L, and Sukharev S (2005) Capping Transmembrane Helices of MscL with Aromatic Residues Changes Channel Response to Membrane Stretch. *Biochemistry*, **44**, 12589-12597.

Cornell RB and Arnold RS. Modulation of the activities of enzymes of membrane lipid metabolism by non-bilayer forming lipids. *Chemistry and Physics of Lipids* **81**, 215-227. 1996.

Cruickshank CC, Minchin RF, Le Dain AC, and Martinac B (1997) Estimation of the pore size of the large-conductance mechanosensitive ion channel of *Escherichia coli*. *biophysical journal*, **74**, 2889-2902.

Dowhan W (1997) Molecular basis for membrane phospholipid diversity: Why are there so many lipids? *annual reviews in biochemistry*, **66**, 199-232.

East JM and Lee AG (1982) Lipid selectivity of the calcium and magnesium ion dependent adenosinetriphosphatase, studied with fluorescence quenching by a brominated phospholipid. *Biochemistry*, **21**, 4144-4151.

Elmore DE and Dougherty DA (2003) Investigating lipid composition effects on the Mechanosensitive channel of Large Conductance (MscL) using molecular dynamics simulations. *biophysical journal*, **85**, 1512-1524.

Elmore DE and Dougherty DA. Molecular dynamics simulations of wild-type and mutant forms of the *Mycobacterium tuberculosis* MscL channel. *Biophys.J.* **81**, 1345-1359. 2001.

Epanand RM (1998) Lipid polymorphism and protein-lipid interactions. *Biochimica et Biophysica Acta-Reviews on Biomembranes*, **1376**, 353-368.

Ewis HE and Lu C (2005) Osmotic Shock: A mechanosensitive channel blocker can prevent release of cytoplasmic but not periplasmic proteins. *FEMS Microbiology Letters*, **253**, 295-301.

Fattal DR and Ben-Shaul A (1993) A molecular model for lipid-protein interaction in membranes: the role of hydrophobic mismatch. *Biophys J*, **65**, 1795-1809.

Flewelling RF and Hubbell WL (1986) The membrane dipole potential in a total membrane potential model. Applications to hydrophobic ion interactions with membranes. *Biophys J*, **49**, 541-552.

Gullingsrud J. Structural determinants of MscL gating studied by molecular dynamics simulations. *Biophys.J.* **80**, 2074-2081. 2001.

Hamill OP and Martinac B (2001) Molecular basis of mechanotransduction in living cells. *Physiological Reviews*, **81**, 685-740.

Häse CC, Le Dain AC, and Martinac B (1995) Purification and functional reconstitution of the recombinant large mechanosensitive ion channel (MscL) of *Escherichia coli*. *J Biol Chem*, **270**, 18329-18334.

Heginbotham L, Kolmakova-Partensky L, and Miller C. Functional reconstitution of a prokaryotic K⁺ channel. *Journal of General Physiology* **111**, 741-749. 1998.

Heijne GV (1996) Principles of membrane protein assembly and structure. *progressions in biophysics and molecular biology*, **66**, 113-139.

Janes N (1996) Curvature stress and polymorphism in membranes. *Chemistry and Physics of Lipids*, **81**, 133-150.

Kloda A and Martinac B. Mechanosensitive channel of *thermoplasma*, the cell-less archaea: cloning and molecular characterisation . *Cell Biochemistry and Biophysics* **34**, 321-347. 2001.

Kong YF, Shen YF, Warth TE, and Ma JP (2002) Conformational pathways in the gating of *Escherichia coli* mechanosensitive channel. *Proceedings of the National Academy of Sciences of the United States of America*, **99**, 5999-6004.

Koprowski P and Kubalski A (2001) Bacterial ion channels and their eukaryotic homologues. *Bioessays*, **23**, 1148-1158.

Kung C and Blount P (2004) Channels in microbes: so many holes to fill. *Molecular Microbiology*, **53**, 373-380.

Ladokhin AS (2000). Fluorescence spectroscopy in peptide and protein analysis. In R.A.Meyers (Ed.), *Encyclopedia of analytical chemistry*, . John Wiley & Sons, Chichester, pp. 5762-5779.

Lakowicz JR (1983). *Principles of Fluorescence Spectroscopy*. Plenum Press, New York.

Lee AG. Membrane Lipids: It's only a phase. *Current Biology* , 377-380. 2000.

Lee AG (2003) Lipid-protein interactions in biological membranes: a structural perspective. *Biochimica et Biophysica Acta-Biomembranes*, **1612**, 1-40.

Lee AG (2004) How lipids affect the activities of integral membrane proteins. *Biochimica et Biophysica Acta-Biomembranes*, **1666**, 62-87.

Lee AG (2005) How lipids and proteins interact in a membrane: a molecular approach. *Molecular biosystems*, **1**, 203-212.

LeMasurier M, Heginbotham L, and Miller C (2001) KcsA:It's a potassium channel. *Journal of General Physiology*, **118**, 303-313.

Madigan MT, Martinko JM, and Parker J (2000). *Brock Biology of microorganisms*. Prentice-Hall Inc., New Jersey.

Mall S, Broadbridge R, Sharma RP, East JM, and Lee AG (2001) Self-association of model transmembrane alpha-helices is modulated by lipid structure. *Biochemistry*, **40**, 12379-12386.

Marsh D (2001) polarity and permeation profiles in lipid membranes. *Proceedings of the National Academy of Sciences of the United States of America*, **98**, 7777.

Martinac B, Buechner M, Delcour AH, Adler J, and Kung C (1987) Pressure-sensitive ion channel in Escherichia coli. *Proceedings of the National Academy of Sciences of the United States of America*, **84**, 2297-2301.

Martinac B (2004) Mechanosensitive ion channels: molecules of mechanotransduction. *journal of cell science*, **117**, 2449-2460.

Moe PC and Blount P (2005) Assessment of Potential stimuli for Mechano-Dependent Gating of MscL: Effects of Pressure, Tension, and Lipid Headgroups. *Biochemistry*, **44**, 12239-12244.

Moe PC, Levin G, and Blount P (2000) Correlating a protein structure with function of a bacterial mechanosensitive channel. *J Biol Chem*, **275**, 31121-31127.

Nelson DL and Cox MM (2005). *Lehninger-principles of biochemistry*. W.H Freeman & Company, New York.

Oakley AJ, Martinac B, and Wilce MCJ (1999) Structure and function of the bacterial mechanosensitive channel of large conductance. *Protein Science*, **8**, 1915-1921.

O'Keefe AH, East JM, and Lee AG (2000) Selectivity in lipid binding to the bacterial outer membrane protein OmpF. *Biophys J*, **79**, 2066-2074.

Ou X, Blount P, Hoffman RJ, and Kung C (1998) one face of a transmembrane helix is crucial in mechanosensitive channel gating. *Proceedings of the National Academy of Sciences of the United States of America*, **95**, 11471-11475.

Palsdottir H and Hunte C (2004) Lipids in membrane protein structures. *Biochimica et Biophysica Acta-Biomembranes*, **1666**, 2-18.

Perozo E, Cortes DM, Sompornpisut P, Kloda A, and Martinac B (2002a) Open channel structure of MscL and the gating mechanism of mechanosensitive channels. *Nature*, **418**, 942-948.

Perozo E, Kloda A, and Martinac B (2002b) Physical principles underlying the transduction of bilayer deformation forces during mechanosensitive channel gating. *Nature Structural Biology*, **9**, 696-703.

Perozo E and Rees DC (2003) Structure and mechanism in prokaryotic mechanosensitive channels. *Current Opinion in Structural Biology*, **13**, 432-442.

Pilot JD, East JM, and Lee AG (2001) Effects of bilayer thickness on the activity of diacylglycerol kinase of *Escherichia coli*. *Biochemistry*.

Pomorski T, Hrafnisdóttir S, and Devaux PvMG (2001) Lipid distribution and transport across cellular membranes. *cell & developmental biology*, **12**, 139-148.

Poolman B, Blount P, Folgering JHA, Friesen RHE, Moe PC, and van der Heide T (2002) How do membrane proteins sense water stress? *Molecular Microbiology*, **44**, 889-902.

Powl AM, East JM, and Lee AG (2003) Lipid-protein interactions studied by introduction of a tryptophan residue: The mechanosensitive channel MscL. *Biochemistry*, **42**, 14306-14317.

Powl AM, East JM, and Lee AG (2005a) Heterogeneity in Binding of Lipid Molecules to the surface of a Membrane Protein: Hot spots for Anionic Lipids on the Mechanosensitive Channel of Large Conductance MscL and Effects on Conformation. *Biochemistry*, **44**, 5873-5883.

Powl AM, Wright N, East JM, and Lee AG (2005b) Identification of the hydrophobic thickness of a membrane protein using fluorescence spectroscopy: Studies with the Mechanosensitive channel MscL. *Biochemistry*, **44**, 5713-5721.

Schulz (2000) β -barrel membrane proteins. *Current Opinion in Structural Biology*, **10**, 443-447.

Spencer RH, Chang G, and Rees DC (1999) 'Feeling the pressure': structural insights into a gated mechanosensitive channel. *Current Opinion in Structural Biology*, **9**, 448-454.

Spencer RH and Rees DC (2002) the α -helix and the organisation and gating of channels. *Annual Review of Biophysics and Biomolecular Structure*, **31**, 207-233.

Stryer L (1996). *Biochemistry*. W.H.Freeman and company, New York.

Stubbs CD and Slater SJ (1996) The effects of non-lamellar forming lipids on membrane protein- lipid interactions. *Chemistry and Physics of Lipids*, **81**, 185-195.

Sukharev S (2000) Pulling the channel in many dimensions. *Trends in Microbiology*, **8**, 12-13.

Sukharev S, Betanzos M, chlang C, and Guy HR (2001a) The gating mechanism of the large mechanosensitive channel MscL. *Nature*, **409**, 720-724.

Sukharev S, Blount P, Martinac B, Blattner FR, and Kung C (1994) A large-conductance mechanosensitive channel in *E.coli* encoded by MscL alone. *Nature*, **368**, 265-268.

Sukharev S, Durell SR, and Guy HR (2001b) Structural models of the MscL gating mechanism. *biophysical journal*, **81**, 917-936.

Sukharev S, Sigurdson WJ, Kung C, and Sachs F (1999) Energetic and spatial parameters for gating of the bacterial large conductance mechanosensitive channel. *Journal of General Physiology*, **113**, 525-540.

valiyaveetil FI, Zhou Y, and Mackinnon R. Lipids in the structure, folding and function of the KcsA K⁺ channel. *Biochemistry* **41**, 10771-10777. 2002.

Werten PJJ, Remigy HW, de Groot BL, Fotiadis D, Philippsen A, Stahlberg H, Grubmuller H, and Engel A (2002) Progress in the analysis of membrane protein structure and function. *Febs Letters*, **529**, 65-72.

White SH and Wimley WC (1999) Membrane protein folding and stability: Physical principles. *Annual Review of Biophysics and Biomolecular Structure*, **28**, 319-365.

Williamson IM, Alvis SJ, East JM, and Lee AG (2003) Interactions of phospholipids with the potassium channel KscA. *Biophys J*, **83**, 2026-2038.

Wood JM, Bremer E, and Csonka LN (2001) Osmosensing and osmoregulatory compatible solute accumulation by bacteria. *comparitive biochemistry and physiology*, **130**, 437-460.

Yoshimura K, Batiza A, Schoeder M, Blount P, and Kung C (1999) Hydrophilicity of a single residue within MscL correlates with increased channel mechanosensitivity. *biophysical journal*, **77**, 1960-1972.

Yoshimura K, Nomura T, and Sokabe M (2004) Loss-of-function mutations at the rim of the funnel of mechanosensitive channel MscL. *biophysical journal*, **86**, 2113-2120.

